LARGE DEFORMATION ANALYSIS OF FLEXIBLE MULTIBODY SYSTEMS

A THESIS SUBMITTED TO
THE GRADUATE SCHOOL OF NATURAL AND APPLIED SCIENCES
OF
MIDDLE EAST TECHNICAL UNIVERSITY

BY

AYDIN TÜZÜN

IN PARTIAL FULFILLMENT OF THE REQUIREMENTS
FOR
THE DEGREE OF DOCTOR OF PHILOSOPHY
IN
MECHANICAL ENGINEERING

SEPTEMBER 2012

Approval of the thesis:

LARGE DEFORMATION ANALYSIS OF FLEXIBLE MULTIBODY SYSTEMS

submitted by **AYDIN TÜZÜN** in partial fulfillment of the requirements for the degree of **Doctor of Philosophy in Mechanical Engineering Department, Middle East Technical University** by,

Prof. Dr. Canan Özgen
Dean, Graduate School of **Natural and Applied Sciences**   ————————

Prof. Dr. Suha Oral
Head of Department, **Mechanical Engineering**   ————————

Prof. Dr. Haluk Darendeliler
Supervisor, **Mechanical Engineering Department, METU**   ————————

Prof. Dr. Kemal İder
Co-supervisor, **Mechanical Engineering Department, METU**   ————————

Examining Committee Members:

Prof. Dr. Suha Oral
Mechanical Engineering Department, METU   ————————

Prof. Dr. Haluk Darendeliler
Mechanical Engineering Department, METU   ————————

Prof. Dr. Can Çoğun
Mechanical Engineering Department, METU   ————————

Prof. Dr. Yavuz Yaman
Aerospace Engineering Department, METU   ————————

Prof. Dr. Müfit Gülgeç
Mechatronics Engineering Department, Çankaya University   ————————

Date: __10.09.2012__

I hereby declare that all information in this document has been obtained and presented in accordance with academic rules and ethical conduct. I also declare that, as required by these rules and conduct, I have fully cited and referenced all material and results that are not original to this work.

Name, Last Name: AYDIN TÜZÜN

Signature   :

ABSTRACT

LARGE DEFORMATION ANALYSIS OF FLEXIBLE MULTIBODY SYSTEMS

Tüzün, Aydın

Ph.D., Department of Mechanical Engineering

Supervisor   : Prof. Dr. Haluk Darendeliler

Co-Supervisor : Prof. Dr. Kemal İder

September 2012, 163 pages

Large displacement and large strain problems of mechanical systems can be solved mainly by four methods. These are Floating Frame of Reference, Incremental Finite Element, Large Rotation Vector and Absolute Nodal Coordinate Formulations (ANCF). Due to exact rigid body representation, simple mass matrix structure and non-incremental formulation, ANCF is more convenient in analyzing flexible multibody systems. However, it is limited to problems with regular boundaries, currently.

The aim of the thesis is to improve the current ANCF in order to handle various problems with irregular boundaries. For this purpose, firstly meshfree ANCF has been developed to analyze flexible multibody systems. Verification of the developed meshfree formulation has been performed for beam type structures and accurate results have been obtained. Then, "ANCF with Virtual Element Mapping Method" has been proposed to overcome the boundary problems of the current formulations. The proposed method has been implemented to plane stress, plane strain, plate/shell and 3D solid finite elements. Verification of the proposed method has been performed by using the patch test problems available in the literature. Besides, it has been verified by various flexible multibody problems with large deformations.

Additionally, shape function polynomials for thin plate assumption have been derived.

It is observed that developed formulations and methods can be useful not only for flexible multibody systems but also for structural mechanics problems subjected to large deformations and/or rotations. The proposed methods and formulations are more efficient than the current formulations in the literature due to extended shape limits of finite elements.

ÖZ

ÇOKLU BÜNYE SİSTEMLERİNİN YÜKSEK DEFORMASYONLU ANALİZİ

Tüzün, Aydın

Doktora, Makina Mühendisliği Bölümü

Tez Yöneticisi   : Prof. Dr. Haluk Darendeliler

Ortak Tez Yöneticisi   : Prof. Dr. Kemal İder

Eylül 2012, 163 sayfa

Mekanik sistemlerde yüksek yer değiştirme ve yüksek gerinim problemleri temel olarak dört yöntem ile çözülebilmektedir. Bunlar, Yüzen Referans Takımı, Basamaklı Sonlu Eleman, Büyük Dönü Vektörü ve Mutlak Nodal Koordinat Formülasyonlarıdır. Doğru katı cisim dinamiği benzetimi, basit kütle matrisi ve basamaksız formülasyonu nedeni ile çoklu bünye dinamiği analizleri için en uygun yöntem, Mutlak Nodal Koordinat Formülasyonu'dur. Fakat, bu yöntem düzgün sınırlara sahip problemler ile sınırlıdır.

Bu tezin amacı, mevcut Mutlak Nodal Koordinat Formülasyonu'nun düzensiz sınırlara sahip problemlerde de kullanılabilecek şekilde geliştirilmesidir. Bu amaçla, ilk önce çoklu bünye dinamiği analizlerinde kullanılmak üzere Ağsız Mutlak Nodal Koordinat Formülasyonu geliştirilmiştir. Geliştirilen ağsız yöntemin doğrulaması kiriş tipi yapılar kullanılarak gerçekleştirilmiş ve uygun sonuçlar elde edilmiştir. Daha sonra, düzensiz sınırlara sahip problemlerin çözümü için "Mutlak Nodal Koordinat Formülasyonu için Sanal Eleman Eşleştirme" Yöntemi geliştirilmiştir. Önerilen yöntem, düzlemsel gerilme, düzlemsel gerinim, plaka/kabuk ve 3 boyutlu sonlu elemanlara uyarlanmıştır. Yöntemin doğrulaması literatürde yer alan ağ doğrulama problemleri ile gerçekleştirilmiştir. Bunun yanında, yüksek

yer değiştirme içeren esnek bünye sistemlerinin analizleri ile de doğrulama yapılmıştır. Ek olarak, ince plaka yaklaşımı için gerekli olan şekil fonksiyonları türetilmiştir.

Bu tezde geliştirilen ve önerilen yöntemlerin, çoklu bünye dinamiği benzetimlerinin dışında yüksek dönü ve/veya deformasyon gerektiren yapısal mekanik problemlerinde de yararlı olacağı gözlenmiştir. Önerilen yöntemler sonlu elemanların şekil sınırlamasını genişlettiğinden dolayı, literatürdeki diğer yöntemlere göre daha verimlidir.

Anahtar Kelimeler: sanal eleman eşleştirme metodu, mutlak nodal koordinat, esnek bünye dinamiği, ağsız yöntemler, plakalar, kabuklar

To my family ...

ACKNOWLEDGMENTS

TABLE OF CONTENTS

LIST OF TABLES

LIST OF FIGURES

FIGURES

xix

CHAPTER 1

INTRODUCTION

Simulation of mechanical systems is an inevitable step of a design process. If the design is limited to mechanics, problems to be solved involve statics or dynamics of the systems. The problems can be solved separately depending on the physical conditions. If the mechanical system consists of bulky parts then it can be assumed that deformation of bulky parts will not influence the dynamics of the system. Therefore, the dynamics and strength of the system can be simulated separately within a certain accuracy. This approach is quite effective for bulky systems due to its solution speed and easy formulation. However, it is not applicable for every mechanical system. If the system has parts that have non-negligible flexibility or the accuracy is the main concern, then the approach will not satisfy the simulation requirements. The study branch that satisfies the requirements is "flexible multibody dynamics".

Flexible multibody dynamics studies started in the early seventies for better simulation of many industrial and technological systems like vehicles, mechanisms, robotics, and space structures [1]. In the past, the systems were designed bulky. Therefore, the dynamics of the systems can be solved easily by using the rigid link assumption. When the deflections of links due to dynamic loadings are not negligible, the rigid link assumption will diverge from the solution. Nowadays, the systems are getting lighter in order to have a weight effective design. Consequently, the importance of flexible multibody dynamics is increasing.

Multibody systems have nonlinear equations of motion due to the large relative displacements and rotations. Therefore, the system equations require certain solution procedures in order to obtain accurate results. Linearization methods are generally applied in order to overcome nonlinearity in statical problems. However, linearization of dynamics equations can be the major source of error when multibody system applications are considered. As a result,

equations of motion for flexible multibody systems are highly nonlinear and require computer implementation based on a non-incremental procedure [2]. In order to show nonlinearity due to dynamics, some publications [2, 3] refers to the simple pendulum example. The example is also shown in Figure 1.1.
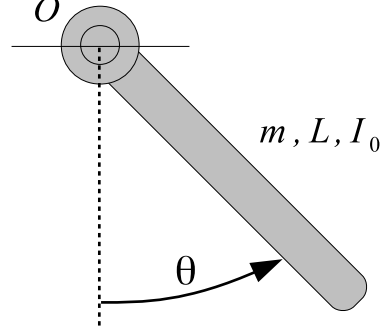
Figure 1.1: Simple pendulum example

The nonlinear equation of motion for a simple rigid pendulum is given below.

$$I_0\ddot{\theta} + mg\frac{L}{2}\sin\theta = 0 \tag{1.1}$$

where I_0, θ, m, g and L are the mass moment of inertia about point O, angle of rotation, mass, gravity and length, respectively. The constant energy integral of motion can be obtained by integration of equation of motion as given in the following equations.

$$I_0\dot{\theta}\frac{d\dot{\theta}}{d\theta} + mg\frac{L}{2}\sin\theta = 0 \tag{1.2a}$$

$$I_0\dot{\theta}d\dot{\theta} + mg\frac{L}{2}\sin\theta d\theta = 0 \tag{1.2b}$$

$$\frac{1}{2}I_0\dot{\theta}^2 - mg\frac{L}{2}\cos\theta = c_1 \tag{1.2c}$$

If the nonlinear equation of motion is linearized with the assumption of small angular

displacement, the equation of motion takes form given below.

$$I_0\ddot{\theta} + mg\frac{L}{2}\theta = 0 \tag{1.3}$$

By substituting $\dot{\theta}(d\dot{\theta}/d\theta)$ for $\ddot{\theta}$ and integrating the equation of motion, one can get following equation for the constant energy integral of motion for small displacement assumption.

$$\frac{1}{2}I_0\dot{\theta}^2 - mg\frac{L}{4}\theta^2 = c_2 \tag{1.4}$$

Equation 1.4 is an approximation for the principle of work and energy if the rotation is small. As a result, any solution that satisfies Equation 1.3 should satisfy Equation 1.4 however it can lead to energy drift as θ increases since the solution is not required to satisfy Equation 1.2 [2, 3]. This problem can arise especially in the incremental approaches.

1.1 Methods used in Flexible Multibody Dynamics

In order to obtain accurate solutions for mechanical systems with flexible parts, some approaches were developed. In 1997, A. A. Shabana reviewed the previous studies and developments [1]. He reported various methods for multibody system formulations in his study [1]. However, most of the methods can be considered as derivatives of other ones. Basically, the methods can be classified with four main formulations, which are the floating frame of reference (FFR) formulation, incremental finite element formulation, large rotation vector formulation and absolute nodal coordinate frame formulation (ANCF) [4–6]. The main difference of the formulations is the nodal coordinate definition for finite elements. The performance and efficiency of a multibody simulation code are mainly dependent on the selected coordinates used for the formulation of the dynamic equations [7]. Short details, advantages and disadvantages of the formulations are described within the following sections.

1.1.1 Floating Frame of Reference Formulation

In this formulation, two coordinate sets (global and floating coordinate frames) are applied [8, 9]. Global coordinate set is used to define the locations and orientations of bodies. However, floating frames are used to describe the deformations of flexible bodies. The deformations with respect to the floating frame of a body is described using nodal variables used in classical

finite element methods. The motion of the floating frames approximates the rigid body motion of the body. Coordinate definitions for the FFR formulation are shown in Figure 1.2.

FFR formulation is specifically efficient for small deformation and large rotation problems. The formulation does not induce deformations under pure rigid body motion. This can be showed by writing the global position vector of an arbitrary point on the deformable body shown in Figure 1.3.
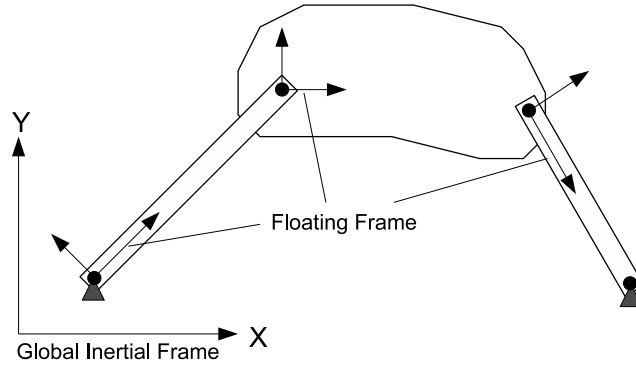
Figure 1.2: Coordinate frames for FFR formulation [10]
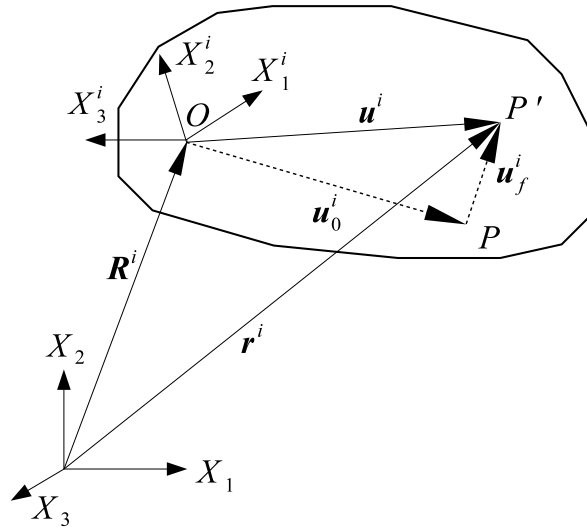
Figure 1.3: Position definition in FFR formulation [8]

4

The global position vector of an arbitrary point P' on body i can be written as given below [8].

$$\mathbf{r}^i = \mathbf{R}^i + \mathbf{A}^i \left(\bar{\mathbf{u}}_0^i + \bar{\mathbf{u}}_f^i \right) \tag{1.5}$$

where $\mathbf{R}^i$ is the global position of the body fixed floating frame of body i, $\mathbf{A}^i$ is the transformation matrix, $\bar{\mathbf{u}}_0^i$ is the undeformed position with respect to the floating frame and $\bar{\mathbf{u}}_f^i$ is the deformation relative to the floating body frame.

As can be seen from the global position vector formulation, when there is no deformation exact rigid body dynamics can be obtained as follows.

$$\mathbf{r}^i = \mathbf{R}^i + \mathbf{A}^i \bar{\mathbf{u}}_0^i \tag{1.6}$$

Dynamic equations of motion of the deformable bodies can be obtained by solving the principle of virtual work or Lagrange's equations. In the FFR formulation, the equations of motion are expressed in terms of a coupled set of reference and elastic coordinates. The elastic coordinates can be introduced using the assumed modes method, the finite element method or experimental identification [1, 8, 11]. In assumed mode method, flexible bodies are usually represented by truncated finite modal series and time-varying mode amplitudes [11]. Additionally, assumed mode method can be used in the finite element method to reduce the dimension of the system matrices.

In addition, there are some studies on the determination of the body coordinate locations (floating frames) as reported in the review of Shabana [1]. It has been shown that there is an optimum location for the floating frame and it requires an additional effort in the simulations.

1.1.2 Incremental Finite Element Formulations

The incremental finite element formulation has a wide range of use in many engineering applications. The method is available for use in many commercial simulation software. Most of the engineering problems can be simulated with this formulation. In order to handle large deformation and rotation problems, lots of finite element procedures are available in the literature. In most of them, large deformations and rotations of finite elements

are described by using nodal coordinates or displacements for continuum elements, and additionally infinitesimal nodal rotations for structural elements like beam, plate and shell elements. Performance of these finite elements mainly depends on parametric description of element geometry in flexible multibody problems. Finite elements can basically be classified as isoparametric or non-isoparametric according to their parametric descriptions. An isoparametric element is defined as an element which has a shape function that can be used to interpolate both location and deformation [12]. Therefore, isoparametric elements can describe exact rigid body dynamics. However, non-isoparametric element types (beams, plates and shells) can not represented the rigid body dynamics, exactly [7, 13]. Additionally, these formulations produce non-zero strain under rigid body displacements or rotations.

For a multibody system modeled by isoparametric finite elements, the procedure is simple. The system equations are formulated with respect to a global coordinate system. Then, the system equations can be solved by explicit direct integration methods over a required duration. If the same procedure is performed for a multibody system modeled with nonisoparametric elements (beams, plates and shells), the obtained results might be erroneous depending on the size of rotations.

In incremental finite element formulations, system equations are linearized and solved with small rotational increments in order to force non-isoparametric elements to behave like isoparametric elements within small rotation increments. Therefore, the major source of error is the incremental rotation approach. In the study of Shin [10], a simple frame of non-isoparametric beam elements is solved for rigid body rotations without using incremental rotation approach as shown in Figure 1.4. As seen in the figure, pure rigid body rotation of the frame causes large deformations in beams for high rotation values. Therefore, incremental rotation approach is used in order to reduce errors due to unreal deformations shown in Figure 1.4. However, the use of the infinitesimal rotations as nodal coordinates leads to a linearization of the kinematic equations of the elements [1, 8]. Consequently, the linearization leads to the loss of the accuracy especially in pure rigid body rotations.
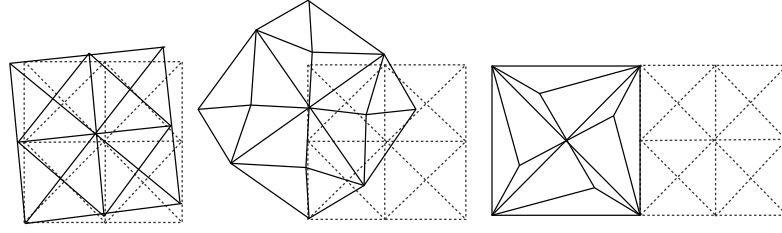
Figure 1.4: Beam elements under clockwise rigid body rotations of 5.73°, 45° and 90° [10]

1.1.3 Large Rotation Vector Formulation

Large Rotation Vector Formulation has been developed in order to circumvent the linearization problem in incremental finite element formulations [14]. In the formulation, finite rotations are used as nodal variables instead of infinitesimal rotations. Therefore, exact rigid body dynamics could be obtained, theoretically. However, the method has an inconsistency problem in the finite rotation degrees of freedom of elements [1]. If a planar beam is considered, the finite rotation consists of the orientation angle, which defines the orientation of the cross-section without shear, and shear deformation. The inconsistency problem is to distinguish the orientation and shear angles. Solving this inconsistency problem in the large rotation vector formulation is not an easy problem but it is possible. It requires to solve highly nonlinear equations in the finite element kinematic description [8]. Additionally, the formulation leads to excessive shear forces due to the finite rotation description of the element cross section [1, 8].

In the formulation, the element configuration is defined with absolute coordinates and finite rotations of the nodes. As a result, a simpler mass matrix and a more complex stiffness matrix can be obtained compared to the incremental finite element formulations [7].

1.1.4 Absolute Nodal Coordinate Formulation

In this formulation, global coordinates and their gradients with respect to the body frame are used as a new set of coordinates [1, 4, 7]. The coordinate formulation makes beam, plate and shell elements behave like isoparametric. Therefore, rigid body dynamics of beams and plates

7

can exactly be modeled by proper element shape functions and element nodal coordinates [7]. Consequently, beam, plate and shell elements show zero strain under rigid body motion. Additionally, ANCF leads to constant mass matrix that simplifies the formulations.

There are lots of studies on beam elements with absolute nodal coordinate formulation in the literature [16–29]. In most of the studies, nonlinear elastic isotropic material assumption is used in formulations. However, few of them consider plasticity with isotropic material assumption in the absolute nodal coordinate frame formulation [27]. The numbers of publications on plates and shells are less than publications on beams. Major studies on plate and shell elements with ANC formulation are [3, 4, 30–33]. Shabana and Mikkola [30] developed a 4-noded generalized plate element, which uses ANCF, and made a simple comparison with the incremental approaches. They studied on a plate having a spherical joint at one corner and subjected to gravitational loading. They used very small elastic modulus in order to observe both rigid body rotations and large elastic deformations. As can be seen from Figure 1.5, incremental methods can not reach the result of an ANCF having 4 elements even for the usage of 100 elements. Additionally, they showed that very complex displacements can be handled with small number of elements.

Some researches were completed to improve the accuracy of the ANCF approach. In [16], a new approach called Hybrid Coordinate Formulation had been studied experimentally and theoretically. The hybrid formulation is based on the modal coordinates for small deformations and absolute nodal coordinates for large deformation. The experimental setup and the obtained results are shown in Figure 1.6. As shown in the figure, a flexible beam with a point mass at the tip is vibrated and displacements of the mass are recorded by high speed camera. The result of hybrid coordinate formulation is almost the same with the experimental outputs.

In order to overcome the difficulties in stiffness matrix formulation, construction and evaluation, some researches were completed. D. G. Vallejo, J. Mayo, J. L. Escalano and J. Dominguez developed a new algorithm to simplify the volume integration during stiffness matrix calculation in ANCF [17]. The developed algorithm is valid for isotropic and elastic materials and very effective for shear deformable beams and plates.
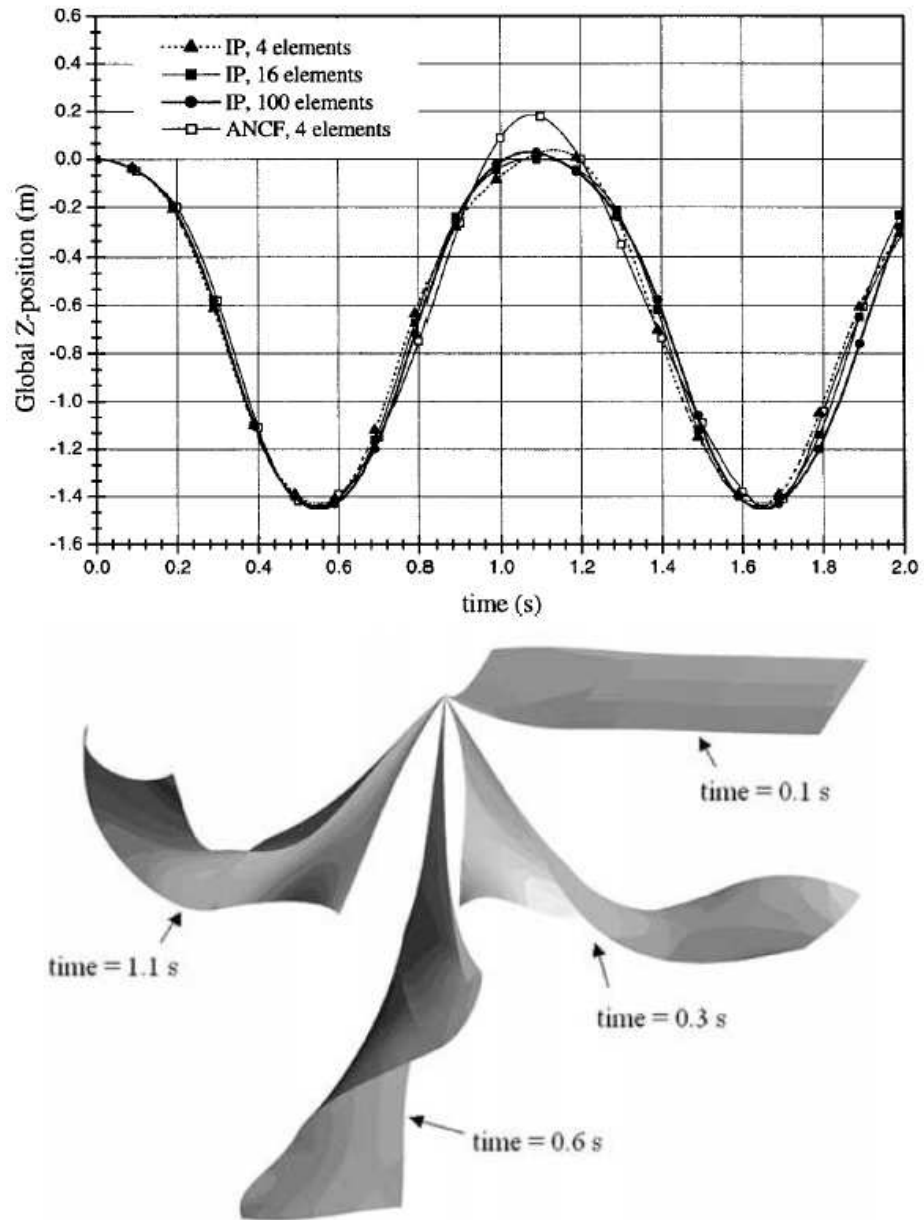
Figure 1.5: Comparison of ANCF with incremental methods (E=20 MPa) [30]
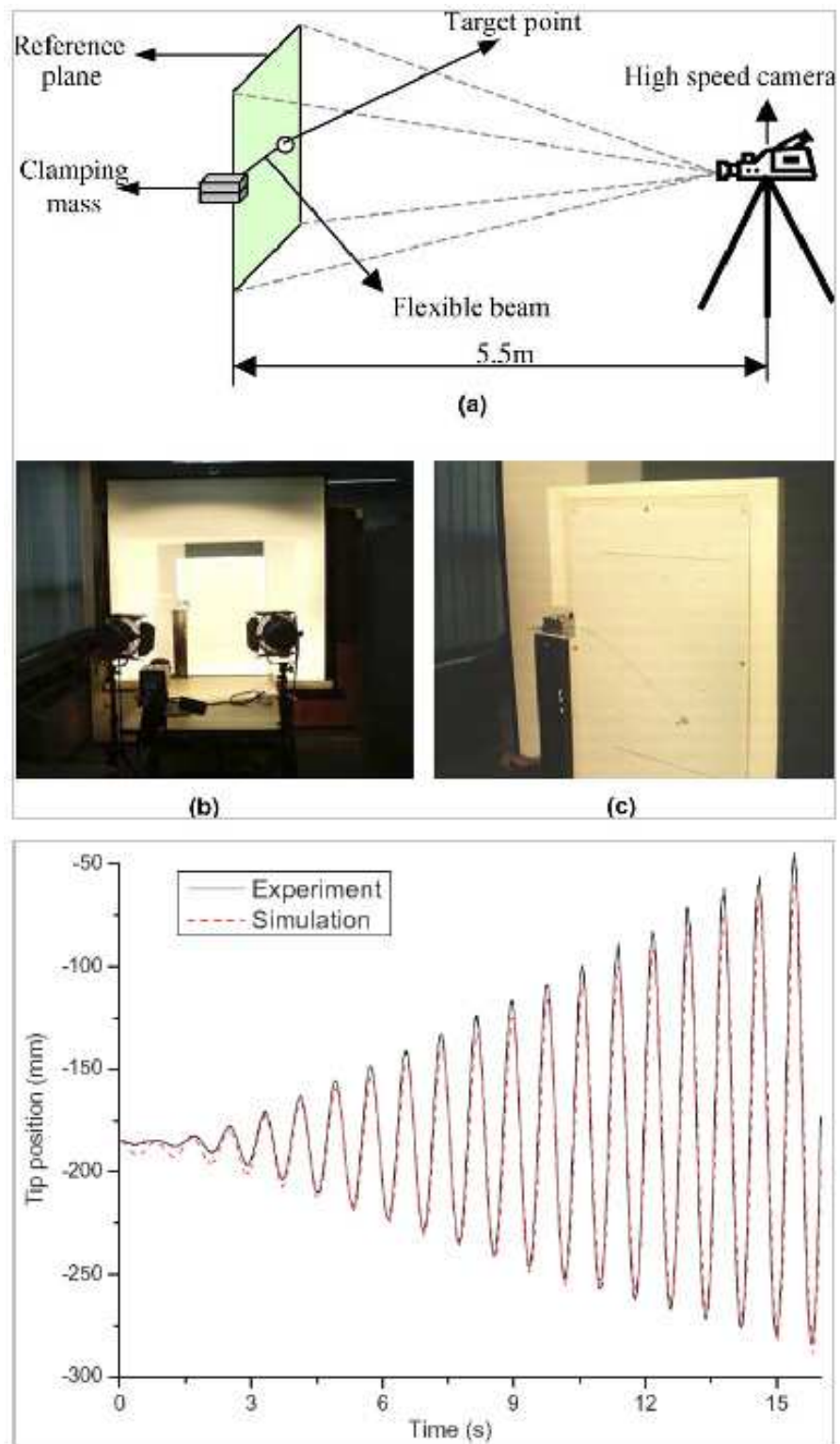
Figure 1.6: Large displacement testing of a beam [15, 16]

A comparison chart for the available methods is shown in Table 1.1. As seen from the comparison chart, each method has some drawbacks. For example, nonlinear elasticity can not be included in FFRF. In IFEF and LRVF, rigid body representation could be erroneous. However, the only disadvantage of ANCF compared to the other methods is highly nonlinear stiffness matrix which can be handled with available solution procedures in the literature.

Table 1.1: Comparison chart for flexible multibody dynamics methods

	FFRF	**IFEF**	**LRVF**	**ANCF**
Application	small def. large rot. large disp.	large def. large rot. large disp.	large def. large rot. large disp.	large def. large rot. large disp.
Increments	-	small rotations	-	-
Mass matrix	nonlinear	nonlinear	nonlinear	constant
Stiffness matrix	linear	nonlinear	nonlinear	nonlinear
Rigid body representation	exact	approximate (may be erroneous)	exact (erroneous for large rot.)	exact

1.2 Research Objectives

Currently, all of the developed ANCF's for quadrilateral plate and shell finite elements are based on regular discretization of flexible bodies. However, flexible bodies may have various shapes, which cannot be modelled by using regular element shapes, in actual engineering problems. Therefore, application region of ANCF is limited to analysis of simple flexible multibody systems, despite high deformation capabilities of the method. Additionally, there is no exact implementation of ANCF to 3D solid elements in literature. Therefore, some additional effort has to be spent on joints between plate or shell elements and 3D solid elements due to inconsistent nodal variables. Currently, there is no 3D solid finite element, which has gradient based absolute nodal variables.

In summary, improvement on the current ANCF is required in order to increase the applications of the method and to make use of it for a wide range of flexible multibody applications.

1.3   Scope of the Thesis

In order to eliminate the current limitations of ANCF and make it applicable to various problems, meshfree methods are introduced to ANCF, firstly. Then, finite element based "Virtual Element Mapping Method" is introduced. The method can also be varied according to the nodal gradient definitions introduced as "Virtual Frame", "Edge Frame" and "Initial Element Frame" methods. By implementing one of the introduced methods, various finite element shapes can be used in flexible multibody problems.

The other objective is to extend ANCF to 3D solid elements in order to generate compatible solid elements with the current plate and shell finite elements based on ANCF. This objective can also be reached by using the introduced "Virtual Element Mapping Methods".

1.4   Outline of the Thesis

The thesis mainly focused on the accurate solution methods for flexible multibody problems under large deformations. Therefore, the main formulation and recent advances related to the ANCF have been summarized in Chapter 2. In the chapter, planar non-shear deformable beam element proposed by Escalano J. L., Hussien H. A. and Shabana A. A. [34], planar shear deformable beam element proposed by Omar M. A. and Shabana A. A. [21] and the generalized plate element proposed by Mikkola A. M., Shabana A. A. [30] are reviewed in detail.

The remaining chapters include new implementations of absolute nodal coordinate formulation. In Chapter 3, meshfree implementation of ANCF for flexible planar beam structures has been presented. Besides the formulations, sample problems and comparisons with ANCF with FEM are given. In Chapter 4, a new finite element formulation based on ANCF has been proposed. Absolute nodal coordinate formulation with virtual element mapping has been developed for plane stress and strain problems. Element shape restriction for quadrilateral elements in ANCF has been eliminated with the proposed formulation. In the chapter, some of the patch tests proposed by Richard H. Macneal and Robert L. Haeder [35] are solved for quasi-static and transient dynamic cases. In Chapter 5, ANCF with virtual element mapping has been implemented to generalized plate finite elements. Additionally,

general guideline for thin plate and shell formulation has been introduced in the chapter. In the next chapter, the proposed method has been extended to 8 noded hexahedral continuum elements. The proposed element in the chapter can be used for a wide range of geometries. Despite being a continuum element, it has all of the flexibilities and advantages of ANCF.

General summary, discussion and conclusion about the proposed methods and finite elements are given in Chapter 7. Additionally, comments on the further improvements and future studies are presented in this last chapter.

CHAPTER 2

REVIEW OF ABSOLUTE NODAL COORDINATE FORMULATIONS

Absolute Nodal Coordinate Formulation (ANCF) has been introduced by Ahmed Shabana in order to improve dynamic representation of beam plate and shell elements. In a review publication by Shabana [1], this drawback of classical finite element methods has been explained as "beam, plate and shell elements are not considered in the classical finite element literature as isoparametric elements because these elements cannot be used to obtain exact modeling of the rigid body dynamics". As compared in Table 1.1, it is the most accurate method within the available formulations related to the flexible multibody dynamics. Besides, mass matrix in the resulting system equations is always constant.

Since, ANCF is used in the thesis, some basic information and recent improvements will be explained in this review chapter.

2.1   Derivation of Equations of Motion

Equations of motion for ANCF can be derived by using Lagrange Equation of an arbitrary flexible body given below.

$$\frac{d}{dt}\left(\frac{\partial T}{\partial \dot{\mathbf{e}}}\right)^T - \left(\frac{\partial T}{\partial \mathbf{e}}\right)^T + \mathbf{C_e}^T \lambda = \mathbf{Q} \tag{2.1}$$

where T is the kinetic energy, $\mathbf{e}$ is the vector of nodal variables, $\mathbf{C_e}$ is the Jacobian matrix of constraint equations, λ is the vector of Lagrange multipliers and $\mathbf{Q}$ is the total generalized force vector including external and elastic forces.

14

If the general definition of kinetic energy ($\dot{\mathbf{e}}^T \mathbf{M} \dot{\mathbf{e}}/2$) is substituted into the Lagrange equation, following equation can be found.

$$\mathbf{M}\ddot{\mathbf{e}} + \mathbf{C_e}^T \lambda = \mathbf{Q} - \mathbf{Q_v} \tag{2.2}$$

where quadratic velocity vector, $\mathbf{Q_v}$, is defined as given below.

$$\mathbf{Q_v} = \dot{\mathbf{M}}\dot{\mathbf{e}} - \left(\frac{\partial}{\partial \mathbf{e}} \left(\frac{1}{2} \dot{\mathbf{e}}^T \mathbf{M} \dot{\mathbf{e}} \right) \right)^T \tag{2.3}$$

It can be said that $\mathbf{Q_v}$ will be zero for ANCF due to constant mass matrix. However, it should also be considered in floating frame of reference formulations in order to take Coriolis effect into account. Then, equations of motion can be simplified for ANCF as follows.

$$\mathbf{M}\ddot{\mathbf{e}} + \mathbf{C_e}^T \lambda = \mathbf{Q} \tag{2.4}$$

However, it can not be solved without including the constraint equations, because number of equations is less than the number of unknowns. Constraint equations ($\mathbf{C}(\mathbf{e}, t) = \mathbf{0}$) can be included in equations of motion by differentiating these equations with respect to time twice. If the constraint equations are differentiated with respect to time once, the following equation can be obtained.

$$\frac{d\mathbf{C}}{dt} = \mathbf{C_e}\dot{\mathbf{e}} + \frac{\partial \mathbf{C}}{\partial t} = \mathbf{0} \tag{2.5}$$

After, second differentiation with respect to time, the constraint equations take the following form.

$$\mathbf{0} = \frac{\partial}{\partial \mathbf{e}} \left(\mathbf{C_e}\dot{\mathbf{e}} \right) \dot{\mathbf{e}} + 2 \frac{\partial \mathbf{C_e}}{\partial t} \dot{\mathbf{e}} + \mathbf{C_e}\ddot{\mathbf{e}} + \frac{\partial^2 \mathbf{C}}{\partial t^2} \tag{2.6}$$

Then, equations of motion can be written by using Equations 2.4 and 2.6 as given below.

$$\begin{bmatrix} \mathbf{M} & \mathbf{C_e}^T \\ \mathbf{C_e} & \mathbf{0} \end{bmatrix} \begin{bmatrix} \ddot{\mathbf{e}} \\ \lambda \end{bmatrix} = \begin{bmatrix} \mathbf{Q} \\ \mathbf{Q_d} \end{bmatrix} \tag{2.7}$$

15

where

$$\mathbf{Q_d} = -\frac{\partial}{\partial \mathbf{e}}(\mathbf{C_e \dot{e}})\,\dot{\mathbf{e}} - 2\frac{\partial \mathbf{C_e}}{\partial t}\,\dot{\mathbf{e}} - \frac{\partial^2 \mathbf{C}}{\partial t^2} = \mathbf{C_e \ddot{e}} \tag{2.8}$$

It can easily be said that the force vector, $\mathbf{Q_d}$, will be zero for simple time independent constraint types like fixed boundary constraints or revolute joints. Generalized force vector, $\mathbf{Q}$, can be found by utilizing virtual work principle for the used nodal variables, $\mathbf{e}$.

2.2   Nodal Variables

The main difference of ANCF is the definition of nodal variables. In the formulation, global coordinates and gradients of global position vector are used as nodal variables. A basic nodal variable representation is given below [8].

$$\mathbf{e}_i = \left[\mathbf{r}_i^T \ \ \frac{\partial \mathbf{r}_i^T}{\partial x} \ \ \frac{\partial \mathbf{r}_i^T}{\partial y} \ \ \frac{\partial \mathbf{r}_i^T}{\partial z}\right]^T \tag{2.9}$$

In the equation, $\mathbf{e}_i$ refers to the nodal variables of the ith node, $\mathbf{r}_i$ refers to the global position vector of the ith node and x, y and z are local coordinates.

2.3   Non-Shear Deformable Planar Beam Element ANCF

Non-shear deformable planar beam element (Figure 2.1) has been proposed by Escalano J.L., Hussien H.A. and Shabana A. A. [34]. They also made some numerical comparisons for flexible multibody dynamics systems in their publication.

The nodal variables defined in Equation 2.9 can be simplified for the nodes of a non-shear deformable planar beam element as given below [34].

$$\mathbf{e}_i = \left[X_i \ Y_i \ \ \frac{\partial X_i}{\partial x} \ \ \frac{\partial Y_i}{\partial x}\right]^T \tag{2.10}$$

16
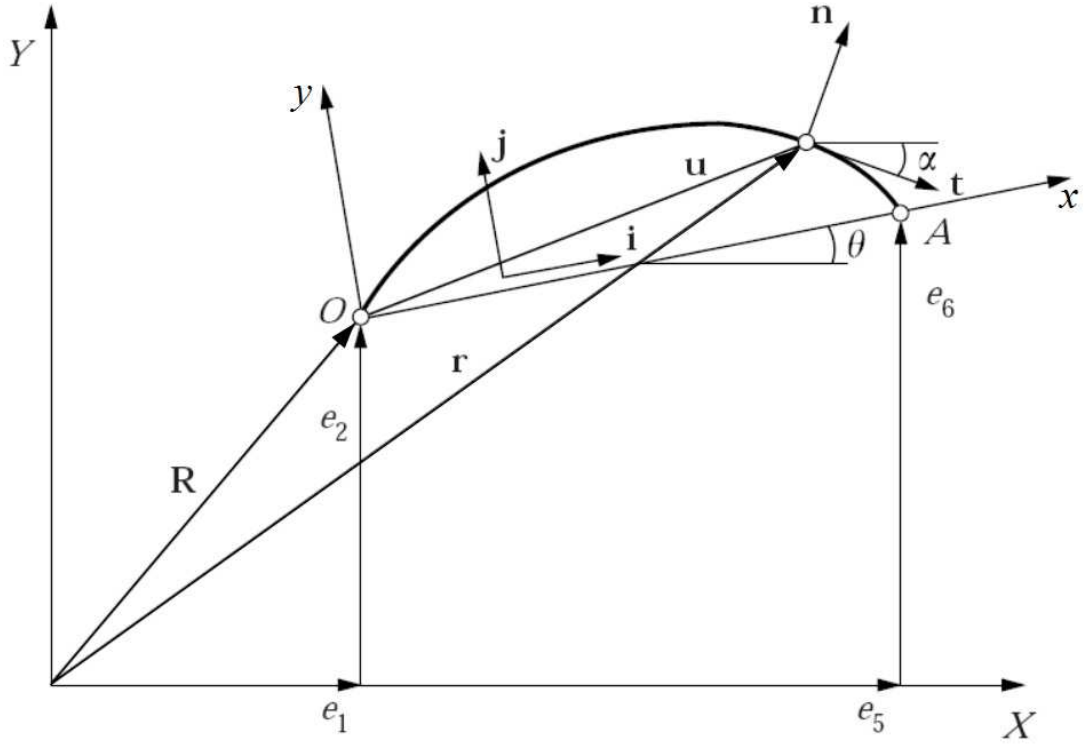
Figure 2.1: Non-shear deformable planar beam element [34]

Then, the vector of nodal variables for an element having the length of L can be written as given in the following equation.

$$\mathbf{e} = \left[(X)_{x=0} \ (Y)_{x=0} \ \left(\frac{\partial X}{\partial x}\right)_{x=0} \ \left(\frac{\partial Y}{\partial x}\right)_{x=0} \ (X)_{x=L} \ (Y)_{x=L} \ \left(\frac{\partial X}{\partial x}\right)_{x=L} \ \left(\frac{\partial Y}{\partial x}\right)_{x=L} \right]^T \qquad (2.11)$$

Then, the global position of an arbitrary point on the element can be approximated by using appropriate shape function polynomials as given below.

$$\mathbf{r} = \begin{bmatrix} X \\ Y \end{bmatrix} = \mathbf{Se} \qquad (2.12)$$

In the equation, $\mathbf{S}$ is the shape function matrix proposed by J.L. Escalano, H.A. Hussien and A. Shabana [34].

17

$$
\mathbf{S} = \begin{bmatrix}
1 - 3\xi^2 + 2\xi^3 & 0 \\
0 & 1 - 3\xi^2 + 2\xi^3 \\
L\left(\xi - 2\xi^2 + \xi^3\right) & 0 \\
0 & L\left(\xi - 2\xi^2 + \xi^3\right) \\
3\xi^2 - 2\xi^3 & 0 \\
0 & 3\xi^2 - 2\xi^3 \\
L\left(\xi^3 - \xi^2\right) & 0 \\
0 & L\left(\xi^3 - \xi^2\right)
\end{bmatrix}^T
\tag{2.13}
$$

where ξ is the reduced local coordinate varying from 0 to 1 and defined as x/L.

2.3.1 Mass Matrix for Non-Shear Deformable Planar Beam Element

Mass matrix of the beam element can be determined from the kinetic energy equation given below.

$$
T = \frac{1}{2} \int_V \rho \, \dot{\mathbf{r}}^T \dot{\mathbf{r}} \, dV
\tag{2.14}
$$

By substituting Equation 2.12 into Equation 2.14, one can obtain the following equation.

$$
T = \frac{1}{2} \int_V \rho \, \dot{\mathbf{e}}^T \mathbf{S}^T \mathbf{S} \dot{\mathbf{e}} \, dV
\tag{2.15}
$$

or it can be written in more compact form as given below.

$$
T = \frac{1}{2} \dot{\mathbf{e}}^T \mathbf{M}_a \dot{\mathbf{e}}
\tag{2.16}
$$

where $\mathbf{M}_a$ is the mass matrix of the beam element and can be formulated using Equations 2.15 and 2.16 as given below.

$$
\mathbf{M}_a = \int_V \rho \, \mathbf{S}^T \mathbf{S} \, dV
\tag{2.17}
$$

If the cross sectional area and the density of the beam element are constant over the length then the mass matrix formulation can be simplified as follows.

18

$$\mathbf{M}_a = m \int\limits_0^1 \mathbf{S}^T \mathbf{S} d\xi \tag{2.18}$$

where m refers to mass per unit length of the element. By introducing shape function matrix, $\mathbf{S}$, given in Equation 2.13, constant mass matrix of the beam element satisfying the kinetic energy equation can be found as given below.

$$\mathbf{M}_a = m \begin{bmatrix} \frac{13}{35} & 0 & \frac{11L}{210} & 0 & \frac{9}{70} & 0 & -\frac{13L}{420} & 0 \\ & \frac{13}{35} & 0 & \frac{11L}{210} & 0 & \frac{9}{70} & 0 & -\frac{13L}{420} \\ & & \frac{L^2}{105} & 0 & \frac{13L}{420} & 0 & -\frac{L^2}{140} & 0 \\ & & & \frac{L^2}{105} & 0 & \frac{13L}{420} & 0 & -\frac{L^2}{140} \\ & & & & \frac{13}{35} & 0 & -\frac{11L}{210} & 0 \\ & & & & & \frac{13}{35} & 0 & -\frac{11L}{210} \\ & & & & & & \frac{L^2}{105} & 0 \\ & & & & & & & \frac{L^2}{105} \end{bmatrix} \tag{2.19}$$

As it is seen from the equation, mass matrix does not depend on global variables or time. It is constant at any positions on the global frame and at any time.

2.3.2 Generalized Elastic Forces for Non-Shear Deformable Planar Beam Element

Generalized elastic force vector for a beam element can be derived by using the strain energy definition. Strain energy for a two dimensional Euler-Bernoulli beam is given below [34].

$$U = \frac{1}{2} \int\limits_0^L \left(Ea \left(\frac{\partial u_l}{\partial x} \right)^2 + EI \left(\frac{\partial^2 u_t}{\partial x^2} \right)^2 \right) dx \tag{2.20}$$

where L, a, I, u_l and u_t refer to length, area, inertia, longitudinal deformation and transverse deformation, respectively. The first term within the integration represents the portion of strain energy due to longitudinal deformation and the second term due to transverse deformation.

In order to find the deformations (u_l and u_t) in terms of nodal variables, $\mathbf{e}$, position of an arbitrary point should be written in the local frame. For this purpose, local position vector, $\mathbf{u}$, at an arbitrary time is written in the global coordinate frame (point O in Figure 2.1), firstly.

19

Then, it will be transformed to the local coordinate by means of local unit vectors defined in global coordinate frame.

Relative position vector of an arbitrary point at an arbitrary time on the element, $\mathbf{u}$, can be written as follows.

$$\mathbf{u} = \begin{bmatrix} u_X \\ u_Y \end{bmatrix} = \begin{bmatrix} (\mathbf{S}_1 - \mathbf{S}_{1O}) \, \mathbf{e} \\ (\mathbf{S}_2 - \mathbf{S}_{2O}) \, \mathbf{e} \end{bmatrix} \tag{2.21}$$

In the equation, $\mathbf{S}_1$ and $\mathbf{S}_2$ refer to the first and second rows of shape function matrix at an arbitrary point, and $\mathbf{S}_{1O}$ and $\mathbf{S}_{2O}$ refer to the first and second rows of shape function matrix at point O in Figure 2.1. Then, $\mathbf{u}$ can be written in local (element) coordinate frame by using unit base vectors, which are shown as $\mathbf{i}$ and $\mathbf{j}$ in Figure 2.1, as given below.

$$\mathbf{u}_{local} = \begin{bmatrix} \mathbf{u}^T \mathbf{i} \\ \mathbf{u}^T \mathbf{j} \end{bmatrix} = \begin{bmatrix} u_X i_X + u_Y i_Y \\ u_X i_Y + u_Y i_X \end{bmatrix} \tag{2.22}$$

Unit base vectors and their components in global frame can be determined by using the locations of end points of the elements as given below.

$$\mathbf{i} = \begin{bmatrix} i_X \\ i_Y \end{bmatrix} = \frac{\mathbf{r}_A - \mathbf{r}_O}{|\mathbf{r}_A - \mathbf{r}_O|} = \frac{\mathbf{S}_A \mathbf{e} - \mathbf{S}_O \mathbf{e}}{|\mathbf{S}_A \mathbf{e} - \mathbf{S}_O \mathbf{e}|} = \begin{bmatrix} \dfrac{e_5 - e_1}{\sqrt{(e_5 - e_1)^2 + (e_6 - e_2)^2}} \\ \dfrac{e_6 - e_2}{\sqrt{(e_5 - e_1)^2 + (e_6 - e_2)^2}} \end{bmatrix} \tag{2.23}$$

where $\mathbf{S}_A$ and $\mathbf{S}_O$ are the shape function matrices evaluated at points A and O, respectively. Then, longitudinal and transverse deformations can be found by substracting initial local position, $[x \ \ 0]^T$, from the deformed local position, $\mathbf{u}_{local}$, as given in the following equation.

$$\begin{bmatrix} u_l \\ u_t \end{bmatrix} = \mathbf{u}_{local} - \begin{bmatrix} x \\ 0 \end{bmatrix} = \begin{bmatrix} u_X i_X + u_Y i_Y - x \\ u_X i_Y + u_Y i_X \end{bmatrix} \tag{2.24}$$

By substituting longitudinal and transverse deformations found in Equation 2.24 into Equation 2.20, one can obtain strain energy definition in terms of nodal variables as given below.

20

$$U = \frac{1}{2} \int_0^L \left(Ea \left(\frac{\partial u_X i_X + u_Y i_Y - x}{\partial x} \right)^2 + EI \left(\frac{\partial^2 u_X i_Y + u_Y i_X}{\partial x^2} \right)^2 \right) dx \qquad (2.25)$$

Then, the generalized elastic force vector can be determined by partial differentiation as given below [34].

$$\mathbf{Q}_k = \frac{\partial U}{\partial \mathbf{e}} \qquad (2.26)$$

Generalized elastic force vector for the beam element can be written explicitly in terms of nodal variables by substituting Equations 2.21, 2.23 and 2.25 into Equation 2.26, as given in the following equation.

$$\mathbf{Q}_k = (\mathbf{A}_{11} + \mathbf{B}_{22}) \, \mathbf{e} i_X^2 + (\mathbf{A}_{22} + \mathbf{B}_{11}) \, \mathbf{e} i_Y^2 + (\mathbf{A}_{12} + \mathbf{A}_{21} - \mathbf{B}_{12} - \mathbf{B}_{21}) \, \mathbf{e} i_X i_Y - \mathbf{A}_1 i_X - \mathbf{A}_2 i_Y$$
$$+ \mathbf{e}^T (\mathbf{A}_{11} + \mathbf{B}_{22}) \, \mathbf{e} i_{X,\mathbf{e}} i_X + \frac{1}{2} \mathbf{e}^T (\mathbf{A}_{12} + \mathbf{A}_{21} - \mathbf{B}_{12} - \mathbf{B}_{21}) \, \mathbf{e} i_{X,\mathbf{e}} i_Y - \mathbf{A}_1^T \mathbf{e} i_{X,\mathbf{e}} \quad (2.27)$$
$$+ \mathbf{e}^T (\mathbf{A}_{22} + \mathbf{B}_{11}) \, \mathbf{e} i_{Y,\mathbf{e}} i_Y + \frac{1}{2} \mathbf{e}^T (\mathbf{A}_{12} + \mathbf{A}_{21} - \mathbf{B}_{12} - \mathbf{B}_{21}) \, \mathbf{e} i_{Y,\mathbf{e}} i_X - \mathbf{A}_2^T \mathbf{e} i_{Y,\mathbf{e}}$$

where $\mathbf{A}_{11}$, $\mathbf{A}_{12}$, $\mathbf{A}_{21}$, $\mathbf{A}_{22}$, $\mathbf{B}_{11}$, $\mathbf{B}_{12}$, $\mathbf{B}_{21}$, $\mathbf{B}_{22}$, $\mathbf{A}_1$ and $\mathbf{A}_2$ are integration constants defined by Escalano J. L., Hussien H. A. and Shabana A. A. [34]. Integration constants are given explicitly in the following equations.

$$\mathbf{A}_{ij} = \frac{Ea}{L} \int_0^1 \mathbf{S}_{i,\xi}^T \, \mathbf{S}_{j,\xi} \, d\xi \qquad (2.28)$$

$$\mathbf{B}_{ij} = \frac{EI}{L^3} \int_0^1 \left(\frac{\partial^2 \mathbf{S}_i}{\partial \xi^2} \right)^T \left(\frac{\partial^2 \mathbf{S}_j}{\partial \xi^2} \right) d\xi \qquad (2.29)$$

$$\mathbf{A}_i = Ea \int_0^1 \mathbf{S}_{i,\xi}^T d\xi \qquad (2.30)$$

$\mathbf{A}_{11}$, $\mathbf{A}_{12}$, $\mathbf{A}_{21}$, $\mathbf{A}_{22}$, $\mathbf{B}_{11}$, $\mathbf{B}_{12}$, $\mathbf{B}_{21}$, $\mathbf{B}_{22}$, $\mathbf{A}_1$, $\mathbf{A}_2$, $\partial \mathbf{S}/\partial \xi$, $\partial^2 \mathbf{S}/\partial \xi^2$, $\partial i_x/\partial \mathbf{e}$ and $\partial i_y/\partial \mathbf{e}$ are presented in simplified form in Appendix A.

2.3.3 Generalized External Forces for Non-Shear Deformable Planar Beam Element

If a force $\mathbf{F}$ acts at an arbitrary point on the finite element, the virtual work done by the force for a virtual displacement of $\delta\mathbf{r}$ can be written as $\mathbf{F}\delta\mathbf{r}$, where $\mathbf{r}$ is the global position vector of the point of application of the force. The virtual change in the vector $\mathbf{r}$ can be expressed in terms of the virtual changes in the nodal variable vector, $\mathbf{e}$. Therefore, the generalized external forces associated with the absolute nodal coordinates can be defined [8]. By using the definition of global position vector given in Equation 2.12, the generalized force vector, $\mathbf{Q}_F$, can be found as given in the following equations.

$$\mathbf{F}^T\delta\mathbf{r} = \mathbf{F}^T\mathbf{S}\delta\mathbf{e} = \mathbf{Q}_F^T\delta\mathbf{e} \tag{2.31a}$$

$$\mathbf{Q}_F = \mathbf{S}^T\mathbf{F} \tag{2.31b}$$

2.3.3.1 Generalized Gravitational Forces for Non-Shear Deformable Planar Beam Element

As an example, distributed gravitational force directed toward the $-Y$ axis is expressed as the generalized force associated to the absolute nodal coordinates of a planar beam element as given below.

$$\mathbf{Q}_F^T = \mathbf{F}^T\mathbf{S} = \int_V \begin{bmatrix} 0 & -\rho g \end{bmatrix} \mathbf{S}\,dV = mg \begin{bmatrix} 0 & -\dfrac{1}{2} & 0 & -\dfrac{L}{12} & 0 & -\dfrac{1}{2} & 0 & \dfrac{L}{12} \end{bmatrix}^T \tag{2.32}$$

2.3.3.2 Generalized Moment for Non-Shear Deformable Planar Beam Element

When a moment M is applied at a cross-section of the beam, the virtual work due to the moment is given by $M\delta\alpha$, where α is the angle of rotation of the cross-section. The orientation of a coordinate system whose origin is rigidly attached to this cross-section can be defined using the transformation matrix given below [8, 34].

22

$$
\begin{bmatrix} cos\alpha & -sin\alpha \\ sin\alpha & cos\alpha \end{bmatrix} = \frac{1}{\sqrt{\left(\frac{\partial X}{\partial x}\right)^2 + \left(\frac{\partial Y}{\partial x}\right)^2}} \begin{bmatrix} \frac{\partial X}{\partial x} & -\frac{\partial Y}{\partial x} \\ \frac{\partial Y}{\partial x} & \frac{\partial X}{\partial x} \end{bmatrix}
\tag{2.33}
$$

By applying virtual change of variables for α, one can get virtual angular rotation in terms of nodal variables as given below [34].

$$
\delta\alpha = \frac{\frac{\partial X}{\partial x}\delta\left(\frac{\partial Y}{\partial x}\right) - \frac{\partial Y}{\partial x}\delta\left(\frac{\partial X}{\partial x}\right)}{\sqrt{\left(\frac{\partial X}{\partial x}\right)^2 + \left(\frac{\partial Y}{\partial x}\right)^2}}
\tag{2.34}
$$

If the moment is applied at node O of the element (Figure 2.1), virtual angular rotation can be calculated as follows.

$$
\delta\alpha = \frac{e_3\delta(e_4) - e_4\delta(e_3)}{e_3^2 + e_4^2} = \begin{bmatrix} 0 & 0 & -\frac{e_4}{e_3^2 + e_4^2} & \frac{e_3}{e_3^2 + e_4^2} & 0 & 0 & 0 & 0 \end{bmatrix}^T \delta\mathbf{e}
\tag{2.35}
$$

Then, the generalized external force, $\mathbf{Q}_F$, for the applied moment, M, can be derived as given below.

$$
\mathbf{Q}_F = \frac{M\delta\alpha}{\delta\mathbf{e}} = \begin{bmatrix} 0 & 0 & -M\frac{e_4}{e_3^2 + e_4^2} & M\frac{e_3}{e_3^2 + e_4^2} & 0 & 0 & 0 & 0 \end{bmatrix}^T
\tag{2.36}
$$

2.4 Absolute Nodal Coordinate Formulation for Shear Deformable Planar Beam Element

Shear deformable planar beam formulation has been introduced by Omar M. A. and Shabana A. A. [21]. They have added two nodal variables, $\partial X_i/\partial y$ and $\partial Y_i/\partial y$, for each nodes and used different shape function with more terms in order to include shear deformation effects. Vector of nodal variables for a shear deformable planar beam element is given below.

$$
\mathbf{e} = \begin{bmatrix} X_1 & Y_1 & \frac{\partial X_1}{\partial x} & \frac{\partial Y_1}{\partial x} & \frac{\partial X_1}{\partial y} & \frac{\partial Y_1}{\partial y} & X_2 & Y_2 & \frac{\partial X_2}{\partial x} & \frac{\partial Y_2}{\partial x} & \frac{\partial X_2}{\partial y} & \frac{\partial Y_2}{\partial y} \end{bmatrix}^T
\tag{2.37}
$$

23

Global position of an arbitrary point on the element can be found by using Equation 2.12. Shape function matrix, proposed by Omar M. A. and Shabana A. A. [21], is given below.

$$\mathbf{S} = \begin{bmatrix} s_1 & 0 & ls_2 & 0 & ls_3 & 0 & s_4 & 0 & ls_5 & 0 & ls_6 & 0 \\ 0 & s_1 & 0 & ls_2 & 0 & ls_3 & 0 & s_4 & 0 & ls_5 & 0 & ls_6 \end{bmatrix} \tag{2.38}$$

where

$$s_1 = 1 - 3\xi^2 + 2\xi^3 \tag{2.39a}$$

$$s_2 = \xi - 2\xi^2 + \xi^3 \tag{2.39b}$$

$$s_3 = \eta - \xi\eta \tag{2.39c}$$

$$s_4 = 3\xi^2 - 2\xi^3 \tag{2.39d}$$

$$s_5 = -\xi^2 + \xi^3 \tag{2.39e}$$

$$s_6 = \xi\eta \tag{2.39f}$$

and ξ and η are the reduced local coordinates and defined as x/l and y/l, respectively.

Mass matrix for the element can be evaluated by using kinetic energy equation given in Equation 2.17 as given below.

$$\mathbf{M} = \int_V \rho\, \mathbf{S}^T \mathbf{S}\, dV \tag{2.40}$$

Constant mass matrix can be evaluated by using Gauss-quadrature method or direct integrations. In [21], mass matrix is published in terms of mass, length, first moment of mass and second moment of mass.

2.4.1 Generalized Elastic Force for Shear Deformable Planar Beam Element

Strain energy equation can be used to find generalized elastic forces as in general flexible multibody formulation procedures. The strain energy equation for a beam element can be in general form written as;

24

$$U = \frac{1}{2} \int_V \boldsymbol{\varepsilon}^T \, \mathbf{E} \, \boldsymbol{\varepsilon} \, dV \tag{2.41}$$

In the equation, $\mathbf{E}$ represents matrix of elastic coefficients and $\boldsymbol{\varepsilon}$ represents the vector form of the strain tensor, $\boldsymbol{\varepsilon}_m$. Matrix of elastic coefficients can be written in terms of modulus of elasticity, E, and Poisson's ratio, ν, as given in the following equation [21].

$$\mathbf{E} = \begin{bmatrix} \lambda + 2\mu & \lambda & 0 \\ \lambda & \lambda + 2\mu & 0 \\ 0 & 0 & 2\mu \end{bmatrix} \tag{2.42}$$

where

$$\lambda = \frac{\nu E}{(1 + \nu)(1 - 2\nu)} \tag{2.43a}$$

$$\mu = \frac{E}{2(1 + \nu)} \tag{2.43b}$$

Nonlinear strain tensor, $\boldsymbol{\varepsilon}_m$, can be formulated in terms of deformation gradient, $\mathbf{J}$, as follows [36].

$$\boldsymbol{\varepsilon}_m = \frac{1}{2}\left(\mathbf{J}^T \, \mathbf{J} - \mathbf{I}\right) \tag{2.44}$$

In Equation 2.44, $\mathbf{I}$ is 2×2 identity matrix and $\mathbf{J}$ is the deformation gradient defined as;

$$\mathbf{J} = \frac{\partial \, \mathbf{r}^t}{\partial \, \mathbf{r}^0} \tag{2.45}$$

where $\mathbf{r}^0$ and $\mathbf{r}^t$ are the global positions of an arbitrary point on the element at initial and arbitrary times, respectively, and defined as follows.

$$\mathbf{r}^t = \begin{bmatrix} X^t & Y^t \end{bmatrix}^T \tag{2.46a}$$

$$\mathbf{r}^0 = \begin{bmatrix} X^0 & Y^0 \end{bmatrix}^T \tag{2.46b}$$

25

By substituting Equations 2.46 and 2.12 into Equation 2.45, deformation gradient, $\mathbf{J}$, can be written in terms of shape function matrix, $\mathbf{S}$, and vector of nodal variables, $\mathbf{e}$, as given below.

$$\mathbf{J} = \frac{\partial \mathbf{r}^t}{\partial \mathbf{r}^0} = \frac{\partial \mathbf{r}^t}{\partial \mathbf{x}} \frac{\partial \mathbf{x}}{\partial \mathbf{r}^0} = \begin{bmatrix} \mathbf{S}_{1,x}\,\mathbf{e} & \mathbf{S}_{1,y}\,\mathbf{e} \\ \mathbf{S}_{2,x}\,\mathbf{e} & \mathbf{S}_{2,y}\,\mathbf{e} \end{bmatrix} \mathbf{D}^{-1} \tag{2.47}$$

If initial body coordinate frame is parallel to the global coordinate frame, then the transformation matrix, $\mathbf{D}$, reduces to identity matrix. By eliminating transformation matrix, components of strain vector can be written as given in the following equations.

$$\varepsilon_1 = \frac{1}{2}(\mathbf{e}^T\,\mathbf{S}_a\,\mathbf{e} - 1) \tag{2.48a}$$

$$\varepsilon_2 = \frac{1}{2}(\mathbf{e}^T\,\mathbf{S}_b\,\mathbf{e} - 1) \tag{2.48b}$$

$$\varepsilon_3 = \frac{1}{2}\mathbf{e}^T\,\mathbf{S}_c\,\mathbf{e} \tag{2.48c}$$

where

$$\mathbf{S}_a = \mathbf{S}_{1,x}^T\,\mathbf{S}_{1,x} + \mathbf{S}_{2,x}^T\,\mathbf{S}_{2,x} \tag{2.49a}$$

$$\mathbf{S}_b = \mathbf{S}_{1,y}^T\,\mathbf{S}_{1,y} + \mathbf{S}_{2,y}^T\,\mathbf{S}_{2,y} \tag{2.49b}$$

$$\mathbf{S}_c = \mathbf{S}_{1,x}^T\,\mathbf{S}_{1,y} + \mathbf{S}_{2,x}^T\,\mathbf{S}_{2,y} \tag{2.49c}$$

Then, the vectorial form of strain tensor and its partial derivative can be written as functions of nodal variables as shown below.

$$\boldsymbol{\varepsilon} = \begin{bmatrix} \varepsilon_1 \\ \varepsilon_2 \\ \varepsilon_3 \end{bmatrix} = \frac{1}{2} \begin{bmatrix} \mathbf{e}^T\,\mathbf{S}_a\,\mathbf{e} - 1 \\ \mathbf{e}^T\,\mathbf{S}_b\,\mathbf{e} - 1 \\ \mathbf{e}^T\,\mathbf{S}_c\,\mathbf{e}_s \end{bmatrix} \tag{2.50a}$$

$$\frac{\partial \boldsymbol{\varepsilon}}{\partial \mathbf{e}} = \begin{bmatrix} \mathbf{e}^T\,\mathbf{S}_a \\ \mathbf{e}^T\,\mathbf{S}_b \\ \frac{1}{2}\,\mathbf{e}^T\left(\mathbf{S}_c + \mathbf{S}_c^T\right) \end{bmatrix} \tag{2.50b}$$

26

The generalized elastic force due to elastic potential can be obtained by differentiating the strain energy with respect to the nodal coordinates as;

$$\mathbf{Q}_k^T = \frac{\partial U}{\partial \mathbf{e}} = \frac{\partial}{\partial \mathbf{e}} \left\{ \frac{1}{2} \int_V \boldsymbol{\varepsilon}^T \mathbf{E} \, \boldsymbol{\varepsilon} \, dV \right\} = \int_V \left(\frac{\partial \boldsymbol{\varepsilon}}{\partial \mathbf{e}} \right)^T \mathbf{E} \, \boldsymbol{\varepsilon} \, dV \qquad (2.51)$$

By substituting Equations 2.50.a and 2.50.b into Equation 2.51, the generalized elastic force vector can be simplified to the following equation.

$$\mathbf{Q}_k^T = \int_V \begin{bmatrix} \mathbf{e}^T \mathbf{S}_a & \mathbf{e}^T \mathbf{S}_b & \frac{1}{2} \mathbf{e}^T \left(\mathbf{S}_c + \mathbf{S}_c^T \right) \end{bmatrix} \begin{bmatrix} \lambda + 2\mu & \lambda & 0 \\ \lambda & \lambda + 2\mu & 0 \\ 0 & 0 & 2\mu \end{bmatrix} \frac{1}{2} \begin{bmatrix} \mathbf{e}^T \mathbf{S}_a \mathbf{e} - 1 \\ \mathbf{e}^T \mathbf{S}_b \mathbf{e} - 1 \\ \mathbf{e}^T \mathbf{S}_c \mathbf{e} \end{bmatrix} dV \quad (2.52a)$$

$$\mathbf{Q}_k^T = \frac{1}{2} \int_V \mathbf{e}^T \begin{bmatrix} ((\lambda + 2\mu) \mathbf{S}_a + \lambda \mathbf{S}_b) \left(\mathbf{e}^T \mathbf{S}_a \mathbf{e} - 1 \right) \cdots \\ + (\lambda \mathbf{S}_a + (\lambda + 2\mu) \mathbf{S}_b) \left(\mathbf{e}^T \mathbf{S}_b \mathbf{e} - 1 \right) + \mu \left(\mathbf{S}_c + \mathbf{S}_c^T \right) \mathbf{e}^T \mathbf{S}_c \mathbf{e} \end{bmatrix} dV \qquad (2.52b)$$

Then, generalized elastic forces of deformable bodies can be assembled by using the forces obtained for each elements in flexible multibody system.

2.4.2 Generalized External Forces for Shear Deformable Planar Beam Element

Generalized external forces for shear deformable planar beam element can be found by using virtual work principle as given in Equation 2.31. As an example, distributed gravitational force directed toward the $-Y$ axis is expressed as the generalized force associated with the absolute nodal coordinates of an arbitrary beam element as follows.

$$\mathbf{Q}_F^T = \mathbf{F}^T \mathbf{S} = \int_V \begin{bmatrix} 0 & -\rho g \end{bmatrix} \mathbf{S} \, d V \qquad (2.53a)$$

$$\mathbf{Q}_F^T = -mg \begin{bmatrix} 0 & \frac{1}{2} & 0 & \frac{l}{12} & 0 & 0 & 0 & \frac{1}{2} & 0 & -\frac{l}{12} & 0 & 0 \end{bmatrix} \qquad (2.53b)$$

27

Additionally, generalized external force vector due to a moment, M, applied at the first node of the beam can be found with a similar procedure given in Section 2.3.3.2 as follows [21].

$$\mathbf{Q}_F^T = \begin{bmatrix} 0 & 0 & 0 & 0 & \dfrac{Me_6}{e_5^2 + e_6^2} & -\dfrac{Me_5}{e_5^2 + e_6^2} & 0 & 0 & 0 & 0 & 0 & 0 \end{bmatrix} \qquad (2.54)$$

2.5 Absolute Nodal Coordinate Formulation for four noded Generalized Plate Element

Plate and shell structures are indispensable parts of mechanical systems. Therefore, ANCF for generalized plates, which was proposed by Mikkola A. M. and Shabana A. A. [30], is also included in this chapter.

The dimensions and the coordinate frames used for a four-noded plate element is shown in Figure 2.2. As shown in the figure, there is one element coordinate frame and one global coordinate frame (or inertial frame) as in general finite element formulations. However, the difference is the used nodal coordinates and the shape functions. Nodal variables of an element are global coordinates and their gradients. By application of different initial gradients, shell structures can also be simulated with the formulation given below.
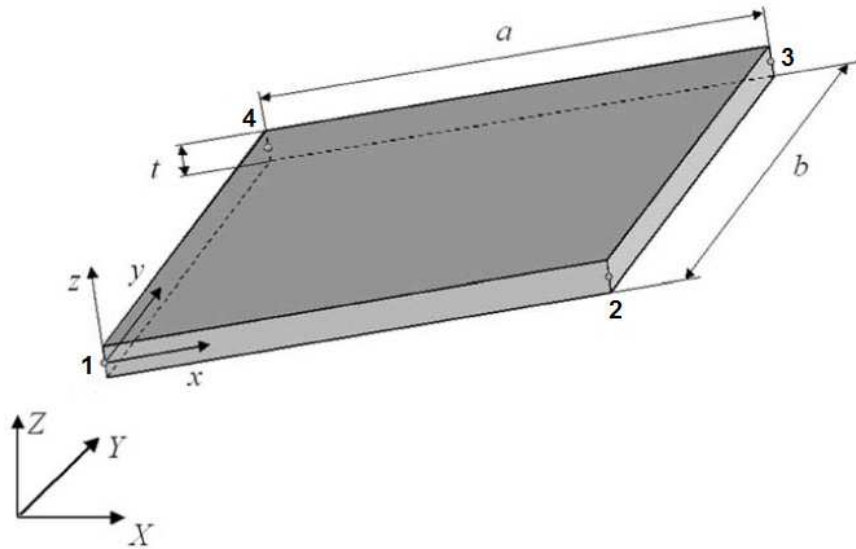
Figure 2.2: Four noded plate element [30]

Nodal variables for an arbitrary plate element can be written by using Equation 2.9 as given below.

$$\mathbf{e} = \begin{bmatrix} \mathbf{e}_1^T & \mathbf{e}_2^T & \mathbf{e}_3^T & \mathbf{e}_4^T \end{bmatrix}^T \tag{2.55}$$

where

$$\mathbf{e}_i = \begin{bmatrix} X_i & Y_i & Z_i & X_{i,x} & Y_{i,x} & Z_{i,x} & X_{i,y} & Y_{i,y} & Z_{i,y} & X_{i,z} & Y_{i,z} & Z_{i,z} \end{bmatrix}^T \tag{2.56}$$

In the equation, X, Y and Z refer to the coordinates with respect to global coordinate frame, and x, y and z refer to the local coordinate frame. With those definitions, the vector of nodal variables for a plate element has the size of 48.

Then, the global position vector, $\mathbf{r}$, can be calculated by using appropriate shape function matrix and Equation 2.12. Mikkola A. M. and Shabana A. A. have introduced two different shape function matrices in their publication [30]. One of them is presented as;

$$\mathbf{S} = [S_1\mathbf{I} \ S_2\mathbf{I} \ S_3\mathbf{I} \ S_4\mathbf{I} \ S_5\mathbf{I} \ S_6\mathbf{I} \ S_7\mathbf{I} \ S_8\mathbf{I} \ S_9\mathbf{I} \ S_{10}\mathbf{I} \ S_{11}\mathbf{I} \ S_{12}\mathbf{I} \ S_{13}\mathbf{I} \ S_{14}\mathbf{I} \ S_{15}\mathbf{I} \ S_{16}\mathbf{I}]$$

$$\tag{2.57}$$

where

$$S_1 = (2\xi + 1)(\xi - 1)^2(2\eta + 1)(\eta - 1)^2$$

$$S_2 = a\xi(\xi - 1)^2(2\eta + 1)(\eta - 1)^2$$

$$S_3 = b\eta(\xi - 1)^2(2\xi + 1)(\eta - 1)^2$$

$$S_4 = t\zeta(\xi - 1)(\eta - 1)$$

$$S_5 = -\xi^2(2\xi - 3)(2\eta + 1)(\eta - 1)^2$$

$$S_6 = a\xi^2(\xi - 1)(2\eta + 1)(\eta - 1)^2$$

$$S_7 = -b\eta\xi^2(2\xi - 3)(\eta - 1)^2$$

$$S_8 = -t\xi\zeta(\eta - 1)$$

$$S_9 = \eta^2\xi^2(2\xi - 3)(2\eta - 3)$$

$$S_{10} = -a\eta^2\xi^2(\xi - 1)(2\eta - 3)$$

29

$$S_{11} = -b\eta^2\xi^2(\eta - 1)(2\xi - 3)$$

$$S_{12} = t\xi\zeta\eta$$

$$S_{13} = -\eta^2(2\xi + 1)(\xi - 1)^2(2\eta - 3)$$

$$S_{14} = -a\xi\eta^2(\xi - 1)^2(2\eta - 3)$$

$$S_{15} = b\eta^2(\xi - 1)^2(2\xi + 1)(\eta - 1)$$

$$S_{16} = -t\eta\zeta(\xi - 1)$$

Additionally, a, b and t are the sizes of plate element given in Figure 2.2, $\mathbf{I}$ is 3×3 identity matrix, and ξ, η and ζ are the reduced local coordinates of an arbitrary point in the element, which are defined as $\xi = x/a$, $\eta = y/b$ and $\zeta = z/t$, respectively. The shape function matrix represents exact rigid body dynamics and produces no strain under rigid body displacements and/or rotations [1, 4, 7, 8, 30, 32]. For the other shape function matrix and their comparison [30] could be reviewed.

2.5.1   Mass matrix for Generalized Plate Element

All of the existing finite element formulations for the large deformation and rotation analysis of plates and shells lead to nonlinear mass matrices [8]. However, it is just a constant matrix in ANCF. Mass matrix of a plate element can easily be formed by writing the kinetic energy equation at an arbitrary time, t, for an element as given below.

$$^tT = \frac{1}{2}\int_{^tV} {}^t\rho \, {}^t\dot{\mathbf{r}}^T {}^t\dot{\mathbf{r}} \, d\,^tV \tag{2.58}$$

In Equation 2.58, $^t\rho$ and ^tV are density and volume of the plate element at an arbitrary time, t. The velocity vector can be obtained by differentiating the position vector as $^t\dot{\mathbf{r}} = \mathbf{S}\,{}^t\dot{\mathbf{e}}$. Density and volume at an arbitrary time t can be written in terms of initial density and volume by using deformation gradient matrix, $\mathbf{J}$, as given in the following equations [36].

$$^t\rho = \frac{^0\rho}{\left|{}_0^t\mathbf{J}\right|} \tag{2.59a}$$

$$d\,^tV = \left|{}_0^t\mathbf{J}\right| d\,^0V \tag{2.59b}$$

Then, mass matrix can be found by substituting velocity vector, $\dot{\mathbf{r}}$, and Equations 2.59.a and 2.59.b into Equation 2.58 as follows.

$$^{t}T = \frac{1}{2} \int_{^{t}V} \frac{^{0}\rho}{\left|^{t}_{0}\mathbf{J}\right|} \left(^{t}\dot{\mathbf{e}}^{T}\right) \mathbf{S}^{T}\mathbf{S}\left(^{t}\dot{\mathbf{e}}\right) \left|^{t}_{0}\mathbf{J}\right| d\,^{0}V \tag{2.60a}$$

$$^{t}T = \frac{1}{2} \left(^{t}\dot{\mathbf{e}}^{T}\right) \left[\int_{^{0}V} {^{0}\rho}\, \mathbf{S}^{T}\mathbf{S}\, d\,^{0}V\right] \left(^{t}\dot{\mathbf{e}}\right) \tag{2.60b}$$

$$^{t}T = \frac{1}{2} \left(^{t}\dot{\mathbf{e}}^{T}\right) {^{t}\mathbf{M}}\left(^{t}\dot{\mathbf{e}}\right) \tag{2.60c}$$

$$^{t}\mathbf{M} = \int_{^{0}V} {^{0}\rho}\, \mathbf{S}^{T}\mathbf{S}\, d\,^{0}V \tag{2.60d}$$

As seen in Equation 2.60d , mass matrix at an arbitrary time, t, does not depend on time and the orientation. It can be evaluated once by using the initial density and volume, then it can be used at any time step during the solution process. However, volume integration is performed on global coordinate frame. Therefore, it should be transformed into local coordinate frame in order to make volume integration easier as given below.

$$\mathbf{M} = \int_{v_e} \rho \mathbf{S}^{T}\mathbf{S} \left|\mathbf{D}\right| dv_e \tag{2.61}$$

where v_e represents volume of the element in local coordinates ($dv_e = dxdydz$) and $\mathbf{D}$ is the gradient tensor defined as;

$$\mathbf{D}^{T} = \frac{\partial \mathbf{X}}{\partial \mathbf{x}} = \begin{bmatrix} \dfrac{\partial X}{\partial x} & \dfrac{\partial X}{\partial y} & \dfrac{\partial X}{\partial z} \\ \dfrac{\partial Y}{\partial x} & \dfrac{\partial Y}{\partial y} & \dfrac{\partial Y}{\partial z} \\ \dfrac{\partial Z}{\partial x} & \dfrac{\partial Z}{\partial y} & \dfrac{\partial Z}{\partial z} \end{bmatrix} \tag{2.62}$$

It is obvious that if the initial local coordinate frame is parallel to the global coordinate frame, then the transformation gradient tensor is equal to identity matrix and $\left|\mathbf{D}\right| = 1$.

31

2.5.2 Generalized Elastic Forces for Generalized Plate Element

In the derivation of generalized elastic forces, continuum mechanics approach has been used. The elastic forces of an arbitrary plate element can be derived using strain energy equation. The strain energy of an element at an arbitrary time, t, can be formulated by using Green-Lagrange strain and 2nd Piola-Kirchhoff stress tensor definitions as given below (Total Lagrangian Formulation) [32].

$$^tU = \frac{1}{2} \int_{^0V} \left(^t\boldsymbol{\varepsilon}^T \right) \mathbf{E} \left(^t\boldsymbol{\varepsilon} \right) d\,^0V \tag{2.63}$$

where $\mathbf{E}$ is the matrix of elastic coefficients and $^t\boldsymbol{\varepsilon}$ is the vector form of the strain tensor, $^t\boldsymbol{\varepsilon}_m$. The matrix of elastic coefficients is given below [36].

$$\mathbf{E} = \begin{bmatrix} \lambda + 2\mu & \lambda & \lambda & 0 & 0 & 0 \\ \lambda & \lambda + 2\mu & \lambda & 0 & 0 & 0 \\ \lambda & \lambda & \lambda + 2\mu & 0 & 0 & 0 \\ 0 & 0 & 0 & \mu & 0 & 0 \\ 0 & 0 & 0 & 0 & \mu & 0 \\ 0 & 0 & 0 & 0 & 0 & \mu \end{bmatrix} \tag{2.64a}$$

$$\lambda = \frac{\nu E}{(1+\nu)(1-2\nu)} \tag{2.64b}$$

$$\mu = \frac{E}{2(1+\nu)} \tag{2.64c}$$

where E and μ are elastic modulus and Poisson's ratio of the material. Then, the generalized elastic force vector of the plate element can be obtained by differentiating the strain energy (Equation 2.63) with respect to the nodal variables as given in the following equation.

$$^t\mathbf{Q}_k^T = \frac{\partial\,^tU}{\partial\,^t\mathbf{e}} = \frac{\partial}{\partial\,^t\mathbf{e}} \left\{ \frac{1}{2} \int_{^0V} {}^t\boldsymbol{\varepsilon}^T \mathbf{E}\,^t\boldsymbol{\varepsilon}\, d\,^0V \right\} = \int_{^0V} \left(\frac{\partial\,^t\boldsymbol{\varepsilon}}{\partial\,^t\mathbf{e}} \right)^T \mathbf{E}\,^t\boldsymbol{\varepsilon}\, d\,^0V \tag{2.65}$$

The nonlinear strain tensor can be defined by using 3×3 identity matrix, $\mathbf{I}$, as given below [36].

$$\varepsilon_m = \frac{1}{2} \left({}_0^t \mathbf{J}^T {}_0^t \mathbf{J} - \mathbf{I} \right) \tag{2.66}$$

Deformation gradient, $\mathbf{J}$, can be written in terms of nodal variables, $\mathbf{e}$, as follows.

$$\mathbf{J} = \frac{\partial\,{}^t\mathbf{r}}{\partial\,{}^0\mathbf{r}} = \begin{bmatrix} \dfrac{\partial\,{}^tX}{\partial\,{}^0X} & \dfrac{\partial\,{}^tX}{\partial\,{}^0Y} & \dfrac{\partial\,{}^tX}{\partial\,{}^0Z} \\[2mm] \dfrac{\partial\,{}^tY}{\partial\,{}^0X} & \dfrac{\partial\,{}^tY}{\partial\,{}^0Y} & \dfrac{\partial\,{}^tY}{\partial\,{}^0Z} \\[2mm] \dfrac{\partial\,{}^tZ}{\partial\,{}^0X} & \dfrac{\partial\,{}^tZ}{\partial\,{}^0Y} & \dfrac{\partial\,{}^tZ}{\partial\,{}^0Z} \end{bmatrix} = \begin{bmatrix} \mathbf{S}_{1,X}\mathbf{e} & \mathbf{S}_{1,Y}\mathbf{e} & \mathbf{S}_{1,Z}\mathbf{e} \\[2mm] \mathbf{S}_{2,X}\mathbf{e} & \mathbf{S}_{2,Y}\mathbf{e} & \mathbf{S}_{2,Z}\mathbf{e} \\[2mm] \mathbf{S}_{3,X}\mathbf{e} & \mathbf{S}_{3,Y}\mathbf{e} & \mathbf{S}_{3,Z}\mathbf{e} \end{bmatrix} \tag{2.67}$$

In Equation 2.67, $\mathbf{S}_1$, $\mathbf{S}_2$ and $\mathbf{S}_3$ are the first, second and third row vectors of shape function matrix, $\mathbf{S}$. The deformation gradient, $\mathbf{J}$, contains partial derivatives of the shape function with respect to the initial global position vector. Therefore, these partial derivatives ($\mathbf{S}_{i,X}$, $\mathbf{S}_{i,Y}$ and $\mathbf{S}_{i,Z}$) should be related to the local coordinate frame as given below.

$$\begin{bmatrix} \dfrac{\partial S_i}{\partial x} \\[2mm] \dfrac{\partial S_i}{\partial y} \\[2mm] \dfrac{\partial S_i}{\partial z} \end{bmatrix} = \begin{bmatrix} \dfrac{\partial X}{\partial x} & \dfrac{\partial Y}{\partial x} & \dfrac{\partial Z}{\partial x} \\[2mm] \dfrac{\partial X}{\partial y} & \dfrac{\partial Y}{\partial y} & \dfrac{\partial Z}{\partial y} \\[2mm] \dfrac{\partial X}{\partial z} & \dfrac{\partial Y}{\partial z} & \dfrac{\partial Z}{\partial z} \end{bmatrix} \begin{bmatrix} \dfrac{\partial S_i}{\partial X} \\[2mm] \dfrac{\partial S_i}{\partial Y} \\[2mm] \dfrac{\partial S_i}{\partial Z} \end{bmatrix} = \mathbf{D} \begin{bmatrix} \dfrac{\partial S_i}{\partial X} \\[2mm] \dfrac{\partial S_i}{\partial Y} \\[2mm] \dfrac{\partial S_i}{\partial Z} \end{bmatrix} \tag{2.68}$$

The transformation matrix, defined in Equations 2.62 and 2.68, can be written in terms of nodal variables as in the following equation.

$$\mathbf{D} = \begin{bmatrix} \dfrac{\partial X}{\partial x} & \dfrac{\partial Y}{\partial x} & \dfrac{\partial Z}{\partial x} \\[2mm] \dfrac{\partial X}{\partial y} & \dfrac{\partial Y}{\partial y} & \dfrac{\partial Z}{\partial y} \\[2mm] \dfrac{\partial X}{\partial z} & \dfrac{\partial Y}{\partial z} & \dfrac{\partial Z}{\partial z} \end{bmatrix} = \begin{bmatrix} \mathbf{S}_{1,x}\,\mathbf{e}_0 & \mathbf{S}_{1,y}\,\mathbf{e}_0 & \mathbf{S}_{1,z}\,\mathbf{e}_0 \\[2mm] \mathbf{S}_{2,x}\,\mathbf{e}_0 & \mathbf{S}_{2,y}\,\mathbf{e}_0 & \mathbf{S}_{2,z}\,\mathbf{e}_0 \\[2mm] \mathbf{S}_{3,x}\,\mathbf{e}_0 & \mathbf{S}_{3,y}\,\mathbf{e}_0 & \mathbf{S}_{3,z}\,\mathbf{e}_0 \end{bmatrix}^T \tag{2.69}$$

Then, partial differentials with respect to the global coordinate frame can be converted into partial differentials with respect to the local coordinate frame as given below.

$$\begin{bmatrix} \dfrac{\partial S_i}{\partial X} \\[2mm] \dfrac{\partial S_i}{\partial Y} \\[2mm] \dfrac{\partial S_i}{\partial Z} \end{bmatrix} = \mathbf{D}^{-1} \begin{bmatrix} \dfrac{\partial S_i}{\partial x} \\[2mm] \dfrac{\partial S_i}{\partial y} \\[2mm] \dfrac{\partial S_i}{\partial z} \end{bmatrix} \tag{2.70}$$

Strain vector and its derivative with respect to the nodal variables should be written in terms of the nodal variables. By using the deformation gradient (Equation 2.67) and nonlinear strain

33

tensor definition (Equation 2.66), nonlinear strain tensor can be rewritten as follows.

$$\boldsymbol{\varepsilon}_m = \begin{bmatrix} \varepsilon_{11} & \varepsilon_{12} & \varepsilon_{13} \\ \varepsilon_{12} & \varepsilon_{22} & \varepsilon_{23} \\ \varepsilon_{13} & \varepsilon_{23} & \varepsilon_{33} \end{bmatrix} = \frac{1}{2} \left(\begin{bmatrix} \frac{\partial\,{}^tX}{\partial\,{}^0X} & \frac{\partial\,{}^tX}{\partial\,{}^0Y} & \frac{\partial\,{}^tX}{\partial\,{}^0Z} \\ \frac{\partial\,{}^tY}{\partial\,{}^0X} & \frac{\partial\,{}^tY}{\partial\,{}^0Y} & \frac{\partial\,{}^tY}{\partial\,{}^0Z} \\ \frac{\partial\,{}^tZ}{\partial\,{}^0X} & \frac{\partial\,{}^tZ}{\partial\,{}^0Y} & \frac{\partial\,{}^tZ}{\partial\,{}^0Z} \end{bmatrix}^T \begin{bmatrix} \frac{\partial\,{}^tX}{\partial\,{}^0X} & \frac{\partial\,{}^tX}{\partial\,{}^0Y} & \frac{\partial\,{}^tX}{\partial\,{}^0Z} \\ \frac{\partial\,{}^tY}{\partial\,{}^0X} & \frac{\partial\,{}^tY}{\partial\,{}^0Y} & \frac{\partial\,{}^tY}{\partial\,{}^0Z} \\ \frac{\partial\,{}^tZ}{\partial\,{}^0X} & \frac{\partial\,{}^tZ}{\partial\,{}^0Y} & \frac{\partial\,{}^tZ}{\partial\,{}^0Z} \end{bmatrix} - \begin{bmatrix} 1 & 0 & 0 \\ 0 & 1 & 0 \\ 0 & 0 & 1 \end{bmatrix} \right) \quad (2.71a)$$

$$\boldsymbol{\varepsilon}_m = \frac{1}{2} \begin{bmatrix} \left(\frac{\partial\mathbf{r}}{\partial\,{}^0X}\right)^T \left(\frac{\partial\mathbf{r}}{\partial\,{}^0X}\right) - 1 & \left(\frac{\partial\mathbf{r}}{\partial\,{}^0X}\right)^T \left(\frac{\partial\mathbf{r}}{\partial\,{}^0Y}\right) & \left(\frac{\partial\mathbf{r}}{\partial\,{}^0X}\right)^T \left(\frac{\partial\mathbf{r}}{\partial\,{}^0Z}\right) \\ \left(\frac{\partial\mathbf{r}}{\partial\,{}^0Y}\right)^T \left(\frac{\partial\mathbf{r}}{\partial\,{}^0X}\right) & \left(\frac{\partial\mathbf{r}}{\partial\,{}^0Y}\right)^T \left(\frac{\partial\mathbf{r}}{\partial\,{}^0Y}\right) - 1 & \left(\frac{\partial\mathbf{r}}{\partial\,{}^0Y}\right)^T \left(\frac{\partial\mathbf{r}}{\partial\,{}^0Z}\right) \\ \left(\frac{\partial\mathbf{r}}{\partial\,{}^0Z}\right)^T \left(\frac{\partial\mathbf{r}}{\partial\,{}^0X}\right) & \left(\frac{\partial\mathbf{r}}{\partial\,{}^0Z}\right)^T \left(\frac{\partial\mathbf{r}}{\partial\,{}^0Y}\right) & \left(\frac{\partial\mathbf{r}}{\partial\,{}^0Z}\right)^T \left(\frac{\partial\mathbf{r}}{\partial\,{}^0Z}\right) - 1 \end{bmatrix} \quad (2.71b)$$

Then, strain tensor can be written in vector form as;

$$\boldsymbol{\varepsilon} = \frac{1}{2} \begin{bmatrix} \left(\frac{\partial\mathbf{r}}{\partial\,{}^0X}\right)^T \left(\frac{\partial\mathbf{r}}{\partial\,{}^0X}\right) - 1 \\ \left(\frac{\partial\mathbf{r}}{\partial\,{}^0Y}\right)^T \left(\frac{\partial\mathbf{r}}{\partial\,{}^0Y}\right) - 1 \\ \left(\frac{\partial\mathbf{r}}{\partial\,{}^0Z}\right)^T \left(\frac{\partial\mathbf{r}}{\partial\,{}^0Z}\right) - 1 \\ 2\left(\frac{\partial\mathbf{r}}{\partial\,{}^0Y}\right)^T \left(\frac{\partial\mathbf{r}}{\partial\,{}^0Z}\right) \\ 2\left(\frac{\partial\mathbf{r}}{\partial\,{}^0X}\right)^T \left(\frac{\partial\mathbf{r}}{\partial\,{}^0Z}\right) \\ 2\left(\frac{\partial\mathbf{r}}{\partial\,{}^0X}\right)^T \left(\frac{\partial\mathbf{r}}{\partial\,{}^0Y}\right) \end{bmatrix} \quad (2.72)$$

The partial differentials appearing in the strain vector (Equation 2.72) can be defined as;

$$\frac{\partial\mathbf{r}}{\partial\,{}^0X_i} = \mathbf{D}_{ei}\mathbf{e} \quad (2.73)$$

where

$$\mathbf{D}_{ei} = \left(a_{1i}\mathbf{S}_{,x} + a_{2i}\mathbf{S}_{,y} + a_{3i}\mathbf{S}_{,z}\right) \quad (2.74)$$

In the equation, a_{1i}, a_{2i} and a_{3i} are the ith element of the column vectors, which are defined as $\mathbf{a}_1$, $\mathbf{a}_2$ and $\mathbf{a}_3$ in the following equation.

$$\begin{bmatrix} \mathbf{a}_1 & \mathbf{a}_2 & \mathbf{a}_3 \end{bmatrix} = \left(\mathbf{D}^T\right)^{-1} \quad (2.75)$$

Finally, the strain vector and its partial derivative with respect to vector of nodal variables can be written in explicit forms by substituting Equation 2.73 into Equation 2.72 as given in the

34

following equations.

$$\boldsymbol{\varepsilon} = \frac{1}{2} \begin{bmatrix} \mathbf{e}^T \mathbf{D}_{e1}{}^T \mathbf{D}_{e1} \mathbf{e} - 1 \\ \mathbf{e}^T \mathbf{D}_{e2}^T \mathbf{D}_{e2} \mathbf{e} - 1 \\ \mathbf{e}^T \mathbf{D}_{e3}^T \mathbf{D}_{e3} \mathbf{e} - 1 \\ 2\mathbf{e}^T \mathbf{D}_{e2}^T \mathbf{D}_{e3} \mathbf{e} \\ 2\mathbf{e}^T \mathbf{D}_{e1}^T \mathbf{D}_{e3} \mathbf{e} \\ 2\mathbf{e}^T \mathbf{D}_{e1}^T \mathbf{D}_{e2} \mathbf{e} \end{bmatrix} \tag{2.76}$$

$$\frac{\partial \boldsymbol{\varepsilon}}{\partial \mathbf{e}} = \begin{bmatrix} \mathbf{e}^T \mathbf{D}_{e1}{}^T \mathbf{D}_{e1} \\ \mathbf{e}^T \mathbf{D}_{e2}^T \mathbf{D}_{e2} \\ \mathbf{e}^T \mathbf{D}_{e3}^T \mathbf{D}_{e3} \\ \mathbf{e}^T (\mathbf{D}_{e2}^T \mathbf{D}_{e3} + \mathbf{D}_{e3}^T \mathbf{D}_{e2}) \\ \mathbf{e}^T \left(\mathbf{D}_{e1}^T \mathbf{D}_{e3} + \mathbf{D}_{e3}^T \mathbf{D}_{e1} \right) \\ \mathbf{e}^T \left(\mathbf{D}_{e1}^T \mathbf{D}_{e2} + \mathbf{D}_{e2}^T \mathbf{D}_{e1} \right) \end{bmatrix} \tag{2.77}$$

Then, the generalized elastic force vector can be written in terms of nodal variables by substituting Equations 2.76 and 2.77 into Equation 2.65 as given below.

$$\mathbf{Q}_k^T = \frac{1}{2} \int_{^0V} \begin{bmatrix} \mathbf{e}^T \mathbf{D}_{e1}{}^T \mathbf{D}_{e1} \\ \mathbf{e}^T \mathbf{D}_{e2}^T \mathbf{D}_{e2} \\ \mathbf{e}^T \mathbf{D}_{e3}^T \mathbf{D}_{e3} \\ \mathbf{e}^T (\mathbf{D}_{e2}^T \mathbf{D}_{e3} + \mathbf{D}_{e3}^T \mathbf{D}_{e2}) \\ \mathbf{e}^T \left(\mathbf{D}_{e1}^T \mathbf{D}_{e3} + \mathbf{D}_{e3}^T \mathbf{D}_{e1} \right) \\ \mathbf{e}^T \left(\mathbf{D}_{e1}^T \mathbf{D}_{e2} + \mathbf{D}_{e2}^T \mathbf{D}_{e1} \right) \end{bmatrix} \mathbf{E} \begin{bmatrix} \mathbf{e}^T \mathbf{D}_{e1}{}^T \mathbf{D}_{e1} \mathbf{e} - 1 \\ \mathbf{e}^T \mathbf{D}_{e2}^T \mathbf{D}_{e2} \mathbf{e} - 1 \\ \mathbf{e}^T \mathbf{D}_{e3}^T \mathbf{D}_{e3} \mathbf{e} - 1 \\ 2\mathbf{e}^T \mathbf{D}_{e2}^T \mathbf{D}_{e3} \mathbf{e} \\ 2\mathbf{e}^T \mathbf{D}_{e1}^T \mathbf{D}_{e3} \mathbf{e} \\ 2\mathbf{e}^T \mathbf{D}_{e1}^T \mathbf{D}_{e2} \mathbf{e} \end{bmatrix} d\,{}^0V \tag{2.78}$$

In order to perform the integration of the generalized elastic force vector, the volume increment should also be transformed into local coordinates as $d\,{}^0V = |\mathbf{D}|\,d\,{}^0v_e$ [30]. Evaluation of the elastic force vector needs to be performed by numerical methods. In most of the finite element procedures, Gauss-Quadrature numerical integration method is applied. By changing the integration variables to the reduced coordinates one can obtain the following equation.

$$\mathbf{Q}_k^T = abt \int_{-\frac{1}{2}}^{\frac{1}{2}} \int_0^1 \int_0^1 \left(\frac{\partial \boldsymbol{\varepsilon}(\xi, \eta, \zeta)}{\partial \mathbf{e}} \right)^T \mathbf{E} \, \boldsymbol{\varepsilon}(\xi, \eta, \zeta) \, |\mathbf{D}| d\xi d\eta d\zeta \qquad (2.79)$$

Volume integration in Equation 2.79 can be converted to simple summations by Gauss-Quadrature method as given in the following equation.

$$\mathbf{Q}_k^T = \frac{abt}{8} \sum_{k=1}^{n_k} \sum_{j=1}^{n_j} \sum_{i=1}^{n_i} w_i w_j w_k \left(\frac{\partial \boldsymbol{\varepsilon}\left(\frac{\xi_i + 1}{2}, \frac{\eta_j + 1}{2}, \frac{\zeta_k}{2} \right)}{\partial \mathbf{e}} \right)^T \mathbf{E} \, \boldsymbol{\varepsilon}\left(\frac{\xi_i + 1}{2}, \frac{\eta_j + 1}{2}, \frac{\zeta_k}{2} \right) |\mathbf{D}| \quad (2.80)$$

where $\left(\xi_i, \eta_j, \zeta_k \right)$ refer to the Gauss-Quadrature points and $\left(w_i, w_j, w_k \right)$ refer to the Gauss-Quadrature weight factors.

2.5.3 Generalized External Forces for Generalized Plate Element

Generalized external forces for the plate element can be found by using virtual work principle as in Equation 2.31. As an example, distributed gravitational force directed toward the $-Z$ axis is expressed as the generalized force associated with the absolute nodal coordinates of an arbitrary plate element as given in the following equations.

$$\mathbf{Q}_F^T = \mathbf{F}^T \mathbf{S} = \int_{^tV} \begin{bmatrix} 0 & 0 & -^t\rho g \end{bmatrix} \mathbf{S} d\,^tV = \int_{^tV} -^t\rho g \mathbf{S}_3 d\,^tV = -\rho g \int_{^0V} \mathbf{S}_3 |\mathbf{D}| dv_e \qquad (2.81a)$$

$$\mathbf{Q}_F^T = \frac{-\rho g abt |\mathbf{D}|}{4} \begin{bmatrix} 0\ 0\ 1\ 0\ 0\ \frac{1}{6}\ 0\ 0\ \frac{b}{6}\ 0\ 0\ \frac{t}{2}\ 0\ 0\ 1\ 0\ 0\ -\frac{a}{6}\ 0\ 0\ \frac{b}{6}\ 0\ 0\ \frac{t}{2}\ \cdots \\ \cdots\ 0\ 0\ 1\ 0\ 0\ -\frac{a}{6}\ 0\ 0\ -\frac{b}{6}\ 0\ 0\ \frac{t}{2}\ 0\ 0\ 1\ 0\ 0\ \frac{a}{6}\ 0\ 0\ -\frac{b}{6}\ 0\ 0\ \frac{t}{2} \end{bmatrix} \qquad (2.81b)$$

2.6 Equation of Motion and Solution Procedure

Using the simplified mass matrix and generalized force vectors, equation of motion of an element can be written as follows [8].

$$\mathbf{M\ddot{e}} + \mathbf{Q}_k = \mathbf{Q}_F \tag{2.82}$$

where $\mathbf{Q}_k$ and $\mathbf{Q}_F$ are the vectors of generalized elastic and external forces, respectively. Using the generalized force vector definition ($\mathbf{Q} = \mathbf{Q}_e - \mathbf{Q}_F$), equation of motion can be written in more compact form as;

$$\mathbf{\ddot{e}} = \mathbf{M}^{-1}\mathbf{Q} \tag{2.83}$$

Mass matrix and force vectors should be assembled in order to get the equations of motion for the whole flexible multibody system. In the literature, there are mainly two assembly procedure. The first one is the same as the procedure used in general finite element problems in which the elements of matrices for finite elements are summed up to the related elements of the system matrices. In the second procedure, the constraint equations between the connected nodes are introduced to the system equations. In the thesis, general finite element assembly procedure is applied. In order to solve the equation of motion over a defined duration, explicit direct integration method can be applied. In the direct integration method, instead of trying to satisfy the equation of motion at any time, it is aimed to satisfy the equilibrium equation only at discrete time intervals [36].

Then, the nodal acceleration vector can be approximated with the central difference method as given below [12].

$$^t\mathbf{\ddot{e}} = \frac{1}{\Delta t^2}\left(^{t+\Delta t}\mathbf{e} - 2\,^t\mathbf{e} + \,^{t-\Delta t}\mathbf{e}\right) \tag{2.84}$$

By substituting Equation 2.84 into Equation 2.83, one can obtain nodal variables at $t + \Delta t$ as shown below.

$$\frac{1}{\Delta t^2}\left(^{t+\Delta t}\mathbf{e} - 2\,^t\mathbf{e} + \,^{t-\Delta t}\mathbf{e}\right) = \mathbf{M}^{-1}\mathbf{Q}(^t\mathbf{e}) \tag{2.85a}$$

$$^{t+\Delta t}\mathbf{e} = 2\,^t\mathbf{e} - \,^{t-\Delta t}\mathbf{e} + \Delta t^2\mathbf{M}^{-1}\mathbf{Q}(^t\mathbf{e}) \tag{2.85b}$$

As seen from Equation 2.85b, the nodal variable at the next increment, $^{t+\Delta t}\mathbf{e}$, can be evaluated by using the nodal variables at times t and $t - \Delta t$. At the first time step, the equation takes the following form.

$$^{\Delta t}\mathbf{e} = 2\,^{0}\mathbf{e} -\,^{-\Delta t}\mathbf{e} + \Delta t^2\mathbf{M}^{-1}\mathbf{Q}(^{0}\mathbf{e}) \tag{2.86}$$

In order to evaluate the nodal variables at the end of the first time step, the nodal variables at time $-\Delta t$ needs to be known besides $^{0}\mathbf{e}$. The unknown nodal variables vector, $^{-\Delta t}\mathbf{e}$, can be written in terms of the nodal velocity and the nodal acceleration vector at $t = 0$ as given below [12, 36].

$$^{-\Delta t}\mathbf{e} =\,^{0}\mathbf{e} - \Delta t\,^{0}\dot{\mathbf{e}} + \frac{\Delta t^2}{2}\,^{0}\ddot{\mathbf{e}} \tag{2.87}$$

Therefore, the vector of nodal variables at any time can be found easily with the known initial configurations.

2.7 Sample Solutions Based on the Literature using ANCF

In order to make comparisons between the current ANCF in the literature and the proposed methods in the following chapters, the reviewed formulations have been used for the solutions of some problems presented in the literature. Obtained results are identical to the published results. As examples, solutions for simple plate structure under time dependent loading and flexible pendulum problem are given in the following sections.

2.7.1 Simple Plate Structure under Time Dependent Point Loading

A simple plate structure under a time dependent point load, which has been studied by Mikkola A. M. and Shabana A. A. [30], is solved by ANCF method. The structure is kinematically fixed, however it undergoes large deformations. The length, width and thickness of the structure are 1.0 m, 1.0 m and 0.1 m, consecutively. Structure is fixed from one edge, and loaded with a time dependent force ($40t$ N) at a corner. In order to

show performance of ANCF in large deformation problem, modulus of elasticity and material density have been chosen as 0.1 MPa and 7800 kg/m^3.
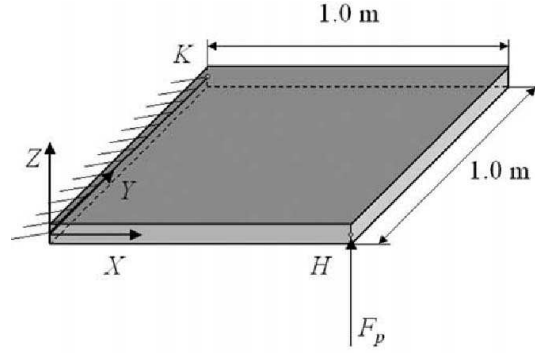
Figure 2.3: Simple plate structure [30]

Mikkola A. M. and Shabana A. A. [30] published solutions for the simple plate structure given in Figure 2.3 by using 4, 9, 25 and 49 ANCF elements. In order to verify the written codes, the structure is modeled with 4 elements in the thesis. Finite element model of the structure is shown in Figure 2.4. As shown in the figure, finite element model has 4 elements and 9 nodes. Total unconstrained degrees of freedom is 108. 3 nodes on the edge (Nodes 1, 4 and 7) are constrained. Time dependent point load is applied in Z direction to Node 3. Equations of motion have been solved with 0.01 s time increment for a total time of 1 s. Global position of Node 3 over time is shown in Figure 2.5. Additionally, deformed shape of the structure at $t = 1$ s is shown in Figure 2.6. Obtained results are identical with the results published by Mikkola A. M. and Shabana A. A. [30].
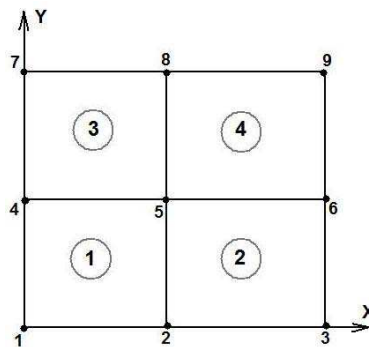
Figure 2.4: Finite element model for simple plate structure
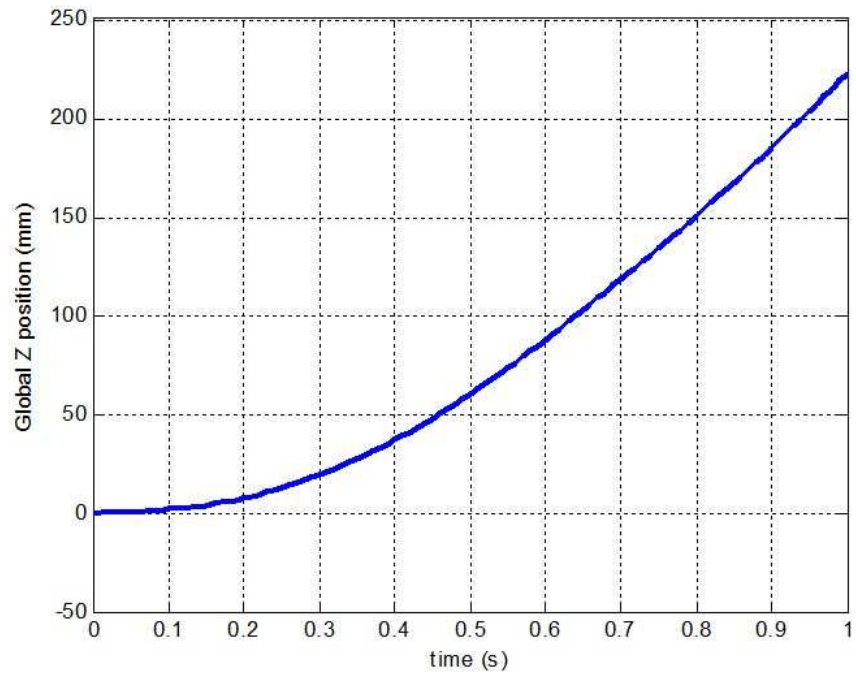
Figure 2.5: Global Z coordinate of Node 3
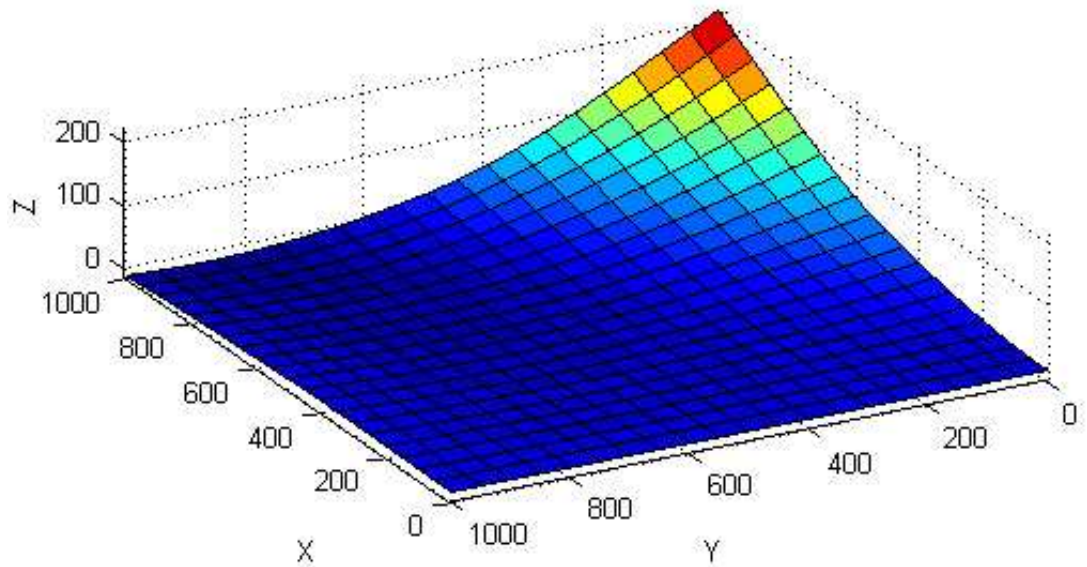
Figure 2.6: Deformed shape of the simple plate structure at $t = 1\ s$

2.7.2 Flexible Plate Pendulum

As a second example, flexible plate pendulum problem published by Mikkola A. M. and Shabana A. A. [30] has been studied. Length and width of the plate are shown in Figure 2.7. Thickness, modulus of elasticity and density of the plate are $10\,mm$, $0.1\,MPa$ and $7810\,kg/m^3$, consecutively. One corner of the structure is constrained by a spherical joint. Then, it is subjected to gravity. Finite element model for the plate is shown in Figure 2.8. As shown in the figure, pendulum is modeled with 3 plate elements and 8 nodes. Total unconstrained degrees of freedom for the system is 96. Equation of motion is solved with a time increment of $10^{-3}\,s$ for a total time of 1.4 seconds.
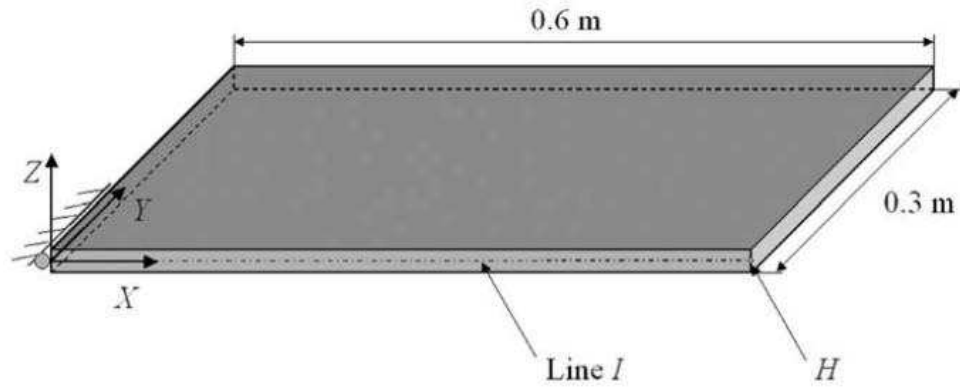
Figure 2.7: Flexible plate pendulum [30]
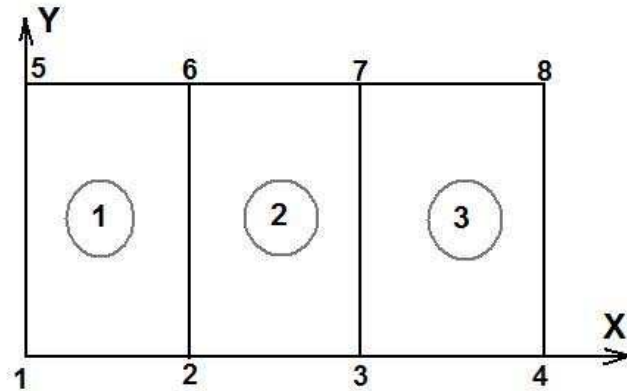
Figure 2.8: Finite element model for flexible plate pendulum

Global position of Node 4 is plotted over time in Figure 2.9. As seen from the graph, magnitude of the global position vector is changing in a large range. If the pendulum were rigid, then the magnitude of position vector would be constant over time. This can give an idea about the flexibility of the pendulum.
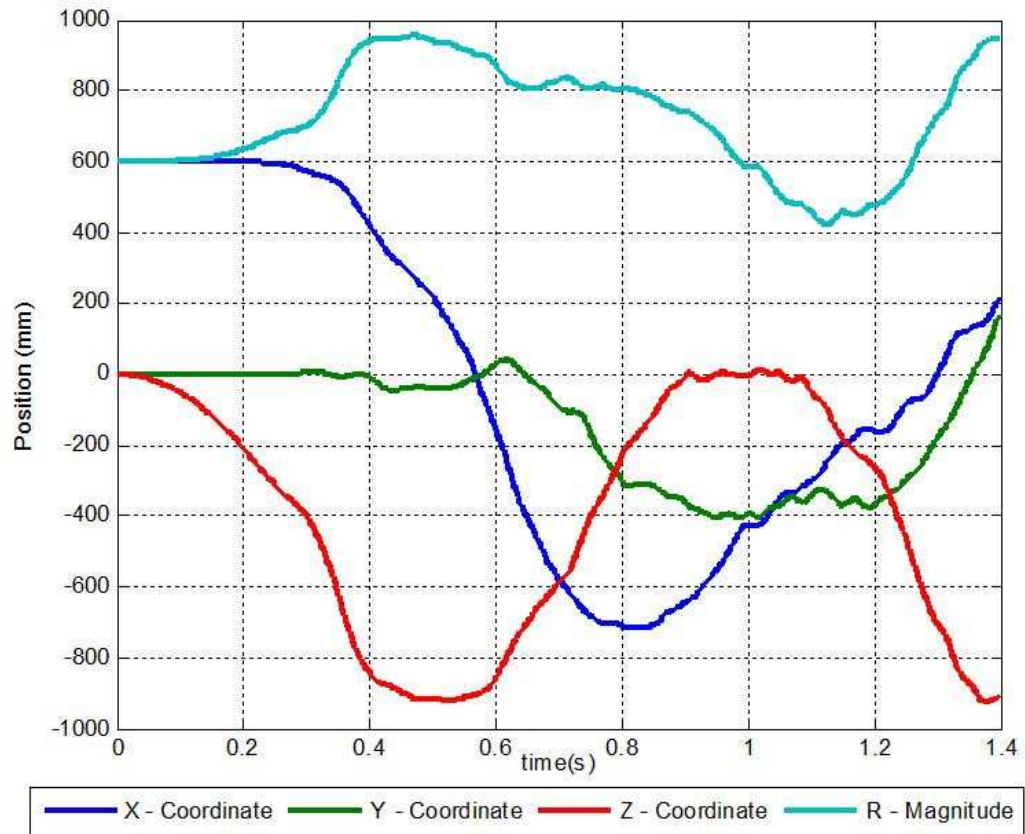
Figure 2.9: Global coordinate of Node 4 over time

Additionally, configurations of the pendulum at some selected instants are shown in Figure 2.10. Despite the small number of elements used in the analysis, large deformation and rotation characteristics of plate have been captured with 4 noded ANCF plate element as shown in the figure. In summary, obtained results are identical to the results published by Mikkola A. M. and Shabana A. A. [30].
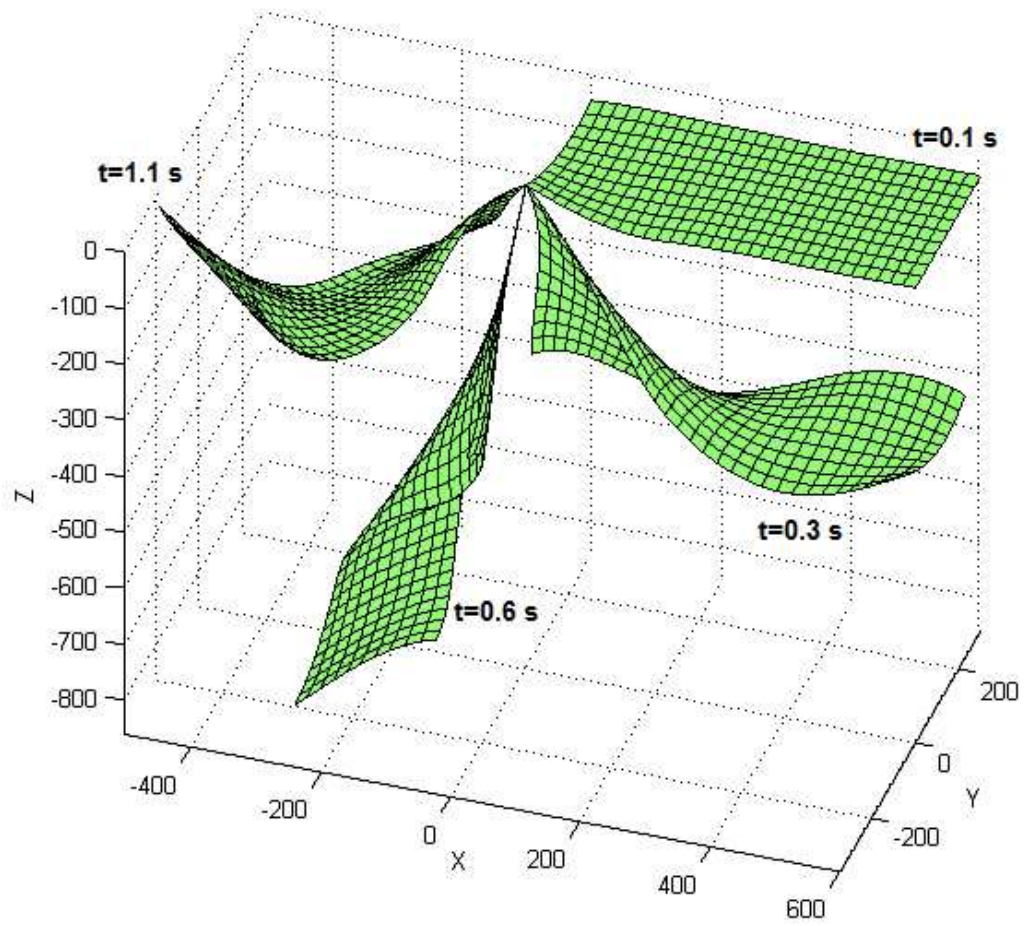
Figure 2.10: Flexible pendulum configurations over time

CHAPTER 3

APPLICATION OF MESHFREE METHOD TO ANCF

3.1 Meshfree Methods

As described in the previous chapters, solution procedures for flexible multibody dynamics problems are mainly based on the Finite Element Method (FEM). Therefore, flexible bodies have to be discretized by predefined meshes. Then, equations of motion could be formulated based on this discretization. It is clear that the shape and the density of the mesh have a great importance in the solution. Therefore, they should be carefully designed to obtain accurate solutions. Despite the flexible multibody dynamics literature has focused on FEM, there are some other methods that could be useful. Meshfree method is a recently developed alternative to FEM for structural mechanics problems. In meshfree method, system equations are established without the use of a predefined mesh [37]. Additionally, it is shown that the accuracy in structural mechanics problems can be increased by using meshfree methods instead of FEM [37, 38].

In this chapter, meshfree method is implemented to flexible multibody problems. Therefore, short definitions and classifications related to the meshfree method are included in the chapter. The most of the literature, which are related to the meshfree method, has been collected within two books by G. R. Liu [37] and G. R. Liu and Y. T. Gu [38]. Those meshfree related books are completing each other. In the thesis, these books were the major references for the meshfree related topics.

The main starting point of the meshfree method was to eliminate mesh generation process from the design cycle, and it was partly succeeded in literature. For beam, plate and shell type structures meshing process is not as difficult as complex solid parts. However, by introducing

meshfree method to flexible multibody dynamics problems, more accurate results could be obtained without the limitations of finite element method, which are listed by G. R. Liu and Y. T. Gu [38] as follows:

1. *High cost in creating an FEM mesh* [38]

2. *Low accuracy of stress:* Many FEM packages do not accurately predict stress. The stresses obtained in FEM are often discontinuous at the interfaces of the elements due to the piecewise (or element-wise) continuous nature of the displacement field assumed in the FEM formulation [38].

3. *Difficulty in adaptive analysis:* One of the current new demands on FEM analysis is to ensure the accuracy of the solution [38].

4. *Limitation in the analysis of some problems [38]:*

   - Under large deformations, considerable loss in accuracy in FEM results can arise from the element distortions [38].

   - It is difficult to simulate crack growth with arbitrary and complex paths which do not coincide with the original element interfaces [38].

   - It is very difficult to simulate the breakage of material with large number of fragments; the FEM is based on continuum mechanics, in which the elements cannot be broken; an element must either stay as a whole, or disappear completely. This usually leads to a misrepresentation of the breakage path [38].

In this chapter, ANCF of shear deformable planar beams using meshfree interpolation polynomials is performed. Structural meshfree formulations are generally starts with the selection of interpolation methods. In the literature, there are various interpolation techniques specialized to specific problems to be solved [37–39]. The most widely used one is the Point Interpolation Method. The method is very simple and adaptable. However, it has some drawbacks besides its advantages. As a starting point, Polynomial Point Interpolation Method (PPIM) was selected. In PPIM, a field variable (global X position in this case) can be written as follows.

$$e_1(x, y, x_Q) = X(x, y, x_Q) = \sum_{i=1}^{3n} p_i(x, y)\, a_i(x_Q) = \mathbf{p}^T(x, y)\, \mathbf{a}(x_Q) = \mathbf{p}\, \mathbf{a} \qquad (3.1)$$

It was seen that PPIM is not appropriate for shear deformable nonlinear beams due to non-invertible moment matrix. Generally, this problem arises from inline node placements. Theoretically, this situation can be circumvented by the following methods [37].

- Moving nodes within the solution domain: If one considers straight beam along a global X axis, it is not possible or realistic to move nodes toward *Y* axis. Therefore, this approach is not applicable to meshfree ANCF of beams.

- Polynomial PIM with Coordinate transformation: This method had been implemented for planar beam problems. However, obtained moment matrix was still non-invertible.

- Matrix triangulation algorithm: The algorithm is based on the proper selection of the interpolating nodes within the solution domain. However, this would not solve the problem for ANCF of beams.

- Radial point interpolation method: The method guarantees non-singular moment matrix. However, number of basis functions is not adequate for the solution of nodal variables. It results in non-square matrices.

- Radial point interpolation with polynomial reproduction: The method guarantees the non-singular moment matrix for meshfree ANCF of planar beams.

As listed above, some methods have been performed for shear deformable planar beam formulation and it is seen that the most appropriate method is the radial point interpolation with polynomial reproduction. Therefore, the following nonlinear beam formulation is based on this method.

3.2 Construction of Shape Function for Planar Beams

In ANCF, nodes have 6 degrees of freedom for planar problems. Those are global positions, *X* and *Y*, and gradients, $\partial X/\partial x$, $\partial Y/\partial x$, $\partial X/\partial y$ and $\partial Y/\partial y$. For the ith node of the system, degrees of freedom are defined as e_1^i, e_2^i, e_3^i, e_4^i, e_5^i and e_6^i. In meshfree methods, support domains, Ω_s, are used to interpolate field variables instead of finite elements. Support domains are generally represented by a point of interest (or quadrature point) at their center as shown in Figure 3.1.
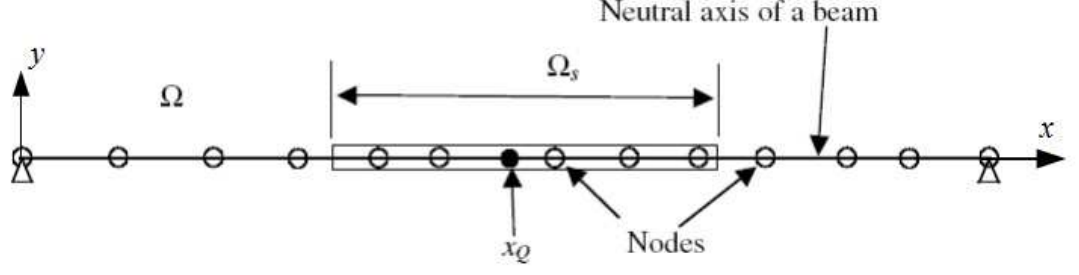
Figure 3.1: Support domain for planar beams [38]

Then, global positions of an arbitrary point in the support domain of a point of interest at x_Q can be written as follows.

$$X(x, y, x_Q) = \sum_{i=1}^{n} R_i(x, y) \, a_i(x_Q) + \sum_{j=1}^{2n} p_j(x, y) \, b_j(x_Q)$$

$$X(x, y, x_Q) = \mathbf{R}^T(x, y) \, \mathbf{a}(x_Q) + \mathbf{P}^T(x, y) \, \mathbf{b}(x_Q) = \mathbf{R}^T \, \mathbf{a} + \mathbf{P}^T \mathbf{b} \qquad (3.2)$$

In Equation 3.2, $\mathbf{P}$ and $\mathbf{R}$ represent polynomial basis and multiquadratic radial basis vectors and they are given below [38].

$$R_i = \left((x - x_i)^2 + (y - y_i)^2 + C^2 \right)^q \qquad (3.3)$$

$$\mathbf{P} = \begin{bmatrix} 1 & x & y & xy & x^2 & x^2y & x^3 & x^3y & x^4 & x^4y & x^5 & x^5y & ... \end{bmatrix}^T \qquad (3.4)$$

where C and q are constants of radial basis function and can be determined depending on the convergence of the problem.

Similarly, Y component of global position vector can be written as follows.

$$Y(x, y, x_Q) = \mathbf{R}^T(x, y) \, \mathbf{c}(x_Q) + \mathbf{P}^T(x, y) \, \mathbf{d}(x_Q) = \mathbf{R}^T \, \mathbf{c} + \mathbf{P}^T \mathbf{d} \qquad (3.5)$$

In Equations 3.2 and 3.5, a_i, b_j, c_i and d_j represent coefficients for basis functions. By using 3.2 and 3.5, global position vector can be written in terms of basis functions in matrix form

47

as given below.

$$\mathbf{r}(x, y, x_Q) = \begin{bmatrix} \mathbf{R}^T(x, y) & \mathbf{P}^T(x, y) & \mathbf{0} & \mathbf{0} \\ \mathbf{0} & \mathbf{0} & \mathbf{R}^T(x, y) & \mathbf{P}^T(x, y) \end{bmatrix} \begin{bmatrix} \mathbf{a} \\ \mathbf{b} \\ \mathbf{c} \\ \mathbf{d} \end{bmatrix} \tag{3.6}$$

Then, the gradients can be determined by partial differentiation with respect to local coordinates x and y as given in the following equations.

$$\frac{\partial X(x, y, x_Q)}{\partial x} = \mathbf{R}_{,x}^T \, \mathbf{a} + \mathbf{P}_{,x}^T \, \mathbf{b} \tag{3.7a}$$

$$\frac{\partial Y(x, y, x_Q)}{\partial x} = \mathbf{R}_{,x}^T \, \mathbf{c} + \mathbf{P}_{,x}^T \, \mathbf{d} \tag{3.7b}$$

$$\frac{\partial X(x, y, x_Q)}{\partial y} = \mathbf{R}_{,y}^T \, \mathbf{a} + \mathbf{P}_{,y}^T \, \mathbf{b} \tag{3.7c}$$

$$\frac{\partial Y(x, y, x_Q)}{\partial y} = \mathbf{R}_{,y}^T \, \mathbf{c} + \mathbf{P}_{,y}^T \, \mathbf{d} \tag{3.7d}$$

Coefficients of basis functions ($\mathbf{a}$, $\mathbf{b}$, $\mathbf{c}$ and $\mathbf{d}$) can be determined by enforcing Equations 3.2, 3.5 and 3.7 to be satisfied at the n nodes within the support domain. For the ith node, degrees of freedom can be calculated as given below.

$$\mathbf{e}^i = \begin{bmatrix} \mathbf{R}_i^T & \mathbf{P}_i^T & \mathbf{0} & \mathbf{0} \\ \mathbf{0} & \mathbf{0} & \mathbf{R}_i^T & \mathbf{P}_i^T \\ \mathbf{R}_{i,x}^T & \mathbf{P}_{i,x}^T & \mathbf{0} & \mathbf{0} \\ \mathbf{0} & \mathbf{0} & \mathbf{R}_{i,x}^T & \mathbf{P}_{i,x}^T \\ \mathbf{R}_{i,y}^T & \mathbf{P}_{i,y}^T & \mathbf{0} & \mathbf{0} \\ \mathbf{0} & \mathbf{0} & \mathbf{R}_{i,y}^T & \mathbf{P}_{i,y}^T \end{bmatrix}_{6x6n} \begin{bmatrix} \mathbf{a} \\ \mathbf{b} \\ \mathbf{c} \\ \mathbf{d} \end{bmatrix}_{6nx1} \tag{3.8}$$

If Equation 3.8 is generalized to n nodes in the support domain, the following set of algebraic equations can be obtained.

$$\mathbf{e}_s = \mathbf{P}_Q \, \mathbf{A} \tag{3.9}$$

48

where $\mathbf{e}_s$ is the vector of nodal variables for the support domain, $\mathbf{P}_Q$ is the generalized moment matrix evaluated at n nodes within the support domain, Ω_s, and $\mathbf{A}$ is the vector of constants of basis functions as shown in the following equations.

$$\mathbf{e}_s = \begin{bmatrix} e_1^1 & e_2^1 & e_3^1 & e_4^1 & e_5^1 & e_6^1 & . & . & e_1^n & e_2^n & e_3^n & e_4^n & e_5^n & e_6^n \end{bmatrix} \tag{3.10a}$$

$$\mathbf{P}_Q = \begin{bmatrix} \mathbf{R}_1^T & \mathbf{P}_1^T & \mathbf{0} & \mathbf{0} \\ \mathbf{0} & \mathbf{0} & \mathbf{R}_1^T & \mathbf{P}_1^T \\ \mathbf{R}_{1,x}^T & \mathbf{P}_{1,x}^T & \mathbf{0} & \mathbf{0} \\ \mathbf{0} & \mathbf{0} & \mathbf{R}_{1,x}^T & \mathbf{P}_{1,x}^T \\ \mathbf{R}_{1,y}^T & \mathbf{P}_{1,y}^T & \mathbf{0} & \mathbf{0} \\ \mathbf{0} & \mathbf{0} & \mathbf{R}_{1,y}^T & \mathbf{P}_{1,y}^T \\ . & . & . & . \\ . & . & . & . \\ \mathbf{R}_n^T & \mathbf{P}_n^T & \mathbf{0} & \mathbf{0} \\ \mathbf{0} & \mathbf{0} & \mathbf{R}_n^T & \mathbf{P}_n^T \\ \mathbf{R}_{n,x}^T & \mathbf{P}_{n,x}^T & \mathbf{0} & \mathbf{0} \\ \mathbf{0} & \mathbf{0} & \mathbf{R}_{n,x}^T & \mathbf{P}_{n,x}^T \\ \mathbf{R}_{n,y}^T & \mathbf{P}_{n,y}^T & \mathbf{0} & \mathbf{0} \\ \mathbf{0} & \mathbf{0} & \mathbf{R}_{n,y}^T & \mathbf{P}_{n,y}^T \end{bmatrix}_{6n x 6n} \tag{3.10b}$$

$$\mathbf{A} = \begin{bmatrix} \mathbf{a}^T & \mathbf{b}^T & \mathbf{c}^T & \mathbf{d}^T \end{bmatrix}_{6n x 1}^T \tag{3.10c}$$

Then, constants of basis functions, $\mathbf{A}$, can be evaluated by matrix inversion as given below.

$$\mathbf{A} = \mathbf{P}_Q^{-1} \, \mathbf{e}_s \tag{3.11}$$

By substituting Equation 3.11 into Equation 3.6, global position vector can be written in terms of known polynomial constants and body coordinates as given in the following equation.

$$\mathbf{r}(x, y, x_Q) = \mathbf{S}(x, y, x_Q) \, \mathbf{e}_s \tag{3.12}$$

where, $\mathbf{S}$ is the shape function matrix for the support domain, Ω_s, and defined below.

$$S(x, y, x_Q) = \begin{bmatrix} \mathbf{R}^T(x, y) & \mathbf{P}^T(x, y) & \mathbf{0} & \mathbf{0} \\ \mathbf{0} & \mathbf{0} & \mathbf{R}^T(x, y) & \mathbf{P}^T(x, y) \end{bmatrix} \mathbf{P}_Q^{-1} \tag{3.13}$$

3.3 Mass Matrix Formulation of Meshfree Planar Beam with ANCF

In meshfree solution procedures, integrations are generally performed within the predefined quadrature domains, Ω_q. Therefore, kinetic energy equation (Equation 2.58) will be integrated over quadrature domains. Then, the kinetic energy of the whole deformable body can be summed by simple assembly procedures as in general finite element methods. Kinetic energy of the quadrature domain, Ω_q, in the support domain, Ω_s, of the body can be evaluated by using shape function matrix as given below.

$$T_q = \frac{1}{2} \int_{V_q} {}^t\rho \, \dot{\mathbf{e}}_s^T \, \mathbf{S}^T(x, y) \, \mathbf{S}(x, y) \, \dot{\mathbf{e}}_s \, d^t V_q \tag{3.14a}$$

$$T_q = \frac{1}{2} \dot{\mathbf{e}}_s^T \left[\int_{V_q} {}^t\rho \, \mathbf{S}^T(x, y) \, \mathbf{S}(x, y) \, d^t V_q \right] \dot{\mathbf{e}}_s \tag{3.14b}$$

$$T_q = \frac{1}{2} \dot{\mathbf{e}}_s^T \mathbf{M}_{sq} \, \dot{\mathbf{e}}_s \tag{3.14c}$$

where $\mathbf{M}_{sq}$ is the mass matrix of the integrated part of the body (quadrature domain) and given explicitly as follows.

$$\mathbf{M}_{sq} = \int_{V_q} {}^t\rho \, \mathbf{S}^T(x, y) \, \mathbf{S}(x, y) \, d^t V_q \tag{3.15}$$

Density and volume increment at an arbitrary time, t, can be written in terms of initial density and volume increment [36]. Then, the volume integration can be performed at initial configuration as given;

$$\mathbf{M}_{sq} = {}^0\rho \int_{V_q} \mathbf{S}^T(x, y) \, \mathbf{S}(x, y) \, d^0 V_q \tag{3.16}$$

50

By introducing the shape function matrix defined in Equation 3.12 into Equation 3.16, one can obtain the explicit form of the mass matrix of quadrature domain as given in the following equation.

$$\mathbf{M_{sq}} = \rho \, (\mathbf{P}_q^{-1})^T \int\limits_{V_q} \begin{bmatrix} \mathbf{R} & \mathbf{0} \\ \mathbf{P} & \mathbf{0} \\ \mathbf{0} & \mathbf{R} \\ \mathbf{0} & \mathbf{P} \end{bmatrix} \begin{bmatrix} \mathbf{R}^T & \mathbf{P}^T & \mathbf{0} & \mathbf{0} \\ \mathbf{0} & \mathbf{0} & \mathbf{R}^T & \mathbf{P}^T \end{bmatrix} dV_q \mathbf{P}_q^{-1} \tag{3.17}$$

3.4 Generalized Elastic Forces for ANCF of Meshfree Planar Beam

Strain energy equation can be used to find generalized elastic forces as in general flexible multibody procedures. The strain energy equation for a quadrature domain, Ω_q, can be written as given below.

$$U_q = \frac{1}{2} \int\limits_V \boldsymbol{\varepsilon}_q^T \, \mathbf{E} \boldsymbol{\varepsilon}_q dV_q \tag{3.18}$$

In Equation 3.18, $\mathbf{E}$ represents matrix of elastic coefficients and $\boldsymbol{\varepsilon}_q$ stands for the vector form of strain tensor, $\boldsymbol{\varepsilon}_m$, within the quadrature domain, Ω_q. Matrix of elastic coefficients can be written in terms of modulus of elasticity, E, and Poisson's Ratio, v, as follows [21].

$$\mathbf{E} = \begin{bmatrix} \lambda + 2\mu & \lambda & 0 \\ \lambda & \lambda + 2\mu & 0 \\ 0 & 0 & 2\mu \end{bmatrix} \tag{3.19a}$$

$$\lambda = \frac{vE}{(1 + v)(1 - 2v)} \tag{3.19b}$$

$$\mu = \frac{E}{2(1 + v)} \tag{3.19c}$$

Nonlinear strain tensor, $\boldsymbol{\varepsilon}_m$, can be formulated in terms of deformation gradient, $\mathbf{J}$, as given below.

51

$$\varepsilon_m = \frac{1}{2}\left(\mathbf{J}^T\,\mathbf{J} - \mathbf{I}\right) \tag{3.20}$$

where $\mathbf{I}$ is identity matrix and $\mathbf{J}$ is the deformation gradient defined as;

$$\mathbf{J} = \frac{\partial\,{}^t\mathbf{r}}{\partial\,{}^0\mathbf{r}} \tag{3.21}$$

Then, it can be written in terms of shape function, $\mathbf{S}$, and vector of nodal variables, $\mathbf{e}_s$, as given below.

$$\mathbf{J} = \frac{\partial\,{}^t\mathbf{r}}{\partial\,{}^0\mathbf{r}} = \frac{\partial\,{}^t\mathbf{r}}{\partial\,\mathbf{x}}\frac{\partial\,\mathbf{x}}{\partial\,{}^0\mathbf{r}} = \begin{bmatrix} \mathbf{S}_{1,x}\,\mathbf{e}_s & \mathbf{S}_{1,y}\,\mathbf{e}_s \\ \mathbf{S}_{2,x}\,\mathbf{e}_s & \mathbf{S}_{2,y}\,\mathbf{e}_s \end{bmatrix}\mathbf{D}^{-1} \tag{3.22}$$

If the body coordinate frame is parallel to the global coordinate frame, then $\mathbf{D}$ reduces to identity matrix. In the meshfree formulation of planar beam, it is assumed that the coordinate frames are parallel. By eliminating transformation matrix, components of strain vector can be written as;

$$\varepsilon_1 = \frac{1}{2}(\mathbf{e}_s^T\,\mathbf{S}_a\,\mathbf{e}_s - 1) \tag{3.23a}$$

$$\varepsilon_2 = \frac{1}{2}(\mathbf{e}_s^T\,\mathbf{S}_b\,\mathbf{e}_s - 1) \tag{3.23b}$$

$$\varepsilon_3 = \frac{1}{2}\mathbf{e}_s^T\,\mathbf{S}_c\,\mathbf{e}_s \tag{3.23c}$$

where

$$\mathbf{S}_a = \mathbf{S}_{1,x}^T\,\mathbf{S}_{1,x} + \mathbf{S}_{2,x}^T\,\mathbf{S}_{2,x} \tag{3.24a}$$

$$\mathbf{S}_b = \mathbf{S}_{1,y}^T\,\mathbf{S}_{1,y} + \mathbf{S}_{2,y}^T\,\mathbf{S}_{2,y} \tag{3.24b}$$

$$\mathbf{S}_c = \mathbf{S}_{1,x}^T\,\mathbf{S}_{1,y} + \mathbf{S}_{2,x}^T\,\mathbf{S}_{2,y} \tag{3.24c}$$

Then, the vectorial form of strain tensor and its partial derivative within the quadrature domain can be written as a function of nodal variables within the support domain as follows.

$$\boldsymbol{\varepsilon}_q = \begin{bmatrix} \varepsilon_1 \\ \varepsilon_2 \\ \varepsilon_3 \end{bmatrix} = \frac{1}{2} \begin{bmatrix} \mathbf{e}_s^T \, \mathbf{S}_{a(q)} \, \mathbf{e}_s - 1 \\ \mathbf{e}_s^T \, \mathbf{S}_{b(q)} \, \mathbf{e}_s - 1 \\ \mathbf{e}_s^T \, \mathbf{S}_{c(q)} \, \mathbf{e}_s \end{bmatrix} \tag{3.25a}$$

$$\frac{\partial \boldsymbol{\varepsilon}_q}{\partial \mathbf{e}_s} = \begin{bmatrix} \mathbf{e}_s^T \, \mathbf{S}_{a(q)} \\ \mathbf{e}_s^T \, \mathbf{S}_{b(q)} \\ \frac{1}{2} \, \mathbf{e}_s^T \left(\mathbf{S}_{c(q)} + \mathbf{S}_{c(q)}^T \right) \end{bmatrix} \tag{3.25b}$$

The generalized elastic forces on nodes within the support domain of a quadrature point due to elastic potential can be obtained by differentiating the strain energy with respect to the nodal variables as given in the following equation.

$$\mathbf{Q}_k^T = \frac{\partial U_q}{\partial \mathbf{e}_s} = \frac{\partial}{\partial \mathbf{e}_s} \left\{ \frac{1}{2} \int_{V_q} \boldsymbol{\varepsilon}_q^T \mathbf{E} \boldsymbol{\varepsilon}_q \, dV_q^0 \right\} = \int_{V_q} \left(\frac{\partial \boldsymbol{\varepsilon}_q}{\partial \mathbf{e}_s} \right)^T \mathbf{E} \boldsymbol{\varepsilon}_q \, dV_q^0 \tag{3.26}$$

By substituting Equations 3.25a and 3.25b into Equation 3.26, the generalized elastic force vector can be written in an explicit form given in the following equation.

$$\mathbf{Q}_k^T = \int_{V_q} \begin{bmatrix} \mathbf{e}_s^T \mathbf{S}_a & \mathbf{e}_s^T \mathbf{S}_b & \frac{1}{2} \mathbf{e}_s^T (\mathbf{S}_c + \mathbf{S}_c^T) \end{bmatrix} \begin{bmatrix} \lambda + 2\mu & \lambda & 0 \\ \lambda & \lambda + 2\mu & 0 \\ 0 & 0 & 2\mu \end{bmatrix} \frac{1}{2} \begin{bmatrix} (\mathbf{e}_s^T \mathbf{S}_a \mathbf{e}_s - 1) \\ (\mathbf{e}_s^T \mathbf{S}_b \mathbf{e}_s - 1) \\ \mathbf{e}_s^T \mathbf{S}_c \mathbf{e}_s \end{bmatrix} dV_q \tag{3.27a}$$

$$\mathbf{Q}_k^T = \frac{1}{2} \int_{V_q} \mathbf{e}_s^T \begin{bmatrix} ((\lambda + 2\mu)\mathbf{S}_a + \lambda \mathbf{S}_b)(\mathbf{e}_s^T \mathbf{S}_a \mathbf{e}_s - 1) \cdots \\ + (\lambda \mathbf{S}_a + (\lambda + 2\mu)\mathbf{S}_b)(\mathbf{e}_s^T \mathbf{S}_b \mathbf{e}_s - 1) + \mu(\mathbf{S}_c + \mathbf{S}_c^T)\mathbf{e}_s^T \mathbf{S}_c \mathbf{e}_s \end{bmatrix} dV_q \tag{3.27b}$$

Then, generalized elastic forces of deformable bodies can be assembled by using the forces obtained for quadrature domains.

3.5   Generalized Gravitational Forces for ANCF of Meshfree Planar Beam

Generalized external forces can be obtained as in the general flexible multibody procedure. As an example, distributed gravitational force directed toward the $-Y$ axis is expressed as the

generalized force associated with the absolute nodal coordinates of an arbitrary quadrature domain as follows.

$$\mathbf{Q}_F^T = \mathbf{F}^T \mathbf{S} = \int\limits_{V_q} [0 - \rho g] \, \mathbf{S} dV_q = \int\limits_{V_q} -\rho g \mathbf{S}_2 dV_q \tag{3.28}$$

3.6 Equation of Motion and Solution Procedure for Meshfree Planar Beams with ANCF

For the solution of system equations, which contain mass matrix and generalized forces, same procedure described in Section 2.6 can be used. However, it is required to assemble quadrature domains instead of elements in order to construct equations of motion for the whole system. Equation of motion for an arbitrary quadrature domain can simply be written as follows;

$$\mathbf{M}_{sq} \ddot{\mathbf{e}}_s + \mathbf{Q}_k(\mathbf{e}_s) = \mathbf{Q}_F \tag{3.29}$$

3.7 Comparison of Meshfree and FEM based ANCFs for Planar Beams

In order to verify performance of the developed meshfree formulation, comparison study for a flexible pendulum problem, which is the major problem for the demonstration of newly developed methods in literature, has been performed. It is assumed that the flexible pendulum has a rectangular cross-section, 1.2 *m* length, density of 7800 kg/m^3 and 1 *MPa* of modulus of elasticity. The pendulum, shown in Figure 3.2, is grounded at $(0, 0)$ local coordinates. Comparison study is performed for three different thicknesses (40 *mm*, 10 *mm* and 2 *mm*).

3.7.1 Results of FEM based ANCF of Shear Deformable Planar Beams

In order to see advantages of meshfree formulation, a convergence study had been performed with finite element based ANCF of shear deformable planar beams. Number of elements is increased up to certain level of convergence. Flexible pendulum problem shown in Figure 3.2 is solved for a duration of 1 *s* with 10^{-5} *s* time intervals using 3, 6, 9 and 12 elements.
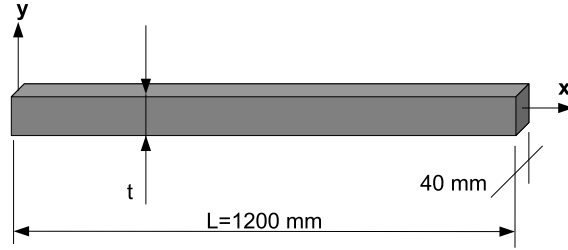
Figure 3.2: Flexible pendulum for comparison study

Obtained results for different thicknesses are presented in Figure 3.3 through Figure 3.11. As seen from the figures, number of elements required for convergence is increasing with decreasing beam thickness. Convergence seems to be satisfied with 12 elements for the beam having thickness of 2 *mm*. However, 9 elements for 10 *mm* thickness and 6 elements for 40 *mm* thickness are adequate.
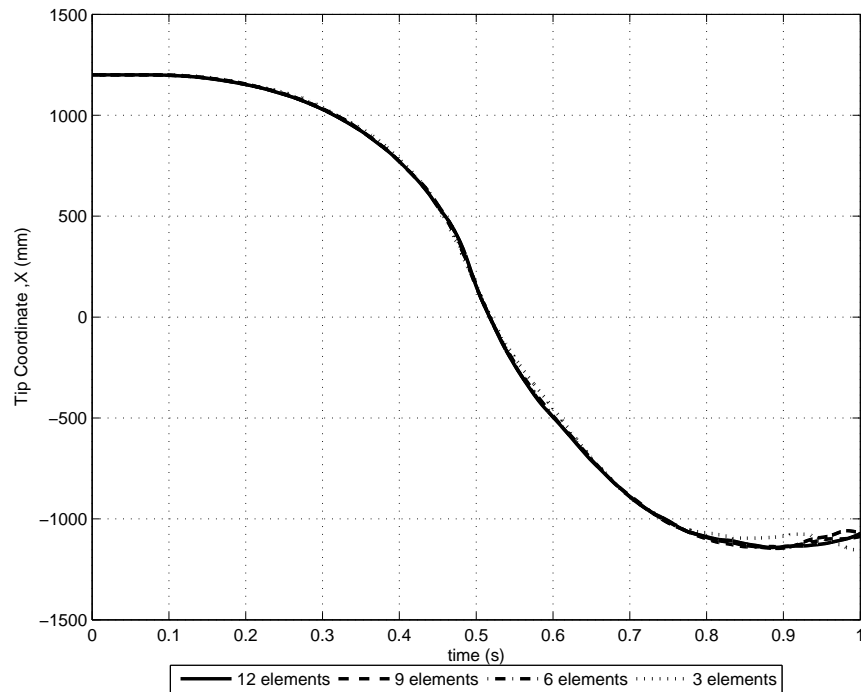
Figure 3.3: Tip coordinate, *X*, versus time for FEM based ANCF (t = 2 mm)
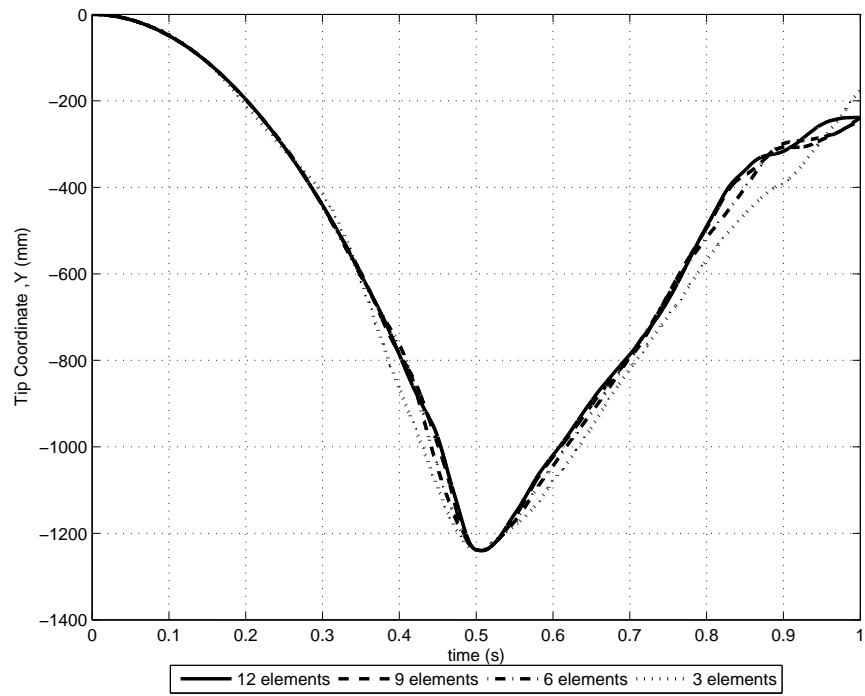
Figure 3.4: Tip coordinate, Y, versus time for FEM based ANCF (t = 2 mm)
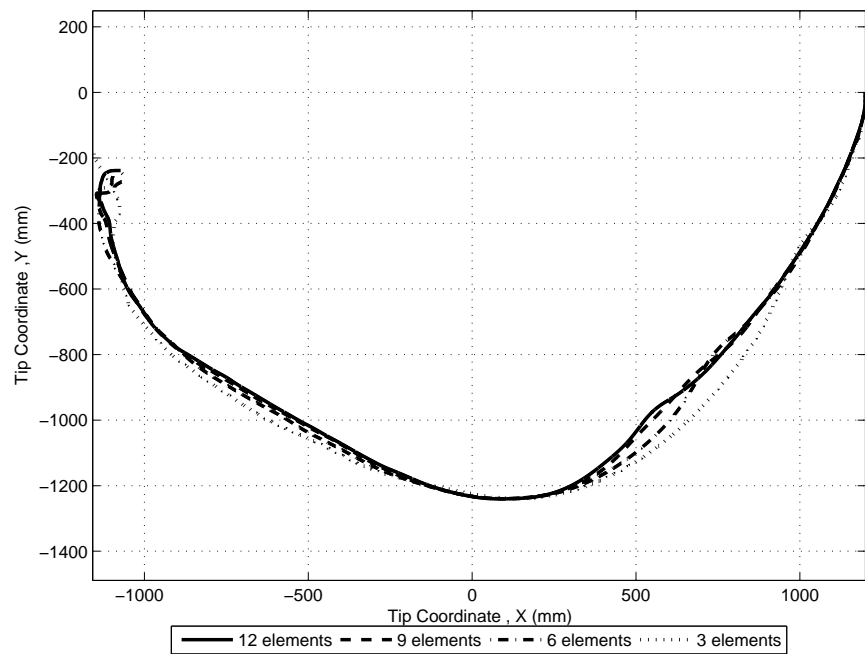
Figure 3.5: Route of the tip for FEM based ANCF (t = 2 mm)

56
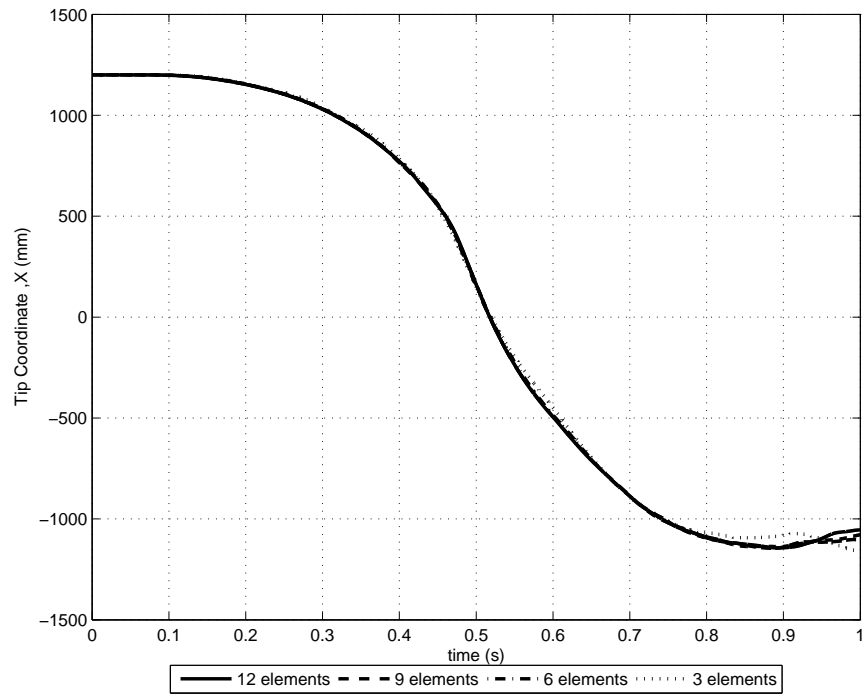
Figure 3.6: Tip coordinate, *X*, versus time for FEM based ANCF (t = 10 mm)
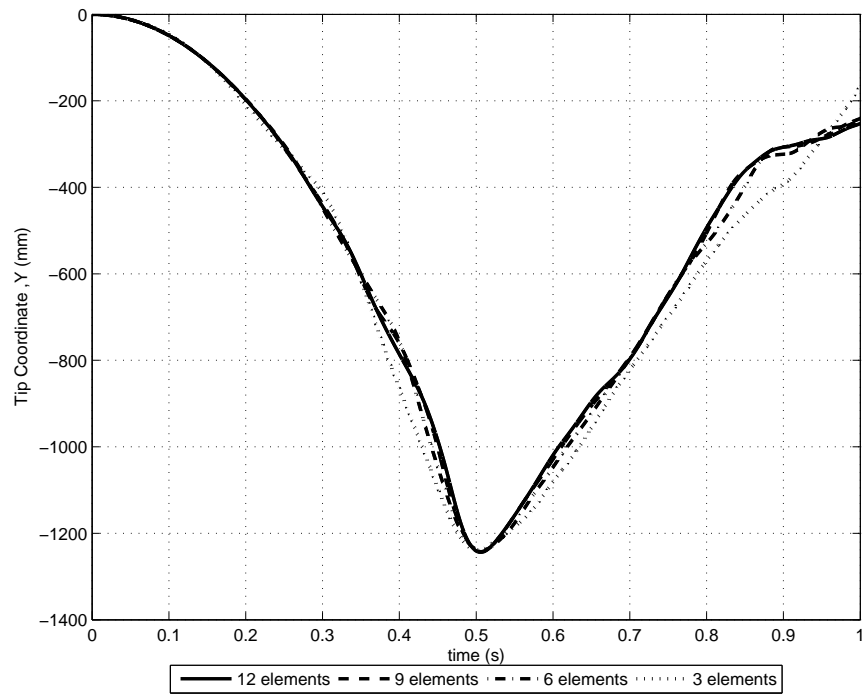
Figure 3.7: Tip coordinate, *Y*, versus time for FEM based ANCF (t = 10 mm)
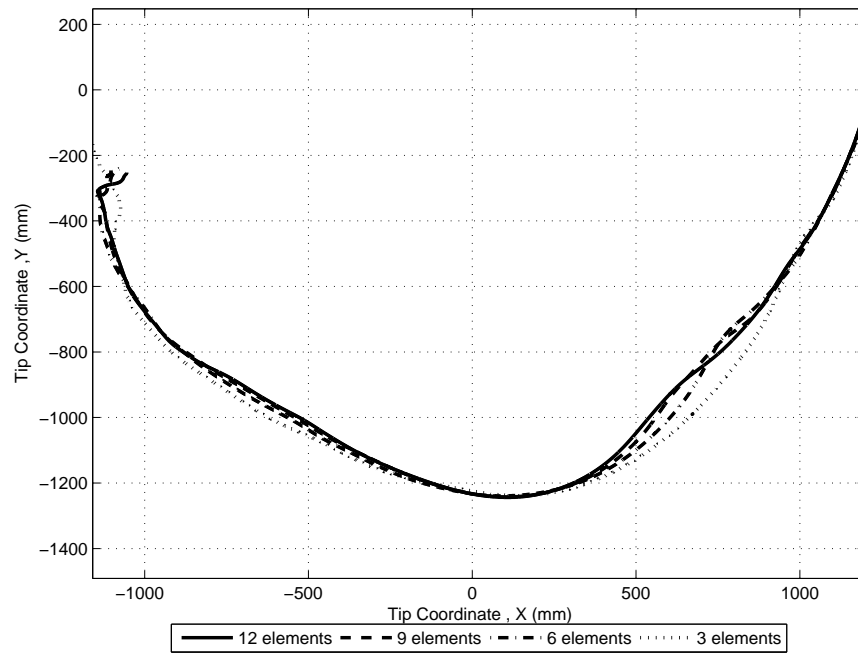
Figure 3.8: Route of the tip for FEM based ANCF (t = 10 mm)
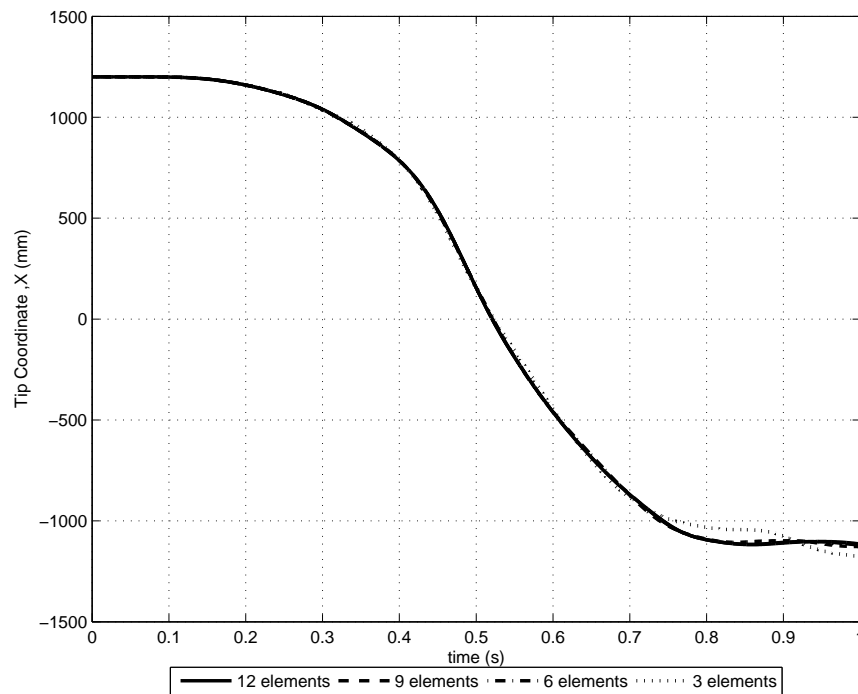
Figure 3.9: Tip coordinate, *X*, versus time for FEM based ANCF (t = 40 mm)
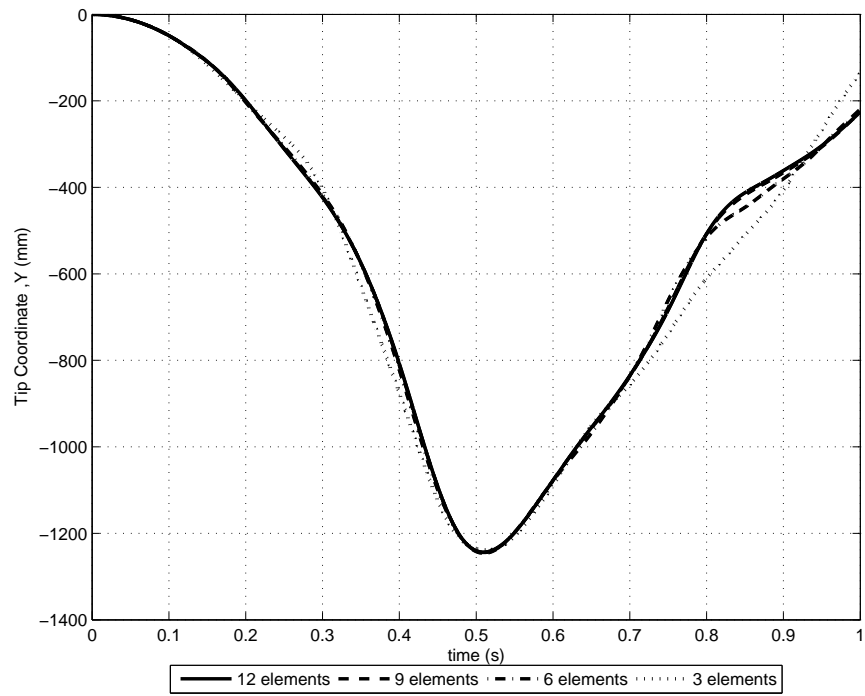
Figure 3.10: Tip coordinate, *Y*, versus time for FEM based ANCF (t = 40 mm)
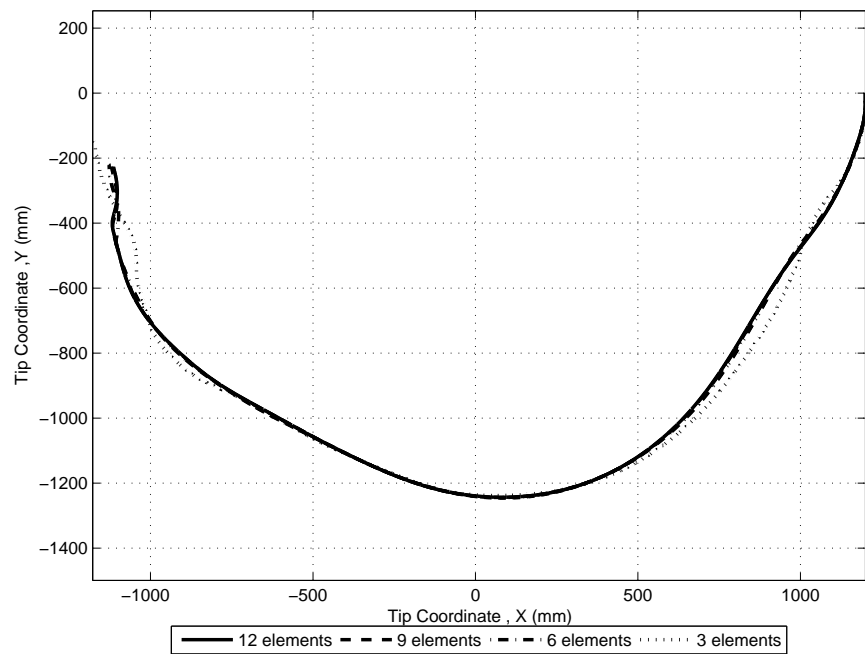
Figure 3.11: Route of the tip for FEM based ANCF (t = 40 mm)

3.7.2 Results Obtained by Meshfree ANCF of Flexible Pendulum

In the meshfree solution of flexible pendulum shown in Figure 3.2, the problem is modeled by using 7 nodes. Volume integrations appearing in the system equations are performed with 6 quadrature domains using 6 support domains as shown in Figure 3.12. In the solution, shape function matrix is not constructed for each quadrature points within the relevant quadrature domain. Instead of this, single shape function matrix is constructed for each quadrature domains using related support domain. Then, they are used for each quadrature points within owning quadrature domains. Obtained results are compared with the results of FEM based ANCF of shear deformable beams for 2 *mm*, 10 *mm* and 40 *mm* thick flexible pendulums in Figure 3.13 through Figure 3.21. Despite fewer number of nodes in meshfree solutions, accurate results are obtained.
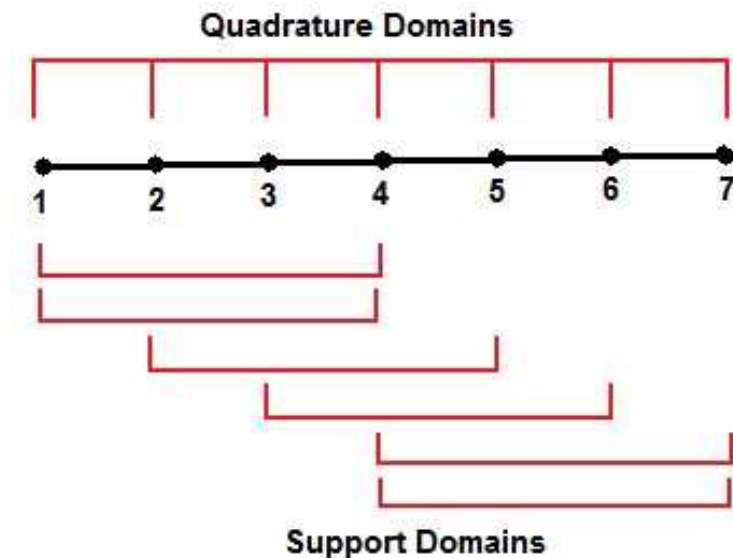
Figure 3.12: Domains used in the solution of flexible pendulum
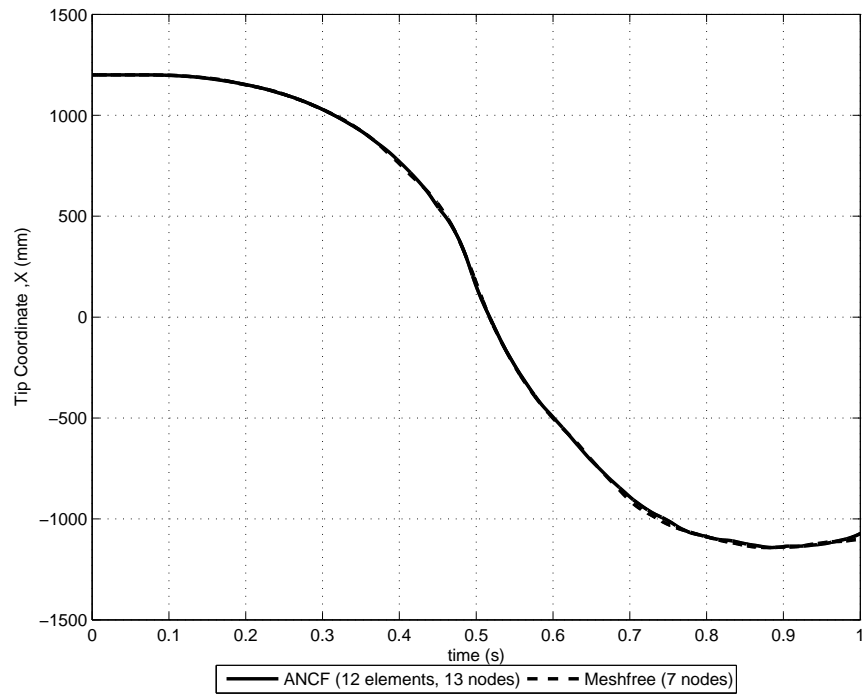
Figure 3.13: Tip coordinate, *X*, versus time for meshfree ANCF (b = 2 mm)
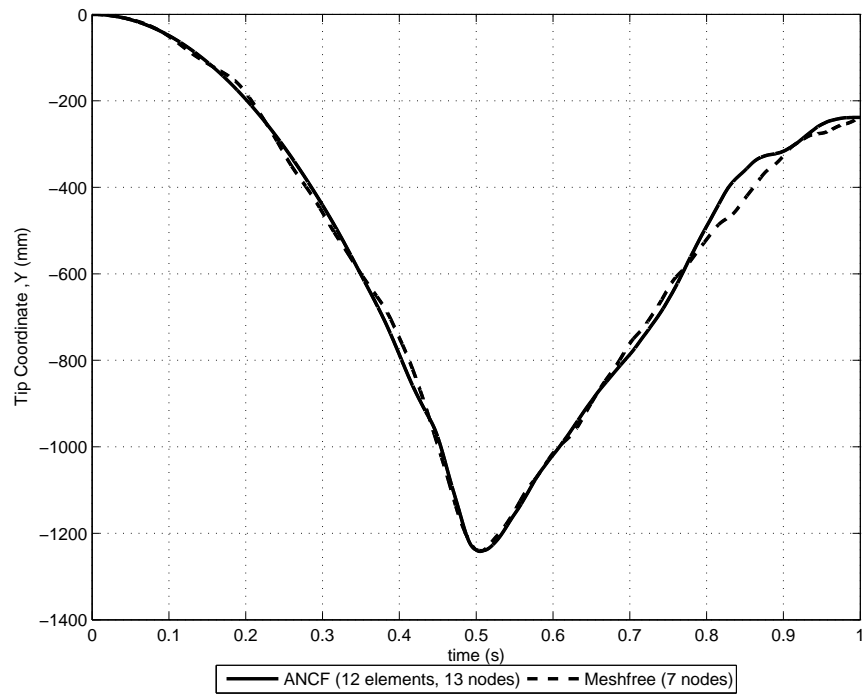
Figure 3.14: Tip coordinate, *Y*, versus time for meshfree ANCF (b = 2 mm)
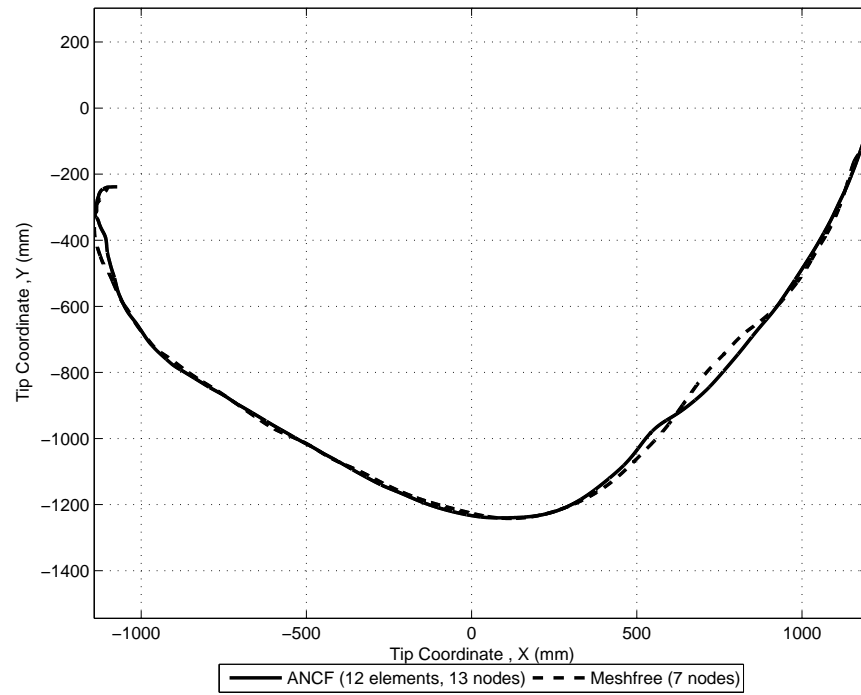
Figure 3.15: Route of the tip for meshfree ANCF (b = 2 mm)
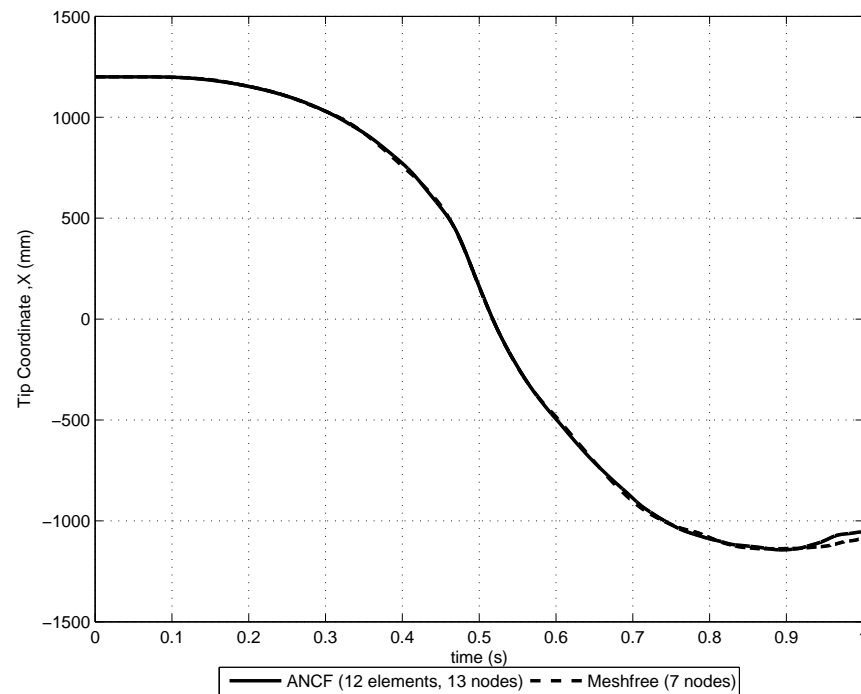
Figure 3.16: Tip coordinate, *X*, versus time for meshfree ANCF (b = 10 mm)
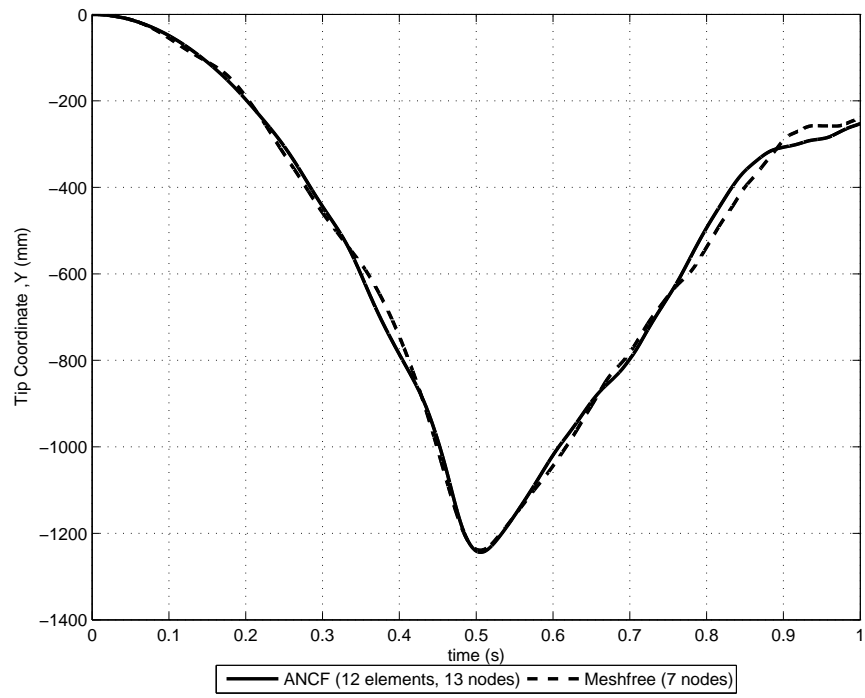
Figure 3.17: Tip coordinate, Y, versus time for meshfree ANCF (b = 10 mm)
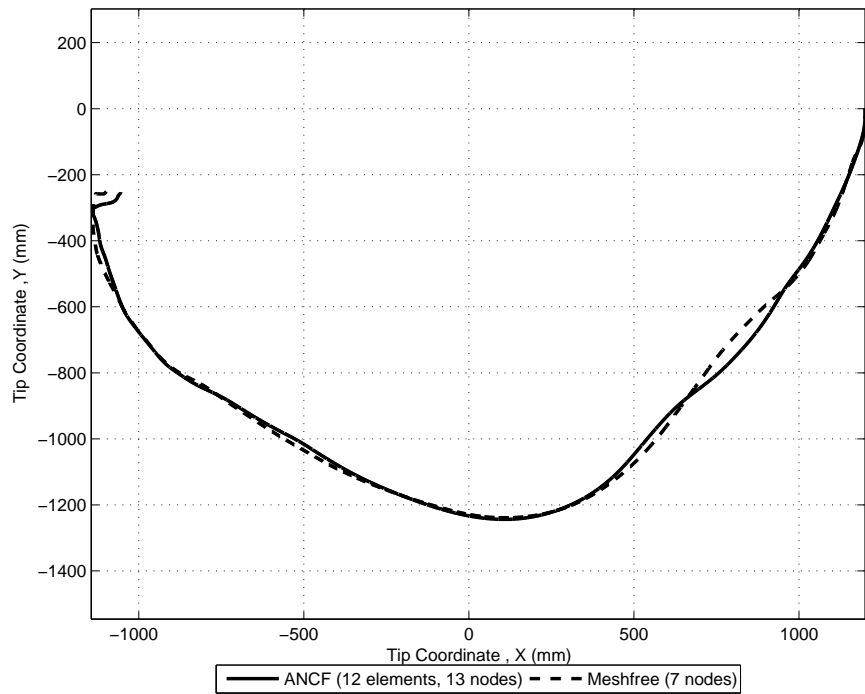
Figure 3.18: Route of the tip for meshfree ANCF (b = 10 mm)
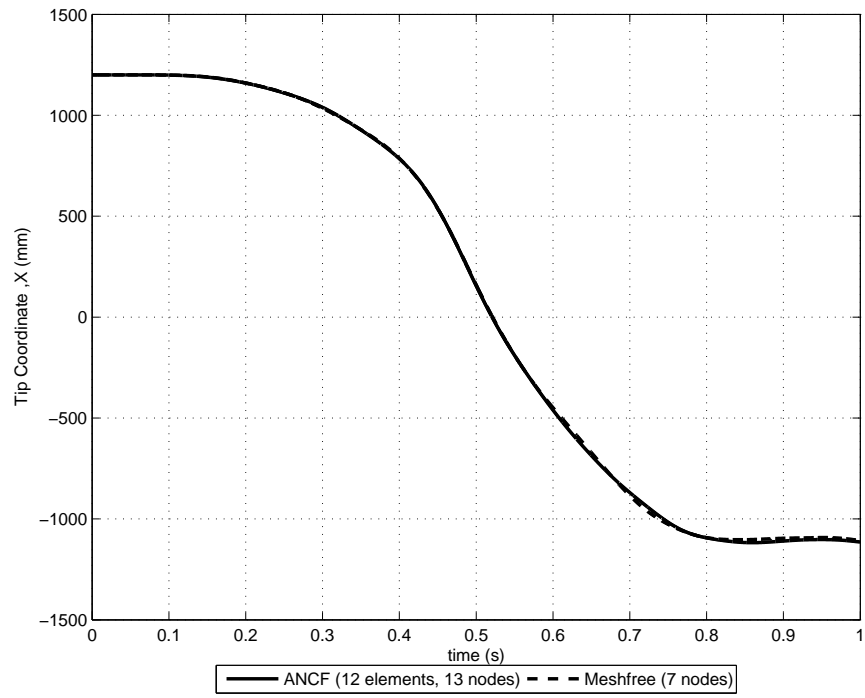
Figure 3.19: Tip coordinate, *X*, versus time for meshfree ANCF (b = 40 mm)
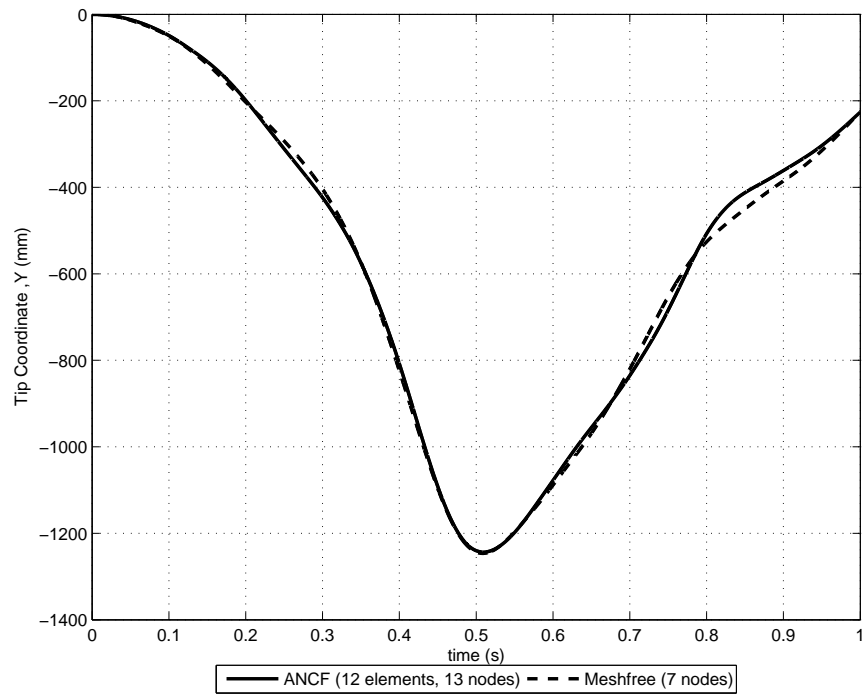
Figure 3.20: Tip coordinate, *Y*, versus time for meshfree ANCF (b = 40 mm)
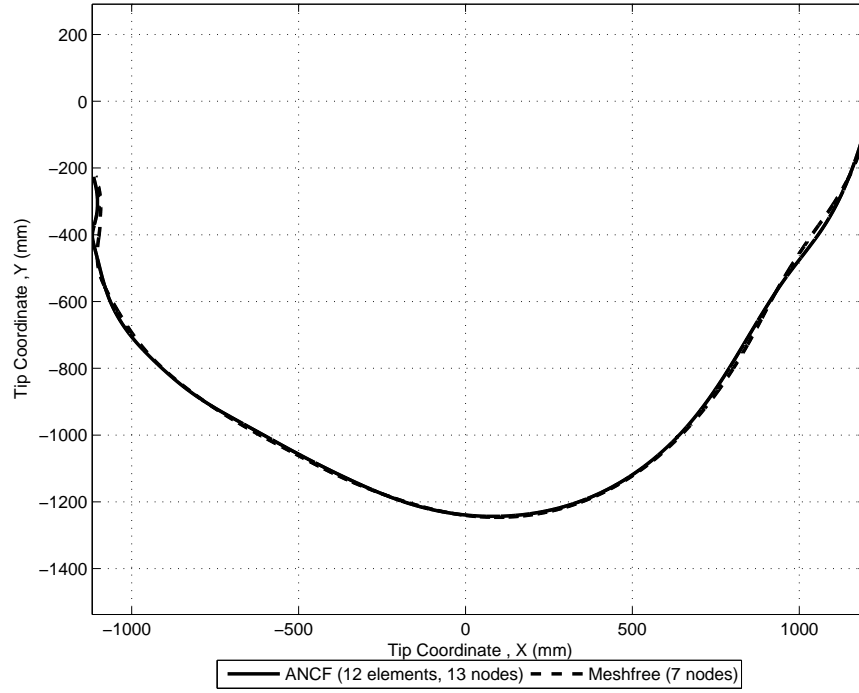
Figure 3.21: Route of the tip for meshfree ANCF (b = 40 mm)

3.8 Discussion

In the chapter, meshfree implementation of ANCF for planar beams has been performed. As can be seen from the comparisons, accurate results can be obtained despite fewer nodes are used. However, cost of computation is relatively high. Required time for the proposed meshfree formulation is at least twice of the time required for finite element based formulation with the same number of nodes. General advantages of the proposed meshfree formulation can be summarized as follows.

- Accuracy is high.

- Extreme nonlinear deformations can be handled due to the higher order of the shape functions.

Additionally, disadvantages of the proposed formulation can be summarized as given below.

- Computational cost is high.

- Formulation still requires background mesh (quadrature domains)

3.8.1 Application of Meshfree ANCF to the Plate/Shell Structure

Due to advantages listed above, meshfree formulation has been tried to be implemented to the ANCF of generalized plates. However, appropriate shape function polynomials, which should work for any kind of node locations and domain selections, could not be found. For particularly selected node locations and quadrature domains, flexible pendulum problem, introduced in Figure 2.7, has been solved accurately with respect to the edge displacements. However, continuity of displacements could not be satisfied over quadrature domain interfaces. Therefore, meshfree generalized plate formulation is not presented in the thesis and left as a future study. Node locations and selected quadrature domains for flexible plate pendulum are presented in Figure 3.22. Comparison of displacements at point H (Figure 2.7) can be found in Figure 3.23. Displacement results are almost identical upto 0.5 s of the simulation, where the kinetic energy is maximum. Then, a negligible difference in the results arises. It can be evaluated that generalized plate formulation is completed with respect to the displacement comparison. However, continuity requirement is not satisfied over the quadrature domains as shown in Figure 3.24.
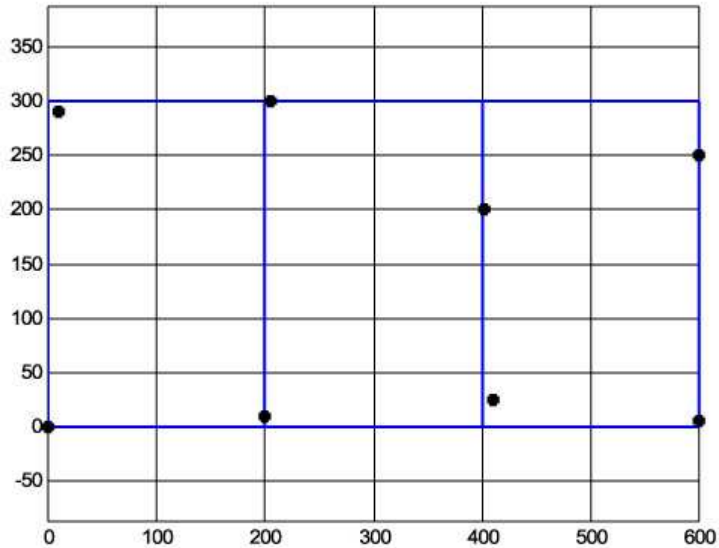
Figure 3.22: Selected node locations and quadrature domains of flexible pendulum for meshfree generalized plate formulation
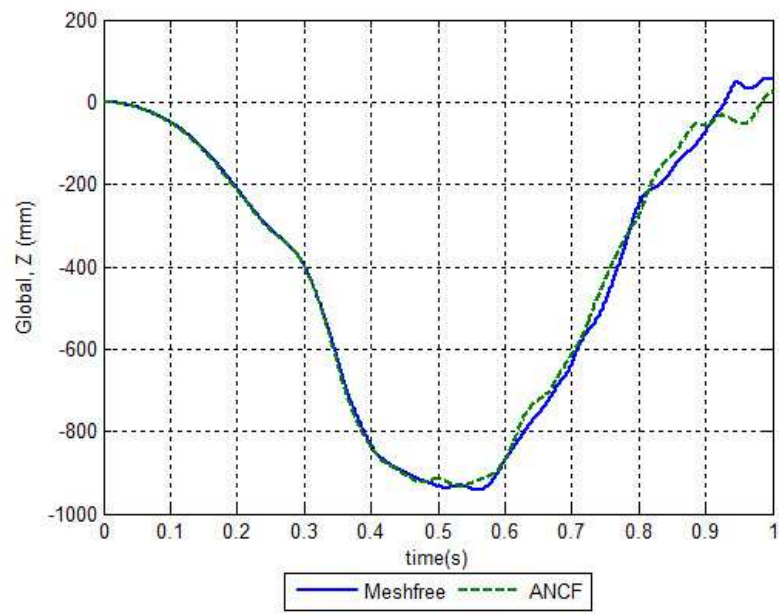
Figure 3.23: Comparison of displacements at point H for FEM and meshfree based ANCF's
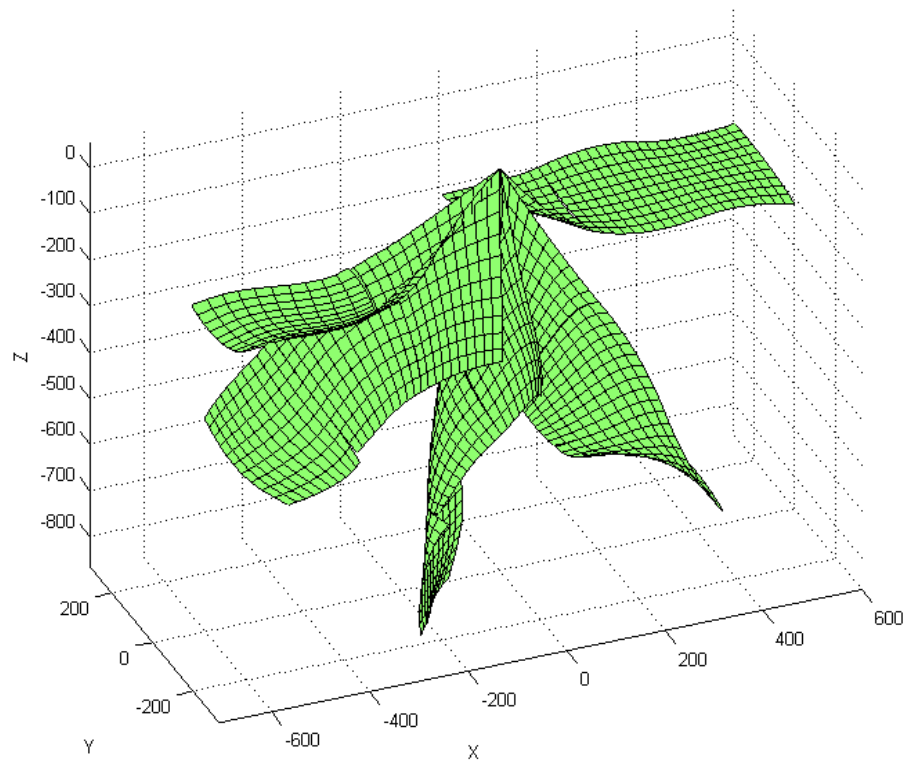
Figure 3.24: Flexible pendulum configurations obtained by using meshfree ANCF

CHAPTER 4

ANCF FOR QUADRILATERAL PLANE STRESS AND PLANE STRAIN ELEMENTS HAVING IRREGULAR SHAPES

Currently, ANCF is used for structural finite elements (beam, plate and shell elements) having regular shapes. However, this method can be extended to irregularly shaped structural elements and also to planar and three dimensional continuum finite elements by using properly selected mapping frames and interpolation polynomials. Main advantages of extending ANCF to continuum finite elements can be summarized as given below:

1. Generalized mass matrix is always constant and independent of the time and the deformation.

2. Hourglass modes, which cause energy loss in finite element simulations, can be eliminated or reduced.

3. Exact representation of rigid body dynamics is possible.

4. Accuracy is high.

Beside these advantages, it has only two drawbacks which are highly nonlinear generalized elastic forces and increased total degrees of freedom. However, these disadvantages could be handled by using available solution procedures, like Newton-Raphson method, in literature.

In this chapter, a new formulation, called "ANCF with Virtual Element Mapping", has been developed in order to eliminate element shape restrictions, to make ANCF be applicable to 3D continuum elements and to make use of the ANCF in general flexible multibody problems. Additionally, three approaches for virtual element mapping are proposed. Developed

formulation and the proposed methods are implemented to four noded plane stress or plane strain quadrilateral finite elements, firstly. Additionally, the performance of the developed ANCF is verified by well known patch test problems proposed by Richard H. Macneal and Robert L. Harder [35]. Implementation of the developed formulation and the proposed methods to plate/shell and 3D hexahedral finite elements are presented in the following chapters.

4.1 Irregular Shaped Quadrilateral Finite Element Representation and Shape Function Creation for Planar Continuum Problems

In general ANCF, nodal degrees of freedom consist of nodal coordinates in global frame and partial derivatives (or gradients) with respect to a local frame or body frame. The mapped coordinate frame given in Figure 4.1 can be chosen in order to define nodal gradients of the finite element.
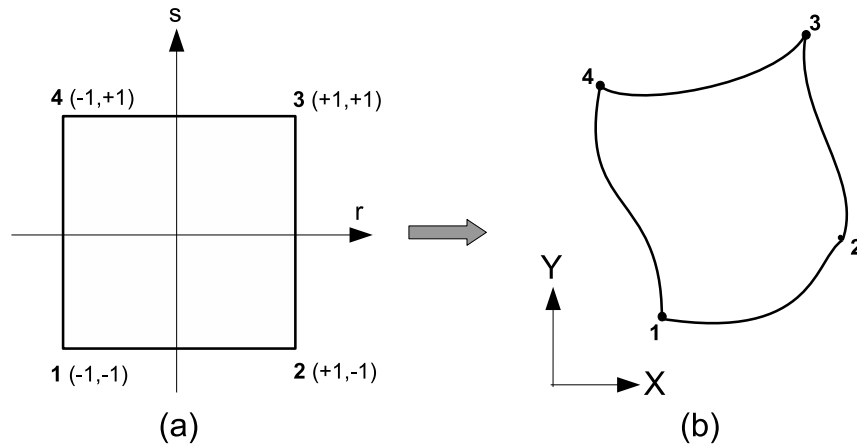
Figure 4.1: The mapped coordinate frame (a) and the global coordinate frame (b)

Then, the nodal degrees of freedom of an arbitrary element at i^{th} node should be written as given below.

$$\mathbf{e}_i^{rs} = \left[X_i \ Y_i \ \frac{\partial X_i}{\partial r} \ \frac{\partial Y_i}{\partial r} \ \frac{\partial X_i}{\partial s} \ \frac{\partial Y_i}{\partial s} \right]^T \tag{4.1}$$

Afterwards, various geometrical finite element shapes could be created by imposing proper polynomial shape functions for global coordinates. The shape function polynomial selected for planar continuum problems is given in the following equation.

$$X = \sum_{i=1}^{12} p_i a_i = \mathbf{p}^T \mathbf{a} \tag{4.2a}$$

$$Y = \sum_{i=1}^{12} p_i b_i = \mathbf{p}^T \mathbf{b} \tag{4.2b}$$

$$\mathbf{p}^T = \begin{bmatrix} 1 & r & s & rs & r^2 & s^2 & r^2s & rs^2 & r^3 & s^3 & r^3s & rs^3 \end{bmatrix} \tag{4.2c}$$

In the equation, $\mathbf{a}$ and $\mathbf{b}$ are vectors of polynomial constants, and $\mathbf{p}$ is the vector of monomials of the shape function. Polynomial constant vectors could be formulated in terms of nodal degrees of freedom of the element as given below.

$$\mathbf{e}_i^{rs} = \mathbf{Q}(r_i, s_i)\mathbf{A} \tag{4.3}$$

where $\mathbf{Q}(r, s)$ and $\mathbf{A}$ are defined in the following equations.

$$\mathbf{Q}(r, s) = \begin{bmatrix} \mathbf{p}^T(r, s) & \mathbf{0} \\ \mathbf{0} & \mathbf{p}^T(r, s) \\ \mathbf{p}_{,r}^T(r, s) & \mathbf{0} \\ \mathbf{0} & \mathbf{p}_{,r}^T(r, s) \\ \mathbf{p}_{,s}^T(r, s) & \mathbf{0} \\ \mathbf{0} & \mathbf{p}_{,s}^T(r, s) \end{bmatrix} \tag{4.4a}$$

$$\mathbf{A} = \begin{bmatrix} \mathbf{a}^T & \mathbf{b}^T \end{bmatrix}^T \tag{4.4b}$$

Here, r_i and s_i represent the mapped coordinates of the ith node on the element as given below.

$$[r_1 \ r_2 \ r_3 \ r_4] = [-1 \ +1 \ +1 \ -1] \tag{4.5a}$$

$$[s_1 \ s_2 \ s_3 \ s_4] = [-1 \ -1 \ +1 \ +1] \tag{4.5b}$$

70

Linear set of algebraic equations to be solved for $\mathbf{A}$ can be derived by using Equation 4.3 for all four nodes of the element as given in the following equation.

$$\mathbf{e}^{rs} = \left[\left(\mathbf{e}_1^{rs}\right)^T \quad \left(\mathbf{e}_2^{rs}\right)^T \quad \left(\mathbf{e}_3^{rs}\right)^T \quad \left(\mathbf{e}_4^{rs}\right)^T \right]^T = \mathbf{P}\,\mathbf{A} \tag{4.6}$$

where

$$\mathbf{P} = \left[\mathbf{Q}^T(r_1, s_1) \quad \mathbf{Q}^T(r_2, s_2) \quad \mathbf{Q}^T(r_3, s_3) \quad \mathbf{Q}^T(r_4, s_4) \right]^T \tag{4.7}$$

Then, polynomial constants vector, $\mathbf{A}$, can be found by using Equation 4.6 as follows.

$$\mathbf{A} = \mathbf{P}^{-1}\mathbf{e}^{rs} \tag{4.8}$$

Additionally, $\mathbf{P}^{-1}$ always exists and be constant as given below.

$$\mathbf{P}^{-1} = \left[\begin{smallmatrix}
0.25 & 0 & 0.125 & 0 & 0.125 & 0 & 0.25 & 0 & -0.125 & 0 & 0.125 & 0 & \dots \\
-0.375 & 0 & -0.125 & 0 & -0.125 & 0 & 0.375 & 0 & -0.125 & 0 & 0.125 & 0 & \dots \\
-0.375 & 0 & -0.125 & 0 & -0.125 & 0 & -0.375 & 0 & 0.125 & 0 & -0.125 & 0 & \dots \\
0.5 & 0 & 0.125 & 0 & 0.125 & 0 & -0.5 & 0 & 0.125 & 0 & -0.125 & 0 & \dots \\
0 & 0 & -0.125 & 0 & 0 & 0 & 0 & 0 & 0.125 & 0 & 0 & 0 & \dots \\
0 & 0 & 0 & 0 & -0.125 & 0 & 0 & 0 & 0 & 0 & -0.125 & 0 & \dots \\
0 & 0 & 0.125 & 0 & 0 & 0 & 0 & 0 & -0.125 & 0 & 0 & 0 & \dots \\
0 & 0 & 0 & 0 & 0.125 & 0 & 0 & 0 & 0 & 0 & -0.125 & 0 & \dots \\
0.125 & 0 & 0.125 & 0 & 0 & 0 & -0.125 & 0 & 0.125 & 0 & 0 & 0 & \dots \\
0.125 & 0 & 0 & 0 & 0.125 & 0 & 0.125 & 0 & 0 & 0 & 0.125 & 0 & \dots \\
-0.125 & 0 & -0.125 & 0 & 0 & 0 & 0.125 & 0 & -0.125 & 0 & 0 & 0 & \dots \\
-0.125 & 0 & 0 & 0 & -0.125 & 0 & 0.125 & 0 & 0 & 0 & 0.125 & 0 & \dots \\
0 & 0.25 & 0 & 0.125 & 0 & 0.125 & 0 & 0.25 & 0 & -0.125 & 0 & 0.125 & \dots \\
0 & -0.375 & 0 & -0.125 & 0 & -0.125 & 0 & 0.375 & 0 & -0.125 & 0 & 0.125 & \dots \\
0 & -0.375 & 0 & -0.125 & 0 & -0.125 & 0 & -0.375 & 0 & 0.125 & 0 & -0.125 & \dots \\
0 & 0.5 & 0 & 0.125 & 0 & 0.125 & 0 & -0.5 & 0 & 0.125 & 0 & -0.125 & \dots \\
0 & 0 & 0 & -0.125 & 0 & 0 & 0 & 0 & 0 & 0.125 & 0 & 0 & \dots \\
0 & 0 & 0 & 0 & 0 & -0.125 & 0 & 0 & 0 & 0 & 0 & -0.125 & \dots \\
0 & 0 & 0 & 0.125 & 0 & 0 & 0 & 0 & 0 & -0.125 & 0 & 0 & \dots \\
0 & 0 & 0 & 0 & 0 & 0.125 & 0 & 0 & 0 & 0 & 0 & -0.125 & \dots \\
0 & 0.125 & 0 & 0.125 & 0 & 0 & 0 & -0.125 & 0 & 0.125 & 0 & 0 & \dots \\
0 & 0.125 & 0 & 0 & 0 & 0.125 & 0 & 0.125 & 0 & 0 & 0 & 0.125 & \dots \\
0 & -0.125 & 0 & -0.125 & 0 & 0 & 0 & 0.125 & 0 & -0.125 & 0 & 0 & \dots \\
0 & -0.125 & 0 & 0 & 0 & -0.125 & 0 & 0.125 & 0 & 0 & 0 & 0.125 & \dots \\
0.25 & 0 & -0.125 & 0 & -0.125 & 0 & 0.25 & 0 & 0.125 & 0 & -0.125 & 0 \\
0.375 & 0 & -0.125 & 0 & -0.125 & 0 & -0.375 & 0 & -0.125 & 0 & 0.125 & 0 \\
0.375 & 0 & -0.125 & 0 & -0.125 & 0 & 0.375 & 0 & 0.125 & 0 & -0.125 & 0 \\
0.5 & 0 & -0.125 & 0 & -0.125 & 0 & -0.5 & 0 & -0.125 & 0 & 0.125 & 0 \\
0 & 0 & 0.125 & 0 & 0 & 0 & 0 & 0 & -0.125 & 0 & 0 & 0 \\
0 & 0 & 0 & 0 & 0.125 & 0 & 0 & 0 & 0 & 0 & 0.125 & 0 \\
0 & 0 & 0.125 & 0 & 0 & 0 & 0 & 0 & -0.125 & 0 & 0 & 0 \\
0 & 0 & 0 & 0 & 0.125 & 0 & 0 & 0 & 0 & 0 & -0.125 & 0 \\
-0.125 & 0 & 0.125 & 0 & 0 & 0 & 0.125 & 0 & 0.125 & 0 & 0 & 0 \\
-0.125 & 0 & 0 & 0 & 0.125 & 0 & -0.125 & 0 & 0 & 0 & 0.125 & 0 \\
-0.125 & 0 & 0.125 & 0 & 0 & 0 & 0.125 & 0 & 0.125 & 0 & 0 & 0 \\
-0.125 & 0 & 0 & 0 & 0.125 & 0 & 0.125 & 0 & 0 & 0 & -0.125 & 0 \\
0 & 0.25 & 0 & -0.125 & 0 & -0.125 & 0 & 0.25 & 0 & 0.125 & 0 & -0.125 \\
0 & 0.375 & 0 & -0.125 & 0 & -0.125 & 0 & -0.375 & 0 & -0.125 & 0 & 0.125 \\
0 & 0.375 & 0 & -0.125 & 0 & -0.125 & 0 & 0.375 & 0 & 0.125 & 0 & -0.125 \\
0 & 0.5 & 0 & -0.125 & 0 & -0.125 & 0 & -0.5 & 0 & -0.125 & 0 & 0.125 \\
0 & 0 & 0 & 0.125 & 0 & 0 & 0 & 0 & 0 & -0.125 & 0 & 0 \\
0 & 0 & 0 & 0 & 0 & 0.125 & 0 & 0 & 0 & 0 & 0 & 0.125 \\
0 & 0 & 0 & 0.125 & 0 & 0 & 0 & 0 & 0 & -0.125 & 0 & 0 \\
0 & 0 & 0 & 0 & 0 & 0.125 & 0 & 0 & 0 & 0 & 0 & -0.125 \\
0 & -0.125 & 0 & 0.125 & 0 & 0 & 0 & 0.125 & 0 & 0.125 & 0 & 0 \\
0 & -0.125 & 0 & 0 & 0 & 0.125 & 0 & -0.125 & 0 & 0 & 0 & 0.125 \\
0 & -0.125 & 0 & 0.125 & 0 & 0 & 0 & 0.125 & 0 & 0.125 & 0 & 0 \\
0 & -0.125 & 0 & 0 & 0 & 0.125 & 0 & 0.125 & 0 & 0 & 0 & -0.125
\end{smallmatrix}\right] \tag{4.9}$$

It is observed that various planar element shapes (samples are shown in Figure 4.2) could be obtained by using the derived shape function constants, given in Equation 4.8, for appropriate nodal degrees of freedom. This feature of the developed formulation allows accurate discretization of irregular shapes of flexible bodies. However, the shape function polynomials for neighboring elements would cause discontinuities on the common element edges. The desired common edge shape might require different nodal gradients for each of the neighboring elements. This problem can be overcome by employing additional constraint equations for each common nodes. However, this method increases the total number of degrees of freedom in the problem to be solved to six times the total node number for planar problems. In addition, added constraint equations should be handled carefully. It is clear that adding constraint equations for assembly of the system equations is not an economical way to use. Therefore, nodal gradients ($\partial X/\partial r$, $\partial Y/\partial r$, $\partial X/\partial s$ and $\partial Y/\partial s$) should be changed or forced to generate the same edge shapes for neighboring elements. Then, system equations can be formed by using general finite element assembly procedures.

As discussed above, using mapped $r-s$ coordinates for nodal gradient definitions is not appropriate. However, shape function polynomials can be generated easily by using the mapped coordinates. Therefore, additional virtual finite elements, which uses the same mapped $r-s$ coordinates with different shape (or mapping) functions, are created on a virtual $X_v - Y_v$ coordinate frame, which is constant and parallel to the global $X-Y$ frame, in order to overcome incompatibility problem in gradients. Then, nodal gradients can be redefined with respect to the virtual coordinate frame. Consequently, shape function matrix, which can generate global coordinates and gradients at an arbitrary point on an element by using nodal degrees of freedom, can be formulated. Various shape function matrices could be formulated depending on the choices made for virtual element's geometrical shape and virtual shape functions. Additionally, using different shape function polynomials for original elements than Equation 4.2 would result alternative shape function matrices, also. Some of the methods, that can be used for shape function matrix generation, are given in the following subsections.
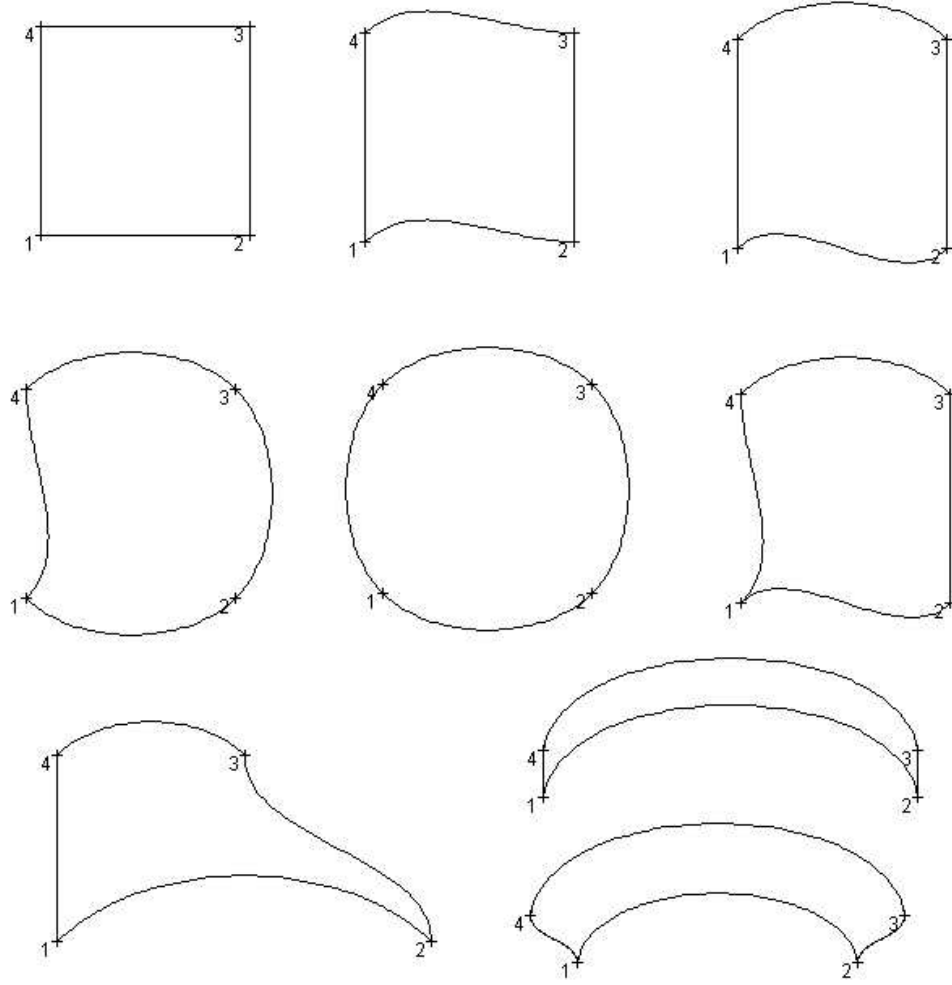
Figure 4.2: Various planar flexible solid element shapes

4.1.1 Method 1: Parallel Virtual Frame and First Order Virtual Element Mapping

In this method, nodal degrees of freedom for the ith node of an arbitrary element is described as given below.

$$\mathbf{e}_i = \left[X_i\ Y_i\ \ \frac{\partial X_i}{\partial X_v}\ \ \frac{\partial Y_i}{\partial X_v}\ \ \frac{\partial X_i}{\partial Y_v}\ \ \frac{\partial Y_i}{\partial Y_v} \right]^T \tag{4.10}$$
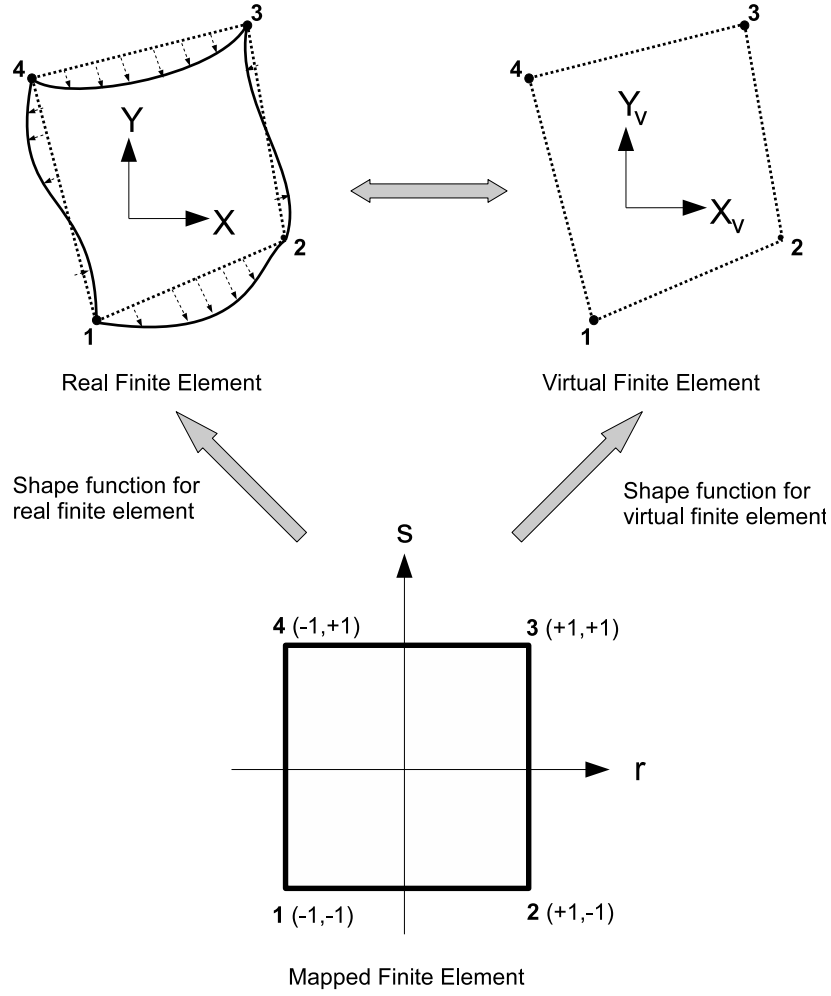
Figure 4.3: Coordinate frames for Parallel Virtual Frame and First Order Virtual Element Mapping Method

In Equation 4.10, nodal gradients are defined with respect to the virtual coordinate frame shown in Figure 4.3. The virtual element is bounded by straight lines connecting initial node coordinates as shown in the figure. Virtual coordinates at an arbitrary point on the element can be found by general first order interpolation functions given below [36].

$$X_v(r, s) = \mathbf{H_v}(r, s) \, ^0\mathbf{X} \qquad (4.11a)$$

$$Y_v(r, s) = \mathbf{H_v}(r, s) \, ^0\mathbf{Y} \qquad (4.11b)$$

where $\mathbf{H_v}(r, s)$ is the first order shape function vector, $^0\mathbf{X}$ is the vector of initial X coordinates of nodes and $^0\mathbf{Y}$ is the vector of initial Y coordinates of the nodes as shown in the following equations.

$$\mathbf{H_v}(r, s) = \frac{1}{4}\left[(1 - r)(1 - s) \quad (1 + r)(1 - s) \quad (1 + r)(1 + s) \quad (1 - r)(1 + s)\right] \tag{4.12a}$$

$$^0\mathbf{X} = \left[^0X_1 \quad ^0X_2 \quad ^0X_3 \quad ^0X_4\right]^T \tag{4.12b}$$

$$^0\mathbf{Y} = \left[^0Y_1 \quad ^0Y_2 \quad ^0Y_3 \quad ^0Y_4\right]^T \tag{4.12c}$$

Then, gradients with respect to the mapped $r - s$ frame can be written in terms of nodal gradients, which are defined in Equation 4.10, in compact form as given below.

$$\mathbf{e}^{rs}(r, s) = \mathbf{T_{m1}}(r, s)\, \mathbf{e}(r, s) \tag{4.13a}$$

$$\mathbf{e}(r, s) = \mathbf{T_{m1}}(r, s)^{-1}\, \mathbf{e}^{rs}(r, s) \tag{4.13b}$$

where

$$\mathbf{T_{m1}}(r, s) = \begin{bmatrix} 1 & 0 & 0 & 0 & 0 & 0 \\ 0 & 1 & 0 & 0 & 0 & 0 \\ 0 & 0 & X_{v,r}(s) & 0 & Y_{v,r}(s) & 0 \\ 0 & 0 & 0 & X_{v,r}(s) & 0 & Y_{v,r}(s) \\ 0 & 0 & X_{v,s}(r) & 0 & Y_{v,s}(r) & 0 \\ 0 & 0 & 0 & X_{v,s}(r) & 0 & Y_{v,s}(r) \end{bmatrix} \tag{4.14}$$

Additionally, $\mathbf{e}^{rs}(r, s)$ and $\mathbf{e}(r, s)$ are vector functions used to evaluate global positions and gradients at arbitrary points on the element as described below.

$$\mathbf{e}^{rs}(r, s) = \left[X(r, s) \quad Y(r, s) \quad X_{,r}(r, s) \quad Y_{,r}(r, s) \quad X_{,s}(r, s) \quad Y_{,s}(r, s)\right]^T \tag{4.15a}$$

$$\mathbf{e}(r, s) = \left[X(r, s) \quad Y(r, s) \quad X_{,X_v}(r, s) \quad Y_{,X_v}(r, s) \quad X_{,Y_v}(r, s) \quad Y_{,Y_v}(r, s)\right]^T \tag{4.15b}$$

Consequently, vector of nodal variables, $\mathbf{e}$, can be converted into the form given in Equation 4.6, $\mathbf{e^{rs}}$, as given below.

$$\mathbf{e^{rs}} = \mathbf{T}_{map1}\,\mathbf{e} \tag{4.16}$$

where the transformation matrix, $\mathbf{T}_{map1}$, can be evaluated by using Equation 4.14 as given below.

$$\mathbf{T}_{map1} = \begin{bmatrix} \mathbf{T}_{m1}(r_1, s_1) & \mathbf{0} & \mathbf{0} & \mathbf{0} \\ \mathbf{0} & \mathbf{T}_{m1}(r_2, s_2) & \mathbf{0} & \mathbf{0} \\ \mathbf{0} & \mathbf{0} & \mathbf{T}_{m1}(r_3, s_3) & \mathbf{0} \\ \mathbf{0} & \mathbf{0} & \mathbf{0} & \mathbf{T}_{m1}(r_4, s_4) \end{bmatrix} \tag{4.17}$$

Finally, global coordinates and gradients with respect to the virtual frame at an arbitrary point can be written in terms of nodal variables by following the procedure given below;

1. Substitute Equation 4.16 into Equation 4.8 to obtain polynomial constants as;

$$\mathbf{A} = \mathbf{P}^{-1}\mathbf{T}_{map1}\,\mathbf{e}$$

2. Substitute polynomial constants into Equation 4.3 in order to obtain vector function used to evaluate global positions and gradients with respect to the mapped rs frame as given below.

$$\mathbf{e}^{rs}(r, s) = \mathbf{Q}(r, s)\mathbf{P}^{-1}\mathbf{T}_{map1}\,\mathbf{e}$$

3. Then, substitute the equation above into Equation 4.13b as:

$$\mathbf{e}(r, s) = \mathbf{T}_{m1}(r, s)^{-1}\,\mathbf{Q}(r, s)\mathbf{P}^{-1}\mathbf{T}_{map1}\,\mathbf{e} \tag{4.18}$$

Then, it can be written in a simple form given below.

$$\mathbf{e}(r, s) = \mathbf{S}(r, s)\,\mathbf{e} \tag{4.19}$$

where the shape function matrix is defined as;

$$\mathbf{S}(r, s) = \mathbf{T}_{m1}(r, s)^{-1}\mathbf{Q}(r, s)\mathbf{P}^{-1}\,\mathbf{T}_{map1} \tag{4.20}$$

In Equation 4.20, $\mathbf{P}^{-1}$ and $\mathbf{T}_{map}$ is independent of local coordinates and time. The derived shape function ensures continuity of nodal parameter at the neighboring node location. Global coordinates are continuous over neighboring element edges, but continuity of gradients is

only guaranteed on node locations. Therefore, stresses or strains will not be continuous over element edges but be continuous over node locations. Continuous stress/strain distributions can be created by linear interpolation over nodal stresses or strains in post-processing stage.

While using Method 1 (Parallel Virtual Frame and First Order Virtual Element Mapping Method), the most difficult part is to define initial nodal gradients ($\partial X/\partial X_v$, $\partial Y/\partial X_v$, $\partial X/\partial Y_v$ and $\partial Y/\partial Y_v$) of the elements. It could be very hard to realize their geometrical meaning for elements having curved edges, initially. In order to overcome this difficulty, alternative nodal representation, Virtual Element Edge Frame and First Order Virtual Element Mapping, have been developed. However, while the method makes definitions of nodal gradients easier, it brings a new restriction for node numbering. Details of the method is given in the next subsection.

4.1.2 Method 2: Virtual Element Edge Frame and First Order Virtual Element Mapping

In this method, nodal gradients are redefined with respect to the edge frame of virtual finite element in order to make geometrical meaning of nodal gradients more understandable. As shown in Figure 4.4, first and second nodes, and third and fourth nodes are connected with straight lines, where S_v is constant. Similarly, second and third nodes, and fourth and first nodes are connected with straight lines, where R_v is constant. These four straight lines connecting the nodes form the boundaries of the virtual element in X_v-Y_v frame. In fact, R_v-S_v is not a new coordinate frame, but they are products of virtual X_v-Y_v frame. If a point, which has the mapped coordinates of (r_a, s_a) on the element, is considered in order to clarify R_v and S_v definitions, then, R_v is defined as the magnitude of the vector from the virtual point at (-1, s_a) to the point at (r, s_a). Similarly, S_v is defined as the magnitude of the vector from the virtual point at (r_a, -1) to the point at (r_a,s). Therefore, they can be defined with respect to the virtual frame X_v-Y_v, defined in Equation 4.11, as given in the following equations.

$$R_v(r) = \sqrt{(\mathbf{H_{vr}}(r)\mathbf{X^0})^2 + (\mathbf{H_{vr}}(r)\mathbf{Y^0})^2} \tag{4.21a}$$

$$S_v(s) = \sqrt{(\mathbf{H_{vs}}(s)\mathbf{X^0})^2 + (\mathbf{H_{vs}}(s)\mathbf{Y^0})^2} \tag{4.21b}$$

where

$$\mathbf{H_{vr}}(r) = \mathbf{H_v}(r, s_a) - \mathbf{H_v}(-1, s_a) = \frac{(1 + r)}{4}\begin{bmatrix} -1 + s_a & 1 - s_a & 1 + s_a & -1 - s_a \end{bmatrix} \quad (4.22a)$$

$$\mathbf{H_{vs}}(s) = \mathbf{H_v}(r_a, s) - \mathbf{H_v}(r_a, -1) = \frac{(1 + s)}{4}\begin{bmatrix} -1 + r_a & -1 - r_a & 1 + r_a & 1 - r_a \end{bmatrix} \quad (4.22b)$$

As can be seen from Equation 4.21, R_v is a function of r and S_v is a function of s, only.
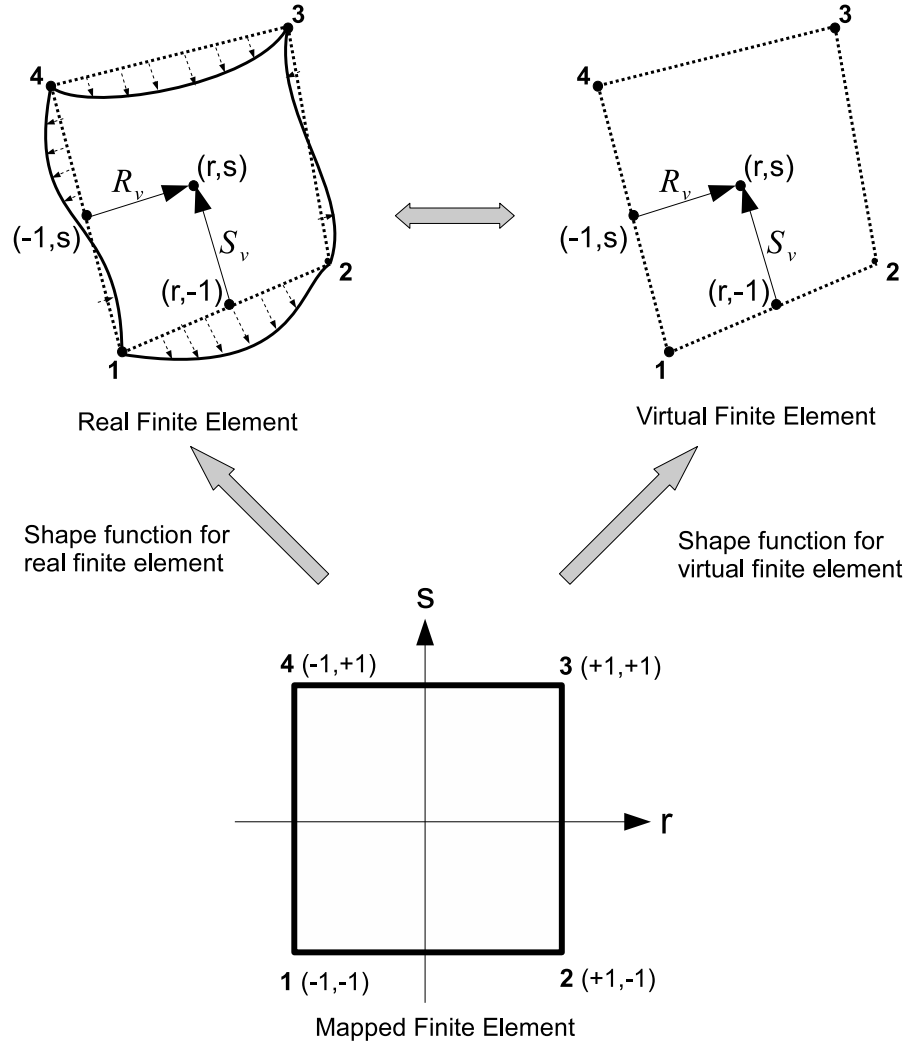
Figure 4.4: Coordinate frames for Virtual Element Edge Frame and First Order Virtual Element Mapping Method

Gradients of virtual R_v-S_v frame with respect to the mapped $r - s$ frame at an arbitrary point

on the element can be written explicitly as given below.

$$\frac{\partial R_v}{\partial r} = \frac{1}{4}\sqrt{(C_{X1} + C_{X2}\, s)^2 + (C_{Y1} + C_{Y2}\, s)^2} \tag{4.23a}$$

$$\frac{\partial S_v}{\partial s} = \frac{1}{4}\sqrt{(C_{X3} + C_{X2}\, r)^2 + (C_{Y3} + C_{Y2}\, r)^2} \tag{4.23b}$$

$$\frac{\partial R_v}{\partial s} = \frac{\partial S_v}{\partial r} = 0 \tag{4.23c}$$

where

$$C_{X1} = -\,^0X_1 + \,^0X_2 + \,^0X_3 - \,^0X_4 \tag{4.24a}$$

$$C_{X2} = +\,^0X_1 - \,^0X_2 + \,^0X_3 - \,^0X_4 \tag{4.24b}$$

$$C_{X3} = -\,^0X_1 - \,^0X_2 + \,^0X_3 + \,^0X_4 \tag{4.24c}$$

$$C_{Y1} = -\,^0Y_1 + \,^0Y_2 + \,^0Y_3 - \,^0Y_4 \tag{4.24d}$$

$$C_{Y2} = +\,^0Y_1 - \,^0Y_2 + \,^0Y_3 - \,^0Y_4 \tag{4.24e}$$

$$C_{Y3} = -\,^0Y_1 - \,^0Y_2 + \,^0Y_3 + \,^0Y_4 \tag{4.24f}$$

Then, nodal variables, $\mathbf{e}$, for the ith node of an arbitrary element can be written as follows.

$$\mathbf{e}_i = \left[X_i \ \ Y_i \ \ \frac{\partial X_i}{\partial R_v} \ \ \frac{\partial Y_i}{\partial R_v} \ \ \frac{\partial X_i}{\partial S_v} \ \ \frac{\partial Y_i}{\partial S_v} \right]^T \tag{4.25}$$

In Equation 4.25, X_i and Y_i are coordinates of the ith node in global frame. In order to make the definitions of nodal variables more clear, the finite element given in Figure 4.4 is redrawn with nodal gradient vectors in Figure 4.5. The gradient vectors are always tangent to the element edges as shown. Additionally, it is advised to use unit vectors for undeformed finite elements despite non-unit gradient vectors are mathematically possible.
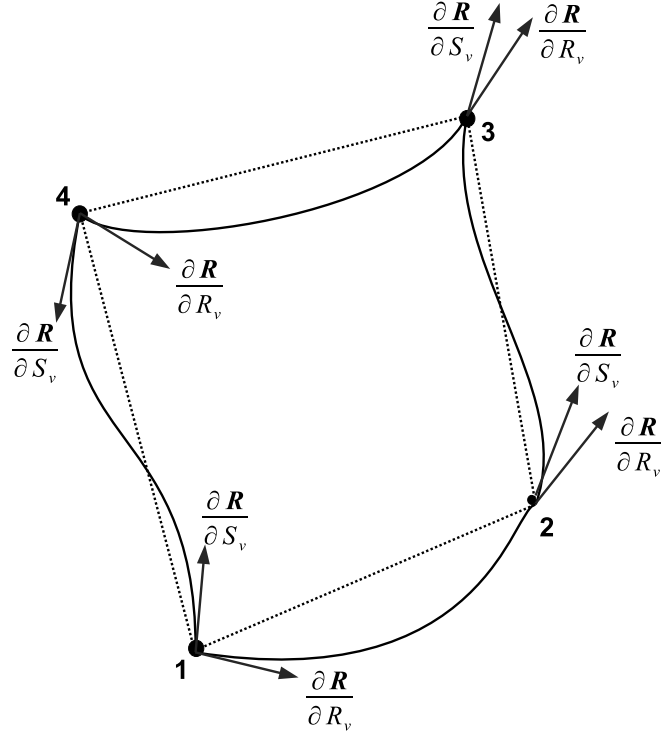
Figure 4.5: Nodal gradient vector representation for Virtual Element Edge Frame and First Order Virtual Element Mapping Method

The gradients with respect to the mapped $r - s$ frame can be written in terms of the nodal gradients ($\partial X/\partial R_v$, $\partial Y/\partial R_v$, $\partial X/\partial S_v$ and $\partial Y/\partial S_v$) as given in the following equation.

$$\mathbf{e}^{rs}(r, s) = \mathbf{T_{m2}}(r, s)\,\mathbf{e}(r, s) \tag{4.26a}$$

$$\mathbf{e}(r, s) = \mathbf{T_{m2}}(r, s)^{-1}\,\mathbf{e}^{rs}(r, s) \tag{4.26b}$$

where

$$\mathbf{T_{m2}}(r, s) = \begin{bmatrix} 1 & 0 & 0 & 0 & 0 & 0 \\ 0 & 1 & 0 & 0 & 0 & 0 \\ 0 & 0 & R_{v,r}(s) & 0 & 0 & 0 \\ 0 & 0 & 0 & R_{v,r}(s) & 0 & 0 \\ 0 & 0 & 0 & 0 & S_{v,s}(r) & 0 \\ 0 & 0 & 0 & 0 & 0 & S_{v,s}(r) \end{bmatrix} \tag{4.27}$$

80

Additionally, $\mathbf{e}(r, s)$ is a vector function used to evaluate global positions and gradients at arbitrary points on the element as described below.

$$\mathbf{e}(r, s) = \left[X(r, s) \quad Y(r, s) \quad X_{,R_v}(r, s) \quad Y_{,R_v}(r, s) \quad X_{,S_v}(r, s) \quad Y_{,S_v}(r, s) \right]^T \tag{4.28}$$

Consequently, vector of nodal variables, $\mathbf{e}$, can be converted into the form given in Equation 4.6, $\mathbf{e^{rs}}$, as given below.

$$\mathbf{e^{rs}} = \mathbf{T}_{map2}\, \mathbf{e} \tag{4.29}$$

where the transformation matrix, $\mathbf{T}_{map2}$, can be evaluated by using Equation 4.27 as given below.

$$\mathbf{T}_{map2} = \begin{bmatrix} \mathbf{T}_{m2}(r_1, s_1) & \mathbf{0} & \mathbf{0} & \mathbf{0} \\ \mathbf{0} & \mathbf{T}_{m2}(r_2, s_2) & \mathbf{0} & \mathbf{0} \\ \mathbf{0} & \mathbf{0} & \mathbf{T}_{m2}(r_3, s_3) & \mathbf{0} \\ \mathbf{0} & \mathbf{0} & \mathbf{0} & \mathbf{T}_{m2}(r_4, s_4) \end{bmatrix} \tag{4.30}$$

Finally, global coordinates and gradients with respect to the virtual frame at an arbitrary point can be written in terms of nodal variables by following similar procedure described for Method 1 as given below.

$$\mathbf{e}(r, s) = \mathbf{T_{m2}}(r, s)^{-1}\, \mathbf{Q}(r, s)\mathbf{P}^{-1}\mathbf{T}_{map2}\, \mathbf{e} \tag{4.31}$$

Then, it can be written in a simple form given below;

$$\mathbf{e}(r, s) = \mathbf{S}(r, s)\, \mathbf{e} \tag{4.32}$$

where the shape function matrix for Method 2 is defined as;

$$\mathbf{S}(r, s) = \mathbf{T}_{m2}(r, s)^{-1}\mathbf{Q}(r, s)\mathbf{P}^{-1}\, \mathbf{T}_{map2} \tag{4.33}$$

81

Transformation matrix for Method 2, $\mathbf{T_{map2}}$, is a diagonal matrix and can be written in explicit form as given below.

$$\mathbf{T_{map2}} = \begin{bmatrix} 1 & 1 & \frac{L_1}{2} & \frac{L_1}{2} & \frac{L_4}{2} & \frac{L_4}{2} & \cdots \\ 1 & 1 & \frac{L_1}{2} & \frac{L_1}{2} & \frac{L_2}{2} & \frac{L_2}{2} & \cdots \\ 1 & 1 & \frac{L_3}{2} & \frac{L_3}{2} & \frac{L_2}{2} & \frac{L_2}{2} & \cdots \\ 1 & 1 & \frac{L_3}{2} & \frac{L_3}{2} & \frac{L_4}{2} & \frac{L_4}{2} & \cdots \end{bmatrix} \mathbf{I_{24 \times 24}} \tag{4.34}$$

where L_1, L_2, L_3 and L_4 represent the virtual edge lengths between nodes 1 and 2, nodes 2 and 3, nodes 3 and 4, and nodes 4 and 1, respectively. Additionally, $\mathbf{I_{24 \times 24}}$ is a 24×24 identity matrix.

While virtual element edge frame, $R_v - S_v$, making geometrical definitions of nodal gradients easier, it brings two major restrictions. First restriction is related to the node numbering. Neighboring elements should be numbered such that, their common virtual element edges should refer to the same virtual coordinate. Indeed, if a common virtual element edge refers to a constant R_v curve of one of the neighboring elements then it should refer to the constant R_v curve for the other element. Therefore, the same nodal gradients will be applicable for both of the elements. The second restriction is about the geometrical descriptions of the neighboring elements. Due to nodal gradient definitions, discontinuous element edge transitions can not be modeled. Actually, this is the outcome of the nodal gradient definitions.

4.1.3 Method 3: Initial Element Frame Mapping Method

In this method, initial shape function polynomials formulated using Method 1 are applied instead of virtual frame having first order mapping as shown in Figure 4.6. Nodal gradients are defined with respect to the initial element configuration. Therefore, initial nodal gradients are always 1 or 0. Curvatures of element edges are created by auxiliary gradients defined with respect to the virtual $X_v Y_v$ frame.
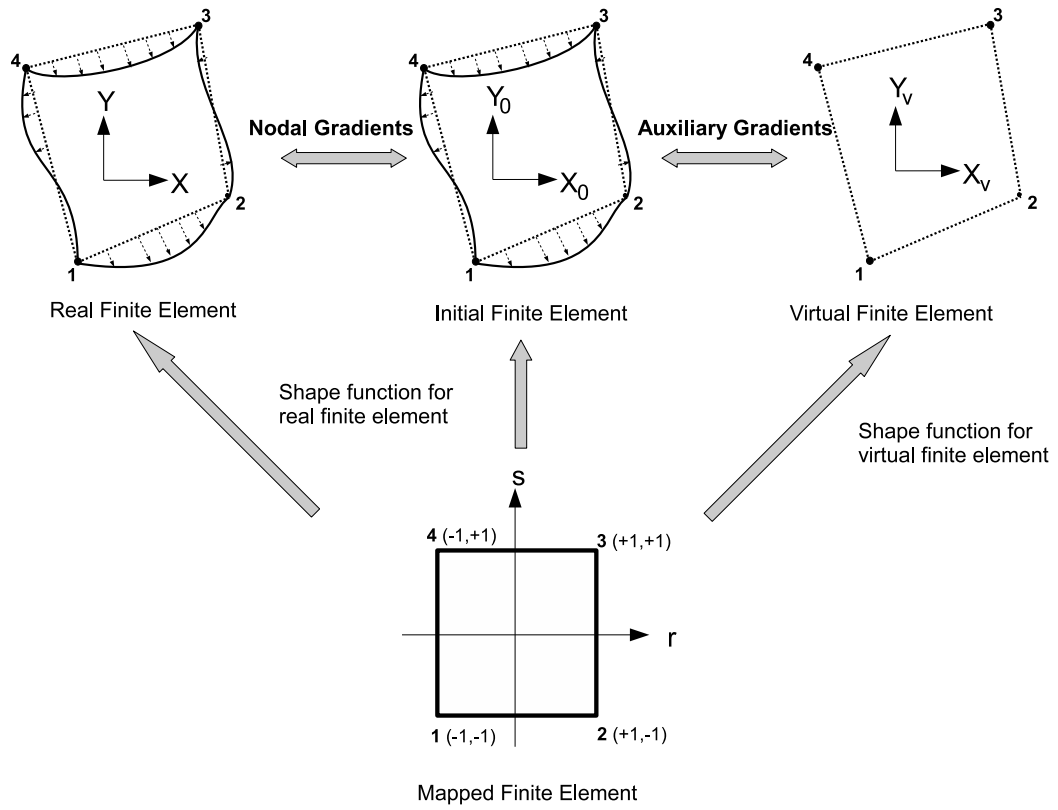
Figure 4.6: Coordinate frames for Initial Element Frame Mapping Method

Then, nodal variables, **e**, for the ith node of an arbitrary element can be written as follows. As seen from the equation, nodal gradients replaced with the actual deformation gradients.

$$\mathbf{e}_i = \left[X_i \; Y_i \; \frac{\partial X_i}{\partial\,^0 X} \; \frac{\partial Y_i}{\partial\,^0 X} \; \frac{\partial X_i}{\partial\,^0 Y} \; \frac{\partial Y_i}{\partial\,^0 Y} \right]^T \tag{4.35}$$

In order to find shape function matrix for the method, the global position vector, which contains gradients with respect to the mapped $r - s$ frame, of an arbitrary point on the element are rewritten in the following two equations for an arbitrary time ($\mathbf{e}^{rs}(r, s)$) and for the initial configuration ($^0\mathbf{e}^{rs}(r, s)$).

$$\mathbf{e}^{rs}(r, s) = \mathbf{S}^{rs}(r, s)\mathbf{e}^{rs} \tag{4.36}$$

$$^0\mathbf{e}^{rs}(r, s) = \mathbf{S}^{rs}(r, s)\,^0\mathbf{e}^{rs} \tag{4.37}$$

83

where the shape function matrix for the mapped frame is defined as;

$$\mathbf{S}^{rs}(r, s) = \mathbf{Q}(r, s)\mathbf{P}^{-1} \tag{4.38}$$

By using Equations 4.36 and 4.37, one can derive global position vector, including deformation gradients, at an arbitrary point in terms of nodal variables for the mapped $r - s$ frame, $\mathbf{e}^{rs}$, as given below.

$$\mathbf{e}(r, s) = \begin{bmatrix} X(r, s) \\ Y(r, s) \\ \partial X/\partial\,^0X(r, s) \\ \partial Y/\partial\,^0X(r, s) \\ \partial X/\partial\,^0Y(r, s) \\ \partial Y/\partial\,^0Y(r, s) \end{bmatrix} = \mathbf{T}_{m3}(r, s)\mathbf{e}^{rs} \tag{4.39}$$

where

$$\mathbf{T}_{m3}(r, s) = \begin{bmatrix} \mathbf{S}_1^{rs} \\ \mathbf{S}_2^{rs} \\ (^0\mathbf{e}^{rs})^T\left(\left(\mathbf{S}_6^{rs}\right)^T \mathbf{S}_3^{rs} - \left(\mathbf{S}_4^{rs}\right)^T \mathbf{S}_5^{rs}\right)/det \\ (^0\mathbf{e}^{rs})^T\left(\left(\mathbf{S}_6^{rs}\right)^T \mathbf{S}_4^{rs} - \left(\mathbf{S}_4^{rs}\right)^T \mathbf{S}_6^{rs}\right)/det \\ (^0\mathbf{e}^{rs})^T\left(\left(\mathbf{S}_3^{rs}\right)^T \mathbf{S}_5^{rs} - \left(\mathbf{S}_5^{rs}\right)^T \mathbf{S}_3^{rs}\right)/det \\ (^0\mathbf{e}^{rs})^T\left(\left(\mathbf{S}_3^{rs}\right)^T \mathbf{S}_6^{rs} - \left(\mathbf{S}_5^{rs}\right)^T \mathbf{S}_4^{rs}\right)/det \end{bmatrix} \tag{4.40}$$

and

$$det = (^0\mathbf{e}^{rs})^T\left(\left(\mathbf{S}_3^{rs}\right)^T \mathbf{S}_6^{rs} - \left(\mathbf{S}_5^{rs}\right)^T \mathbf{S}_4^{rs}\right)^0\mathbf{e}^{rs} \tag{4.41}$$

In Equations 4.40 and 4.41, $\mathbf{S}_i^{rs}$ represents the ith row vector of $\mathbf{S}^{rs}$.

Finally, nodal variable vector with respect to $r - s$ frame can be written in terms of nodal variable vector of the element as described below.

$$\mathbf{e} = \mathbf{T}_{map3}\,\mathbf{e}^{rs} \tag{4.42a}$$

$$\mathbf{e}^{rs} = \left(\mathbf{T}_{map3}\right)^{-1}\mathbf{e} \tag{4.42b}$$

where

$$\mathbf{T}_{map3} = \begin{bmatrix} \mathbf{T}_{m3}(r_1, s_1) \\ \mathbf{T}_{m3}(r_2, s_2) \\ \mathbf{T}_{m3}(r_3, s_3) \\ \mathbf{T}_{m3}(r_4, s_4) \end{bmatrix} \tag{4.43}$$

Then, global position and gradients with respect to the initial configuration of an arbitrary point on the element can be found by substituting Equation 4.42 into Equation 4.39 as given below.

$$\mathbf{e}(r, s) = \mathbf{T}_{m3}(r, s)\mathbf{T}_{map3}^{-1}\mathbf{e} \tag{4.44}$$

In addition, the shape function matrix for Method 3 can be defined as;

$$\mathbf{S}(r, s) = \mathbf{T}_{m3}(r, s)\mathbf{T}_{map3}^{-1} \tag{4.45}$$

The most important advantage of Method 3 is simple generalized elastic force derivation. Elastic force vector can be found directly by using nodal gradients. Although, virtual element shape functions do not appear in the formulation, they are still needed for determination of initial nodal variables, $^0\mathbf{e}^{rs}$, containing gradients with respect to the mapped $r - s$ frame. If the shape function polynomials for the real finite element and the virtual finite elements are identical for all three methods, then the results to be obtained will be identical. Therefore, selection of appropriate method should be based on the preferred geometrical representations and complexity of the formulations.

4.1.4 Other Applicable Methods for Shape Function Matrix Formulation

Basically, irregular shaped quadrilateral finite elements require two shape function polynomials for shape function matrix generation. Depending on the selected shape functions, various alternative solution methods can be generated using one of the three methods described above.

4.2 Mass Matrix Formulation

All of the existing classical finite element formulations for the large deformation and rotation analysis lead to nonlinear mass matrices [8]. However, it is just a constant matrix in ANCF. This feature of the formulation is valid for the newly developed planar elements, also. Mass matrix can easily be formulated by writing the kinetic energy equation at an arbitrary time, t, for an element as given in Equation 2.58. In the equation, ${}^t\rho$ and ${}^tV$ are density and volume of the element at an arbitrary time, t. The velocity vector, $\dot{\mathbf{r}}$, at an arbitrary point on the element can be obtained by differentiating the nodal position vector as ${}^t\dot{\mathbf{r}} = \mathbf{S_{12}}(r,s)\,({}^t\dot{\mathbf{e}})$, where, $\mathbf{S_{12}}(r,s)$ is the reduced shape function matrix, which contains only the first and the second rows of shape function matrix given in Equations 4.20 or 4.33 or 4.45. Density and volume at an arbitrary time, t, can be written in terms of initial density and volume by using deformation gradient matrix, $\mathbf{J}$ [36]. Then, the mass matrix can be found by substituting velocity vector, $\dot{\mathbf{r}}$, and Equation 2.59 into Equation 2.58 as given below.

$$ {}^tT = \frac{1}{2} \int_{{}^tV} \frac{{}^0\rho}{|{}^t_0\mathbf{J}|} \left({}^t\dot{\mathbf{e}}^T\right) \mathbf{S_{12}}^T \mathbf{S_{12}} \left({}^t\dot{\mathbf{e}}\right) |{}^t_0\mathbf{J}| d\,{}^0V \tag{4.46a} $$

$$ {}^tT = \frac{1}{2} \left({}^t\dot{\mathbf{e}}^T\right) \left[\int_{{}^0V} {}^0\rho\, \mathbf{S_{12}}^T \mathbf{S_{12}}\, d\,{}^0V \right] \left({}^t\dot{\mathbf{e}}\right) \tag{4.46b} $$

$$ {}^tT = \frac{1}{2} \left({}^t\dot{\mathbf{e}}^T\right) {}^t\mathbf{M} \left({}^t\dot{\mathbf{e}}\right) \tag{4.46c} $$

$$ {}^t\mathbf{M} = \int_{{}^0V} {}^0\rho\, \mathbf{S_{12}}^T \mathbf{S_{12}}\, d\,{}^0V \tag{4.46d} $$

As seen in Equation 4.46d , mass matrix at an arbitrary time, t, does not depend on time. It can be evaluated once by using the initial density and volume, then it can be used at any time step during the solution process. However, it is very difficult to integrate mass matrix over initial complex volume on global coordinate frame, ${}^0V$. Therefore, it should be transformed into the mapped $r - s$ frame in order to make volume integration easier as given below.

86

$$\mathbf{M} = \int_{V^{rs}} \rho \, \mathbf{S_{12}}^T \mathbf{S_{12}} \, |\mathbf{D}| \, drds \tag{4.47a}$$

$$\mathbf{D} = \frac{\partial \mathbf{X}_0}{\partial \mathbf{r}} = \begin{bmatrix} \dfrac{\partial X_0}{\partial r} & \dfrac{\partial X_0}{\partial s} \\ \dfrac{\partial Y_0}{\partial r} & \dfrac{\partial Y_0}{\partial s} \end{bmatrix} \tag{4.47b}$$

4.3 Generalized Elastic Forces

In the derivation of generalized elastic forces, continuum mechanics approach has been used. The generalized elastic forces of an arbitrary element can be derived using strain energy equation. The strain energy of an element at an arbitrary time, t, can be formulated by using Green-Lagrange strain and 2nd Piola-Kirchhoff stress tensor definitions as given in the following equation (Total Lagrangian Formulation) [32].

$$^t U = \frac{1}{2} \int_{^0V} \left({}^t \boldsymbol{\varepsilon}^T \right) \mathbf{E} \left({}^t \boldsymbol{\varepsilon} \right) d \, {}^0V \tag{4.48}$$

where $\mathbf{E}$ is the matrix of elastic coefficients and ${}^t \boldsymbol{\varepsilon}$ is the vector form of the strain tensor, ${}^t \boldsymbol{\varepsilon}_m$. The matrices of elastic coefficients for plane-stress and plane-strain problems are given below [36].

$$\mathbf{E} = \frac{E}{(1-v^2)} \begin{bmatrix} 1 & v & 0 \\ v & 1 & 0 \\ 0 & 0 & 1-v \end{bmatrix} \quad (plane-stress) \tag{4.49a}$$

$$\mathbf{E} = \frac{E(1-v)}{(1+v)(1-2v)} \begin{bmatrix} 1 & \dfrac{v}{1-v} & 0 \\ \dfrac{v}{1-v} & 1 & 0 \\ 0 & 0 & \dfrac{2(1-2v)}{(1-v)} \end{bmatrix} \quad (plane-strain) \tag{4.49b}$$

where E and v are modulus of elasticity and Poisson's ratio of material. The generalized elastic forces of the element can be obtained by differentiating the strain energy (Equation 4.48) with respect to the nodal variables as given in the following equation.

$$ {}^t\mathbf{Q}_k = \frac{\partial {}^t U}{\partial {}^t\mathbf{e}} = \frac{\partial}{\partial {}^t\mathbf{e}} \left\{ \frac{1}{2} \int\limits_{0V} {}^t\boldsymbol{\varepsilon}^T \mathbf{E}\, {}^t\boldsymbol{\varepsilon}\, d\,{}^0V \right\} = \int\limits_{0V} \left(\frac{\partial {}^t\boldsymbol{\varepsilon}}{\partial {}^t\mathbf{e}} \right)^T \mathbf{E}\, {}^t\boldsymbol{\varepsilon}\, d\,{}^0V \tag{4.50} $$

In order to find nonlinear strain tensor, deformation gradient should be written in terms of nodal variables. Due to different nodal variable definitions, formulation of deformation gradients for Method 1, Method 2 and Method 3 will be different as given below.

$$ \mathbf{J} = \frac{\partial \mathbf{X}^t}{\partial \mathbf{X}^0} = \underbrace{\begin{bmatrix} \frac{\partial X}{\partial X_0} & \frac{\partial X}{\partial Y_0} \\ \frac{\partial Y}{\partial X_0} & \frac{\partial Y}{\partial Y_0} \end{bmatrix}}_{Method\ 3} = \underbrace{\begin{bmatrix} \frac{\partial X}{\partial X_v} & \frac{\partial X}{\partial Y_v} \\ \frac{\partial Y}{\partial X_v} & \frac{\partial Y}{\partial Y_v} \end{bmatrix} \begin{bmatrix} \frac{\partial X_0}{\partial X_v} & \frac{\partial X_0}{\partial Y_v} \\ \frac{\partial Y_0}{\partial X_v} & \frac{\partial Y_0}{\partial Y_v} \end{bmatrix}^{-1}}_{Method\ 1} = \underbrace{\begin{bmatrix} \frac{\partial X}{\partial R_v} & \frac{\partial X}{\partial S_v} \\ \frac{\partial Y}{\partial R_v} & \frac{\partial Y}{\partial S_v} \end{bmatrix} \begin{bmatrix} \frac{\partial X_0}{\partial R_v} & \frac{\partial X_0}{\partial S_v} \\ \frac{\partial Y_0}{\partial R_v} & \frac{\partial Y_0}{\partial S_v} \end{bmatrix}^{-1}}_{Method\ 2} \tag{4.51} $$

In general form, deformation gradient tensor can be written as given below.

$$ \mathbf{J} = \begin{bmatrix} \mathbf{S_3 e} & \mathbf{S_5 e} \\ \mathbf{S_4 e} & \mathbf{S_6 e} \end{bmatrix} \begin{bmatrix} d_{11} & d_{12} \\ d_{21} & d_{22} \end{bmatrix} = \begin{bmatrix} (d_{11}\mathbf{S_3} + d_{21}\mathbf{S_5})\,\mathbf{e} & (d_{12}\mathbf{S_3} + d_{22}\mathbf{S_5})\,\mathbf{e} \\ (d_{11}\mathbf{S_4} + d_{21}\mathbf{S_6})\,\mathbf{e} & (d_{12}\mathbf{S_4} + d_{22}\mathbf{S_6})\,\mathbf{e} \end{bmatrix} \tag{4.52} $$

In the equation, d_{11}, d_{12}, d_{21} and d_{22} are the elements of inverse of initial nodal gradient tensor and defined in the equation given below for the three shape function matrix methods.

$$ \begin{bmatrix} d_{11} & d_{12} \\ d_{21} & d_{22} \end{bmatrix} = \begin{bmatrix} \frac{\partial X_0}{\partial X_v} & \frac{\partial X_0}{\partial Y_v} \\ \frac{\partial Y_0}{\partial X_v} & \frac{\partial Y_0}{\partial Y_v} \end{bmatrix}^{-1} = \begin{bmatrix} \mathbf{S_3}^0\mathbf{e} & \mathbf{S_5}^0\mathbf{e} \\ \mathbf{S_4}^0\mathbf{e} & \mathbf{S_6}^0\mathbf{e} \end{bmatrix}^{-1} \cdots Method\ 1 \tag{4.53a} $$

$$ \begin{bmatrix} d_{11} & d_{12} \\ d_{21} & d_{22} \end{bmatrix} = \begin{bmatrix} \frac{\partial X_0}{\partial R_v} & \frac{\partial X_0}{\partial S_v} \\ \frac{\partial Y_0}{\partial R_v} & \frac{\partial Y_0}{\partial S_v} \end{bmatrix}^{-1} = \begin{bmatrix} \mathbf{S_3}^0\mathbf{e} & \mathbf{S_5}^0\mathbf{e} \\ \mathbf{S_4}^0\mathbf{e} & \mathbf{S_6}^0\mathbf{e} \end{bmatrix}^{-1} \cdots Method\ 2 \tag{4.53b} $$

$$ \begin{bmatrix} d_{11} & d_{12} \\ d_{21} & d_{22} \end{bmatrix} = \begin{bmatrix} 1 & 0 \\ 0 & 1 \end{bmatrix} \cdots Method\ 3 \tag{4.53c} $$

Then, general definition of nonlinear Lagrangian strain tensor can be written as;

$$ \varepsilon_{\mathbf{m}} = \frac{1}{2} \left({}_0^t\mathbf{J}^T {}_0^t\mathbf{J} - \mathbf{I} \right) \tag{4.54a} $$

$$ \varepsilon_{\mathbf{m}} = \frac{1}{2} \begin{bmatrix} \mathbf{e}^T \mathbf{N}_{11}\mathbf{e} - 1 & \mathbf{e}^T \mathbf{N}_{12}\mathbf{e} \\ \mathbf{e}^T \mathbf{N}_{12}\mathbf{e} & \mathbf{e}^T \mathbf{N}_{22}\mathbf{e} - 1 \end{bmatrix} \tag{4.54b} $$

88

where

$$\mathbf{N}_{11} = (d_{11}\mathbf{S_3} + d_{21}\mathbf{S_5})^T (d_{11}\mathbf{S_3} + d_{21}\mathbf{S_5}) + (d_{11}\mathbf{S_4} + d_{21}\mathbf{S_6})^T (d_{11}\mathbf{S_4} + d_{21}\mathbf{S_6}) \qquad (4.55a)$$

$$\mathbf{N}_{12} = (d_{11}\mathbf{S_3} + d_{21}\mathbf{S_5})^T (d_{12}\mathbf{S_3} + d_{22}\mathbf{S_5}) + (d_{11}\mathbf{S_4} + d_{21}\mathbf{S_6})^T (d_{12}\mathbf{S_4} + d_{22}\mathbf{S_6}) \qquad (4.55b)$$

$$\mathbf{N}_{22} = (d_{12}\mathbf{S_3} + d_{22}\mathbf{S_5})^T (d_{12}\mathbf{S_3} + d_{22}\mathbf{S_5}) + (d_{12}\mathbf{S_4} + d_{22}\mathbf{S_6})^T (d_{12}\mathbf{S_4} + d_{22}\mathbf{S_6}) \qquad (4.55c)$$

Then, the strain vector and its partial derivative with respect to the nodal variables can be written in terms of the nodal variables by using Equation 4.54b as given below.

$$\boldsymbol{\varepsilon} = \begin{bmatrix} \varepsilon_{11} \\ \varepsilon_{22} \\ \varepsilon_{12} \end{bmatrix} = \frac{1}{2} \begin{bmatrix} \mathbf{e}^T \mathbf{N}_{11}\mathbf{e} - 1 \\ \mathbf{e}^T \mathbf{N}_{22}\mathbf{e} - 1 \\ \mathbf{e}^T \mathbf{N}_{12}\mathbf{e} \end{bmatrix} \qquad (4.56)$$

$$\frac{\partial \boldsymbol{\varepsilon}}{\partial \mathbf{e}} = \begin{bmatrix} \mathbf{e}^T \mathbf{N}_{11} \\ \mathbf{e}^T \mathbf{N}_{22} \\ \frac{1}{2}\,\mathbf{e}^T \left(\mathbf{N}_{12} + \mathbf{N}_{12}{}^T \right) \end{bmatrix} \qquad (4.57)$$

Finally, the generalized elastic force equation can be written in terms of nodal variables by substituting Equations 4.56 and 4.57 into Equation 4.50 as given below.

$$\mathbf{Q}_k = \frac{1}{2} \int_{V^{rs}} \begin{bmatrix} \mathbf{e}^T \mathbf{N}_{11} \\ \mathbf{e}^T \mathbf{N}_{22} \\ \mathbf{e}^T \left(\mathbf{N}_{12} + \mathbf{N}_{12}{}^T \right) \end{bmatrix}^T \mathbf{E} \begin{bmatrix} \mathbf{e}^T \mathbf{N}_{11}\mathbf{e} - 1 \\ \mathbf{e}^T \mathbf{N}_{22}\mathbf{e} - 1 \\ 2\mathbf{e}^T \mathbf{N}_{12}\mathbf{e} \end{bmatrix} |\mathbf{D}| \; drds \qquad (4.58)$$

Evaluation of the generalized elastic force vector can be performed by numerical integration methods like Gauss-Quadrature method. Additionally, tangent stiffness matrix can be used for nonlinear static analysis. It can be formulated by partial differentiation of generalized elastic force vector with respect to the nodal variables as given below.

$$\mathbf{K}_t = \frac{\partial \mathbf{Q}_k}{\partial \mathbf{e}} \qquad (4.59)$$

4.4   Generalized External Forces

If a force $\mathbf{F}$ acts at an arbitrary point on the finite element, the virtual work done by the force for a virtual displacement of $\delta\mathbf{r}$ can be written as $\mathbf{F}\delta\mathbf{r}$, where $\mathbf{r}$ is the global position vector of the point of application of the force. The virtual change in the vector $\mathbf{r}$ can be expressed in terms of the virtual changes in the nodal variable, $\mathbf{e}$. Therefore, the generalized external forces associated with the absolute nodal coordinates can be defined [8]. By using the definitions of global position vector given in Equations 4.19 or 4.32 or 4.44, the generalized force vector, $\mathbf{Q}_F$, can be found for the point loads as given below.

$$\mathbf{F}^T \delta\mathbf{r} = \mathbf{F}^T \mathbf{S}_{12} \delta\mathbf{e} = \mathbf{Q}_F^T \delta\mathbf{e} \tag{4.60a}$$

$$\mathbf{Q}_F = \mathbf{S}_{12}^T \mathbf{F} \tag{4.60b}$$

where $\mathbf{S}_{12}$ is a matrix formed by first two rows of the shape function matrix. Other loading types can be derived by using the virtual work principle.

4.5   Equation of Motion for ANCF with Virtual Element Mapping

Using the mass matrix (Equation 4.47a) and generalized force vector (Equation 4.58), equation of motion of the flexible multibody system can be constructed as given below [8].

$$\mathbf{M}\ddot{\mathbf{e}} + \mathbf{Q}_k = \mathbf{Q}_F \tag{4.61}$$

Using the generalized force vector definition ($\mathbf{Q} = \mathbf{Q}_F - \mathbf{Q}_k$) and including constraint equations, equation of motion can be written in more compact form as given below. Here, λ is the vector of Lagrange Multipliers.

$$\begin{bmatrix} \ddot{\mathbf{e}} \\ \lambda \end{bmatrix} = \begin{bmatrix} \mathbf{M} & \mathbf{C}^T \\ \mathbf{C} & 0 \end{bmatrix}^{-1} \begin{bmatrix} \mathbf{Q} \\ 0 \end{bmatrix} \tag{4.62}$$

If the inertial effects are ignorable, then the problem can be reduced to static case by ignoring kinetic energy terms in the equations. In order to solve nonlinear static problems, iterative Newton-Raphson algorithm can be applied by using tangent stiffness matrix.

4.6   Patch Tests

In order to verify the developed ANCF and the proposed finite element for planar problems, some of the patch tests proposed by Richard H. Macneal and Robert L. Harder [35] have been performed for both static and dynamic solution procedures. In nonlinear static solutions, Optimization Toolbox in MATLAB® has been used. However, simple explicit direct integration algorithm presented in Chapter 2 has been utilized in order to solve transient dynamics problems. In dynamic solutions, loadings are converted to time dependent functions which are zero, initially. It is observed that steady state response obtained by transient solutions are almost identical to solutions obtained for static cases.

4.6.1   Membrane Plate Patch Test

The first patch test problem given in Figure 4.7 is used to verify the constant strain property of finite elements. Height, length, thickness, modulus of elasticity and Poisson's ratio of the plate are $a = 0.12$, $b = 0.24$, $t = 0.001$, $E = 1.0x10^6$ and $v = 0.25$, respectively. Initial nodal variables with respect to Method 1 are given in Table 4.1.
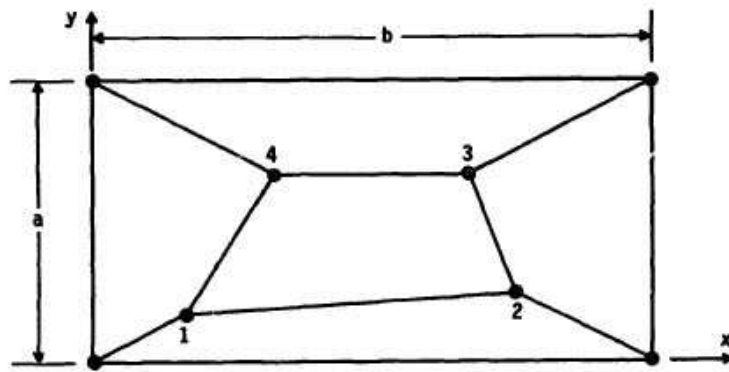
Figure 4.7: Membrane plate patch test [35]

Table 4.1: Initial nodal variables for membrane plate patch test

	X	Y	$\partial X/\partial X_v$	$\partial Y/\partial X_v$	$\partial X/\partial Y_v$	$\partial Y/\partial Y_v$
	Initial Configuration					
Node 1	0.04	0.02	1	0	0	1
Node 2	0.18	0.03	1	0	0	1
Node 3	0.16	0.08	1	0	0	1
Node 4	0.08	0.08	1	0	0	1
Node 5	0	0	1	0	0	1
Node 6	0.24	0	1	0	0	1
Node 7	0.24	0.12	1	0	0	1
Node 8	0	0.12	1	0	0	1

Final configurations of external nodes have been determined using the boundary conditions, $u = 10^{-3}(x+y/2)$ and $v = 10^{-3}(y+x/2)$, given in [35]. Nodal boundary conditions have been converted to functions of time for transient dynamic simulation as given below.

$$e_i(t) = {}^0e_i + \Delta e_i \ f(t) \tag{4.63}$$

where e_i is the ith nodal variable, ${}^0e_i$ is the initial value of ith nodal variable and Δe_i is the steady state change of ith nodal variable of the system. Additionally, time dependent function is given below [40].

$$f(t) = \begin{cases} 0.5\,(1 - cos(\pi \ t/t_r)) & if \quad t < t_r \\ 1 & if \quad t \ge t_r \end{cases} \tag{4.64}$$

where t_r is the rise time for boundary conditions. In the simulation, 0.08 s rise time has been used. Selected density and time step size are 0.8 and 1×10^{-5}, respectively.

Steady state response of the system has been obtained at 0.08 s of the simulation. Obtained stresses are shown in Figures 4.8, 4.9 and 4.10. As seen from figures, stress distributions are almost constant over elements. Comparison of the results with theoretical values are listed in Table 4.2.
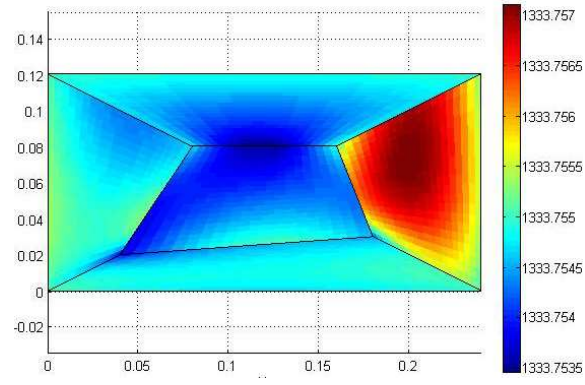
Figure 4.8: Membrane plate patch test σ_{xx} distribution
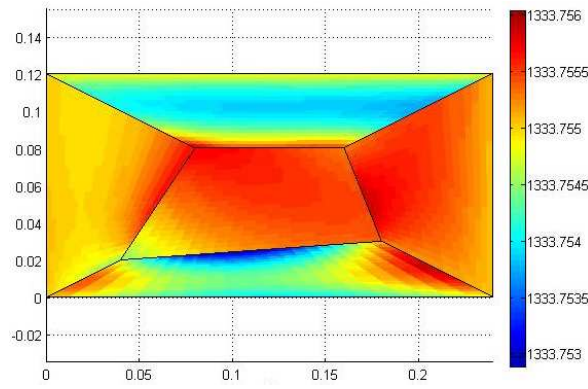
Figure 4.9: Membrane plate patch test σ_{22} distribution
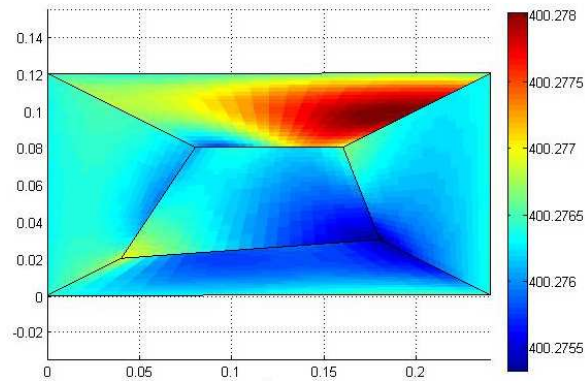
Figure 4.10: Membrane plate patch test τ_{12} distribution

Table 4.2: Results for membrane plate patch test

	Theoretical Solution [35]	**Average of the result**	**Error**
ϵ_x	10^{-3}	1.0006×10^{-3}	0.057%
ϵ_y	10^{-3}	1.0006×10^{-3}	0.057%
γ	10^{-3}	1.0007×10^{-3}	0.069%
σ_x	1333	1333.755	0.057%
σ_y	1333	1333.755	0.057%
τ_{xy}	400	400.277	0.069%

4.6.2 Straight Cantilever Beam Patch Test

Patch test problems proposed by Richard H. Macneal and Robert L. Harder [35] are given in Figure 4.11. Effects of skew angle and taperness of the element on the results can be verified by these tests. The first patch test contains regular rectangular elements having the aspect ratio of 5. In the second test, 45° taper angle is implemented to the elements. At the last case, elements are exposed to 45° skew angle. The beam to be solved has the length of 6.0, the width of 0.2, the depth of 0.1, modulus elasticity of $1.0x10^7$ and Poisson's ratio of 0.3. Patch test problems are solved for in-plane shear and extension cases with a unit force at the free end.
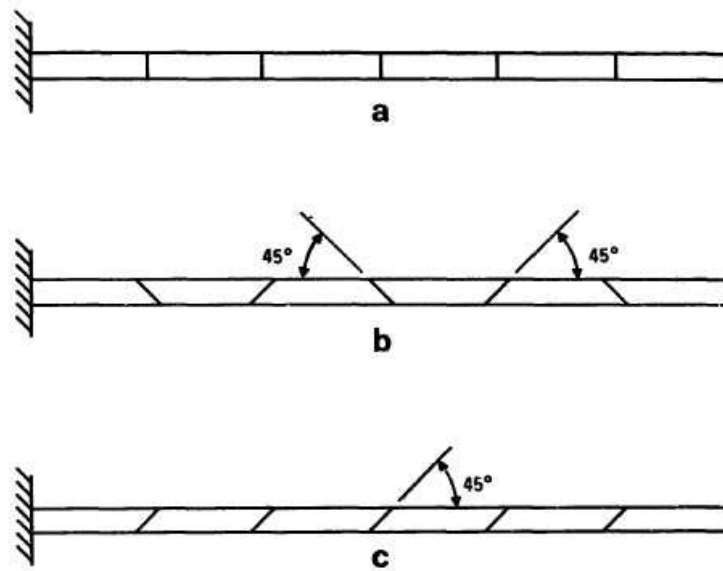
Figure 4.11: Straight cantilever beam patch test [35]

Finite element discretization of the beam is shown in Figure 4.12 and nodal connectivities of elements are described in Table 4.3. Initial nodal gradients are determined according to the virtual $X_v - Y_v$ frame, which is described in Section 5.1.1 as Method 1, and listed for regular, trapezoidal and parallelogram shape elements in Table 4.4. Fixed boundary conditions are applied for X, Y and $\partial X / \partial Y_v$ degrees of freedom of Node 1 and Node 8.
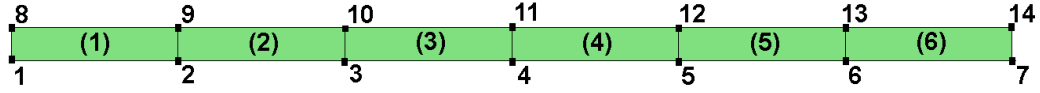
Figure 4.12: Discretized beam for patch test problem

Table 4.3: Connectivity of the elements

	1st Node	2nd Node	3rd Node	4th Node
Element 1	1	2	9	8
Element 2	2	3	10	9
Element 3	3	4	11	10
Element 4	4	5	12	11
Element 5	5	6	13	12
Element 6	6	7	14	13

Theoretically, regular element shapes will result continuous distributions for all stress components. However, discontinuous distributions for σ_{YY} and σ_{XY} will occur at the element transitions for the trapezoidal and parallelogram shaped elements given in Figure 4.11. Despite some discontinuities on two stress components, discontinuity on von Misses stress distributions for trapezoidal and parallelogram elements are negligible. The obtained von Misses stress distributions for regular, trapezoidal and parallelogram elements are given in Figures 4.13, 4.14 and 4.15. As can be seen from the figures, discontinuities on trapezoidal and parallelogram elements are negligible. In fact, just a single element is enough for the beam problem as given in Figure 4.16 due to third order shape function polynomials used.

Displacements on the load directions and their errors are listed in Table 4.5. As seen on the table, all of the results are in the acceptable ranges defined in the publication of Richard H.

Table 4.4: Initial nodal variables of straight cantilever beam for Method 1

	X			Y	$\partial X/\partial X_v$	$\partial Y/\partial X_v$	$\partial X/\partial Y_v$	$\partial Y/\partial Y_v$
	Regular	Trapezoidal	Parallelogram					
Node 1	0	0	0	0	1	0	0	1
Node 2	1	1.1	0.9	0	1	0	0	1
Node 3	2	1.9	1.9	0	1	0	0	1
Node 4	3	3.1	2.9	0	1	0	0	1
Node 5	4	3.9	3.9	0	1	0	0	1
Node 6	5	5.1	4.9	0	1	0	0	1
Node 7	6	6	6	0	1	0	0	1
Node 8	0	0	0	0.2	1	0	0	1
Node 9	1	0.9	1.1	0.2	1	0	0	1
Node 10	2	2.1	2.1	0.2	1	0	0	1
Node 11	3	2.9	3.1	0.2	1	0	0	1
Node 12	4	4.1	4.1	0.2	1	0	0	1
Node 13	5	4.9	5.1	0.2	1	0	0	1
Node 14	6	6	6	0.2	1	0	0	1

Macneal and Robert L. Harder [35]. As stated before, single regular element, which has the aspect ratio of 30, results almost exact displacement solutions. The maximum error has been obtained at the trapezoidal element solutions. Actually, this is not due to the taperness of the elements but due to differences in the edge lengths of neighboring elements. It is expected that the error will be reduced if the number of elements is increased even for the trapezoidal element shapes.
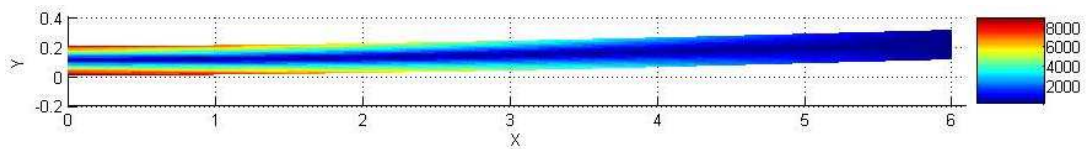
Figure 4.13: Von Misses stress distribution for straight cantilever beam with regular elements (In-plane shear)
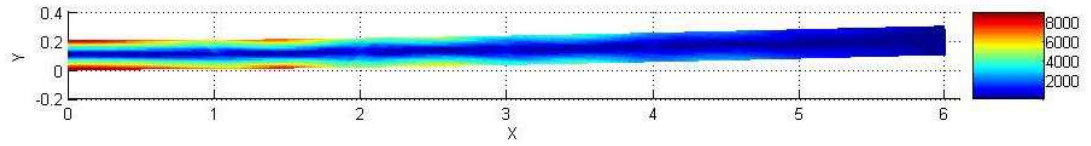
Figure 4.14: Von Misses stress distribution for straight cantilever beam with trapezoidal elements (In-plane shear)
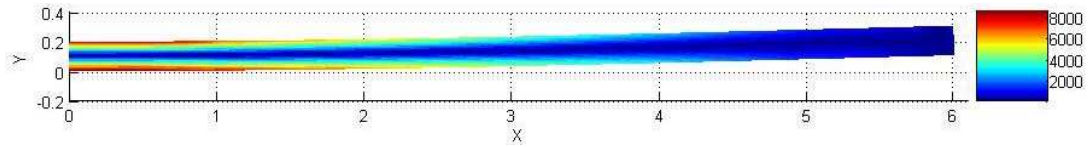
Figure 4.15: Von Misses stress distribution for straight cantilever beam with parallelogram elements (In-plane shear)
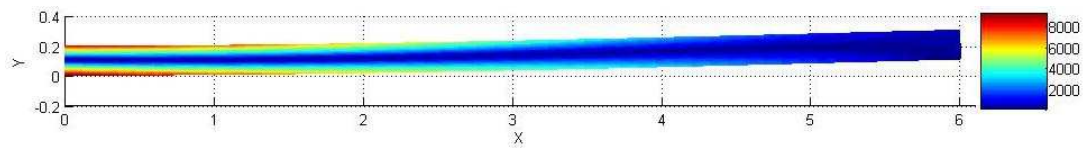
Figure 4.16: Von Misses stress distribution for straight cantilever beam with a single rectangular element (In-plane shear)

Table 4.5: Patch test results for straight beam

	Maximum tip displacement on the loading direction					
	In-plane shear			Extension ($\times 10^{-5}$)		
	Exact	Calculated	Error	Exact	Calculated	Error
Regular	0.1081	0.1081	0.00%	3.0	3.0126	0.42%
Trapezoidal	0.1081	0.0998	−7.68%	3.0	3.0205	0.68%
Parallelogram	0.1081	0.1077	−0.37%	3.0	3.0150	0.50%
One Element	0.1081	0.1077	−0.37%	3.0	2.9847	−0.51%

4.6.3 Curved Beam Patch Test

Curved beam patch test problem, proposed by Richard H. Macneal and Robert L. Harder [35], is discretized as given in Figure 4.17. Element connectivity matrix given in Table 4.3 has been used with the nodal variables defined according to Method 2 and listed in Table 4.6. The problem has been solved using the following parameters.

$$Inner/Outer \ Radius = 4.12/4.32$$

$$Arc \ Angle = 90°$$

$$thickness = 0.1$$

$$E = 1.0x10^7$$

$$\nu = 0.25$$
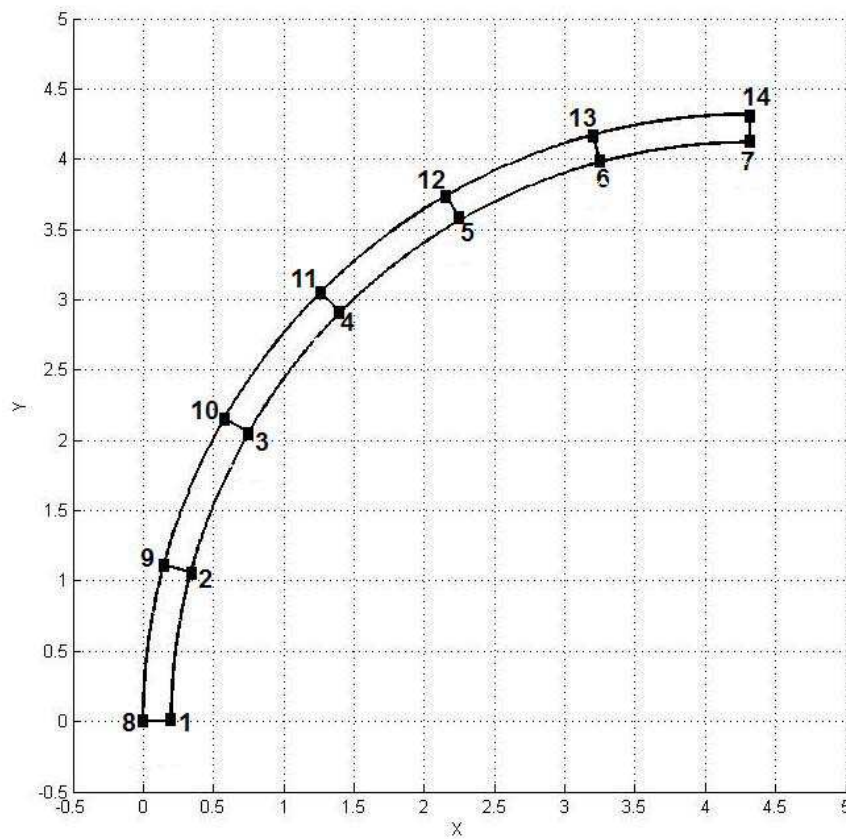
Figure 4.17: Discretized curved beam for the patch test problem

Table 4.6: Initial nodal variables of the curved beam for Method 2

Node	X	Y	$\partial X/\partial R_v$	$\partial Y/\partial R_v$	$\partial X/\partial S_v$	$\partial Y/\partial S_v$
1	0.2	0	0	1	-1	0
2	0.3403856	1.066334	0.2588190	0.9659258	-0.9659258	0.2588190
3	0.7519753	2.06	0.5	0.8660254	-0.8660254	0.5
4	1.406720	2.913280	0.7071068	0.7071068	-0.7071068	0.7071068
5	2.26	3.568025	0.8660254	0.5	-0.5	0.8660254
6	3.2537	3.979614	0.9659258	0.2588190	-0.2588190	0.9659258
7	4.32	4.12	1	0	0	1
8	0	0	0	1	-1	0
9	0.1472004	1.118098	0.2588190	0.9659258	-0.9659258	0.2588190
10	0.5787703	2.16	0.5	0.8660254	-0.8660254	0.5
11	1.265299	3.054701	0.7071068	0.7071068	-0.7071068	0.7071068
12	2.16	3.741230	0.8660254	0.5	-0.5	0.8660254
13	3.201902	4.172800	0.9659258	0.2588190	-0.2588190	0.9659258
14	4.32	4.32	1	0	0	1

The main objective of the test is to verify accuracy of finite elements under combined loading conditions. The curved beam is subjected to both normal and shear stresses with an in-plane shear force at the tip.

The original patch test problem contains 6 elements. However, the total number of elements can be reduced to 3 in the proposed formulation without losing accuracy in stresses and displacements. As the number of elements decreases discretized geometry starts to differ from the original geometry. Using single element for the finite element modeling results geometrical discrepancies and unacceptable stress distributions. However, single element can be used if the only concern is the accuracy in the tip displacement. For the simulation with 3 elements, Nodes 1, 3, 5, 7, 8, 10, 12 and 14 have been used without changing their nodal descriptions defined in Table 4.6. Similarly, Nodes 1, 4, 7, 8, 11 and 14 have been used for 2 elements, and Nodes 1, 7, 8 and 14 are used for single element simulations.

The von Misses stress distributions for 6 and 3 total element solutions are given in Figures 4.18 and 4.19. As seen from the figures, stresses are continuous over the element edges. Continuity is also valid for all stress components due to identical element shapes used in the discretization of the geometry. Tip displacements obtained by using 1, 2, 3 and 6 total number of elements in the loading direction are listed in Table 4.7. As the total number of elements decreases, the error encountered increases. However, errors in the tip displacement are in the

acceptable range even for a single element.
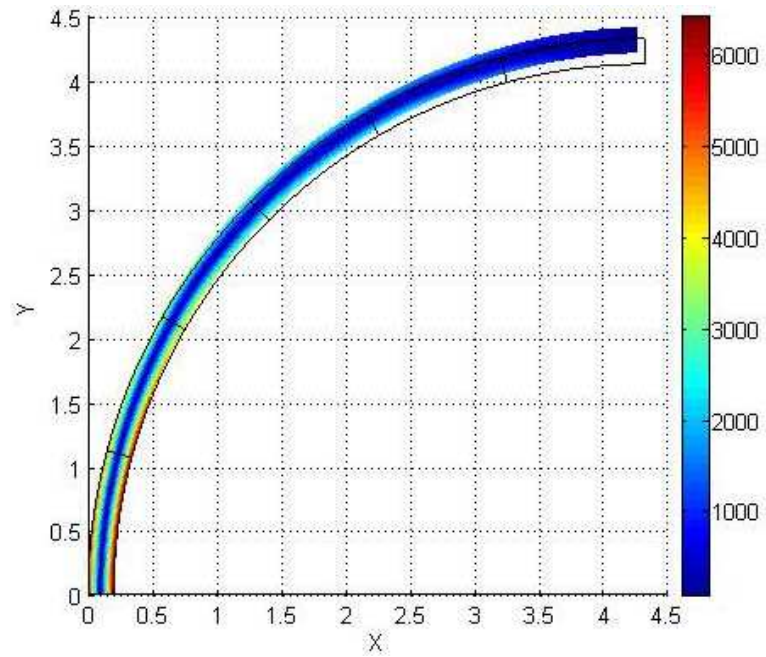
Figure 4.18: Von Misses stress distribution for curved beam with 6 elements (In-plane shear)
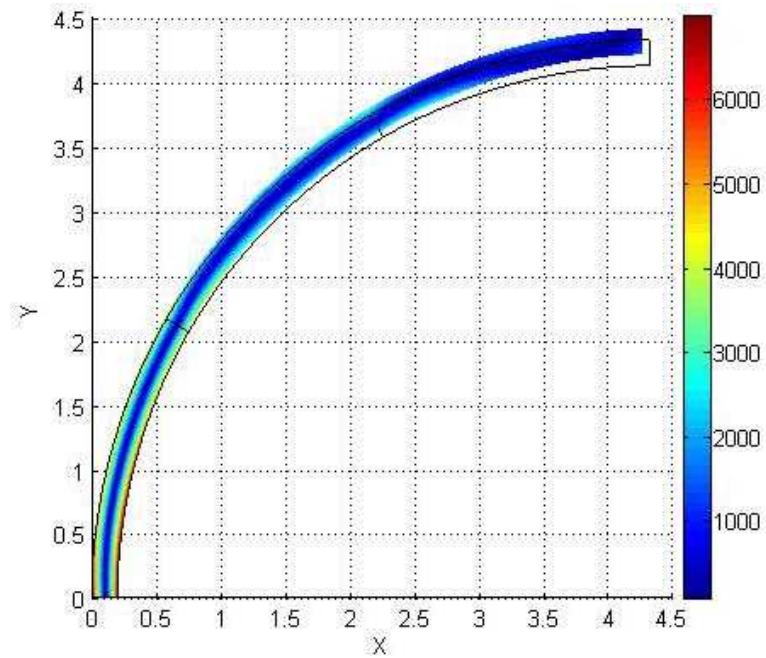
Figure 4.19: Von Misses stress distribution for curved beam with 3 elements (In-plane shear)

Table 4.7: Patch test results for the curved beam

	Maximum Tip Displacement		
	Theoretical	Calculated	Error
6 curved elements	0.08734	0.087122	−0.25%
3 curved elements	0.08734	0.086365	−1.12%
2 curved elements	0.08734	0.084826	−2.88%
1 curved element	0.08734	0.083818	−4.03%

4.7   Discussion

In this chapter, a completely new ANCF has been developed by using "virtual elements". Then, it is implemented to planar engineering problems. Accuracies of the developed methods and the proposed finite element formulation have been verified by some of the standard patch test problems proposed by Richard H. Macneal and Robert L. Harder [35].

Average of the grades for the proposed finite elements is **A**. The lowest grade, which is **B**, has been encountered in the test of in-plane loading of straight beam with trapezoidal elements. However, it is still in the acceptable range. The patch test results show that the proposed formulation works well for planar problems. However, these tests do not cover all of the geometrical shapes, which could be created with ANCF with Virtual Element Mapping. Therefore, the proposed method still needs to be verified for other geometrical shapes. These additional verification tests are left as future studies.

CHAPTER 5

ANCF FOR PLATE AND SHELL ELEMENTS HAVING IRREGULAR SHAPES

Currently, available ANCF's for quadrilateral plate and shell elements in the literature can only handle regular shapes like square or rectangle. However, the proposed methods in Chapter 4 can be adapted to plate and shell elements in order to handle irregular shapes of plate and shell elements, also. In this chapter, ANCF with Virtual Element Mapping has been implemented to four noded plate and shell finite elements. Presented formulation is based on the generalized plate assumption. In addition, shape functions for thin shell assumptions are also derived in the chapter. Therefore, thin plate and shell problems can easily be solved by using the derived shape functions and following the steps of generalized plate formulation.

5.1 Irregular Shaped Quadrilateral Finite Element Representation and Shape Function Creation for Generalized Plate Problems

In the generalized plate formulation the mapped t coordinate is added to the formulation presented in Chapter 4. One can chose the mapped coordinate frame given in Figure 5.1 as a local frame of the finite element. Then, the nodal degrees of freedom of an arbitrary element at the ith node should be written as given below.

$$\mathbf{e}_i^{rst} = \left[X_i\ Y_i\ Z_i\ \frac{\partial X_i}{\partial r}\ \frac{\partial Y_i}{\partial r}\ \frac{\partial Z_i}{\partial r}\ \frac{\partial X_i}{\partial s}\ \frac{\partial Y_i}{\partial s}\ \frac{\partial Z_i}{\partial s}\ \frac{\partial X_i}{\partial t}\ \frac{\partial Y_i}{\partial t}\ \frac{\partial Z_i}{\partial t} \right]^T \tag{5.1}$$

Figure 5.1: Mapped *rst* coordinate frame for the generalized plate/shell elements

Then, various geometrical finite element shapes could be created by imposing proper polynomial shape functions for global coordinates. The shape function selected for the generalized plate problems is given in the following equations.

$$X = \sum_{i=1}^{12} p_i a_i = \mathbf{p}^T \mathbf{a} \tag{5.2a}$$

$$Y = \sum_{i=1}^{12} p_i b_i = \mathbf{p}^T \mathbf{b} \tag{5.2b}$$

$$Z = \sum_{i=1}^{12} p_i c_i = \mathbf{p}^T \mathbf{c} \tag{5.2c}$$

$$\mathbf{p}^T = \begin{bmatrix} 1 & r & s & t & rs & rt & st & rst & r^2 & s^2 & r^2 s & rs^2 & r^3 & s^3 & r^3 s & rs^3 \end{bmatrix} \tag{5.2d}$$

In the equation, **a**, **b** and **c** are vectors of polynomial constants, and **p** is the vector of monomials of the shape function. Vector of polynomial constants could be formulated in terms of nodal degrees of freedom of the element as given below.

$$\mathbf{e}_i^{rst} = \mathbf{Q}(r_i, s_i, t_i)\mathbf{A} \tag{5.3}$$

103

where

$$
\mathbf{Q}(r, s, t) =
\begin{vmatrix}
\mathbf{p}^T(r, s, t) & \mathbf{0} & \mathbf{0} \\
\mathbf{0} & \mathbf{p}^T(r, s, t) & \mathbf{0} \\
\mathbf{0} & \mathbf{0} & \mathbf{p}^T(r, s, t) \\
\mathbf{p}^T_{,r}(r, s, t) & \mathbf{0} & \mathbf{0} \\
\mathbf{0} & \mathbf{p}^T_{,r}(r, s, t) & \mathbf{0} \\
\mathbf{0} & \mathbf{0} & \mathbf{p}^T_{,r}(r, s, t) \\
\mathbf{p}^T_{,s}(r, s, t) & \mathbf{0} & \mathbf{0} \\
\mathbf{0} & \mathbf{p}^T_{,s}(r, s, t) & \mathbf{0} \\
\mathbf{0} & \mathbf{0} & \mathbf{p}^T_{,s}(r, s, t) \\
\mathbf{p}^T_{,t}(r, s, t) & \mathbf{0} & \mathbf{0} \\
\mathbf{0} & \mathbf{p}^T_{,t}(r, s, t) & \mathbf{0} \\
\mathbf{0} & \mathbf{0} & \mathbf{p}^T_{,t}(r, s, t)
\end{vmatrix}
\tag{5.4a}
$$

$$
\mathbf{A} = \begin{bmatrix} \mathbf{a}^T & \mathbf{b}^T & \mathbf{c}^T \end{bmatrix}^T
\tag{5.4b}
$$

and, r_i, s_i and t_i represent the mapped coordinates of the ith node on the element and are defined as given below.

$$
[r_1 \ r_2 \ r_3 \ r_4] = [-1 \ +1 \ +1 \ -1]
\tag{5.5a}
$$

$$
[s_1 \ s_2 \ s_3 \ s_4] = [-1 \ -1 \ +1 \ +1]
\tag{5.5b}
$$

$$
[t_1 \ t_2 \ t_3 \ t_4] = [0 \ 0 \ 0 \ 0]
\tag{5.5c}
$$

While the ranges of r and s are between -1 and $+1$, the range of t is between $-^0t/2$ and $+^0t/2$, where ^0t is the thickness of the flexible structure.

Linear set of algebraic equations to be solved for $\mathbf{A}$ can be derived by using Equation 5.3 for all four nodes of the element as given in the following equation.

$$
\mathbf{e}^{rst} = \mathbf{PA}
\tag{5.6a}
$$

$$
\mathbf{A} = \mathbf{P}^{-1}\mathbf{e}^{rst}
\tag{5.6b}
$$

104

where

$$\mathbf{P} = \begin{bmatrix} \mathbf{Q}(r_1, s_1, t_1) \\ \mathbf{Q}(r_2, s_2, t_2) \\ \mathbf{Q}(r_3, s_3, t_3) \\ \mathbf{Q}(r_4, s_4, t_4) \end{bmatrix} \tag{5.7a}$$

Then, vector of polynomial constants, $\mathbf{A}$, can be found by using Equation 5.6.b. Additionally, $\mathbf{P}^{-1}$ always exists and is constant as given in the previous formulations.

Various 3D plate/shell element shapes (samples are shown in Figure 5.2) could be generated by using the derived shape function polynomials, given in Equation 5.6, for appropriate nodal degrees of freedom. This feature of the developed formulation allows accurate discretization of irregular geometries. However, the shape function polynomials for neighboring elements would cause discontinuities on the common element edges as in the planar elements presented in Chapter 4. The desired common edge shape might require different nodal gradients for neighboring elements. This problem can be overcome by changing or forcing nodal gradients ($\partial X/\partial r$, $\partial Y/\partial r$, $\partial Z/\partial r$, $\partial X/\partial s$, $\partial Y/\partial s$, $\partial Z/\partial s$, $\partial X/\partial t$, $\partial Y/\partial t$, $\partial Z/\partial t$) to generate the same edge shapes for neighboring elements. Then, system equations can be formed by using general finite element assembly procedures.

As discussed above, using mapped rst coordinates for nodal gradient definitions is not appropriate. However, shape function polynomials can be generated easily by using the mapped coordinates. Therefore, additional virtual finite elements, which uses the same mapped rst coordinates with different shape (or mapping) functions, are created on a virtual $X_v Y_v Z_v$ coordinate frame, which is constant and parallel to the global XYZ frame, in order to overcome incompatibility problem in gradients. Then, nodal gradients can be redefined with respect to the virtual coordinate frame. Consequently, shape function matrix, which can generate global coordinates and gradients at an arbitrary point on an element by using nodal degrees of freedom, can be formulated. Various shape function matrices could be formulated depending on the choices made for virtual element's geometrical shape and virtual shape functions. Additionally, using different shape function polynomials for original elements than Equation 5.2 would result alternative shape function matrices, also. Some of the methods,

that can be used for shape function matrix generation, are given in the following subsections.
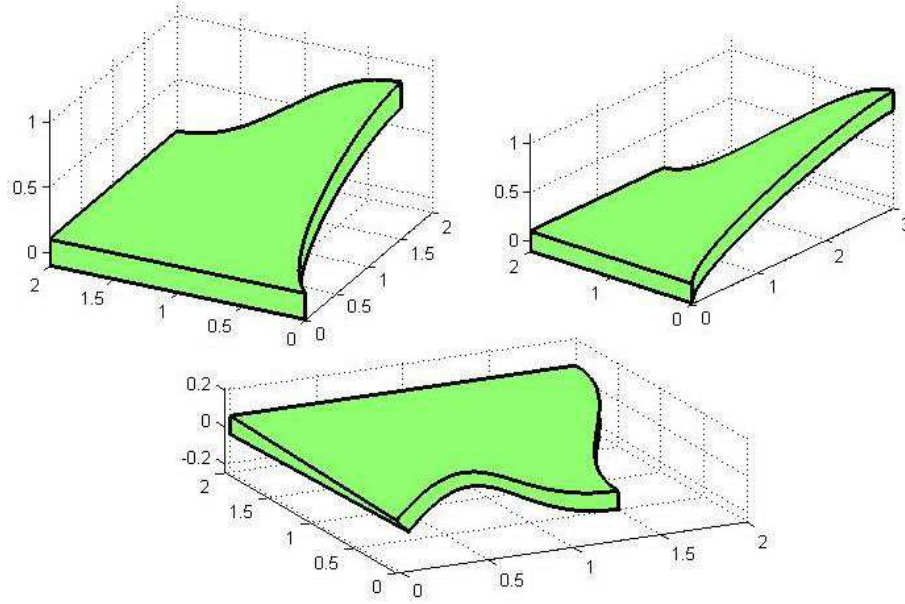
Figure 5.2: Various 3D plate/shell element shapes

5.1.1   Method 1: Parallel Virtual Frame and First Order Virtual Element Mapping

In this method, nodal degrees of freedom for the ith node of an arbitrary element is described as given below.

$$\mathbf{e}_i = \left[X_i \ Y_i \ Z_i \ \frac{\partial X_i}{\partial X_v} \ \frac{\partial Y_i}{\partial X_v} \ \frac{\partial Z_i}{\partial X_v} \ \frac{\partial X_i}{\partial Y_v} \ \frac{\partial Y_i}{\partial Y_v} \ \frac{\partial Z_i}{\partial Y_v} \ \frac{\partial X_i}{\partial Z_v} \ \frac{\partial Y_i}{\partial Z_v} \ \frac{\partial Z_i}{\partial Z_v} \right]^T \tag{5.8}$$
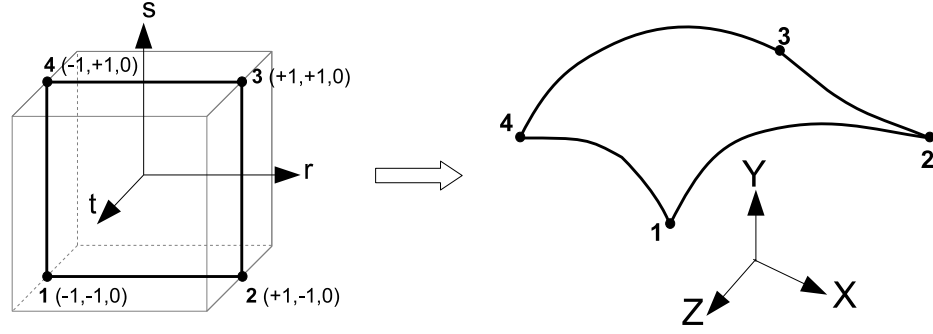
In the equation, nodal gradients are defined with respect to the virtual coordinate frame shown in Figure 5.3. Mapping functions for virtual coordinates at an arbitrary point on the element can be constructed by using interpolation polynomial of a general first order interpolation functions for 3D isoparametric hexahedral elements [36] as given in the following equation.

$$X_v(r, s, t) = \mathbf{H_v}(r, s) \left({}^0\mathbf{X} + t \, {}^0\mathbf{X}_{,t} \right) \tag{5.9a}$$

$$Y_v(r, s, t) = \mathbf{H_v}(r, s) \left({}^0\mathbf{Y} + t \, {}^0\mathbf{Y}_{,t} \right) \tag{5.9b}$$

$$Z_v(r, s, t) = \mathbf{H_v}(r, s) \left({}^0\mathbf{Z} + t \, {}^0\mathbf{Z}_{,t} \right) \tag{5.9c}$$
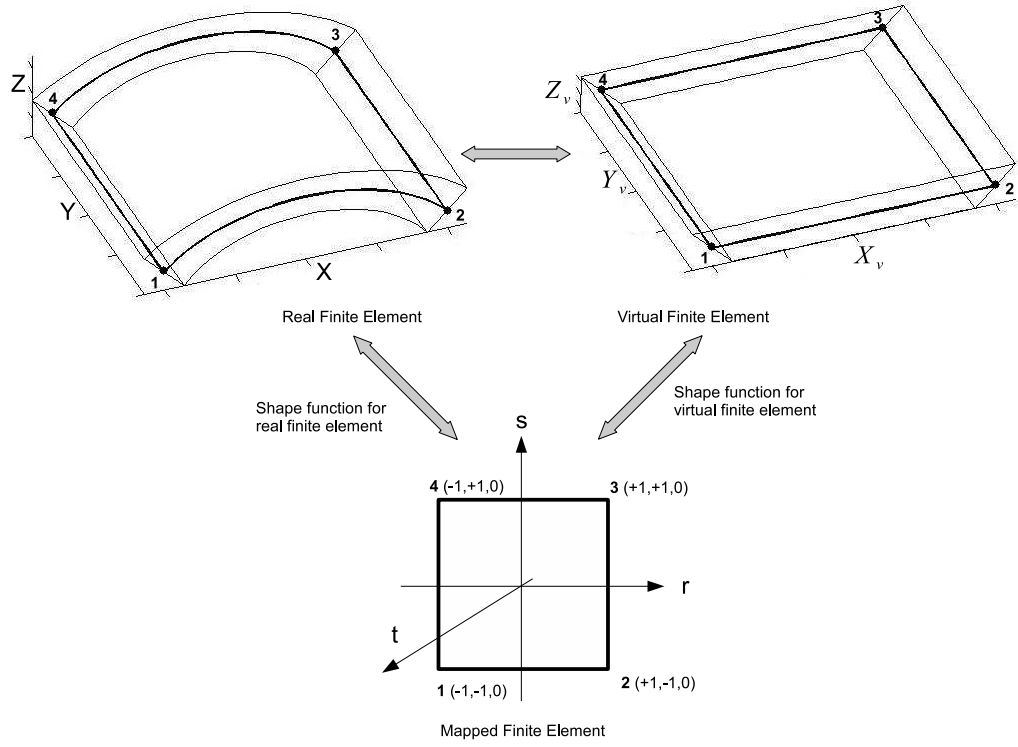
Figure 5.3: Coordinate frames for Parallel Virtual Frame and First Order Virtual Element Mapping Method

where

$$\mathbf{H_v} = \frac{1}{4}\left[(1-r)(1-s) \quad (1+r)(1-s) \quad (1+r)(1+s) \quad (1-r)(1+s)\right] \tag{5.10a}$$

$${}^0\mathbf{X} = \begin{bmatrix}{}^0X_1 & {}^0X_2 & {}^0X_3 & {}^0X_4\end{bmatrix}^T \tag{5.10b}$$

$${}^0\mathbf{Y} = \begin{bmatrix}{}^0Y_1 & {}^0Y_2 & {}^0Y_3 & {}^0Y_4\end{bmatrix}^T \tag{5.10c}$$

$${}^0\mathbf{Z} = \begin{bmatrix}{}^0Z_1 & {}^0Z_2 & {}^0Z_3 & {}^0Z_4\end{bmatrix}^T \tag{5.10d}$$

$${}^0\mathbf{X}_{,t} = \begin{bmatrix}{}^0X_{1,t} & {}^0X_{2,t} & {}^0X_{3,t} & {}^0X_{4,t}\end{bmatrix}^T \tag{5.10e}$$

$${}^0\mathbf{Y}_{,t} = \begin{bmatrix}{}^0Y_{1,t} & {}^0Y_{2,t} & {}^0Y_{3,t} & {}^0Y_{4,t}\end{bmatrix}^T \tag{5.10f}$$

$${}^0\mathbf{Z}_{,t} = \begin{bmatrix}{}^0Z_{1,t} & {}^0Z_{2,t} & {}^0Z_{3,t} & {}^0Z_{4,t}\end{bmatrix}^T \tag{5.10g}$$

As seen from Equation 5.9, the virtual 3D element is constructed by using not only initial node

locations but also the initial gradients in the thickness directions. Therefore, these gradient terms should be defined, initially. Then, three of the nodal gradients appearing in Equation 5.8 are redundant and do not have to be defined, initially. In the thesis, starting nodal gradients are selected as $\partial \mathbf{X}_i / \partial X_v$, $\partial \mathbf{X}_i / \partial Y_v$ and $\partial \mathbf{X}_i / \partial t$. However, Equation 5.8 is still valid, therefore, initial $\partial \mathbf{X}_i / \partial Z_v$ has to be calculated by using predefined nodal gradients.

Then, gradients with respect to the mapped rst frame can be written in terms of nodal gradients in compact form as given below.

$$\mathbf{e}^{rst}(r, s, t) = \mathbf{T}_{m1}(r, s, t)\mathbf{e}(r, s, t) \tag{5.11a}$$

$$\mathbf{e}(r, s, t) = (\mathbf{T}_{m1}(r, s, t))^{-1} \mathbf{e}^{rst}(r, s, t) \tag{5.11b}$$

where

$$\mathbf{T}_{m1}(r, s, t) =
\begin{bmatrix}
1 & 0 & 0 & 0 & 0 & 0 & 0 & 0 & 0 & 0 & 0 & 0 \\
0 & 1 & 0 & 0 & 0 & 0 & 0 & 0 & 0 & 0 & 0 & 0 \\
0 & 0 & 1 & 0 & 0 & 0 & 0 & 0 & 0 & 0 & 0 & 0 \\
0 & 0 & 0 & X_{v,r} & 0 & 0 & Y_{v,r} & 0 & 0 & Z_{v,r} & 0 & 0 \\
0 & 0 & 0 & 0 & X_{v,r} & 0 & 0 & Y_{v,r} & 0 & 0 & Z_{v,r} & 0 \\
0 & 0 & 0 & 0 & 0 & X_{v,r} & 0 & 0 & Y_{v,r} & 0 & 0 & Z_{v,r} \\
0 & 0 & 0 & X_{v,s} & 0 & 0 & Y_{v,s} & 0 & 0 & Z_{v,s} & 0 & 0 \\
0 & 0 & 0 & 0 & X_{v,s} & 0 & 0 & Y_{v,s} & 0 & 0 & Z_{v,s} & 0 \\
0 & 0 & 0 & 0 & 0 & X_{v,s} & 0 & 0 & Y_{v,s} & 0 & 0 & Z_{v,s} \\
0 & 0 & 0 & X_{v,t} & 0 & 0 & Y_{v,t} & 0 & 0 & Z_{v,t} & 0 & 0 \\
0 & 0 & 0 & 0 & X_{v,t} & 0 & 0 & Y_{v,t} & 0 & 0 & Z_{v,t} & 0 \\
0 & 0 & 0 & 0 & 0 & X_{v,t} & 0 & 0 & Y_{v,t} & 0 & 0 & Z_{v,t}
\end{bmatrix} \tag{5.12}$$

Consequently, degrees of freedom vector, $\mathbf{e}$, can be converted into the form given in Equation 5.6, $\mathbf{e}^{rst}$, as formulated in the following equation.

$$\mathbf{e}^{rst} = \mathbf{T}_{map1}\mathbf{e} \tag{5.13}$$

where the transformation matrix, $\mathbf{T}_{map1}$, can be evaluated by using Equation 5.11 for all four nodes of the element as given below.

$$\mathbf{T}_{map1} =
\begin{bmatrix}
\mathbf{T}_{m1}(r_1, s_1, t_1) & \mathbf{0} & \mathbf{0} & \mathbf{0} \\
\mathbf{0} & \mathbf{T}_{m1}(r_2, s_2, t_2) & \mathbf{0} & \mathbf{0} \\
\mathbf{0} & \mathbf{0} & \mathbf{T}_{m1}(r_3, s_3, t_3) & \mathbf{0} \\
\mathbf{0} & \mathbf{0} & \mathbf{0} & \mathbf{T}_{m1}(r_4, s_4, t_4)
\end{bmatrix} \tag{5.14}$$

Finally, global coordinates and gradients with respect to the virtual frame at an arbitrary point can be written in terms of nodal variables by following the procedure given below;

1. Substitute Equation 5.13 into Equation 5.6b to obtain polynomial constants as;

$$\mathbf{A} = \mathbf{P}^{-1}\mathbf{T}_{map1}\,\mathbf{e}$$

2. Substitute polynomial constants into Equation 5.3 in order to obtain vector function used to evaluate global positions and gradients with respect to the mapped *rst* frame as given below;

$$\mathbf{e}^{rst}(r, s, t) = \mathbf{Q}(r, s, t)\mathbf{P}^{-1}\mathbf{T}_{map1}\,\mathbf{e}$$

3. Then, substitute the equation above into Equation 5.11b as;

$$\mathbf{e}(r, s, t) = \mathbf{T}_{\mathbf{m1}}(r, s, t)^{-1}\,\mathbf{Q}(r, s, t)\mathbf{P}^{-1}\mathbf{T}_{map1}\,\mathbf{e} \tag{5.15}$$

Then, it can be written in a simple form given below;

$$\mathbf{e}(r, s, t) = \mathbf{S}(r, s, t)\,\mathbf{e} \tag{5.16}$$

where the shape function matrix is defined as;

$$\mathbf{S}(r, s, t) = \mathbf{T}_{m1}(r, s, t)^{-1}\mathbf{Q}(r, s, t)\mathbf{P}^{-1}\,\mathbf{T}_{map1} \tag{5.17}$$

In the equation, $\mathbf{P}^{-1}$ and $\mathbf{T}_{map}$ are independent of local coordinates and time. The derived shape function ensures continuity of nodal parameter at the neighboring node location. Global coordinates are continuous over neighboring element edges. However, continuity of gradients is only guaranteed on node locations. Therefore, stresses or strains will not be continuous over element edges but be continuous over node locations. Continuous stress/strain distributions can be created by linear interpolation over nodal stresses or strains in post-processing stage.

Similar to the planar formulation in Chapter 4, it is hard to define initial nodal gradients ($\partial X/\partial X_v$, $\partial Y/\partial X_v$, $\partial Z/\partial X_v$, $\partial X/\partial Y_v$, $\partial Y/\partial Y_v$ and $\partial Z/\partial Y_v$) of the elements. In order to

overcome this difficulty, alternative nodal representation, Virtual Element Edge Frame and First Order Virtual Element Mapping, has been implemented in following section.

5.1.2 Method 2: Virtual Element Edge Frame and First Order Virtual Element Mapping

In this method, nodal gradients are redefined with respect to the linear edges and T_v vector, which is created according to the gradients in the thickness direction of virtual finite element, in order to make geometrical meaning of nodal gradients more understandable. As shown in Figure 5.3, first and second nodes, and third and fourth nodes are connected with straight lines, where S_v and T_v are constant. Similarly, second and third nodes, and fourth and first nodes are connected with straight lines, where R_v and T_v are constant. These four straight lines connecting the nodes form the boundaries of the virtual element in $X_v Y_v Z_v$ frame. In fact, $R_v S_v T_v$ is not a new coordinate frame, but they are products of virtual $X_v Y_v Z_v$ frame. Let's consider a point, which has the mapped coordinates of (r_a, s_a, t_a) on the element, in order to clarify R_v, S_v and T_v definitions. Then, R_v is defined as the magnitude of the vector from the virtual point at $(-1, s_a, t_a)$ to the point at (r, s_a, t_a). Similarly, S_v is defined as the magnitude of the vector from the virtual point at $(r_a, -1, t_a)$ to the point at (r_a, s, t_a). Finally, T_v is defined as the magnitude of the vector from the virtual point at $(r_a, t_a, -^0t/2)$ to the point at (r_a, s_a, t). Therefore, they can be defined with respect to the virtual coordinate frame, $X_v Y_v Z_v$, defined in Equation 5.9, as given in the following equations. As can be seen from the equations, R_v is a function of r, S_v is a function of s and T_v is a function of t, only.

$$R_v(r) = \sqrt{\left(\mathbf{H_{vr}}(r)\left(\mathbf{X}^0 + t_a\mathbf{X}^0_{,t}\right)\right)^2 + \left(\mathbf{H_{vr}}(r)\left(\mathbf{Y}^0 + t_a\mathbf{Y}^0_{,t}\right)\right)^2 + \left(\mathbf{H_{vr}}(r)\left(\mathbf{Z}^0 + t_a\mathbf{Z}^0_{,t}\right)\right)^2} \quad (5.18a)$$

$$S_v(s) = \sqrt{\left(\mathbf{H_{vs}}(s)\left(\mathbf{X}^0 + t_a\mathbf{X}^0_{,t}\right)\right)^2 + \left(\mathbf{H_{vs}}(s)\left(\mathbf{Y}^0 + t_a\mathbf{Y}^0_{,t}\right)\right)^2 + \left(\mathbf{H_{vs}}(s)\left(\mathbf{Z}^0 + t_a\mathbf{Z}^0_{,t}\right)\right)^2} \quad (5.18b)$$

$$T_v(t) = \left(t + \frac{^0t}{2}\right)\sqrt{\left(\mathbf{H_v}(r_a, s_a)\mathbf{X}^0_{,t}\right)^2 + \left(\mathbf{H_v}(r_a, s_a)\mathbf{Y}^0_{,t}\right)^2 + \left(\mathbf{H_v}(r_a, s_a)\mathbf{Z}^0_{,t}\right)^2} \quad (5.18c)$$

where

$$\mathbf{H_{vr}}(r) = \mathbf{H_v}(r, s_a) - \mathbf{H_v}(-1, s_a) = \frac{(1+r)}{4}\left[-1+s_a \quad 1-s_a \quad 1+s_a \quad -1-s_a\right] \qquad (5.19a)$$

$$\mathbf{H_{vs}}(s) = \mathbf{H_v}(r_a, s) - \mathbf{H_v}(r_a, -1) = \frac{(1+s)}{4}\left[-1+r_a \quad -1-r_a \quad 1+r_a \quad 1-r_a\right] \qquad (5.19b)$$

Gradients of virtual $R_v S_v T_v$ frame with respect to the mapped rst frame at an arbitrary point on the element can be written explicitly as given below.

$$\frac{\partial R_v}{\partial r} = \frac{1}{4}\sqrt{\begin{array}{c}(C_{X1}+C_{X2}\,s+t\,(D_{X1}+D_{X2}\,s))^2+(C_{Y1}+C_{Y2}\,s+t\,(D_{Y1}+D_{Y2}\,s))^2\\ \cdots+(C_{Z1}+C_{Z2}\,s+t\,(D_{Z1}+D_{Z2}\,s))^2\end{array}} \qquad (5.20a)$$

$$\frac{\partial S_v}{\partial s} = \frac{1}{4}\sqrt{\begin{array}{c}(C_{X3}+C_{X2}\,r+t\,(D_{X3}+D_{X2}\,r))^2+(C_{Y3}+C_{Y2}\,r+t\,(D_{Y3}+D_{Y2}\,r))^2\\ \cdots+(C_{Z3}+C_{Z2}\,r+t\,(D_{Z3}+D_{Z2}\,r))^2\end{array}} \qquad (5.20b)$$

$$\frac{\partial T_v}{\partial t} = \sqrt{\left(\mathbf{H_v}(r,s)\mathbf{X}^0_{,t}\right)^2+\left(\mathbf{H_v}(r,s)\mathbf{Y}^0_{,t}\right)^2+\left(\mathbf{H_v}(r,s)\mathbf{Z}^0_{,t}\right)^2} \qquad (5.20c)$$

$$\frac{\partial R_v}{\partial s} = \frac{\partial R_v}{\partial t} = \frac{\partial S_v}{\partial r} = \frac{\partial S_v}{\partial t} = \frac{\partial T_v}{\partial r} = \frac{\partial T_v}{\partial s} = 0 \qquad (5.20d)$$

where

$$\begin{bmatrix} C_{X1} & C_{Y1} & C_{Z1} \\ C_{X2} & C_{Y2} & C_{Z2} \\ C_{X3} & C_{Y3} & C_{Z3} \\ D_{X1} & D_{Y1} & D_{Z1} \\ D_{X2} & D_{Y2} & D_{Z2} \\ D_{X3} & D_{Y3} & D_{Z3} \end{bmatrix} = \begin{bmatrix} (-X^0_1+X^0_2+X^0_3-X^0_4) & (-Y^0_1+Y^0_2+Y^0_3-Y^0_4) & (-Z^0_1+Z^0_2+Z^0_3-Z^0_4) \\ (+X^0_1-X^0_2+X^0_3-X^0_4) & (+Y^0_1-Y^0_2+Y^0_3-Y^0_4) & (+Z^0_1-Z^0_2+Z^0_3-Z^0_4) \\ (-X^0_1-X^0_2+X^0_3+X^0_4) & (-Y^0_1-Y^0_2+Y^0_3+Y^0_4) & (-Y^0_1-Y^0_2+Y^0_3+Y^0_4) \\ (-X^0_{1,t}+X^0_{2,t}+X^0_{3,t}-X^0_{4,t}) & (-Y^0_{1,t}+Y^0_{2,t}+Y^0_{3,t}-Y^0_{4,t}) & (-Z^0_{1,t}+Z^0_{2,t}+Z^0_{3,t}-Z^0_{4,t}) \\ (+X^0_{1,t}-X^0_{2,t}+X^0_{3,t}-X^0_{4,t}) & (+Y^0_{1,t}-Y^0_{2,t}+Y^0_{3,t}-Y^0_{4,t}) & (+Z^0_{1,t}-Z^0_{2,t}+Z^0_{3,t}-Z^0_{4,t}) \\ (-X^0_{1,t}-X^0_{2,t}+X^0_{3,t}+X^0_{4,t}) & (-Y^0_{1,t}-Y^0_{2,t}+Y^0_{3,t}+Y^0_{4,t}) & (-Y^0_{1,t}-Y^0_{2,t}+Y^0_{3,t}+Y^0_{4,t}) \end{bmatrix} \qquad (5.21)$$

Then, nodal variables, $\mathbf{e}$, for the ith node of an arbitrary element can be written as follows.

$$\mathbf{e}_i = \left[X_i \ Y_i \ Z_i \ \frac{\partial X_i}{\partial R_v} \ \frac{\partial Y_i}{\partial R_v} \ \frac{\partial Z_i}{\partial R_v} \ \frac{\partial X_i}{\partial S_v} \ \frac{\partial Y_i}{\partial S_v} \ \frac{\partial Z_i}{\partial S_v} \ \frac{\partial X_i}{\partial T_v} \ \frac{\partial Y_i}{\partial T_v} \ \frac{\partial Z_i}{\partial T_v}\right]^T \qquad (5.22)$$

In the equation, X_i, Y_i and Z_i are coordinates of the ith node in global frame. As stated in the previous chapter, the gradient vectors at nodes are always tangent to the element edges.

The gradients with respect to the mapped rst frame can be written in terms of the nodal gradients ($\partial X/\partial R_v$, $\partial Y/\partial R_v$, $\partial Z/\partial R_v$, $\partial X/\partial S_v$, $\partial Y/\partial S_v$, $\partial Z/\partial S_v$, $\partial X/\partial T_v$, $\partial Y/\partial T_v$ and $\partial Z/\partial T_v$) as given in the following equation.

$$\mathbf{e}^{rst}(r, s, t) = \mathbf{T_{m2}}(r, s, t) \, \mathbf{e}(r, s, t) \qquad (5.23a)$$

$$\mathbf{e}(r, s, t) = (\mathbf{T_{m2}}(r, s, t))^{-1} \, \mathbf{e}^{rst}(r, s, t) \qquad (5.23b)$$

where

$$\mathbf{T_{m2}}(r, s, t) = \mathbf{I_{12x12}} \begin{bmatrix} 1 & 1 & 1 & R_{v,r} & R_{v,r} & R_{v,r} & S_{v,s} & S_{v,s} & S_{v,s} & T_{v,t} & T_{v,t} & T_{v,t} \end{bmatrix} \qquad (5.24)$$

Consequently, degrees of freedom vector, $\mathbf{e}$, can be converted into the form given in Equation 5.6, $\mathbf{e^{rst}}$, as formulated in the following equation.

$$\mathbf{e^{rst}} = \mathbf{T}_{map2}\mathbf{e} \qquad (5.25)$$

where the transformation matrix, $\mathbf{T}_{map2}$, can be evaluated by using Equation 5.23 as given below.

$$\mathbf{T}_{map2} = \begin{bmatrix} \mathbf{T}_{m2}(r_1, s_1, t_1) & \mathbf{0} & \mathbf{0} & \mathbf{0} \\ \mathbf{0} & \mathbf{T}_{m2}(r_2, s_2, t_2) & \mathbf{0} & \mathbf{0} \\ \mathbf{0} & \mathbf{0} & \mathbf{T}_{m2}(r_3, s_3, t_3) & \mathbf{0} \\ \mathbf{0} & \mathbf{0} & \mathbf{0} & \mathbf{T}_{m2}(r_4, s_4, t_4) \end{bmatrix} \qquad (5.26)$$

Similar to the planar formulation presented in the previous chapter, $\mathbf{T_{map2}}$ matrix can be written in terms of the virtual edge lengths of the element similar.

Finally, global coordinates and gradients with respect to the virtual frame at an arbitrary point can be written in terms of nodal variables by following the similar procedure described for Method 1 as given below.

$$\mathbf{e}(r, s, t) = \mathbf{T_{m2}}(r, s, t)^{-1} \, \mathbf{Q}(r, s, t)\mathbf{P}^{-1}\mathbf{T}_{map2} \, \mathbf{e} \qquad (5.27)$$

Then, it can be written in the following simple form.

$$\mathbf{e}(r, s, t) = \mathbf{S}(r, s, t) \, \mathbf{e} \qquad (5.28)$$

where the shape function matrix for Method 2 is defined as

$$\mathbf{S}(r, s, t) = \mathbf{T}_{m2}(r, s, t)^{-1}\mathbf{Q}(r, s, t)\mathbf{P}^{-1}\,\mathbf{T}_{map2} \tag{5.29}$$

Similar to the planar formulation for virtual $R_v S_v$ frame, while $R_v S_v T_v$ frame making geometrical definitions of nodal gradients easier, it brings following restrictions:

- Neighboring elements should be numbered such that their common virtual element edges should refer to the same virtual coordinate.

- Due to nodal gradient definitions, discontinuous element edge transitions (Figure 5.4) can not be modeled.
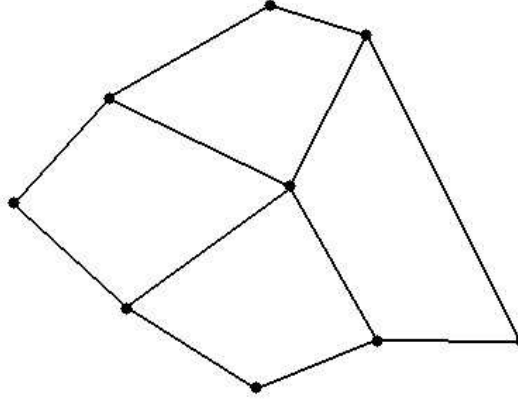
Figure 5.4: Not applicable element transitions for Method 2

5.1.3 Other Applicable Methods for Shape Function Matrix Formulation

Basically, quadrilateral plate and shell finite elements require two shape function polynomials for shape function matrix generation. Depending on the selected shape functions, various alternative solution methods can be generated. In the previous chapter, another alternative method called "Method 3: Initial Element Frame Mapping Method" was proposed. The same method can also be used for plate and shell element formulations. In the method, initial shape function polynomials are used instead of virtual $X_v Y_v Z_v$ or $R_v S_v T_v$ frames. Then, nodal variables, $\mathbf{e}_i$, for the ith node of an arbitrary element can be written as follows.

113

$$\mathbf{e}_i = \left[X_i \ Y_i \ Z_i \ \frac{\partial X_i}{\partial^0 X} \ \frac{\partial Y_i}{\partial^0 X} \ \frac{\partial Z_i}{\partial^0 X} \ \frac{\partial X_i}{\partial^0 Y} \ \frac{\partial Y_i}{\partial^0 Y} \ \frac{\partial Z_i}{\partial^0 Y} \ \frac{\partial X_i}{\partial^0 Z} \ \frac{\partial Y_i}{\partial^0 Z} \ \frac{\partial Z_i}{\partial^0 Z} \right]^T \qquad (5.30)$$

Derivation of the shape function matrix can easily be performed by following the procedure given in Chapter 4. Finally, simpler generalized elastic force formulation can be obtained.

5.2   Mass Matrix Formulation

The constant mass matrix of the proposed plate/shell element can be derived using the general kinetic energy equation similar to the derivation performed in Chapter 4. The mass matrix at an arbitrary time, t, is independent of time and can be evaluated once by using the initial density and volume. Then, it can be used at any time step during the solution process. The derived mass matrix equation is given below.

$$\mathbf{M} = \int_{V^{rst}} \rho \, \mathbf{S}_{123}^T \mathbf{S}_{123} \, |\mathbf{D}| \, dr \, ds \, dt \qquad (5.31)$$

where the gradient tensor between initial global coordinates and the mapped frame is defined below.

$$\mathbf{D} = \frac{\partial \mathbf{X}_0}{\partial \mathbf{r}} = \begin{bmatrix} \frac{\partial X_0}{\partial r} & \frac{\partial X_0}{\partial s} & \frac{\partial X_0}{\partial t} \\ \frac{\partial Y_0}{\partial r} & \frac{\partial Y_0}{\partial s} & \frac{\partial Y_0}{\partial t} \\ \frac{\partial Z_0}{\partial r} & \frac{\partial Z_0}{\partial s} & \frac{\partial Z_0}{\partial t} \end{bmatrix} \qquad (5.32)$$

In Equation 5.31, $\mathbf{S}_{123}$ is the shape function matrix of global coordinates, which contains first three rows of the shape function matrices given in Equations 5.17 or 5.29. Additionally, it is important to remember that t varies from $-^0 t/2$ to $+^0 t/2$.

5.3   Generalized Elastic Forces

The generalized elastic forces of an arbitrary element can be derived using strain energy equation. The strain energy of an element at an arbitrary time, t, can be formulated by using

Green-Lagrange strain and 2nd Piola-Kirchhoff stress tensor definitions. Recall the derived generalized elastic force equations given below.

$$
{}^{t}\mathbf{Q}_{k} = \frac{\partial\,{}^{t}U}{\partial\,{}^{t}\mathbf{e}} = \frac{\partial}{\partial\,{}^{t}\mathbf{e}}\left\{\frac{1}{2}\int\limits_{0_V}{}^{t}\boldsymbol{\varepsilon}^{T}\mathbf{E}\,{}^{t}\boldsymbol{\varepsilon}\,d\,{}^{0}V\right\} = \int\limits_{0_V}\left(\frac{\partial\,{}^{t}\boldsymbol{\varepsilon}}{\partial\,{}^{t}\mathbf{e}}\right)^{T}\mathbf{E}\,{}^{t}\boldsymbol{\varepsilon}\,d\,{}^{0}V \tag{5.33}
$$

In order to find nonlinear strain tensor, deformation gradient should be written in terms of nodal variables given in Equation 5.8 for Method 1 or Equation 5.22 for Method 2. Due to different nodal variable definitions used, formulations of deformation gradients for Method 1 and Method 2 will be different.

Deformation gradient for Method 1;

$$
\mathbf{J} = \begin{bmatrix} \frac{\partial X}{\partial X_v} & \frac{\partial X}{\partial Y_v} & \frac{\partial X}{\partial Z_v} \\ \frac{\partial Y}{\partial X_v} & \frac{\partial Y}{\partial Y_v} & \frac{\partial Y}{\partial Z_v} \\ \frac{\partial Z}{\partial X_v} & \frac{\partial Z}{\partial Y_v} & \frac{\partial Z}{\partial Z_v} \end{bmatrix} \begin{bmatrix} \frac{\partial X_0}{\partial X_v} & \frac{\partial X_0}{\partial Y_v} & \frac{\partial X_0}{\partial Z_v} \\ \frac{\partial Y_0}{\partial X_v} & \frac{\partial Y_0}{\partial Y_v} & \frac{\partial Y_0}{\partial Z_v} \\ \frac{\partial Z_0}{\partial X_v} & \frac{\partial Z_0}{\partial Y_v} & \frac{\partial Z_0}{\partial Z_v} \end{bmatrix}^{-1} \tag{5.34}
$$

Deformation gradient for Method 2;

$$
\mathbf{J} = \begin{bmatrix} \frac{\partial X}{\partial R_v} & \frac{\partial X}{\partial S_v} & \frac{\partial X}{\partial T_v} \\ \frac{\partial Y}{\partial R_v} & \frac{\partial Y}{\partial S_v} & \frac{\partial Y}{\partial T_v} \\ \frac{\partial Z}{\partial R_v} & \frac{\partial Z}{\partial S_v} & \frac{\partial Z}{\partial T_v} \end{bmatrix} \begin{bmatrix} \frac{\partial X_0}{\partial R_v} & \frac{\partial X_0}{\partial S_v} & \frac{\partial X_0}{\partial T_v} \\ \frac{\partial Y_0}{\partial R_v} & \frac{\partial Y_0}{\partial S_v} & \frac{\partial Y_0}{\partial T_v} \\ \frac{\partial Z_0}{\partial R_v} & \frac{\partial Z_0}{\partial S_v} & \frac{\partial Z_0}{\partial T_v} \end{bmatrix}^{-1} \tag{5.35}
$$

In general form, deformation gradient tensor can be written as given below.

$$
\mathbf{J} = \begin{bmatrix} \mathbf{S_4e} & \mathbf{S_7e} & \mathbf{S_{10}e} \\ \mathbf{S_5e} & \mathbf{S_8e} & \mathbf{S_{11}e} \\ \mathbf{S_6e} & \mathbf{S_9e} & \mathbf{S_{12}e} \end{bmatrix} \begin{bmatrix} d_{11} & d_{12} & d_{13} \\ d_{21} & d_{22} & d_{23} \\ d_{31} & d_{32} & d_{33} \end{bmatrix} = \begin{bmatrix} \mathbf{V_{11}e} & \mathbf{V_{12}e} & \mathbf{V_{13}e} \\ \mathbf{V_{21}e} & \mathbf{V_{22}e} & \mathbf{V_{23}e} \\ \mathbf{V_{31}e} & \mathbf{V_{32}e} & \mathbf{V_{33}e} \end{bmatrix} \tag{5.36}
$$

where the row vectors, $\mathbf{V_{ij}}$, defined as given below.

$$
\begin{bmatrix}
\mathbf{V_{11}}(r,s,t) \\
\mathbf{V_{12}}(r,s,t) \\
\mathbf{V_{13}}(r,s,t) \\
\mathbf{V_{21}}(r,s,t) \\
\mathbf{V_{22}}(r,s,t) \\
\mathbf{V_{23}}(r,s,t) \\
\mathbf{V_{31}}(r,s,t) \\
\mathbf{V_{32}}(r,s,t) \\
\mathbf{V_{33}}(r,s,t)
\end{bmatrix}
=
\begin{bmatrix}
d_{11}\mathbf{S_4} + d_{21}\mathbf{S_7} + d_{31}\mathbf{S_{10}} \\
d_{12}\mathbf{S_4} + d_{22}\mathbf{S_7} + d_{32}\mathbf{S_{10}} \\
d_{13}\mathbf{S_4} + d_{23}\mathbf{S_7} + d_{33}\mathbf{S_{10}} \\
d_{11}\mathbf{S_5} + d_{21}\mathbf{S_8} + d_{31}\mathbf{S_{11}} \\
d_{12}\mathbf{S_5} + d_{22}\mathbf{S_8} + d_{32}\mathbf{S_{11}} \\
d_{13}\mathbf{S_5} + d_{23}\mathbf{S_8} + d_{33}\mathbf{S_{11}} \\
d_{11}\mathbf{S_6} + d_{21}\mathbf{S_9} + d_{31}\mathbf{S_{12}} \\
d_{12}\mathbf{S_6} + d_{22}\mathbf{S_9} + d_{32}\mathbf{S_{12}} \\
d_{13}\mathbf{S_6} + d_{23}\mathbf{S_9} + d_{33}\mathbf{S_{12}}
\end{bmatrix}
\tag{5.37}
$$

In the deformation gradient tensor equation, d_{11}, d_{12}, d_{13}, d_{21}, d_{22}, d_{23}, d_{31}, d_{32} and d_{33} are the elements of inverse of initial nodal gradient tensor and defined for the two shape function matrix methods as given in the following equations.

$$
\begin{bmatrix}
d_{11} & d_{12} & d_{13} \\
d_{21} & d_{22} & d_{23} \\
d_{31} & d_{32} & d_{33}
\end{bmatrix}
=
\begin{bmatrix}
\frac{\partial X_0}{\partial X_v} & \frac{\partial X_0}{\partial Y_v} & \frac{\partial X_0}{\partial Z_v} \\
\frac{\partial Y_0}{\partial X_v} & \frac{\partial Y_0}{\partial Y_v} & \frac{\partial Y_0}{\partial Z_v} \\
\frac{\partial Z_0}{\partial X_v} & \frac{\partial Z_0}{\partial Y_v} & \frac{\partial Z_0}{\partial Z_v}
\end{bmatrix}^{-1}
=
\begin{bmatrix}
\mathbf{S_4}^0\mathbf{e} & \mathbf{S_7}^0\mathbf{e} & \mathbf{S_{10}}^0\mathbf{e} \\
\mathbf{S_5}^0\mathbf{e} & \mathbf{S_8}^0\mathbf{e} & \mathbf{S_{11}}^0\mathbf{e} \\
\mathbf{S_6}^0\mathbf{e} & \mathbf{S_9}^0\mathbf{e} & \mathbf{S_{12}}^0\mathbf{e}
\end{bmatrix}^{-1}
\cdots Method\ 1 \tag{5.38a}
$$

$$
\begin{bmatrix}
d_{11} & d_{12} & d_{13} \\
d_{21} & d_{22} & d_{23} \\
d_{31} & d_{32} & d_{33}
\end{bmatrix}
=
\begin{bmatrix}
\frac{\partial X_0}{\partial R_v} & \frac{\partial X_0}{\partial S_v} & \frac{\partial X_0}{\partial T_v} \\
\frac{\partial Y_0}{\partial R_v} & \frac{\partial Y_0}{\partial S_v} & \frac{\partial Y_0}{\partial T_v} \\
\frac{\partial Z_0}{\partial R_v} & \frac{\partial Z_0}{\partial S_v} & \frac{\partial Z_0}{\partial T_v}
\end{bmatrix}^{-1}
=
\begin{bmatrix}
\mathbf{S_4}^0\mathbf{e} & \mathbf{S_7}^0\mathbf{e} & \mathbf{S_{10}}^0\mathbf{e} \\
\mathbf{S_5}^0\mathbf{e} & \mathbf{S_8}^0\mathbf{e} & \mathbf{S_{11}}^0\mathbf{e} \\
\mathbf{S_6}^0\mathbf{e} & \mathbf{S_9}^0\mathbf{e} & \mathbf{S_{12}}^0\mathbf{e}
\end{bmatrix}^{-1}
\cdots Method\ 2 \tag{5.38b}
$$

General definition of nonlinear Lagrangian strain tensor is given in Equation 5.39a [36], where $\mathbf{I}$ is 3 by 3 identity matrix. Then, strain tensor, $\boldsymbol{\varepsilon}_m$, can be written in terms of nodal variables, $\mathbf{e}$, by using Equation 5.36 as given below.

$$
\boldsymbol{\varepsilon}_m = \frac{1}{2}\left({}_0^t\mathbf{J}^{T}{}_0^t\mathbf{J} - \mathbf{I}\right) \tag{5.39a}
$$

$$
\boldsymbol{\varepsilon}_m = \frac{1}{2}
\begin{bmatrix}
\mathbf{e}^T\mathbf{N}_{11}\mathbf{e} - 1 & \mathbf{e}^T\mathbf{N}_{12}\mathbf{e} & \mathbf{e}^T\mathbf{N}_{13}\mathbf{e} \\
\mathbf{e}^T\mathbf{N}_{12}\mathbf{e} & \mathbf{e}^T\mathbf{N}_{22}\mathbf{e} - 1 & \mathbf{e}^T\mathbf{N}_{23}\mathbf{e} \\
\mathbf{e}^T\mathbf{N}_{13}\mathbf{e} & \mathbf{e}^T\mathbf{N}_{23}\mathbf{e} & \mathbf{e}^T\mathbf{N}_{33}\mathbf{e} - 1
\end{bmatrix}
\tag{5.39b}
$$

116

where the square matrices, $\mathbf{N}_{ij}$, are defined as follows.

$$\mathbf{N}_{11} = \mathbf{V_{11}}^T\mathbf{V_{11}} + \mathbf{V_{21}}^T\mathbf{V_{21}} + \mathbf{V_{31}}^T\mathbf{V_{31}} \tag{5.40a}$$

$$\mathbf{N}_{12} = \mathbf{V_{11}}^T\mathbf{V_{12}} + \mathbf{V_{21}}^T\mathbf{V_{22}} + \mathbf{V_{31}}^T\mathbf{V_{32}} \tag{5.40b}$$

$$\mathbf{N}_{13} = \mathbf{V_{11}}^T\mathbf{V_{13}} + \mathbf{V_{21}}^T\mathbf{V_{23}} + \mathbf{V_{31}}^T\mathbf{V_{33}} \tag{5.40c}$$

$$\mathbf{N}_{22} = \mathbf{V_{12}}^T\mathbf{V_{12}} + \mathbf{V_{22}}^T\mathbf{V_{22}} + \mathbf{V_{32}}^T\mathbf{V_{32}} \tag{5.40d}$$

$$\mathbf{N}_{23} = \mathbf{V_{12}}^T\mathbf{V_{13}} + \mathbf{V_{22}}^T\mathbf{V_{23}} + \mathbf{V_{32}}^T\mathbf{V_{33}} \tag{5.40e}$$

$$\mathbf{N}_{33} = \mathbf{V_{13}}^T\mathbf{V_{13}} + \mathbf{V_{23}}^T\mathbf{V_{23}} + \mathbf{V_{33}}^T\mathbf{V_{33}} \tag{5.40f}$$

Then, the strain vector and its partial derivative with respect to the nodal variables can be written in terms of the nodal variables as given below.

$$\boldsymbol{\varepsilon} = \begin{bmatrix} \varepsilon_{11} \\ \varepsilon_{22} \\ \varepsilon_{33} \\ \varepsilon_{23} \\ \varepsilon_{13} \\ \varepsilon_{12} \end{bmatrix} = \frac{1}{2}\begin{bmatrix} \mathbf{e}^T\mathbf{N}_{11}\mathbf{e} - 1 \\ \mathbf{e}^T\mathbf{N}_{22}\mathbf{e} - 1 \\ \mathbf{e}^T\mathbf{N}_{33}\mathbf{e} - 1 \\ \mathbf{e}^T\mathbf{N}_{23}\mathbf{e} \\ \mathbf{e}^T\mathbf{N}_{13}\mathbf{e} \\ \mathbf{e}^T\mathbf{N}_{12}\mathbf{e} \end{bmatrix} \qquad \frac{\partial\boldsymbol{\varepsilon}}{\partial\mathbf{e}} = \begin{bmatrix} \mathbf{e}^T\mathbf{N}_{11} \\ \mathbf{e}^T\mathbf{N}_{22} \\ \mathbf{e}^T\mathbf{N}_{33} \\ \frac{1}{2}\,\mathbf{e}^T\left(\mathbf{N}_{23} + \mathbf{N}_{23}{}^T\right) \\ \frac{1}{2}\,\mathbf{e}^T\left(\mathbf{N}_{13} + \mathbf{N}_{13}{}^T\right) \\ \frac{1}{2}\,\mathbf{e}^T\left(\mathbf{N}_{12} + \mathbf{N}_{12}{}^T\right) \end{bmatrix} \tag{5.41}$$

Finally, the generalized elastic force equation can be written in terms of nodal variables by substituting Equation 5.41 into Equation 5.33 as given in the following equation. Evaluation of the generalized elastic force vector can be performed by numerical integration methods like Gauss-Quadrature.

$$\mathbf{Q}_k = \frac{1}{2}\int_{V_{rst}} \begin{bmatrix} \mathbf{e}^T\mathbf{N}_{11} \\ \mathbf{e}^T\mathbf{N}_{22} \\ \mathbf{e}^T\mathbf{N}_{33} \\ \frac{1}{2}\,\mathbf{e}^T\left(\mathbf{N}_{23} + \mathbf{N}_{23}{}^T\right) \\ \frac{1}{2}\,\mathbf{e}^T\left(\mathbf{N}_{13} + \mathbf{N}_{13}{}^T\right) \\ \frac{1}{2}\,\mathbf{e}^T\left(\mathbf{N}_{12} + \mathbf{N}_{12}{}^T\right) \end{bmatrix}^T \mathbf{E} \begin{bmatrix} \mathbf{e}^T\mathbf{N}_{11}\mathbf{e} - 1 \\ \mathbf{e}^T\mathbf{N}_{22}\mathbf{e} - 1 \\ \mathbf{e}^T\mathbf{N}_{33}\mathbf{e} - 1 \\ \mathbf{e}^T\mathbf{N}_{23}\mathbf{e} \\ \mathbf{e}^T\mathbf{N}_{13}\mathbf{e} \\ \mathbf{e}^T\mathbf{N}_{12}\mathbf{e} \end{bmatrix} |\mathbf{D}|\ drdsdt \tag{5.42}$$

5.4   Generalized External Forces

It is known that the generalized external force vectors can be found by virtual work principle. If a point force, $\mathbf{F}$, acts on a point having global coordinates of $\mathbf{r}$, than the external force vector, $\mathbf{Q}_F$, can be found by virtual work principle as follows.

$$\mathbf{F}^T \delta\mathbf{r} = \mathbf{F}^T \mathbf{S}_{123} \delta\mathbf{e} = \mathbf{Q}_F^T \delta\mathbf{e} \qquad (5.43a)$$

$$\mathbf{Q}_F = \mathbf{S}_{123}^T \mathbf{F} \qquad (5.43b)$$

5.5   Straight Cantilever Beam Patch Test for the Proposed Plate/Shell Finite Element

In order to verify the developed finite element for problems containing plate and shell structures, straight cantilever beam patch tests proposed by Richard H. Macneal and Robert L. Harder [35], have been performed for three types of element geometries. The patch test problems are defined in Figure 4.11 of Section 4.6.2. In planar tests, finite elements were tested against in-plane shear and extension loadings. Out-of-plane shear loading is also included in the patch tests of the proposed plate and shell elements.

Finite element discretization and nodal connectivities of the elements are the same as ones used in planar problem and given in Figure 4.12 and Table 4.3, respectively. Initial nodal gradients are determined according to the virtual $X_v Y_v Z_v$ frame and listed for regular, trapezoidal and parallelogram shape elements in Tables 4.4 and 5.1. Fixed boundary conditions are applied for X, Y, Z, $\partial Z/\partial X_v$ and $\partial X/\partial Y_v$ degrees of freedom of Node 1 and Node 8.

Table 5.1: Added nodal variables for Method 1

	Z	$\partial X/\partial Z_v$	$\partial Y/\partial Z_v$	$\partial X/\partial Z_v$	$\partial Y/\partial Z_v$	$\partial Z/\partial Z_v$
All Nodes	0	0	0	0	0	1

118

Similar to the planar formulation, discontinuities on some of the stress components have been evaluated after solving the problem for trapezoidal and parallelogram elements. However, von Misses stress distributions are almost continuous. Obtained stress distributions and displacements for in-plane shear loadings are almost identical to planar element results given in Figures 4.13, 4.14 and 4.15. Stress distributions for in-plane loading obtained by the generalized plate formulation are given in Figures 5.5, 5.6 and 5.7. Deformed configurations of the cantilever beam under out-of-plane shear loading for regular, trapezoidal and parallelogram elements are given in Figures 5.8, 5.9 and 5.10. Obtained displacement results are in the acceptable range as shown in Table 5.2 despite relatively high error levels in out-of-plane loading solutions. It is expected that the error would be reduced if the number of elements is increased.
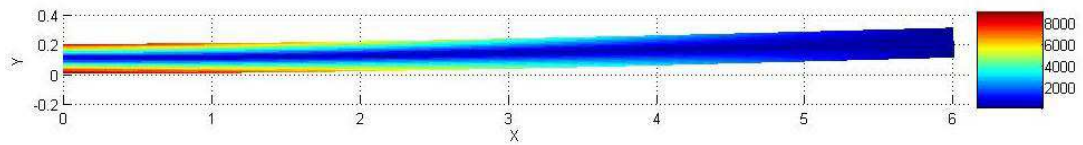
Figure 5.5: Von Misses stress distribution for straight cantilever beam with regular elements (in-plane shear)
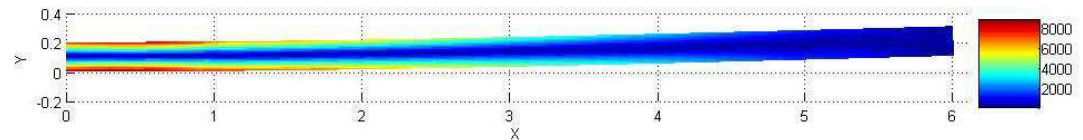
Figure 5.6: Von Misses stress distribution for straight cantilever beam with trapezoidal elements (in-plane shear)
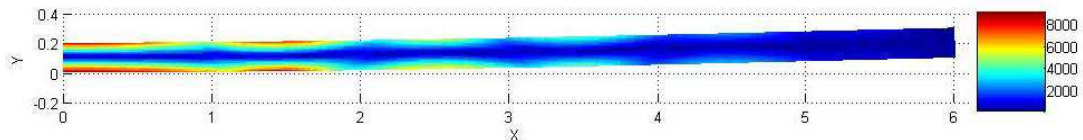
Figure 5.7: Von Misses stress distribution for straight cantilever beam with parallelogram elements (in-plane shear)
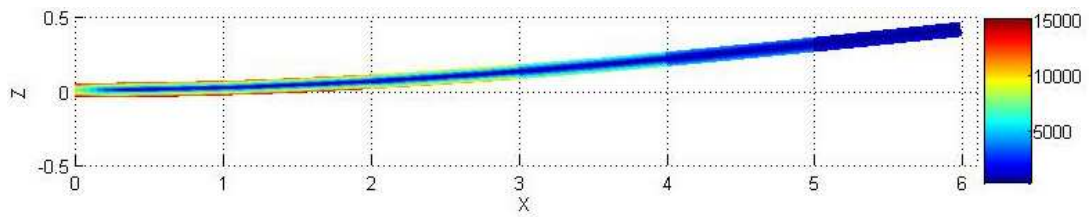
Figure 5.8: Von Misses stress distribution for straight cantilever beam with regular elements (out-of-plane shear)
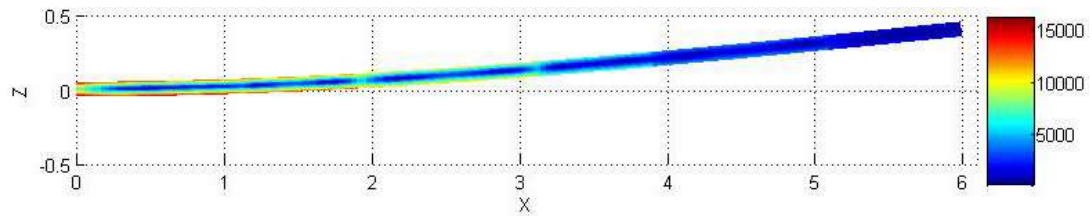
Figure 5.9: Von Misses stress distribution for straight cantilever beam with trapezoidal elements (out-of-plane shear)
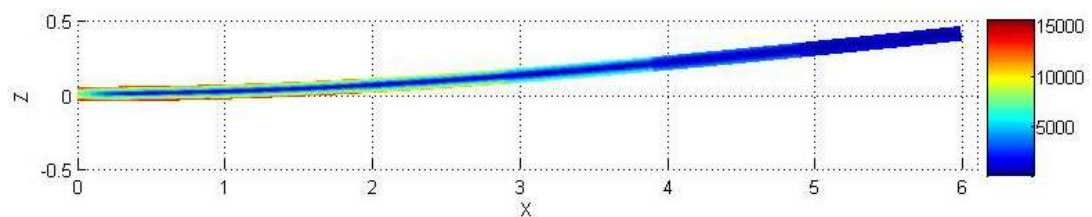
Figure 5.10: Von Misses stress distribution for straight cantilever beam with parallelogram elements (out-of-plane shear)

Table 5.2: Straight cantilever beam patch test results for the generalized plate/shell formulation

	Maximum tip displacement on the loading direction			
	Theoretical	Calculated	Error	Grade
	In-plane shear loading			
Regular	0.1081	0.1081	0.00%	A
Trapezoidal	0.1081	0.1000	−7.47%	B
Parallelogram	0.1081	0.1078	−0.23%	A
	Extension loading			
Regular	3.0×10^{-5}	3.0537×10^{-5}	1.79%	A
Trapezoidal	3.0×10^{-5}	3.0632×10^{-5}	2.11%	B
Parallelogram	3.0×10^{-5}	3.0540×10^{-5}	1.80%	A
	Out-of-plane shear loading			
Regular	0.4321	0.4052	−6.23%	B
Trapezoidal	0.4321	0.3912	−9.47%	B
Parallelogram	0.4321	0.4033	−6.66%	B

5.6 Discussion on the Proposed Generalized Plate/Shell Formulation

In this chapter, implementation of ANCF using virtual element mapping to the generalized plate element has been performed. Despite acceptable results have been obtained in the patch tests, out-of-plane bending results are not as accurate as expected. In fact, it is evaluated that relatively higher errors in out-of-plane loadings are due to the thickness terms in shape function polynomial and the nature of generalized plate assumption. Accuracy of the results could be increased by using different interpolation functions or using thin plate or shell assumption for the formulation. Shape function matrix derivation for thin plate and shell elements is given in the following section for future use.

5.7 Irregular Shaped Quadrilateral Finite Element Representation and Shape Function Creation for Thin Plates and Shells

In the thin plate/shell formulation, nodal gradients along the thickness direction are removed from the nodal degrees of freedom as shown in the following equation because of thin plate assumption.

121

$$\mathbf{e}_i^{rs} = \left[X_i \ Y_i \ Z_i \ \frac{\partial X_i}{\partial r} \ \frac{\partial Y_i}{\partial r} \ \frac{\partial Z_i}{\partial r} \ \frac{\partial X_i}{\partial s} \ \frac{\partial Y_i}{\partial s} \ \frac{\partial Z_i}{\partial s} \right]^T \qquad (5.44)$$

Gradients along the thickness direction ($\partial X/\partial t$, $\partial Y/\partial t$ and $\partial Z/\partial t$) can be evaluated by using orthogonality of rst frame if they are needed. The shape function selected for the thin plate/shell problems is given below.

$$X(r, s, t) = \mathbf{p}^T(r, s) \, \mathbf{a} + t \, \frac{\partial X}{\partial t} \qquad (5.45a)$$

$$Y(r, s, t) = \mathbf{p}^T(r, s) \, \mathbf{b} + t \, \frac{\partial Y}{\partial t} \qquad (5.45b)$$

$$Z(r, s, t) = \mathbf{p}^T(r, s) \, \mathbf{c} + t \, \frac{\partial Z}{\partial t} \qquad (5.45c)$$

$$\mathbf{p}^T = \left[1 \ r \ s \ rs \ r^2 \ s^2 \ r^2s \ rs^2 \ r^3 \ s^3 \ r^3s \ rs^3 \right] \qquad (5.45d)$$

Then, polynomial constants ($\mathbf{A} = [\mathbf{a}^T \ \mathbf{b}^T \ \mathbf{c}^T]^T$) can be formulated in terms of nodal degrees of freedom of the element as given in the following equation.

$$\mathbf{e}_i^{rs} = \mathbf{Q}(r_i, s_i)\mathbf{A} \qquad (5.46)$$

where

$$\mathbf{Q}(r, s) = \begin{vmatrix} \mathbf{p}^T(r, s) & 0 & 0 \\ 0 & \mathbf{p}^T(r, s) & 0 \\ 0 & 0 & \mathbf{p}^T(r, s) \\ \mathbf{p}_{,r}^T(r, s) & 0 & 0 \\ 0 & \mathbf{p}_{,r}^T(r, s) & 0 \\ 0 & 0 & \mathbf{p}_{,r}^T(r, s) \\ \mathbf{p}_{,s}^T(r, s) & 0 & 0 \\ 0 & \mathbf{p}_{,s}^T(r, s) & 0 \\ 0 & 0 & \mathbf{p}_{,s}^T(r, s) \end{vmatrix} \qquad (5.47)$$

Here, r_i and s_i represent the mapped coordinates of the ith node on the element as given below.

$$[r_1 \quad r_2 \quad r_3 \quad r_4] = [-1 \quad +1 \quad +1 \quad -1] \tag{5.48a}$$

$$[s_1 \quad s_2 \quad s_3 \quad s_4] = [-1 \quad -1 \quad +1 \quad +1] \tag{5.48b}$$

Then, linear set of algebraic equations to be solved for **A** can be derived by using Equation 5.46 for all four nodes of the element as given in the following equation.

$$\mathbf{e}^{rs} = \mathbf{P}\,\mathbf{A} \tag{5.49}$$

where

$$\mathbf{P} = \left[\mathbf{Q}^T(r_1, s_1) \quad \mathbf{Q}^T(r_2, s_2) \quad \mathbf{Q}^T(r_3, s_3) \quad \mathbf{Q}^T(r_4, s_4) \right]^T \tag{5.50}$$

Then, polynomial constants vector, **A**, can be found by using Equation 5.49 as follows.

$$\mathbf{A} = \mathbf{P}^{-1}\mathbf{e}^{rs} \tag{5.51}$$

In order to overcome discontinuity problem at the element transitions, nodal gradients are rewritten with respect to the $R_v S_v$ virtual frame as given below.

$$\mathbf{e}_i = \left[X_i \ Y_i \ Z_i \ \frac{\partial X_i}{\partial R_v} \ \frac{\partial Y_i}{\partial R_v} \ \frac{\partial Z_i}{\partial R_v} \ \frac{\partial X_i}{\partial S_v} \ \frac{\partial Y_i}{\partial S_v} \ \frac{\partial Z_i}{\partial S_v} \right]^T \tag{5.52}$$

Relationship between rs and $R_v S_v$ frames are rewritten below for the midplane ($t = 0$) of the element.

$$R_v(r) = \sqrt{(\mathbf{H_{vr}}(r)\mathbf{X}^0)^2 + (\mathbf{H_{vr}}(r)\mathbf{Y}^0)^2 + (\mathbf{H_{vr}}(r)\mathbf{Z}^0)^2} \tag{5.53a}$$

$$S_v(s) = \sqrt{(\mathbf{H_{vs}}(s)\mathbf{X}^0)^2 + (\mathbf{H_{vs}}(s)\mathbf{Y}^0)^2 + (\mathbf{H_{vs}}(s)\mathbf{Z}^0)^2} \tag{5.53b}$$

$$\tag{5.53c}$$

123

where

$$\mathbf{H_{vr}}(r) = \mathbf{H_v}(r, s_a) - \mathbf{H_v}(-1, s_a) = \frac{(1 + r)}{4}\left[-1 + s_a \quad 1 - s_a \quad 1 + s_a \quad -1 - s_a\right] \quad (5.54a)$$

$$\mathbf{H_{vs}}(s) = \mathbf{H_v}(r_a, s) - \mathbf{H_v}(r_a, -1) = \frac{(1 + s)}{4}\left[-1 + r_a \quad -1 - r_a \quad 1 + r_a \quad 1 - r_a\right] \quad (5.54b)$$

Then, the gradients of $R_v S_v$ frame with respect to the mapped rs frame at an arbitrary point on the element can be written explicitly as given in the following equations.

$$\frac{\partial R_v}{\partial r} = \frac{1}{4}\sqrt{(C_{X1} + C_{X2}\ s)^2 + (C_{Y1} + C_{Y2}\ s)^2 + (C_{Z1} + C_{Z2}\ s)^2} \quad (5.55a)$$

$$\frac{\partial S_v}{\partial s} = \frac{1}{4}\sqrt{(C_{X3} + C_{X2}\ r)^2 + (C_{Y3} + C_{Y2}\ r)^2 + (C_{Z3} + C_{Z2}\ r)^2} \quad (5.55b)$$

$$\frac{\partial R_v}{\partial s} = \frac{\partial S_v}{\partial r} = 0 \quad (5.55c)$$

where C_{Xi}, C_{Yi} and C_{Zi} are defined in Equation 5.20.

The gradients with respect to the mapped rs frame can be written in terms of the nodal gradients ($\partial X/\partial R_v$, $\partial Y/\partial R_v$, $\partial Z/\partial R_v$, $\partial X/\partial S_v$, $\partial Y/\partial S_v$ and $\partial Z/\partial S_v$) as given in the following equation.

$$\mathbf{e^{rs}}(r, s, 0) = \mathbf{T_{m2}}(r, s)\ \mathbf{e}(r, s, 0) \quad (5.56)$$

where

$$\mathbf{T_{m2}}(r, s) = \begin{bmatrix} 1 & 1 & 1 & R_{v,r} & R_{v,r} & R_{v,r} & S_{v,s} & S_{v,s} & S_{v,s} \end{bmatrix} \mathbf{I_{12x12}} \quad (5.57)$$

Then, global position and gradients with respect to the mapped frame can be evaluated by using the equation given below.

$$\mathbf{e}^{rs}(r, s, 0) = \mathbf{S^{rs}}(r, s)\mathbf{e} \quad (5.58)$$

where

$$\mathbf{S^{rs}}(r, s) = \mathbf{Q}(r, s)\ \mathbf{P}^{-1}\ \mathbf{T}_{map2} \quad (5.59)$$

Finally, global position and gradients with respect to the virtual $R_v S_v$ frame can be evaluated by using the equation given below.

$$\mathbf{e}(r, s, 0) = \mathbf{S}(r, s)\mathbf{e} \tag{5.60}$$

where

$$\mathbf{S}(r, s) = \mathbf{T}_{m2}(r, s)^{-1}\mathbf{S}^{\mathbf{rs}}(r, s) \tag{5.61}$$

In the formulation of equations of motion, $\mathbf{S^{rs}}(r, s)$ will be used in order to make derivations and calculations simpler. Then, gradients with respect to the thickness direction can be evaluated by using orthogonality condition as given below.

$$\frac{\partial \mathbf{X}}{\partial t} = \frac{\frac{\partial \mathbf{X}}{\partial r} \times \frac{\partial \mathbf{X}}{\partial s}}{\left|\frac{\partial \mathbf{X}}{\partial r} \times \frac{\partial \mathbf{X}}{\partial s}\right|} \tag{5.62a}$$

$$\begin{bmatrix} \partial X/\partial t \\ \partial Y/\partial t \\ \partial Z/\partial t \end{bmatrix} = \frac{1}{\sqrt{(\mathbf{e}^T\mathbf{S}_{t1}\mathbf{e})^2 + (\mathbf{e}^T\mathbf{S}_{t2}\mathbf{e})^2 + (\mathbf{e}^T\mathbf{S}_{t3}\mathbf{e})^2}} \begin{bmatrix} \mathbf{e}^T\mathbf{S}_{t1}\mathbf{e} \\ \mathbf{e}^T\mathbf{S}_{t2}\mathbf{e} \\ \mathbf{e}^T\mathbf{S}_{t3}\mathbf{e} \end{bmatrix} \tag{5.62b}$$

where

$$\mathbf{S}_{t1} = \mathbf{S}_5^{\mathbf{rs}T}\mathbf{S}_9^{\mathbf{rs}} - \mathbf{S}_6^{\mathbf{rs}T}\mathbf{S}_8^{\mathbf{rs}} \tag{5.63a}$$

$$\mathbf{S}_{t2} = \mathbf{S}_6^{\mathbf{rs}T}\mathbf{S}_7^{\mathbf{rs}} - \mathbf{S}_4^{\mathbf{rs}T}\mathbf{S}_9^{\mathbf{rs}} \tag{5.63b}$$

$$\mathbf{S}_{t3} = \mathbf{S}_4^{\mathbf{rs}T}\mathbf{S}_8^{\mathbf{rs}} - \mathbf{S}_5^{\mathbf{rs}T}\mathbf{S}_7^{\mathbf{rs}} \tag{5.63c}$$

Finally, global position vector of an arbitrary point can be written as follows.

$$\begin{bmatrix} X(r, s, t) \\ Y(r, s, t) \\ Z(r, s, t) \end{bmatrix} = \mathbf{S}_{123}^{\mathbf{rs}}\mathbf{e} + \frac{t}{\sqrt{(\mathbf{e}^T\mathbf{S}_{t1}\mathbf{e})^2 + (\mathbf{e}^T\mathbf{S}_{t2}\mathbf{e})^2 + (\mathbf{e}^T\mathbf{S}_{t3}\mathbf{e})^2}} \begin{bmatrix} \mathbf{e}^T\mathbf{S}_{t1}\mathbf{e} \\ \mathbf{e}^T\mathbf{S}_{t2}\mathbf{e} \\ \mathbf{e}^T\mathbf{S}_{t3}\mathbf{e} \end{bmatrix} \tag{5.64}$$

Then, mass matrix and generalized elastic force vector can be derived by following the similar procedure described for the generalized plate formulation.

CHAPTER 6

ANCF FOR SOLID ELEMENTS HAVING IRREGULAR SHAPES

In Chapter 4, ANCF extended to plane stress and strain problems for four noded quadrilateral elements having irregular shapes. In Chapter 5, the proposed continuum formulation applied to plate and shell problems, successfully. Developed formulations show that a wide range of element shapes can be generated and solved. The next step for the formulation is extending to eight noded hexahedral elements, which can various shapes. Actually, there is an attempt to generate absolute nodal coordinate formulation for 3D brick elements by Lars Kübler, Peter Eberhard and Johannes Geisler [41]. However, their proposed finite element [41] does not have exact representation of ANCF. The element only use global positions as nodal variables instead of displacements without including nodal gradients, which are the most powerful feature of the formulation making the difference. In summary, they have proposed a new 8 noded brick element, which can be assembled with the ANCF beams, plates and shells, having the same deformation capabilities as in classical finite element methods. However, better implementation could be performed by including nodal gradients as degrees of freedom of nodes.

Currently, ANCF is used for regular shaped structural finite elements (beam , plate and shell elements). In Chapters 4 and 5, regular shape limitation has been solved with the proposed formulation, which uses virtual elements. In this chapter, the developed formulations and approaches are directly applied to the 8 noded 3D solid elements in order to take advantages of ANCF for 3D continuum problems. Additionally, success of the developed element has been verified by some of the patch tests proposed by Richard H. MACNEAL and Robert L. HARDER [35] and a flexible pendulum problem available in the literature.

126

6.1 Finite Element Representation and Shape Function Creation for 3D Solid Elements with Virtual Element Methods

Finite element representation and virtual element shape functions of 3D solid elements are very similar to the planar elements developed in Chapter 4. The only difference is the addition of the mapped t coordinate which has a range of $[-1, +1]$.

One can select the mapped coordinate frame given in Figure 6.1 in order to define nodal gradients for the element. Then, the nodal degrees of freedom at the ith node of an arbitrary element should be written as given below.

$$\mathbf{e}_i = \left[X_i \ Y_i \ Z_i \ \frac{\partial X_i}{\partial r} \ \frac{\partial Y_i}{\partial r} \ \frac{\partial Z_i}{\partial r} \ \frac{\partial X_i}{\partial s} \ \frac{\partial Y_i}{\partial s} \ \frac{\partial Z_i}{\partial s} \ \frac{\partial X_i}{\partial t} \ \frac{\partial Y_i}{\partial t} \ \frac{\partial Z_i}{\partial t} \right]^T \tag{6.1}$$
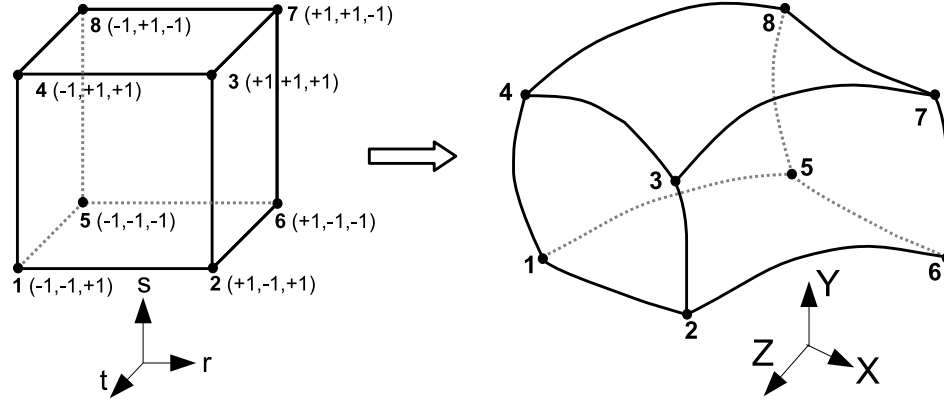
Figure 6.1: *rst* coordinate frame mapping for 3D solid elements

A third order polynomial given below is selected as the shape function polynomial of the eight noded hexahedral solid element.

$$\begin{bmatrix} X(r,s,t) \\ Y(r,s,t) \\ Z(r,s,t) \end{bmatrix} = \begin{bmatrix} \mathbf{p}^T(r,s,t) & \mathbf{0} & \mathbf{0} \\ \mathbf{0} & \mathbf{p}^T(r,s,t) & \mathbf{0} \\ \mathbf{0} & \mathbf{0} & \mathbf{p}^T(r,s,t) \end{bmatrix} \mathbf{A} \qquad (6.2a)$$

$$\mathbf{p}^T(r,s,t) = \begin{vmatrix} 1 & r & s & t & rs & rt & st & rst & \cdots \\ r^2 & s^2 & t^2 & r^2s & r^2t & rs^2 & ts^2 & rt^2 & \cdots \\ st^2 & r^3 & s^3 & t^3 & r^3s & r^3t & rs^3 & ts^3 & \cdots \\ rt^3 & st^3 & r^2st & rs^2t & rst^2 & r^3st & rs^3t & rst^3 & \end{vmatrix} \qquad (6.2b)$$

where $\mathbf{A}$ is the vector of polynomial constants, which contain constants for $X(r,s,t)$, $Y(r,s,t)$ and $Z(r,s,t)$.

Then, polynomial constants ($\mathbf{A}$) could be formulated in terms of nodal degrees of freedom of the element as given in the following equations.

$$\mathbf{e}_i = \mathbf{Q}(r_i, s_i, t_i)\mathbf{A} \qquad (6.3)$$

where $\mathbf{Q}(r,s,t)$ is a matrix of functions defined in Equation 5.4a and r_i, s_i and t_i represent the mapped coordinates of the ith node on the element as given below.

$$[r_1 \ r_2 \ r_3 \ r_4 \ r_5 \ r_6 \ r_7 \ r_8] = [-1 \ +1 \ +1 \ -1 \ -1 \ +1 \ +1 \ -1] \qquad (6.4a)$$

$$[s_1 \ s_2 \ s_3 \ s_4 \ s_5 \ s_6 \ s_7 \ s_8] = [-1 \ -1 \ +1 \ +1 \ -1 \ -1 \ +1 \ +1] \qquad (6.4b)$$

$$[t_1 \ t_2 \ t_3 \ t_4 \ t_5 \ t_6 \ t_7 \ t_8] = [+1 \ +1 \ +1 \ +1 \ -1 \ -1 \ -1 \ -1] \qquad (6.4c)$$

Then, the vector of polynomial constants, $\mathbf{A}$, can be found by solving the linear algebraic equation given below. Similar to the previous finite element applications, $\mathbf{P}^{-1}$ is always exist and constant for the selected shape function polynomials.

$$\mathbf{e} = \mathbf{P}\mathbf{A} \qquad (6.5a)$$

$$\mathbf{A} = \mathbf{P}^{-1}\mathbf{e} \qquad (6.5b)$$

where

$$\mathbf{P} = \begin{bmatrix} \mathbf{Q}(r_1, s_1, t_1) \\ \mathbf{Q}(r_2, s_2, t_2) \\ \mathbf{Q}(r_3, s_3, t_3) \\ \mathbf{Q}(r_4, s_4, t_4) \\ \mathbf{Q}(r_5, s_5, t_5) \\ \mathbf{Q}(r_6, s_6, t_6) \\ \mathbf{Q}(r_7, s_7, t_7) \\ \mathbf{Q}(r_8, s_8, t_8) \end{bmatrix} \tag{6.6}$$

Various 3D solid element shapes given in Figure 6.2 could be generated by using the derived shape function polynomials, given in Equation 6.5, and appropriate nodal degrees of freedom. However, discontinuity problem discussed in Chapters 4 and 5 is also valid for 3D solid elements. Similarly, this problem can be overcome by changing or forcing nodal gradients ($\partial X/\partial r$, $\partial Y/\partial r$, $\partial Z/\partial r$, $\partial X/\partial s$, $\partial Y/\partial s$, $\partial Z/\partial s$, $\partial X/\partial t$, $\partial Y/\partial t$, $\partial Z/\partial t$) to generate the same edge shapes for neighbouring elements. Then, system equations can be formed by using general finite element assembly procedures. Two alternative mapping methods are discussed in the following sections for 3D solid elements.
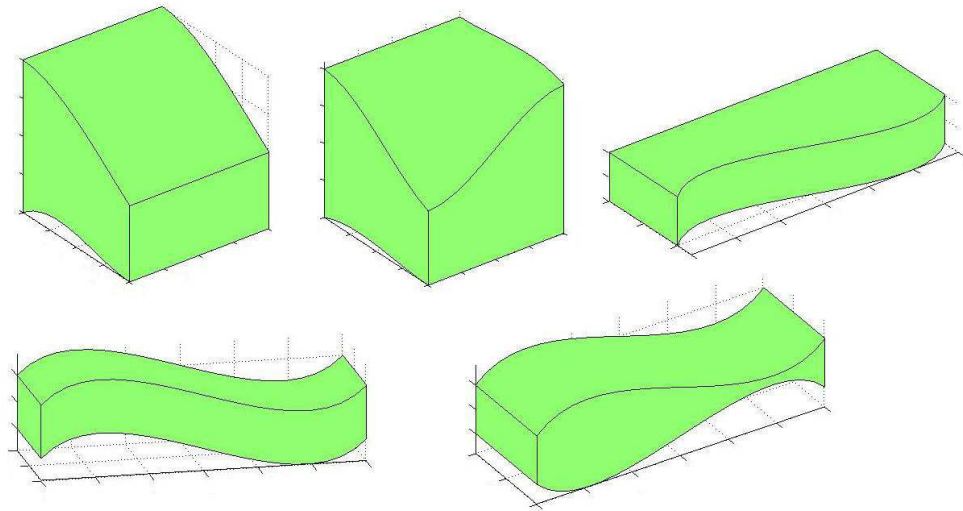
Figure 6.2: Various 3D solid element shapes

6.1.1   Method 1: Parallel Virtual Frame and First Order Virtual Element Mapping

In this method, nodal gradients are defined with respect to the virtual coordinate frame of virtual element shown in Figure 6.3. Then, nodal degrees of freedom for the ith node of an arbitrary element is described as given in the following equation.

$$\mathbf{e}_i = \left[X_i \ Y_i \ Z_i \ \frac{\partial X_i}{\partial X_v} \ \frac{\partial Y_i}{\partial X_v} \ \frac{\partial Z_i}{\partial X_v} \ \frac{\partial X_i}{\partial Y_v} \ \frac{\partial Y_i}{\partial Y_v} \ \frac{\partial Z_i}{\partial Y_v} \ \frac{\partial X_i}{\partial Z_v} \ \frac{\partial Y_i}{\partial Z_v} \ \frac{\partial Z_i}{\partial Z_v} \right]^T \tag{6.7}$$
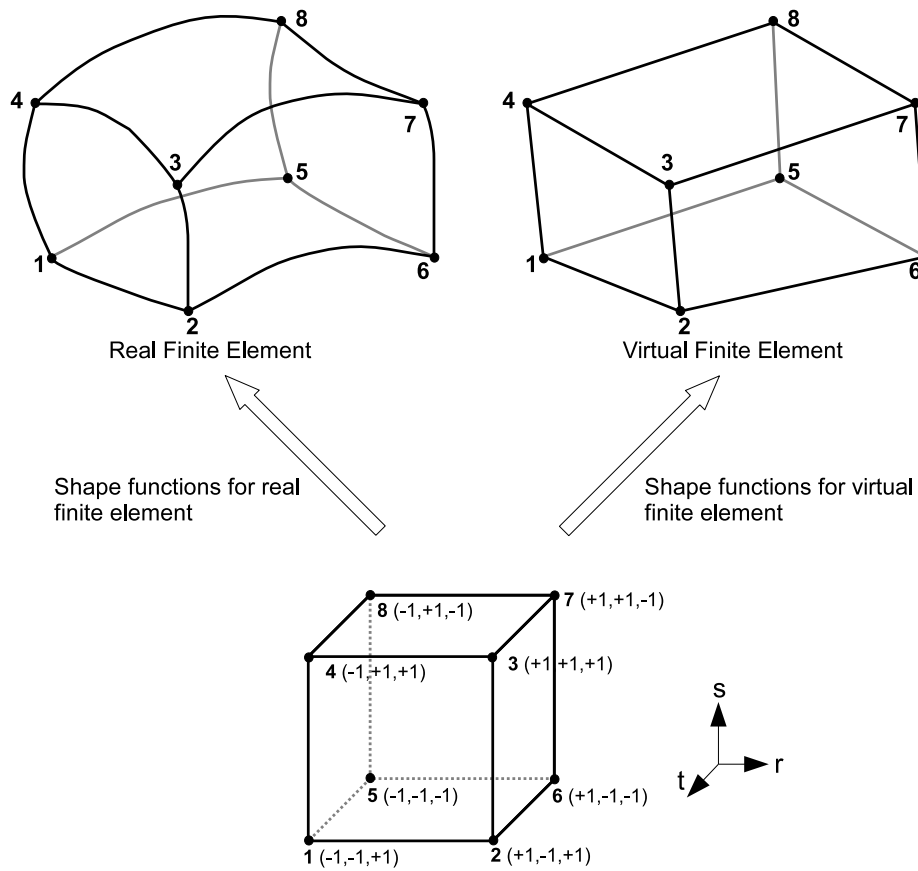
Figure 6.3: Virtual finite element frame in 3D continuum element for Method 1

Mapping functions for virtual finite element shown in Figure 6.3 can be constructed by using general first order interpolation functions for 3D isoparametric hexahedral element [36] as given in the following equation.

$$X_v(r, s, t) = \mathbf{H_{v3d}}(r, s, t)\,{}^0\mathbf{X} \tag{6.8a}$$

$$Y_v(r, s, t) = \mathbf{H_{v3d}}(r, s, t)\,{}^0\mathbf{Y} \tag{6.8b}$$

$$Z_v(r, s, t) = \mathbf{H_{v3d}}(r, s, t)\,{}^0\mathbf{Z} \tag{6.8c}$$

where

$$\mathbf{H_{v3d}}(r, s, t) = \frac{1}{2}\left[\mathbf{H_v}(r, s)(1 + t) \quad \mathbf{H_v}(r, s)(1 - t)\right] \tag{6.9}$$

and $\mathbf{H_v}(r, s)$ is the first order shape function matrix used for virtual planar elements presented in Chapter 4.

Then, gradients with respect to the mapped *rst* frame can be written in terms of nodal gradients in compact form by using Equation 5.11 and 5.12 in the previous chapter. Consequently, gradient terms in vector of nodal variables can be converted into the gradients with respect to the mapped *rst* frame as given below.

$$\mathbf{e^{rst}} = \mathbf{T}_{map1}\mathbf{e} \tag{6.10}$$

where $\mathbf{T}_{map1}$ is defined in Equation 5.14.

Finally, global coordinates and gradients with respect to the virtual frame can be found by using polynomial constants derived in Equation 6.5 as given below.

$$\mathbf{e}(r, s, t) = \mathbf{S}(r, s, t)\mathbf{e} \tag{6.11}$$

where

$$\mathbf{S}(r, s, t) = \mathbf{T}_{m1}(r, s, t)^{-1}\mathbf{Q}(r, s, t)\,\mathbf{P^{-1}}\,\mathbf{T}_{map1} \tag{6.12}$$

While $\mathbf{P^{-1}}$ is the same for all finite elements, $\mathbf{T}_{map1}$ depends on the initial element geometry. The derived shape function matrix ensures continuity of nodal parameter at the neighboring node location. Global coordinates are continuous over neighboring element faces. However, continuity of gradients is only guaranteed on node locations. Therefore, stresses or strains

131

will not be continuous over element edges but be identical for neighboring elements at the same node locations. Continuous stress and strain distributions can be created by linear interpolation over nodal stresses or strains in post-processing stage.

6.1.2 Method 2: Virtual Element Edge Frame and First Order Virtual Element Mapping

In this method, nodal gradients are redefined with respect to the linear edges of virtual finite element shown in Figure 6.3. Straight lines from nodes 1 to 2, 4 to 3, 5 to 6 and 8 to 7 represent the virtual coordinate, where S_v and T_v are constant. Similarly, lines from nodes 1 to 4, 2 to 3, 5 to 8 and 6 to 7 represent the virtual coordinate, where R_v and T_v are constant. Finally, lines from nodes 5 to 1, 6 to 2, 8 to 4 and 7 to 3 represent the virtual coordinate, where R_v and S_v are constant. These 12 straight lines connecting the nodes form the boundaries of the virtual element in $X_v Y_v Z_v$ frame. Similar to the 2D planar formulation, $R_v S_v T_v$ is not a new coordinate frame, but they are products of virtual $X_v Y_v Z_v$ frame.

If a point, which has the mapped coordinates of (r_a, s_a, t_a) on the element, is consider in order to clarify R_v, S_v and T_v definitions, then, R_v is defined as the magnitude of the vector from the virtual point at $(-1, s_a, t_a)$ to the point at (r, s_a, t_a). Similarly, S_v is defined as the magnitude of the vector from the virtual point at $(r_a, -1, t_a)$ to the point at (r_a, s, t_a). Finally, T_v is defined as the magnitude of the vector from the virtual point at $(r_a, s_a, -1)$ to the point at (r_a, s_a, t). Therefore, they can be defined with respect to the virtual frame $(X_v Y_v Z_v)$ defined in Equation 6.8 as given in the following equations. As can be seen from the equations, R_v is a function of r, S_v is a function of s and T_v is a function of t, only.

$$R_v(r) = \sqrt{(\mathbf{H_{v3dr}}(r)\ ^0\mathbf{X})^2 + (\mathbf{H_{v3dr}}(r)\ ^0\mathbf{Y})^2 + (\mathbf{H_{v3dr}}(r)\ ^0\mathbf{Z})^2} \qquad (6.13a)$$

$$S_v(s) = \sqrt{(\mathbf{H_{v3ds}}(s)\ ^0\mathbf{X})^2 + (\mathbf{H_{v3ds}}(s)\ ^0\mathbf{Y})^2 + (\mathbf{H_{v3ds}}(s)\ ^0\mathbf{Z})^2} \qquad (6.13b)$$

$$T_v(t) = \sqrt{(\mathbf{H_{v3dt}}(t)\ ^0\mathbf{X})^2 + (\mathbf{H_{v3dt}}(t)\ ^0\mathbf{Y})^2 + (\mathbf{H_{v3dt}}(t)\ ^0\mathbf{Z})^2} \qquad (6.13c)$$

where

$$\mathbf{H_{v3dr}}(r) = \mathbf{H_{v3d}}(r, s_a, t_a) - \mathbf{H_{v3d}}(-1, s_a, t_a) = \frac{1}{2}\left[(1 + t_a)\mathbf{H_{vr}}(r) \quad (1 - t_a)\mathbf{H_{vr}}(r)\right] \quad (6.14a)$$

$$\mathbf{H_{v3ds}}(s) = \mathbf{H_{v3d}}(r_a, s, t_a) - \mathbf{H_{v3d}}(r_a, -1, t_a) = \frac{1}{2}\left[(1 + t_a)\mathbf{H_{vs}}(s) \quad (1 - t_a)\mathbf{H_{vs}}(s)\right] \quad (6.14b)$$

$$\mathbf{H_{v3dt}}(t) = \mathbf{H_{v3d}}(r_a, s_a, t) - \mathbf{H_{v3d}}(r_a, s_a, -1) = \frac{(1 + t)}{2}\left[\mathbf{H_v}(r_a, s_a) \quad - \mathbf{H_v}(r_a, s_a)\right] \quad (6.14c)$$

Then, gradients of virtual $R_v S_v T_v$ frame with respect to the mapped rst frame at an arbitrary point on the element can be written in explicit forms as given below.

$$\frac{\partial R_v}{\partial r} = \frac{1}{8}\sqrt{\begin{array}{c}(C_{X1} + C_{X2}\,s + C_{X3}t + C_{X4}\,st)^2 + (C_{Y1} + C_{Y2}\,s + C_{Y3}t + C_{Y4}\,st)^2 \\ \cdots + (C_{Z1} + C_{Z2}\,s + C_{Z3}t + C_{Z4}\,st)^2\end{array}} \quad (6.15a)$$

$$\frac{\partial S_v}{\partial s} = \frac{1}{8}\sqrt{\begin{array}{c}(C_{X5} + C_{X2}\,r + C_{X6}t + C_{X4}\,rt)^2 + (C_{Y5} + C_{Y2}\,r + C_{Y6}t + C_{Y4}\,rt)^2 \\ \cdots + (C_{Z5} + C_{Z2}\,r + C_{Z6}t + C_{Z4}\,rt)^2\end{array}} \quad (6.15b)$$

$$\frac{\partial T_v}{\partial t} = \frac{1}{8}\sqrt{\begin{array}{c}(C_{X7} + C_{X3}\,r + C_{X6}s + C_{X4}\,rs)^2 + (C_{Y7} + C_{Y3}\,r + C_{Y6}s + C_{Y4}\,rs)^2 \\ \cdots + (C_{Z7} + C_{Z3}\,r + C_{Z6}s + C_{Z4}\,rs)^2\end{array}} \quad (6.15c)$$

$$\frac{\partial R_v}{\partial s} = \frac{\partial R_v}{\partial t} = \frac{\partial S_v}{\partial r} = \frac{\partial S_v}{\partial t} = \frac{\partial T_v}{\partial r} = \frac{\partial T_v}{\partial s} = 0 \quad (6.15d)$$

where the constants of virtual element are given in the following equations.

$$C_{X1} = -\,^0X_1 + \,^0X_2 + \,^0X_3 - \,^0X_4 - \,^0X_5 + \,^0X_6 + \,^0X_7 - \,^0X_8$$

$$C_{X2} = +\,^0X_1 - \,^0X_2 + \,^0X_3 - \,^0X_4 + \,^0X_5 - \,^0X_6 + \,^0X_7 - \,^0X_8$$

$$C_{X3} = -\,^0X_1 + \,^0X_2 + \,^0X_3 - \,^0X_4 + \,^0X_5 - \,^0X_6 - \,^0X_7 + \,^0X_8$$

$$C_{X4} = +\,^0X_1 - \,^0X_2 + \,^0X_3 - \,^0X_4 - \,^0X_5 + \,^0X_6 - \,^0X_7 + \,^0X_8$$

$$C_{X5} = -\,^0X_1 - \,^0X_2 + \,^0X_3 + \,^0X_4 - \,^0X_5 - \,^0X_6 + \,^0X_7 + \,^0X_8$$

$$C_{X6} = -\,^0X_1 - \,^0X_2 + \,^0X_3 + \,^0X_4 + \,^0X_5 + \,^0X_6 - \,^0X_7 - \,^0X_8$$

$$C_{X7} = +\,^0X_1 + \,^0X_2 + \,^0X_3 + \,^0X_4 - \,^0X_5 - \,^0X_6 - \,^0X_7 - \,^0X_8$$

$$C_{Y1} = -\,^0Y_1 + \,^0Y_2 + \,^0Y_3 - \,^0Y_4 - \,^0Y_5 + \,^0Y_6 + \,^0Y_7 - \,^0Y_8$$

133

$$C_{Y2} = + {}^0Y_1 - {}^0Y_2 + {}^0Y_3 - {}^0Y_4 + {}^0Y_5 - {}^0Y_6 + {}^0Y_7 - {}^0Y_8$$

$$C_{Y3} = - {}^0Y_1 + {}^0Y_2 + {}^0Y_3 - {}^0Y_4 + {}^0Y_5 - {}^0Y_6 - {}^0Y_7 + {}^0Y_8$$

$$C_{Y4} = + {}^0Y_1 - {}^0Y_2 + {}^0Y_3 - {}^0Y_4 - {}^0Y_5 + {}^0Y_6 - {}^0Y_7 + {}^0Y_8$$

$$C_{Y5} = - {}^0Y_1 - {}^0Y_2 + {}^0Y_3 + {}^0Y_4 - {}^0Y_5 - {}^0Y_6 + {}^0Y_7 + {}^0Y_8$$

$$C_{Y6} = - {}^0Y_1 - {}^0Y_2 + {}^0Y_3 + {}^0Y_4 + {}^0Y_5 + {}^0Y_6 - {}^0Y_7 - {}^0Y_8$$

$$C_{Y7} = + {}^0Y_1 + {}^0Y_2 + {}^0Y_3 + {}^0Y_4 - {}^0Y_5 - {}^0Y_6 - {}^0Y_7 - {}^0Y_8$$

$$C_{Z1} = - {}^0Z_1 + {}^0Z_2 + {}^0Z_3 - {}^0Z_4 - {}^0Z_5 + {}^0Z_6 + {}^0Z_7 - {}^0Z_8$$

$$C_{Z2} = + {}^0Z_1 - {}^0Z_2 + {}^0Z_3 - {}^0Z_4 + {}^0Z_5 - {}^0Z_6 + {}^0Z_7 - {}^0Z_8$$

$$C_{Z3} = - {}^0Z_1 + {}^0Z_2 + {}^0Z_3 - {}^0Z_4 + {}^0Z_5 - {}^0Z_6 - {}^0Z_7 + {}^0Z_8$$

$$C_{Z4} = + {}^0Z_1 - {}^0Z_2 + {}^0Z_3 - {}^0Z_4 - {}^0Z_5 + {}^0Z_6 - {}^0Z_7 + {}^0Z_8$$

$$C_{Z5} = - {}^0Z_1 - {}^0Z_2 + {}^0Z_3 + {}^0Z_4 - {}^0Z_5 - {}^0Z_6 + {}^0Z_7 + {}^0Z_8$$

$$C_{Z6} = - {}^0Z_1 - {}^0Z_2 + {}^0Z_3 + {}^0Z_4 + {}^0Z_5 + {}^0Z_6 - {}^0Z_7 - {}^0Z_8$$

$$C_{Z7} = + {}^0Z_1 + {}^0Z_2 + {}^0Z_3 + {}^0Z_4 - {}^0Z_5 - {}^0Z_6 - {}^0Z_7 - {}^0Z_8$$

Then, vector of nodal variables, $\mathbf{e}$, for the ith node of an arbitrary element can be written as follows.

$$\mathbf{e}_i = \left[X_i \ Y_i \ Z_i \ \frac{\partial X_i}{\partial R_v} \ \frac{\partial Y_i}{\partial R_v} \ \frac{\partial Z_i}{\partial R_v} \ \frac{\partial X_i}{\partial S_v} \ \frac{\partial Y_i}{\partial S_v} \ \frac{\partial Z_i}{\partial S_v} \ \frac{\partial X_i}{\partial T_v} \ \frac{\partial Y_i}{\partial T_v} \ \frac{\partial Z_i}{\partial T_v} \right]^T \tag{6.16}$$

In the equation, X_i, Y_i and Z_i are coordinates of the ith node in global frame. As stated in Chapter 4, the gradient vectors are always tangent to the element edges.

The nodal gradients with respect to the mapped *rst* frame can be written in terms of the nodal gradients with respect to the virtual $R_v S_v T_v$ frame ($\partial X/\partial R_v$, $\partial Y/\partial R_v$, $\partial Z/\partial R_v$, $\partial X/\partial S_v$, $\partial Y/\partial S_v$, $\partial Z/\partial S_v$, $\partial X/\partial T_v$, $\partial Y/\partial T_v$ and $\partial Z/\partial T_v$) as given in the following equation.

$$\mathbf{e}^{\mathbf{rst}} = \mathbf{T}_{map2}\mathbf{e} \tag{6.17}$$

134

where

$$\mathbf{T}_{map2} = \begin{bmatrix} \mathbf{T}_{m2}(r_1, s_1, t_1) \\ \mathbf{T}_{m2}(r_2, s_2, t_2) \\ \mathbf{T}_{m2}(r_3, s_3, t_3) \\ \mathbf{T}_{m2}(r_4, s_4, t_4) \\ \mathbf{T}_{m2}(r_5, s_5, t_5) \\ \mathbf{T}_{m2}(r_6, s_6, t_6) \\ \mathbf{T}_{m2}(r_7, s_7, t_7) \\ \mathbf{T}_{m2}(r_8, s_8, t_8) \end{bmatrix} \tag{6.18}$$

$\mathbf{T}_{m2}$ matrix for 3D hexahedral element is defined in the following equation.

$$\mathbf{T}_{m2}(r, s, t) = \mathbf{I}_{12x12} \begin{bmatrix} 1 & 1 & 1 & R_{v,r} & R_{v,r} & R_{v,r} & S_{v,s} & S_{v,s} & S_{v,s} & T_{v,t} & T_{v,t} & T_{v,t} \end{bmatrix} \tag{6.19}$$

where $\mathbf{I}_{12x12}$ is $12x12$ identity matrix.

Finally, global coordinates and gradients with respect to the virtual frame at an arbitrary point can be written in terms of nodal variables as given below.

$$\mathbf{e}(r, s, t) = \mathbf{T}_{m2}(r, s, t)^{-1} \mathbf{Q}(r, s, t) \mathbf{P}^{-1} \mathbf{T}_{map2} \mathbf{e} \tag{6.20}$$

Then, it can be written in a simple form given below.

$$\mathbf{e}(r, s, t) = \mathbf{S}(r, s, t)\mathbf{e} \tag{6.21}$$

where

$$\mathbf{S}(r, s, t) = \mathbf{T}_{m2}(r, s, t)^{-1} \mathbf{Q}(r, s, t) \mathbf{P}^{-1} \mathbf{T}_{map2} \tag{6.22}$$

Similar to the previous planar formulations, $\mathbf{T}_{map2}$ matrix in the shape function definition can be written in terms of the virtual edge lengths of the element.

6.2 Generalized System Parameters for 3D Hexahedral Finite Elements

The mass matrix and the generalized elastic and external force vectors can be derived using the same procedure described in Chapter 5. Despite the formulation is exactly the same,

135

integration boundaries of the mapped t coordinate are different. Integration limits of the mapped t coordinate should be changed from $[-{}^{0}t/2, +{}^{0}t/2]$ to $[-1, +1]$. Then, Equations 5.31, 5.42 and 5.43 can be used to calculate the mass matrix, the generalized elastic forces and the generalized external forces, respectively.

6.3 Straight Cantilever Beam Patch Test for the Proposed Solid Element

In order to verify performance of the proposed hexahedral finite element under quasi-static loading conditions, straight cantilever beam patch test problems proposed by Richard H. Macneal and Robert L. Harder [35], have been solved. Geometries of the problems are defined in Figure 4.11 of Section 4.6.2. Analyses are performed for in-plane shear and extension loading cases. Finite element model has been generated using 28 nodes and 6 elements as shown in Figure 6.4 with the connectivity matrix given in Table 6.1. Initial nodal gradients are determined according to the virtual $X_v Y_v Z_v$ frame similar to the planar patch test analyses in Section 4.6.2. Fixed boundary conditions are applied for X, Y, Z, $\partial X/\partial Y_v$, $\partial Z/\partial Y_v$, $\partial X/\partial Z_v$ and $\partial Y/\partial Z_v$ degrees of freedom of nodes 1, 8, 15 and 22.
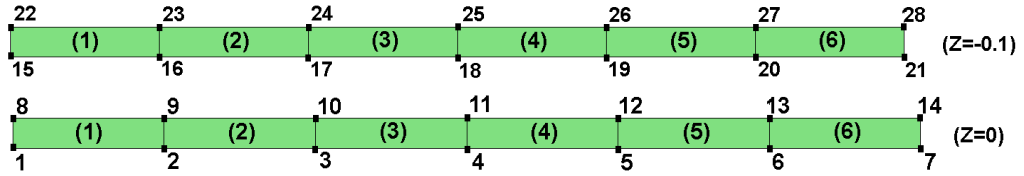
Figure 6.4: Discretized beam for patch test problem

Table 6.1: Connectivity of the elements

	Node Numbers							
Element 1	1	2	9	8	15	16	23	22
Element 2	2	3	10	9	16	17	24	23
Element 3	3	4	11	10	17	18	25	24
Element 4	4	5	12	11	18	19	26	25
Element 5	5	6	13	12	19	20	27	26
Element 6	6	7	14	13	20	21	28	27

Similar to the planar formulation, discontinuities on some of the stress components have been observed after solving the problem for trapezoidal and parallelogram elements. However, von Misses stress distributions are almost continuous and almost identical to 2D planar element results as shown in Figures 6.5, 6.6 and 6.7. Displacements on the load directions and their errors are listed in Table 6.2. As seen on the table, all of the results are in the acceptable ranges defined in the publication of Richard H. Macneal and Robert L. Harder [35]. In addition, the patch test problem has been solved by using single regular element, which has the aspect ratio of 30, with a high accuracy as shown in the table. Similar to the results of planar finite element formulations, the maximum error is obtained for the trapezoidal element solutions due to differences in the edge lengths of neighboring elements.

Figure 6.5: Von Misses stress distribution for straight cantilever beam with 3D regular elements (in-plane shear)

Figure 6.6: Von Misses stress distribution for straight cantilever beam with 3D trapezoidal elements (in-plane shear)
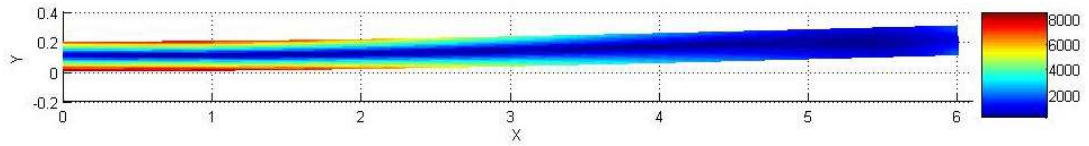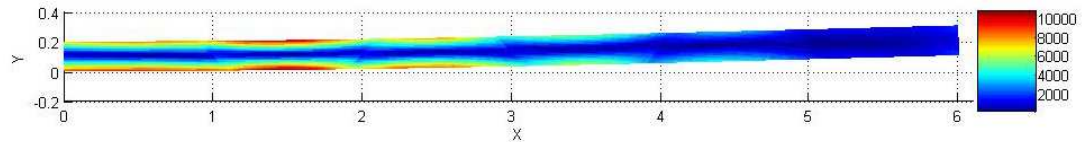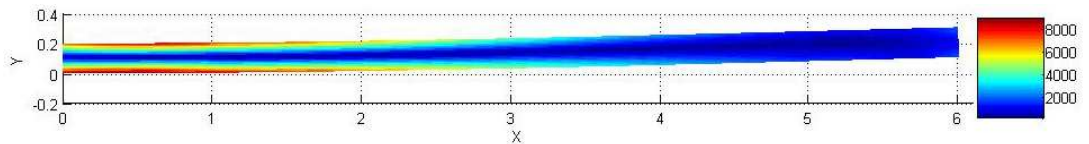

Figure 6.7: Von Misses stress distribution for straight cantilever beam with 3D parallelogram elements (in-plane shear)

137

Table 6.2: Patch test results for straight beam

| | Maximum tip displacement on the loading direction | | | |
	Theoretical	Calculated	Error	Grade
	In-plane shear loading			
Regular	0.1081	0.1077	−0.40%	A
Trapezoidal	0.1081	0.0992	−8.20%	B
Parallelogram	0.1081	0.1072	−0.81%	A
One Element	0.1081	0.1080	−0.08%	A
	Extension loading			
Regular	3.0×10^{-5}	3.0284×10^{-5}	0.95%	A
Trapezoidal	3.0×10^{-5}	3.0278×10^{-5}	0.93%	A
Parallelogram	3.0×10^{-5}	3.0345×10^{-5}	1.15%	A
One Element	3.0×10^{-5}	2.9515×10^{-5}	−1.62%	A

6.4 Flexible Pendulum Solutions using the Proposed Hexahedral Finite Element

In order to verify the proposed finite element formulation in flexible multibody dynamics, flexible pendulum problem, which was published by K. Dufva and A. A. Shabana [32], has been studied. K. Dufva and A. A. Shabana have solved the problem using thin plate assumption. Therefore, they applied all loads and boundary conditions to the mid-plane of the structure. However, it is not possible to apply fixed boundary conditions to the midplane of 8 noded hexahedral solid elements. Therefore, all translational degrees of freedom of the node at [0, 0, 0] are fixed. The geometry of the pendulum is shown in Figure 6.8. Thickness, modulus of elasticity, Poisson's ratio and density of the plate are 0.01 m, 1.0×10^5 Pa, 0.3 and 7810 kg/m^3, respectively.

Firstly, flexible pendulum under gravitational load has been solved by using 1×1, 2×2, 3×3 and 4×4 elements in order to observe convergence characteristic of the finite element. Then, the 2×2 finite element model has been studied with element shape irregularities in order to observe error contributions of irregular shapes.
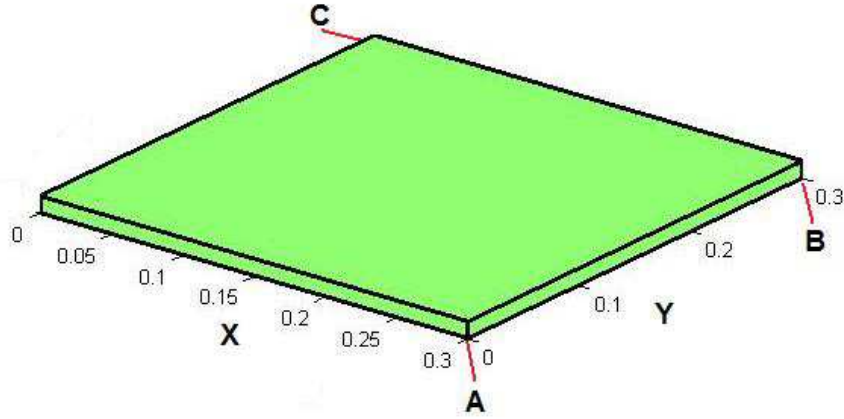
Figure 6.8: Geometry of the flexible pendulum

Deformed shapes of flexible pendulum obtained by using 1×1, 2×2, 3×3 and 4×4 finite elements are shown in Figure 6.9. Change of global positions of points A and B (Figure 6.8) with time are shown in Figures 6.10 and 6.11. Due to symmetric locations of points A and C, results are posted for point A, only. As can be seen from the graphs, relative error is decreasing with the increasing total number of elements. However, it can be stated that, the problem can be solved by using 4 hexahedral elements (2×2 mesh configuration) with a certain accuracy, by examining the deformed shapes in Figure 6.9 and change of global positions with time in Figures 6.10 and 6.11. Additionally, deformed shapes obtained by using single element prove the capabilities of the proposed finite element formulation under large rigid body rotation and extreme deformation cases.

Relative percent errors between consecutive total element numbers are plotted over time in Figures 6.12 and 6.13. Relative percent errors have been calculated not on the absolute positions but on the absolute displacements of points A and B. Therefore, error percentages are high, although relatively close absolute coordinates have been obtained for various total number of elements as shown in Figures 6.10 and 6.11. Effect of total number of elements can clearly be identified from relative percent absolute displacement error curves in Figures 6.12 and 6.13. Magnitude of the maximum error is decreasing with increasing total number of elements as shown in the figures. In addition, it can be observed that, the total number of fluctuations in error versus time plots are increasing with the increasing total number of elements due to introduced degrees of freedom and added natural frequencies to the system.

139
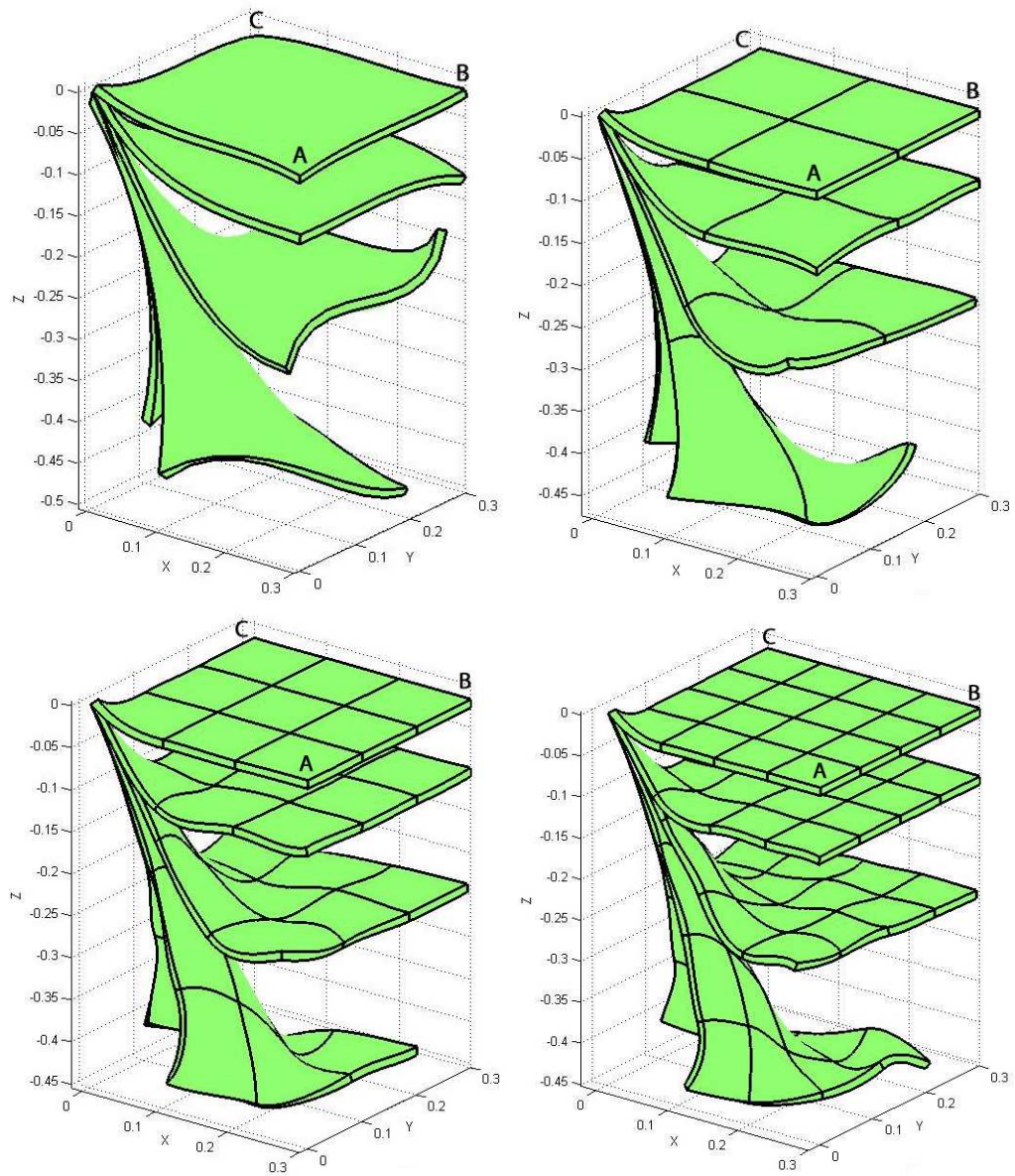
Figure 6.9: Deformed pendulum shapes at 0.075 s, 0.15 s, 0.225 s and 0.3 s with 1x1, 2x2, 3x3 and 4x4 finite element mesh
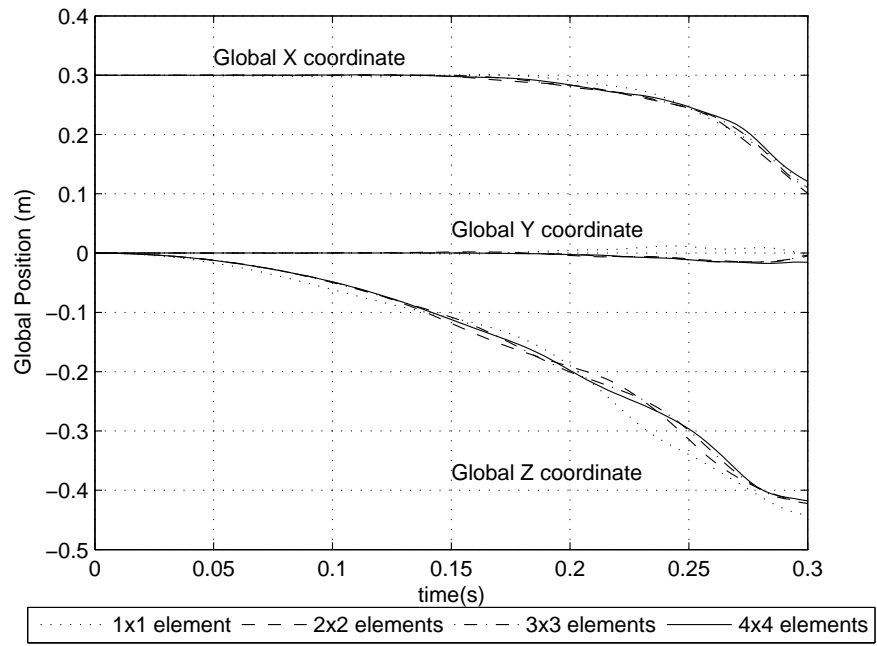
140

Figure 6.10: Flexible pendulum - global positions of Point A
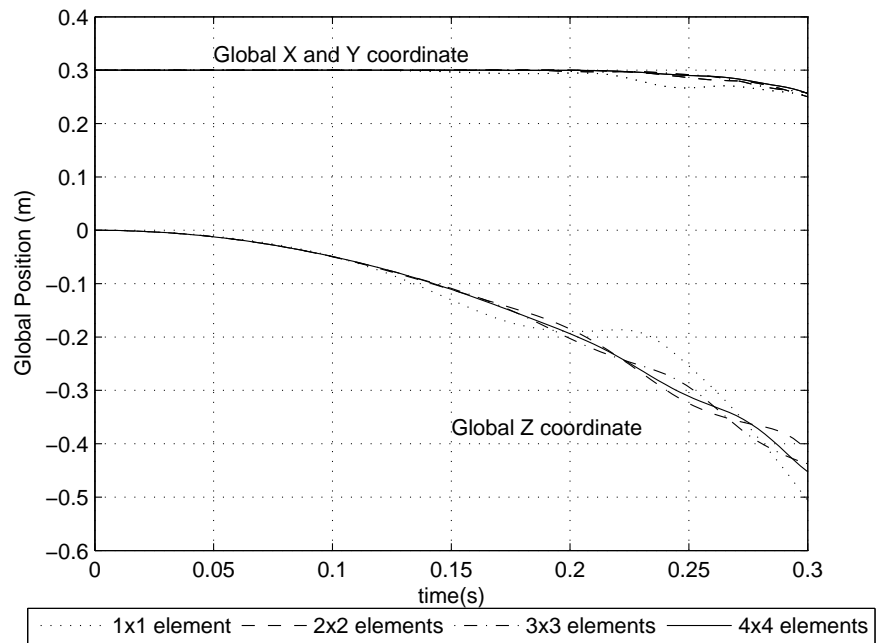

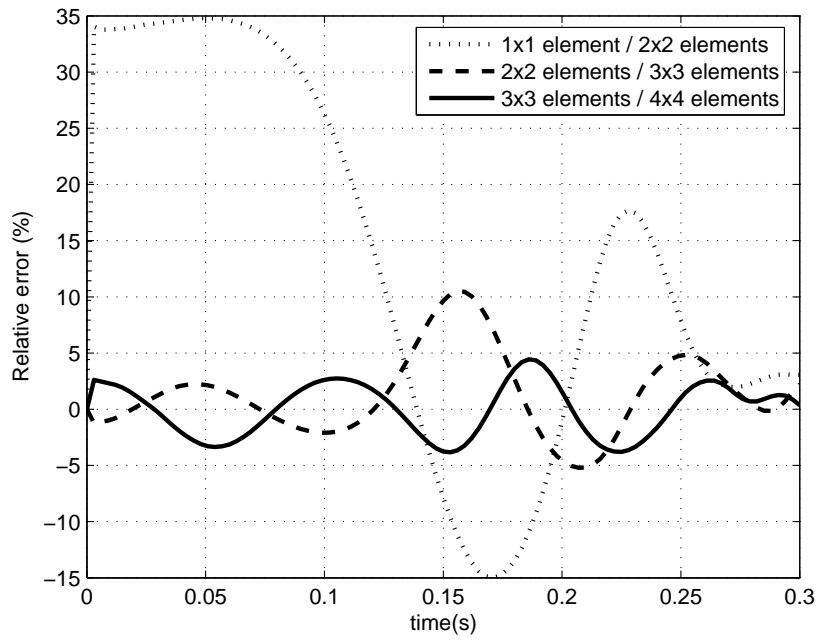Figure 6.11: Flexible pendulum - global positions of Point B

141

Figure 6.12: Flexible pendulum - relative error in the absolute displacements of Point A
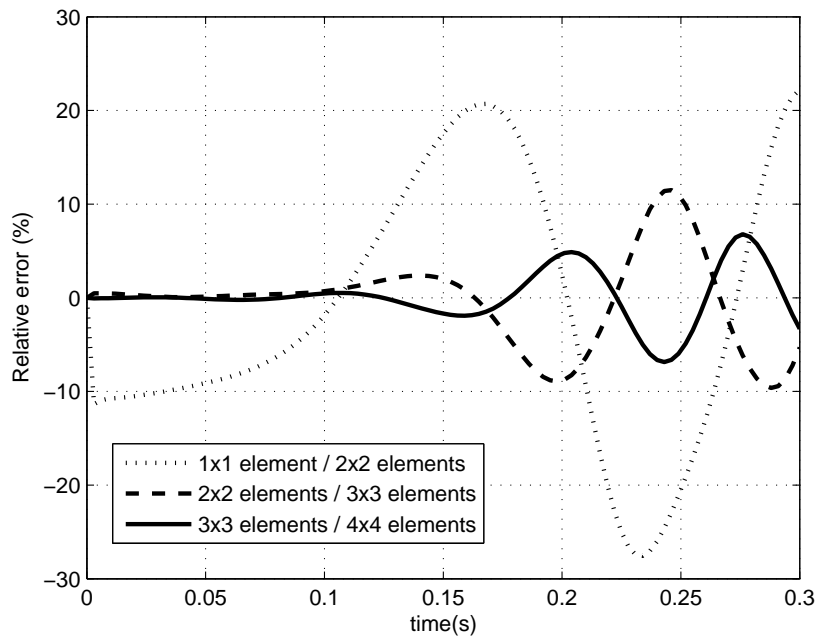

Figure 6.13: Flexible pendulum - relative error in the absolute displacements of Point B

In fact, flexible pendulum problem is not physically possible, despite lots of studies have been performed on it in the literature [30, 32]. However, it is very effective method in testing new finite element formulations under large rigid body rotations and extreme deformations. It has been seen that comparable results with the results of K. Dufva and A. A. Shabana [32] are obtained using 2×2 elements. A detailed comparison of the results has not been performed due to differences in boundary conditions and element topologies. Therefore, no further mesh refinement has been performed. Major advantages of the proposed finite element over the available formulations are sensitivity in the deformations along thickness direction and irregular element shape capability.

6.4.1 Effects of Irregular Element Shapes on Flexible Pendulum Solutions

The previous patch tests show that the major error sources are not high aspect ratio, skew angle or taperness of the finite elements. In the previous chapters, cantilever beam patch test problems are successfully solved by using single element having a high aspect ratio of 30. Negligible effect of skew angle has been proven by patch tests using trapezoidal finite elements in Chapters 4 and 5. Additionally, the curved beam problem has been solved with tapered elements, accurately. The major error source for ANCF with Virtual Element Mapping is dissimilar neighboring virtual element shapes. Similarity of the neighboring elements is defined by the ratio of edge lengths of neighboring virtual elements. It is expected to obtain the best results for the similarity ratio of 1. Similarity ratio for the flexible pendulum problem is defined as the ratio of lengths (a/b) shown in Figure 6.14. Then, 2×2 elements analyses are repeated for the similarity ratio of 0.03/0.27 to 0.27/0.03. Deformed pendulum shapes for various similarity ratios are shown in Figures 6.15 and 6.16. It is very difficult to distinguish the difference between obtained results from the figures. Therefore, the results obtained by similarity ratio of 1 are selected as reference and displacement errors at points A, B and C are determined, relatively. Obtained error distributions for points A, B and C are shown in Figures 6.17, 6.18 and 6.19, respectively. Displacement errors vary from -7.86% to 7.13% for Point A, -9.39% to 14.24% for Point B, and -8.13% to 5.44% for Point C. Despite reasonable error levels, it is suggested that the similarity ratio should not exceed the range of (0.5, 2). In addition, significance of similarity ratio would be reduced with the increasing total number of elements.
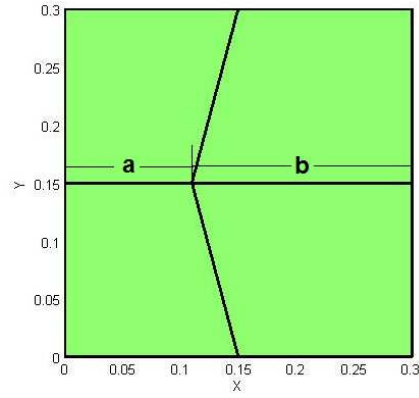
Figure 6.14: Definition similarity ratio for the flexible pendulum problem, a/b

6.5 Discussion on the Proposed Hexahedral Finite Element

In this chapter, implementation of ANCF with Virtual Element Mapping to eight noded hexahedral element has been performed. Performance of the proposed element has been tested with well known cantilever beam patch test problems in finite element literature and flexible pendulum problem, which is the most common test case in flexible multibody dynamics literature. In cantilever patch test solutions, the main aim was to verify nonlinear static solution procedure for the proposed finite element. Performed test results show that the proposed finite element generate accurate results for regular, parallelogram and trapezoidal element shapes. The lowest grade has been obtained for trapezoidal element shape as in the planar finite element formulation.

In flexible pendulum solutions, the main aim was to show accuracy of the proposed element under large rotation and deformation cases. Firstly, convergence study has been performed for different number of elements. It has been shown that accurate results can be obtained similar to the results published for different element formulations and topologies in literature. Then, effect of irregular element geometries has been investigated in flexible pendulum problem. In order to define irregularity level, a new definition called "similarity ratio" has been made. It is shown that up to 14.24% error can be obtained with the similarity ratio between 1/9 and 9/1. However, error level can be decreased to accurate levels by increasing number of elements or using similarity ratio between 1/2 and 2/1.

144
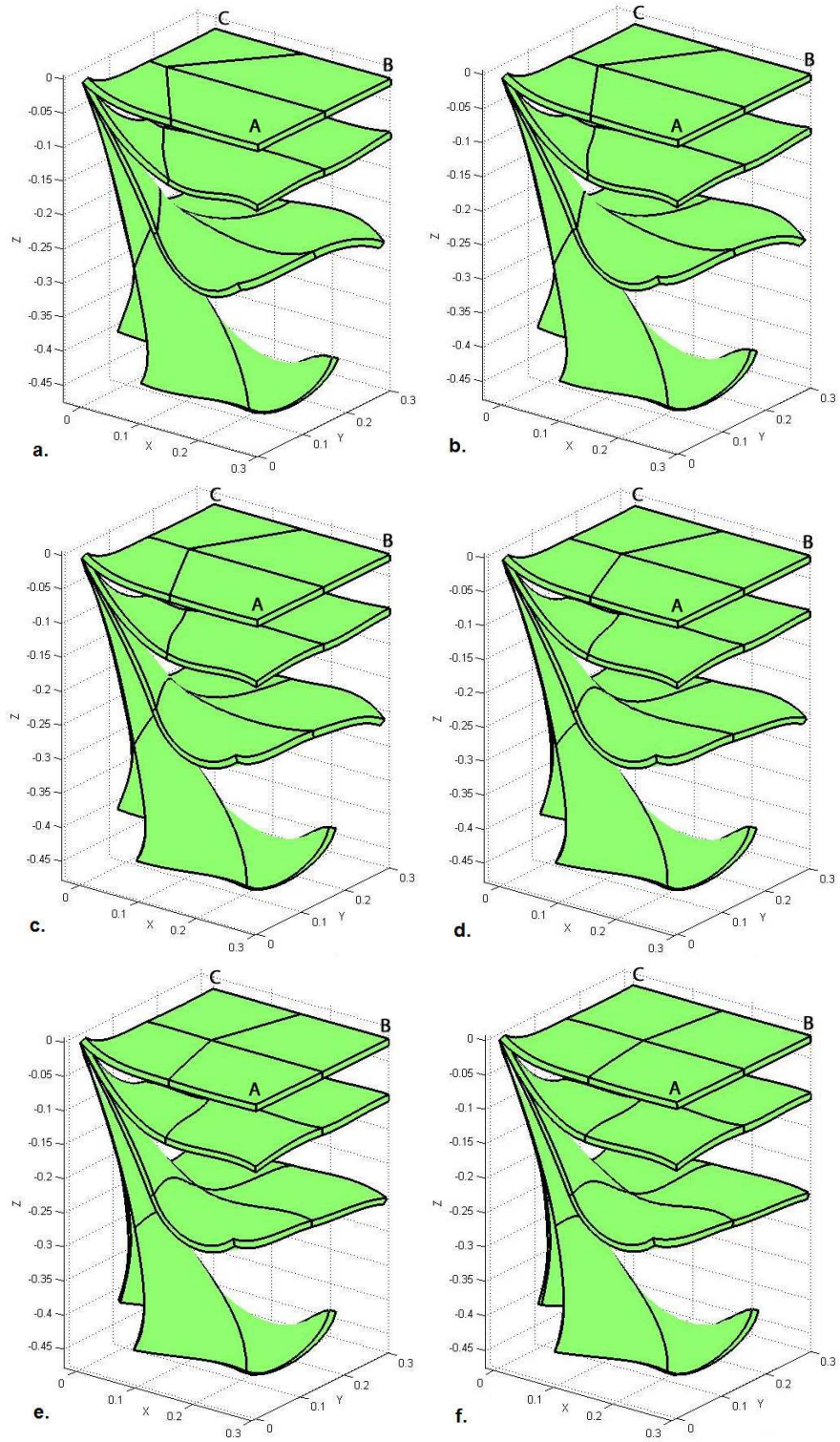
Figure 6.15: Deformed flexible pendulum shapes at 0.075 s, 0.15 s, 0.225 s and 0.3 s (a. a/b=0.03/0.27, b. a/b=0.05/0.25, c. a/b=0.07/0.23, d. a/b=0.09/0.21, e. a/b=0.11/0.19, f. a/b=0.13/0.17)
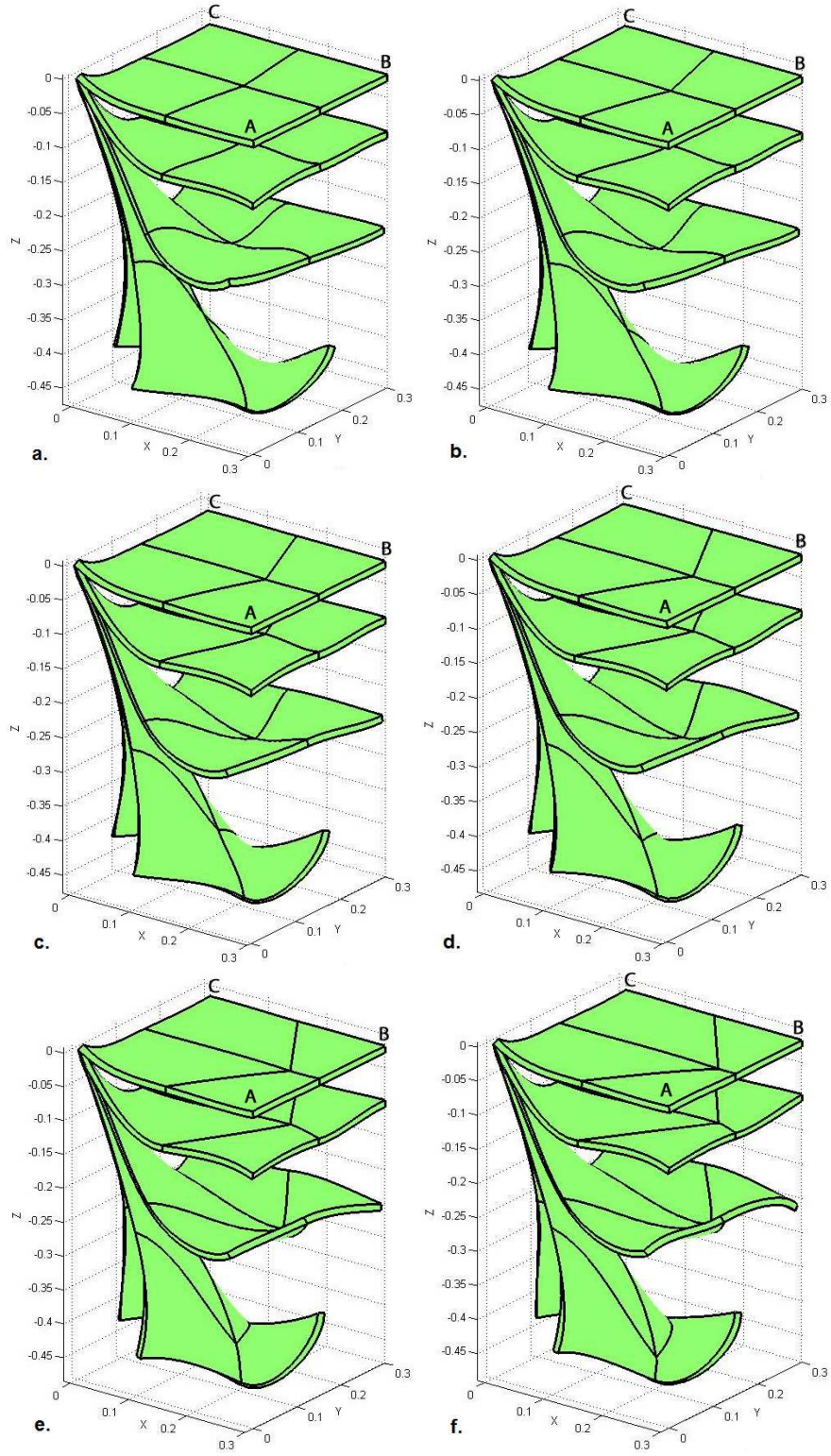
Figure 6.16: Deformed flexible pendulums at 0.075 s, 0.15 s, 0.225 s and 0.3 s (a. a/b=0.17/0.13, b. a/b=0.19/0.11, c. a/b=0.21/0.09, d. a/b=0.23/0.07, e. a/b=0.25/0.05, f. a/b=0.27/0.03)
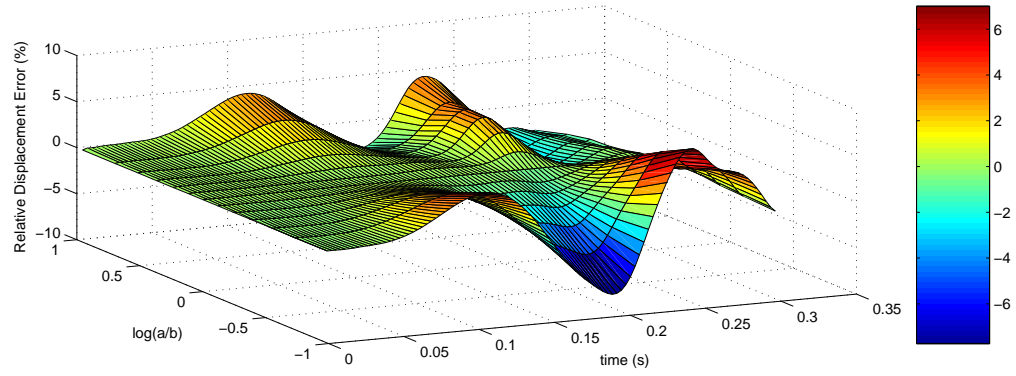
Figure 6.17: Flexible pendulum - relative displacement error distribution at Point A over time for various similarity ratios
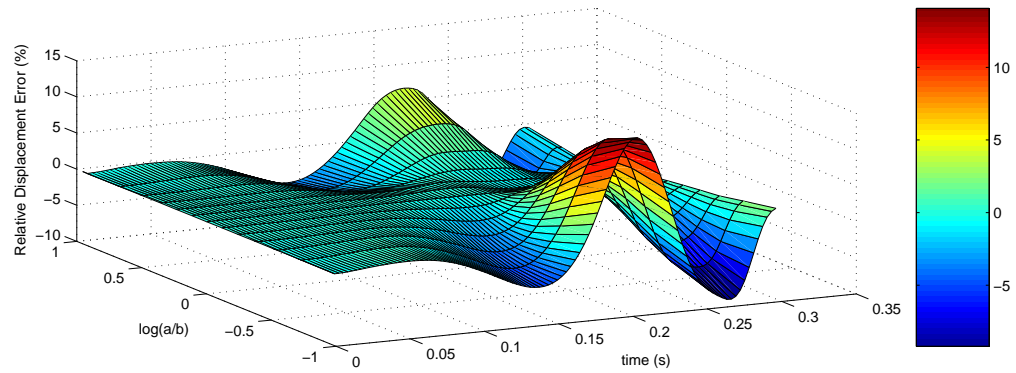
Figure 6.18: Flexible pendulum - relative displacement error distribution at Point B over time for various similarity ratios
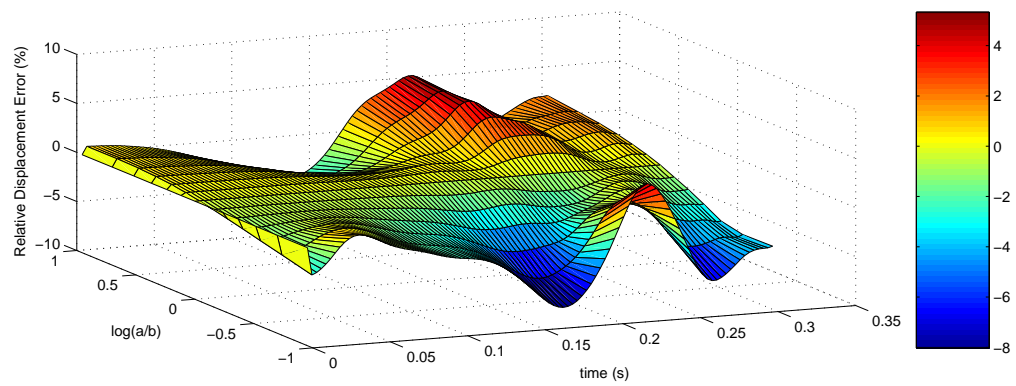
Figure 6.19: Flexible pendulum - relative displacement error distribution at Point C over time for various similarity ratios

CHAPTER 7

DISCUSSION AND CONCLUSION

7.1   Discussion of the Thesis

The main goal of the thesis is to improve current plate/shell finite element formulations for flexible multibody dynamics problems or develop a new approach. In the thesis, both of the aims have been completed not only for plates and shell elements but also for beams, plane stress/plane strain elements and 3D hexahedral solid elements. Firstly, available flexible multibody formulations have been investigated and compared, and as a result of the comparison study, Absolute Nodal Coordinate Formulation has been selected as the basis of the thesis.

The first attempt in the thesis is to introduce meshfree methods to Absolute Nodal Coordinate Formulation. For this purpose, the meshfree ANCF for planar shear deformable beams has been proposed. The proposed formulation has been verified by solving the flexible beam pendulum problem, which is well known in the flexible multibody dynamics literature. Obtained solutions show that accurate results can be obtained with a less number of nodes compared to finite element method based ANCF.

After verifying planar beam formulation, meshfree ANCF of plates and shells have been studied. However, it is observed that it is not possible to satisfy the displacement continuity between quadrature domains by using the developed formulation. Therefore, only the results and their comparisons have been presented without detailed derivations for plates and shells instead of working on this formulation further. Despite the discontinuity problem, it is observed that the most appropriate polynomial based shape function method is the radial point interpolation with polynomial reproduction.

The second attempt in the thesis is to eliminate regular element shape limitation of available ANCF. This attempt is successfully completed and verified. Firstly, "ANCF with Virtual Element Mapping" has been proposed with three alternative nodal coordinate definitions. Then, 4 noded planar quadrilateral finite element formulation has been performed. Nonlinear static and time dependent dynamic finite element analyses have been solved accurately with the proposed method for some of the available patch test problems. Additionally, it is seen that steady state responses in transient dynamics analyses are almost identical to the results obtained by nonlinear static analyses. In fact, this also shows that transient dynamic simulations with finite elements, which use the proposed methods, would not need additional control and solution algorithms for hourglass effect, which is the major error source in explicit finite element solution methods.

It can be thought that the proposed methods are not cost effective due to high number of nodal degrees of freedom and highly nonlinear stiffness matrix or generalized elastic force vector. However, these are actually the advantages of the proposed formulations for transients dynamics flexible multibody simulations, since;

1. the mass matrix is always constant and independent of time,

2. deformable bodies can be discretized with less number of elements relative to the classical finite element methods due to higher order of shape function polynomials and

3. accurate stress and strain results could be obtained due to the use of nonlinear strain tensor in formulation without approximation or linearization.

After verification of the proposed methods for planar finite elements, it has been extended to the generalized plate and shell problems. The detailed formulations of 4 noded generalized plate element have been presented with verification tests. However, performance of the developed finite element under out-of-plane shear loading conditions is not as satisfactory as the performance under in-plane shear or extension loading conditions for thin plates. Actually, this is the general feature of all generalized plate/shell finite elements. In order to increase accuracy in out-of-plane shear loading, thin plate/shell shape functions have been proposed, but, detailed derivation and verification of thin plate/shell formulation have not been presented in the thesis.

149

ANCF with Virtual Element Mapping method has been applied to 3D hexahedral finite elements. Besides verification with cantilever beam patch tests, flexible pendulum problem has also been studied in detail. Firstly, convergence characteristic of the proposed finite element formulation has been observed. Then effect of irregular shaped elements on displacement results has been examined. It is seen that the major element shape factor contributing the results is the similarity ratio, which is defined as the ratio of the edge lengths of neighboring virtual elements. In fact, this ratio is not related with the single element shape but it is related to the finite element mesh of the flexible body. As a result, it is shown that a wide range of similarity ratio can be used without losing accuracy, significantly.

7.2 Conclusions

It is observed that the developed finite element based methods in this thesis are efficient for the solution of flexible multibody problems. The major contributions of the current study can be listed as follows;

1. Meshfree Absolute Nodal Coordinate Formulation for planar shear deformable beams has been developed. It is observed that accuracy is high in the solution and extreme deformations can be handled, easily.

2. Absolute Nodal Coordinate Formulation with Virtual Element Mapping Method is introduced and it is seen that various finite element geometries can be modeled and advantages of ANCF can know be used in 3D continuum problems.

3. ANCF with Virtual Element Mapping has been developed for the solution of plane stress/plane strain problems. Four noded quadrilateral plane stress/plane strain finite elements have been developed for the solution of irregular problems.

4. ANCF with Virtual Element Mapping has been developed for the solution of plate and shell problems. Four noded plate and shell finite elements have been developed for the solution of irregular problems.

5. Derivation of thin plate and shell shape functions for ANCF with Virtual Element Mapping has been made.

6. ANCF with Virtual Element Mapping has been developed for the solution of 3D problems. Eight noded hexahedral finite element has been developed for the solution of irregular problems.

7.3 Further Improvements and Future Studies

The proposed methods and implementations in this thesis study can be improved in the following subjects:

1. Meshfree plate/shell ANCF can be improved by implementing different interpolation functions available in the literature. It is obvious that the accuracy can be increased with the improved shape function polynomials.

2. The proposed Virtual Element Mapping method and related finite elements in the thesis have been tested for a limited range of element geometries, which can be generated by the proposed shape functions. Therefore, additional patch tests should be performed in order to determine geometric limits of the elements.

3. The accuracy of the solutions can be changed by using different shape function polynomials. Therefore, this could be studied in order to increase accuracy.

4. Finite element formulation for "Virtual Element Mapping using Initial Shape Function Polynomials" has been proposed. In most of the regular element shapes this method produce the same shape functions as in Method 1 or 2. However, accuracy of the method for elements having curved edges could be different. Therefore, the method can be studied in detail in order to improve accuracy.

5. For the proposed thin plate/shell shape functions, detailed formulation and verification of the thin plate/shell elements could be performed.

6. ANCF is not very effective for quasi-static simulations. Therefore, an improvement can be made by studying on the solution algorithms or linearization of stiffness matrix.

7. It is also thought that extending the proposed methods to nonlinear elasticity problems would be useful. Especially, accurate results would be expected for hyperelastic and viscoelastic materials.

8. In addition to the improvement requirements, the proposed finite element methods can also be extended to plasticity problems, such as metal forming simulations or crashworthiness applications. These applications also require contact algorithms. Therefore, plasticity and contact algorithms should be considered together.

REFERENCES

[1] Shabana A. A., "Flexible multibody dynamics: Review of past and recent development", Multibody System Dynamics 1: 189-222, 1997, Kluwer Academic Publishers

[2] Shabana A. A., "Non-linear dynamics of multibody systems with generalized and non-generalized coordinates", W. Schiehlen and M. Valasek (eds), Virtual Nonlinear Multibody Systems, 1-16, 2003, Kluwer Academic Publishers

[3] Shabana A. A., Mikkola A. M., "On the use of the degenerate plate and the absolute nodal co-ordinate formulations in multibody system applications", Journal of Sound and Vibration (2003) 259(2), 481-489

[4] Shabana A. A., Christensen A. P., "Three-Dimensional absolute nodal co-ordinate formulation: Plate problem", Int. Journal for Num. Met. in Eng., Vol. 40, 2775-2790, 1997

[5] Yoo W. S., Dmitrochenko O., Pogorelov D. Y., "Review of finite elements using absolute nodal coordinates for large-deformation problems and matching physical experiments", Procedings of DETC'05, ASME International Conference on Multibody Systems, Nonlinear Dynamics and Controls, 2005, DETC2005-84720

[6] Christensen A. P., "Three dimensional finite element absolute nodal coordinate formulation", PhD Thesis, University of Illinois at Chicago, 1998

[7] Shabana A. A., "Computer implementation of the absolute nodal coordinate formulation for flexible multibody dynamics", Nonlinear Dynamics 16: 293-306, 1998, Kluwer Academic Publishers

[8] Shabana A. A., "Dynamics of multibody systems", John Wiley &Sons, New York, 1989

[9] Shabana, A. A., Wehage, R. A., "A coordinate reduction technique for dynamic analysis of spatial substructures with large angular rotations", Mechanics Based Design of Structures and Machines, 11:3, 401-431, 1983

[10] Shin J., "A study of flexible multibody system with finite shell elements", PhD Thesis, The University of Michigan, 2007

[11] Dwivedy K. S., Eberhard P., "Dynamic analysis of flexible manipulators, a literature review", Mechanism and Machine Theory 41: 749-777, 2006

[12] Cook R. D., Malkus D. S., Plesha M. E., Witt R. J., "Concepts and applications of finite element analysis", 4th edition, John Wiley & Sons, 2001

[13] Shabana A. A., "Definition of the Slopes and the Finite Element Absolute Nodal Coordinate Formulation", Multibody System Dynamics 1: 339-348, 1997, Kluwer Academic Publishers

[14] Simo J. C., Vu-Quoc L., "On the dynamics of flexible beams under large overall motions - the plane case: parts I&II", ASME Journal of Applied Mechanics 53, 1986, 849-863

[15] Yoo W. S., Kim K. N., Kim H. W., Sohn J. H., "Developments of multibody system dynamics: computer simulations and experiments", Multibody Syst. Dyn 18:35-58, 2007

[16] Yoo W. S., Kim M. S., Mun S. H., Sohn J. H., "Large displacement of beam with base motion: flexible multibody simulations and experiments", Comput. Methods Appl. Mech. Engrg. 195: 7036-7051, 2006

[17] Vallejo D. G., Mayo J., Escalano J. L., Dominguez J., "A new algorithm for the evaluation of the elastic forces in the absolute nodal coordinate formulation", European Congress on Computational Methods in Applied Sciences And Engineering, 24-28 July 2004

[18] Shabana A. A., Schwertassek R., "Equivalence of the floating frame of reference approach and finite element formulations", Int. J. Non-Linear Mechanics. Vol. 33, No. 3, 417-432,1998

[19] Takahashi Y., Shimizu N., "Study on elastic forces of the absolute nodal coordinate formulation for deformable beams", Proceedings of the 1999 ASME Design Eng. Technical Conferences, DETC99/VIB-8203, 1999

[20] Berzeri M., Shabana A. A., "Development of simple models for elastic forces in the absolute nodal co-ordinate formulation", Journal of Sound and Vibration, 2000, 235 (4), 539-565

[21] Omar M. A., Shabana A. A., "A two dimensional shear deformable beam for large rotation and deformation problems", Journal of Sound and Vibration, 2001, 243 (3), 565-576

[22] Dombrowski S. V., "Analysis of large flexible body deformation in multibody systems using absolute coordinates", Multibody System Dynamics 8: 409-432, 2002, Kluwer Academic Publishers

[23] Yoo W. S., Lee J. H., Park S. J., Sohn J. H., Dmitrotchenko O., Pogorelov D., "Large Oscillations of thin cantilever beam: Physical experiments and simulation using absolute nodal coordinate formulation", Nonlinear Dynamics Vol. 34 (1-2), 3-29, 2003

[24] Vallejo D. G., Mayo J., Escalano J. L., Dominguez J., "Efficient evaluation of the elastic forces and the jacobian in the absolute nodal coordinate formulation", Nonlinear Dynamics 35: 313-329, 2004

[25] Dufva K. E., Sopanen J. T., Mikkola, "A two-dimensional shear deformable beam element based on the absolute nodal coordinate formulation", Journal of Sound and Vibration 280 (2005), 719-738

[26] Schwab A. L., Meijaard J. P., "Comparison of three-dimensional flexible beam elements for dynamic analysis: Finite element method and absolute nodal coordinate formulation", Proceedings of IDETC/CIE 2005 ASME Int. Design Eng. Technical Conferences & Comp. and Information in Eng Conference, DETC2005-85104

[27] Gerstmayr J., Matikainen M. K., "Analysis of stress and strain in the absolute nodal coordinate formulation with nonlinear material behavior", III European Conference on Computational Mechanics Solids, Structures and Coupled Problems in Engineering

[28] Sugiyama H., Gerstmayr J., Shabana A. A., "Deformation modes in the finite element absolute nodal coordinate formulation", Journal of Sound and Vibration 298 (2006), 1129-1149

[29] Gerstmayr J., "Strain tensors in the absolute nodal coordinate and the floating frame of reference formulation", Nonlinear dynamics 34: 133-145, 2003

[30] Mikkola A. M., Shabana A. A., "A Non-incremental finite element procedure for the analysis of large deformation of plates and shells in mechanical system applications", Multibody System Dynamics 9: 283-309, 2003

[31] Yoo W. S., Lee J. H., Park S. J., Sohn J. H., Pogorelov D., Dmitrochenko O., "Large deflection analysis of a thin plate: Computer simulations and experiments", Multibody system dynamics 11: 185-208, 2004

[32] Dufva K., Shabana A. A., "Analysis of thin plate structures using the absolute nodal coordinate formulation", Proceedings of the Institution of Mechanical Engineers, Part K: Journal of Multi-body Dynamics, Vol. 219, Number 4 / 2005, 345-355

[33] Schwab A. L., Gerstmayr J., Meijaard J. P., "Comparison of three-dimensional flexible thin plate elements for multibody dynamics analysis: Finite element formulation and absolute nodal coordinate formulation", Proceedings of the ASME 2007 International Design Engineering Technical Conferences & Computers and Information in Engineering Conference IDETC/CIE 2007, DETC2007-34754

[34] Escalona J. L., Hussien H. A., Shabana A. A., "Application of the absolute nodal co-ordinate formulation to multibody system dynamics", Journal of Sound and Vib. 214(5), 833-851, 1998

[35] Macneal R. H., Harder R. L., "A Proposed Standard Set of Problems to Test Finite Element Accuracy", Finite Elements in Analysis and Design ,Vol 1, 3-20, 1985

[36] Bathe K. J., "Finite Element Procedures", Prentice Hall, 1996

[37] Liu G. R., "Mesh Free Methods: Moving beyond the Finite Element Method", CRC Press, 2003

[38] Liu G. R., Gu Y. T., "An Introduction to Meshfree Methods and Their Programming", Springer, 2005

[39] Belytschko T., Krongauz Y., Organ D., Fleming M., Krysl P., "Meshless Methods: An Overview and recent developments", Computational Methods in Applied Mechanics and Engineering, Vol. 139, 3-47, 1996

[40] Schwer L. E., Key S. W., Pucik T. A., Bindeman L.P., "An Assessment of the LS-DYNA Hourglass Formulations via the 3D Patch Test", 5th European LS-DYNA Users Conference, 2005

[41] Kübler L., Eberhand P., Geisler J., "Flexible Multibody Systems with Large Deformations using Absolute Nodal Coordinates for Isoparametric Solid Brick Elements", ASME 2003 Design Engineering Technical Conferences and Computers and Information in Engineering Conference ,Chicago, Illinois, USA, September 2-6, 2003

APPENDIX A

INTEGRATION CONSTANTS FOR NON-SHEAR DEFORMABLE PLANAR BEAM ANCF

By using the shape function matrix given in Equation 2.13, $\partial \mathbf{S}/\partial \xi$ and $\partial^2 \mathbf{S}/\partial \xi^2$ can be calculated as given in Equations A.1 and A.2.

$$
\frac{\partial \mathbf{S}}{\partial \xi} = \begin{bmatrix}
-6\xi + 6\xi^2 & 0 \\
0 & -6\xi + 6\xi^2 \\
L\left(1 - 4\xi + 3\xi^2\right) & 0 \\
0 & L\left(1 - 4\xi + 3\xi^2\right) \\
6\xi - 6\xi^2 & 0 \\
0 & 6\xi - 6\xi^2 \\
L\left(3\xi^2 - 2\xi\right) & 0 \\
0 & L\left(3\xi^2 - 2\xi\right)
\end{bmatrix}^T
\tag{A.1}
$$

$$
\frac{\partial^2 \mathbf{S}}{\partial \xi^2} = \begin{bmatrix}
-6 + 12\xi & 0 \\
0 & -6 + 12\xi \\
L\left(-4 + 6\xi\right) & 0 \\
0 & L\left(-4 + 6\xi\right) \\
6 - 12\xi & 0 \\
0 & 6 - 12\xi \\
L\left(6\xi - 2\right) & 0 \\
0 & L\left(6\xi - 2\right)
\end{bmatrix}^T
\tag{A.2}
$$

Then, integration constants appearing in Equation 2.28 can be calculated as given in Equations A.3 - A.12.

$$\mathbf{A}_{11} = \frac{Ea}{L} \int_0^1 \mathbf{S}_{1,\xi}^T \mathbf{S}_{1,\xi} d\xi = \frac{Ea}{L} \begin{bmatrix} \frac{6}{5} & 0 & \frac{L}{10} & 0 & -\frac{6}{5} & 0 & \frac{L}{10} & 0 \\ 0 & 0 & 0 & 0 & 0 & 0 & 0 & 0 \\ \frac{L}{10} & 0 & \frac{2L^2}{15} & 0 & -\frac{L}{10} & 0 & -\frac{L^2}{30} & 0 \\ 0 & 0 & 0 & 0 & 0 & 0 & 0 & 0 \\ -\frac{6}{5} & 0 & -\frac{L}{10} & 0 & \frac{6}{5} & 0 & -\frac{L}{10} & 0 \\ 0 & 0 & 0 & 0 & 0 & 0 & 0 & 0 \\ \frac{L}{10} & 0 & -\frac{L^2}{30} & 0 & -\frac{L}{10} & 0 & \frac{2L^2}{15} & 0 \\ 0 & 0 & 0 & 0 & 0 & 0 & 0 & 0 \end{bmatrix} \tag{A.3}$$

$$\mathbf{A}_{21} = \frac{Ea}{L} \int_0^1 \mathbf{S}_{2,\xi}^T \mathbf{S}_{1,\xi} d\xi = \frac{Ea}{L} \begin{bmatrix} 0 & 0 & 0 & 0 & 0 & 0 & 0 & 0 \\ \frac{6}{5} & 0 & \frac{L}{10} & 0 & -\frac{6}{5} & 0 & \frac{L}{10} & 0 \\ 0 & 0 & 0 & 0 & 0 & 0 & 0 & 0 \\ \frac{L}{10} & 0 & \frac{2L^2}{15} & 0 & -\frac{L}{10} & 0 & -\frac{L^2}{30} & 0 \\ 0 & 0 & 0 & 0 & 0 & 0 & 0 & 0 \\ -\frac{6}{5} & 0 & -\frac{L}{10} & 0 & \frac{6}{5} & 0 & -\frac{L}{10} & 0 \\ 0 & 0 & 0 & 0 & 0 & 0 & 0 & 0 \\ \frac{L}{10} & 0 & -\frac{L^2}{30} & 0 & -\frac{L}{10} & 0 & \frac{2L^2}{15} & 0 \end{bmatrix} \tag{A.4}$$

$$\mathbf{A}_{12} = \frac{Ea}{L} \int_0^1 \mathbf{S}_{1,\xi}^T \mathbf{S}_{2,\xi} d\xi = \frac{Ea}{L} \begin{bmatrix} 0 & 0 & 0 & 0 & 0 & 0 & 0 & 0 \\ \frac{6}{5} & 0 & \frac{L}{10} & 0 & -\frac{6}{5} & 0 & \frac{L}{10} & 0 \\ 0 & 0 & 0 & 0 & 0 & 0 & 0 & 0 \\ \frac{L}{10} & 0 & \frac{2L^2}{15} & 0 & -\frac{L}{10} & 0 & -\frac{L^2}{30} & 0 \\ 0 & 0 & 0 & 0 & 0 & 0 & 0 & 0 \\ -\frac{6}{5} & 0 & -\frac{L}{10} & 0 & \frac{6}{5} & 0 & -\frac{L}{10} & 0 \\ 0 & 0 & 0 & 0 & 0 & 0 & 0 & 0 \\ \frac{L}{10} & 0 & -\frac{L^2}{30} & 0 & -\frac{L}{10} & 0 & \frac{2L^2}{15} & 0 \end{bmatrix}^T \tag{A.5}$$

158

$$\mathbf{A}_{22} = \frac{Ea}{L} \int_0^1 \mathbf{S}_{2,\xi}^T \mathbf{S}_{2,\xi} d\xi = \frac{Ea}{L}
\begin{bmatrix}
0 & 0 & 0 & 0 & 0 & 0 & 0 & 0 \\
0 & \frac{6}{5} & 0 & \frac{L}{10} & 0 & -\frac{6}{5} & 0 & \frac{L}{10} \\
0 & 0 & 0 & 0 & 0 & 0 & 0 & 0 \\
0 & \frac{L}{10} & 0 & \frac{2L^2}{15} & 0 & -\frac{L}{10} & 0 & -\frac{L^2}{30} \\
0 & 0 & 0 & 0 & 0 & 0 & 0 & 0 \\
0 & -\frac{6}{5} & 0 & -\frac{L}{10} & 0 & \frac{6}{5} & 0 & -\frac{L}{10} \\
0 & 0 & 0 & 0 & 0 & 0 & 0 & 0 \\
0 & \frac{L}{10} & 0 & -\frac{L^2}{30} & 0 & -\frac{L}{10} & 0 & \frac{2L^2}{15}
\end{bmatrix}
\tag{A.6}$$

$$\mathbf{B}_{11} = \frac{EI}{L^3} \int_0^1 \left(\frac{\partial^2 \mathbf{S}_1}{\partial \xi^2}\right)^T \left(\frac{\partial^2 \mathbf{S}_1}{\partial \xi^2}\right) d\xi = \frac{EI}{L^3}
\begin{bmatrix}
12 & 0 & 6L & 0 & -12 & 0 & 6L & 0 \\
0 & 0 & 0 & 0 & 0 & 0 & 0 & 0 \\
6L & 0 & 4L^2 & 0 & -6L & 0 & 2L^2 & 0 \\
0 & 0 & 0 & 0 & 0 & 0 & 0 & 0 \\
-12 & 0 & -6L & 0 & 12 & 0 & -6L & 0 \\
0 & 0 & 0 & 0 & 0 & 0 & 0 & 0 \\
6L & 0 & 2L^2 & 0 & -6L & 0 & 4L^2 & 0 \\
0 & 0 & 0 & 0 & 0 & 0 & 0 & 0
\end{bmatrix}
\tag{A.7}$$

$$\mathbf{B}_{21} = \frac{EI}{L^3} \int_0^1 \left(\frac{\partial^2 \mathbf{S}_2}{\partial \xi^2}\right)^T \left(\frac{\partial^2 \mathbf{S}_1}{\partial \xi^2}\right) d\xi = \frac{EI}{L^3}
\begin{bmatrix}
0 & 0 & 0 & 0 & 0 & 0 & 0 & 0 \\
12 & 0 & 6L & 0 & -12 & 0 & 6L & 0 \\
0 & 0 & 0 & 0 & 0 & 0 & 0 & 0 \\
6L & 0 & 4L^2 & 0 & -6L & 0 & 2L^2 & 0 \\
0 & 0 & 0 & 0 & 0 & 0 & 0 & 0 \\
-12 & 0 & -6L & 0 & 12 & 0 & -6L & 0 \\
0 & 0 & 0 & 0 & 0 & 0 & 0 & 0 \\
6L & 0 & 2L^2 & 0 & -6L & 0 & 4L^2 & 0
\end{bmatrix}
\tag{A.8}$$

$$\mathbf{B}_{12} = \frac{EI}{L^3} \int_0^1 \left(\frac{\partial^2 \mathbf{S}_1}{\partial \xi^2}\right)^T \left(\frac{\partial^2 \mathbf{S}_2}{\partial \xi^2}\right) d\xi = \frac{EI}{L^3} \begin{bmatrix} 0 & 0 & 0 & 0 & 0 & 0 & 0 & 0 \\ 12 & 0 & 6L & 0 & -12 & 0 & 6L & 0 \\ 0 & 0 & 0 & 0 & 0 & 0 & 0 & 0 \\ 6L & 0 & 4L^2 & 0 & -6L & 0 & 2L^2 & 0 \\ 0 & 0 & 0 & 0 & 0 & 0 & 0 & 0 \\ -12 & 0 & -6L & 0 & 12 & 0 & -6L & 0 \\ 0 & 0 & 0 & 0 & 0 & 0 & 0 & 0 \\ 6L & 0 & 2L^2 & 0 & -6L & 0 & 4L^2 & 0 \end{bmatrix}^T \tag{A.9}$$

$$\mathbf{B}_{22} = \frac{EI}{L^3} \int_0^1 \left(\frac{\partial^2 \mathbf{S}_2}{\partial \xi^2}\right)^T \left(\frac{\partial^2 \mathbf{S}_2}{\partial \xi^2}\right) d\xi = \frac{EI}{L^3} \begin{bmatrix} 0 & 0 & 0 & 0 & 0 & 0 & 0 & 0 \\ 0 & 12 & 0 & 6L & 0 & -12 & 0 & 6L \\ 0 & 0 & 0 & 0 & 0 & 0 & 0 & 0 \\ 0 & 6L & 0 & 4L^2 & 0 & -6L & 0 & 2L^2 \\ 0 & 0 & 0 & 0 & 0 & 0 & 0 & 0 \\ 0 & -12 & 0 & -6L & 0 & 12 & 0 & -6L \\ 0 & 0 & 0 & 0 & 0 & 0 & 0 & 0 \\ 0 & 6L & 0 & 2L^2 & 0 & -6L & 0 & 4L^2 \end{bmatrix} \tag{A.10}$$

$$\mathbf{A}_1 = Ea \int_0^1 \mathbf{S}_{1,\xi}^T d\xi = Ea \begin{bmatrix} -1 & 0 & 0 & 0 & 1 & 0 & 0 & 0 \end{bmatrix}^T \tag{A.11}$$

$$\mathbf{A}_2 = Ea \int_0^1 \mathbf{S}_{2,\xi}^T d\xi = Ea \begin{bmatrix} 0 & -1 & 0 & 0 & 0 & 1 & 0 & 0 \end{bmatrix}^T \tag{A.12}$$

Additionally, $\partial i_x / \partial \mathbf{e}$ and $\partial i_y / \partial \mathbf{e}$ can be simplified as given in the following equations.

$$\frac{\partial i_x}{\partial \mathbf{e}} = \frac{1}{\left((e_5 - e_1)^2 + (e_6 - e_2)^2\right)^{3/2}} \begin{bmatrix} -(e_6 - e_2)^2 \\ (e_5 - e_1)(e_6 - e_2) \\ 0 \\ 0 \\ (e_6 - e_2)^2 \\ -(e_5 - e_1)(e_6 - e_2) \\ 0 \\ 0 \end{bmatrix}$$ (A.13)

$$\frac{\partial i_y}{\partial \mathbf{e}} = \frac{1}{\left((e_5 - e_1)^2 + (e_6 - e_2)^2\right)^{3/2}} \begin{bmatrix} (e_5 - e_1)(e_6 - e_2) \\ -(e_5 - e_1)^2 \\ 0 \\ 0 \\ -(e_5 - e_1)(e_6 - e_2) \\ (e_5 - e_1)^2 \\ 0 \\ 0 \end{bmatrix}$$ (A.14)

CURRICULUM VITAE

PERSONAL INFORMATION

Surname, Name	: Tüzün, Aydın
Date/Place of birth	: 17 February 1979, ANKARA
Nationality	: Turkish
Marital Status	: Single
Work address	: TÜBİTAK-SAGE P.K. 16, 06261 Mamak, ANKARA / TÜRKİYE
Phone	: +90 (312) 590 92 13
Fax	: +90 (312) 590 91 48-49
E-mail	: aydin.tuzun@tubitak.gov.tr
	aydintuzun@yahoo.com

EDUCATION

Degree	Institution	Years
PhD.	Department of Mechanical Engineering, METU	2005-2012
MSc.	Department of Mechanical Engineering, METU	2001-2004
BSc.	Department of Mechanical Engineering, METU	1996-2001
High School	Ankara Dikmen Lisesi	1993-1995

WORK EXPERIENCE

Enrollment	Organization	Years
Chief Research Engineer	Structural Mechanics and Control Group, TÜBİTAK-SAGE, Ankara, TÜRKİYE	2004-present
Research Assistant	Department of Mechanical Engineering, METU, Ankara, TÜRKİYE	2001-2004

LANGUAGE SKILLS

Native Language: Turkish

Other Languages: English

AREAS OF TECHNICAL INTEREST

Structural Mechanics/Dynamics	Mechanical design, design of composite structures, wing box design, aeroelasticity, mechanical shock, fixture design, metal forming, structural optimization
Structural Testing	Structural integrity tests, Ground Vibration Testing, vibration and mechanical shock tests, ejection tests

PUBLICATIONS

1. Atik H., Baran Ö. U. and Tüzün A., "Static Aeroelastic Calculations for a Wing under Large Deformations", AIAA-APA 2012, New Orleans, U.S.A., June 2012.

2. Atik H., Baran Ö. U. and Tüzün A., "Static Aeroelastic Calculations for a High Aspect Ratio Wing", AIAC 2011, Ankara, Türkiye, September 2011.